Retrieval Analysis and Finite Element Modeling of Orthopaedic Porous-Coated Implants

A Dissertation

Submitted to the Faculty

of

Drexel University

by

Josa Ann Hanzlik

in partial fulfillment of the

requirements for the degree

of

Doctor of Philosophy

August 2015

Dedication

This dissertation is dedicated to my patient, loving and demanding husband,

who always believed in me, even when I didn't.

Acknowledgements

I would like to thank my advisor Dr. Steven Kurtz for his guidance, advice and supporting me to go abroad for a year.

Thank you to Dr. Judd Day for his constant probing questions and ideas. His genius and humor is unparalleled.

Thank you to my committee members, Dr. Sri Balasubramanian, Dr. Kara Spiller and Dr. Shieh for their significant insight and constructive criticism that improved the quality of my work.

I would like to acknowledge Dr. Lim, the Graduate Studies Office and everyone in the Biomed Office for their support, smiles and belief in me.

It's hard to imagine my time at Drexel without acknowledging all the wonderful people I met through my student activities. My DGWISE ladies: Jules, Chetana, Kerry, Marissa, Danni and many more.

My friends who I met at the ORL in Netherlands, words cannot express how much I enjoyed my time there. Dr. Nico Verdonschot and Dr. Dennis Janssen, thank you for your guidance, support, humor and friendship. Lennert, Thom, Priyanka, Veronica, Sanaz and Florieke, thank you for the amazing year in the Netherlands.

My IRC labmates: Dan, Genymphas, Mariya, Sevi, Michael, Alex, Tina, Lenny and Liza. There have been so many found memories, such as ORS trips and Researchgiving.

My two rocks that I am fortunate to call friends, Jaimie and Chetana.

To my sisters, Stephanie and Mary, who are so similar to me, yet so vastly different. Edward and Cheryl, my parents, for their support in all my endeavors.

To my husband Kevin, you have been my sounding board and support through this process. Thank you for everything.

Table of Contents

List of Tables

List of Figures

Dissertation Abstract

Retrieval Analysis and Finite Element Modeling of Orthopaedic Porous-Coated Implants
Josa Ann Hanzlik
Steven M. Kurtz, Ph.D.

Recent Nationwide Inpatient Sample (NIS) studies have shown that implant loosening remains one of the common reasons for revision in total joint replacement. In an effort to reduce loosening caused by long-term breakdown of the cement mantle, manufacturers introduced cementless technologies to provide biological fixation by hard tissue ingrowth at the bone-implant interface. One new material, porous tantalum, has had promising clinical results with well-fixed implants and relatively few reported cases of loosening. The factors that may be causing the lower incidence of aseptic loosening remain unknown. Therefore, the goal of this dissertation was to investigate the factors affecting bone fixation in porous tantalum implants through retrieval analysis and finite element (FE) modeling. Through the Implant Research Center's retrieval program, the proportion of implants revised for aseptic loosening was compared between the porous tantalum implants and historical porous-coated implants. Retrieval analysis protocols were developed to assess and determine factors that affect bone ingrowth in porous tantalum hip and knee implants. Porous tantalum tibial trays were histologically analyzed to determine locations of fibrous tissue or bone ingrowth. The results showed that the amount of bone observed varied by implant type and location within each implant for retrieved porous tantalum acetabular shells, femoral stems, patellas and tibial trays. Retrieval results showed that modular tibial tray implants had higher bone ingrowth than the monoblock tibial trays. However, the bone ingrowth in the porous tantalum was lower than that observed in historical porous-coated implants. Histological analyses of tibial trays demonstrated bone ingrowth primarily in the superficial depth of the tibial trays,

with fibrous tissue also present. The FE models showed that there was more favorable initial implant stability in the modular tibial tray compared to the monoblock implant. This study showed that the lower incidence of aseptic loosening did not appear to be associated with increased bone ingrowth for the retrieved porous tantalum hip and knee implants. Initial FE models showed that lower micromotion for the modular tibial tray compared the monoblock. This dissertation presents a multifaceted approach for analysis of highly porous biomaterials.

Specific Aims

Aim 1: Within the Implant Research Center's retrieval program, determine the reasons for revision of retrieved porous tantalum implants. Determine the association between previous number of surgeries, coating type and fixation method (cementless or cemented) on the proportion of implants revised for aseptic loosening.

Aim 2: Characterize retrieved porous tantalum implants for bone ingrowth. Determine factors associated with bone ingrowth in retrieved porous tantalum implants.

Aim 3: Create FE models to investigate factors affecting initial implant stability and stress on the bone/implant.

a) Investigate the effect of implant design (modular vs monoblock), implant properties, bone quality and patient activity on micromotion.
b) Assess the difference in stress and stress on the tibial implant and tibial bone based on implant design type (modular vs monoblock).

Introduction (Literature Review)

Anatomy and Biomechanics of the Hip and Knee

Anatomy of the Hip

The hip joint consists of the acetabulum (socket) and the femoral head (ball). The acetabulum is the socket in the pelvis formed by three bones: the ilium, the ischium and the pubis. The socket faces laterally and also slightly inferiorly and anteriorly. The femoral head is mostly semispherical, with a short “neck of the femur” angling the head anteriorly, medially and superiorly to fit into the socket. The angle of inclination is created by the femur head and the long bone of the femur. The inclination angle is normally 125°in adults, however, greater in infants. The bones of the hip are the femur (the thigh bone) and the pelvis. The superior end of the femur is shaped like a ball. This ball is called the femoral head. The femoral head fits into a round socket on the side of the pelvis. This socket is called the acetabulum (Figure 0-1).

The femoral neck attaches the femoral head to the rest of the femur. The greater trochanter is a bump that juts outward from the top of the femur. Muscles attach to the greater trochanter. One of these muscles is the gluteus medius, which is an important muscle for keeping the pelvis level during walking.

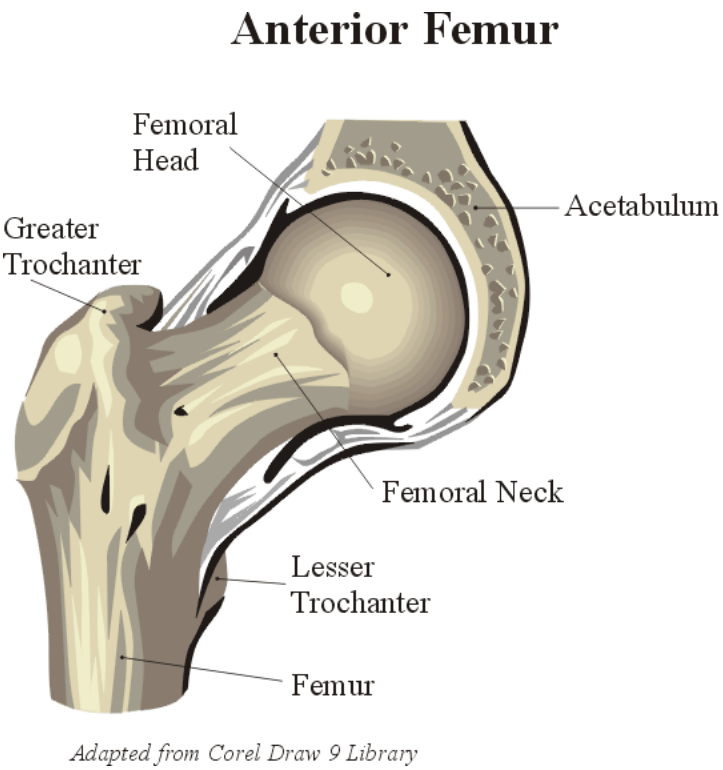

Figure 0-1: Anatomy of the hip joint [1].

In any joint, the bones at the ends are covered in *articular cartilage*. In the hip, the articular cartilage is approximately ¼ inch thick. It has a white, shiny appearance and rubbery consistency. Articular cartilage is slippery allowing for the joint surfaces to slide against one another without causing damage (Figure 0-2). Articular cartilage absorbs shock and provides an extremely smooth surface that makes motion easier. Articular cartilage is present everywhere that two bony surfaces articulate or move against one another.

In the hip, articular cartilage covers the socket portion of the acetabulum in the pelvis and the end of the femur. The cartilage is especially thick in the back portion of the acetabulum, as this is where most of the force occurs during walking and running.

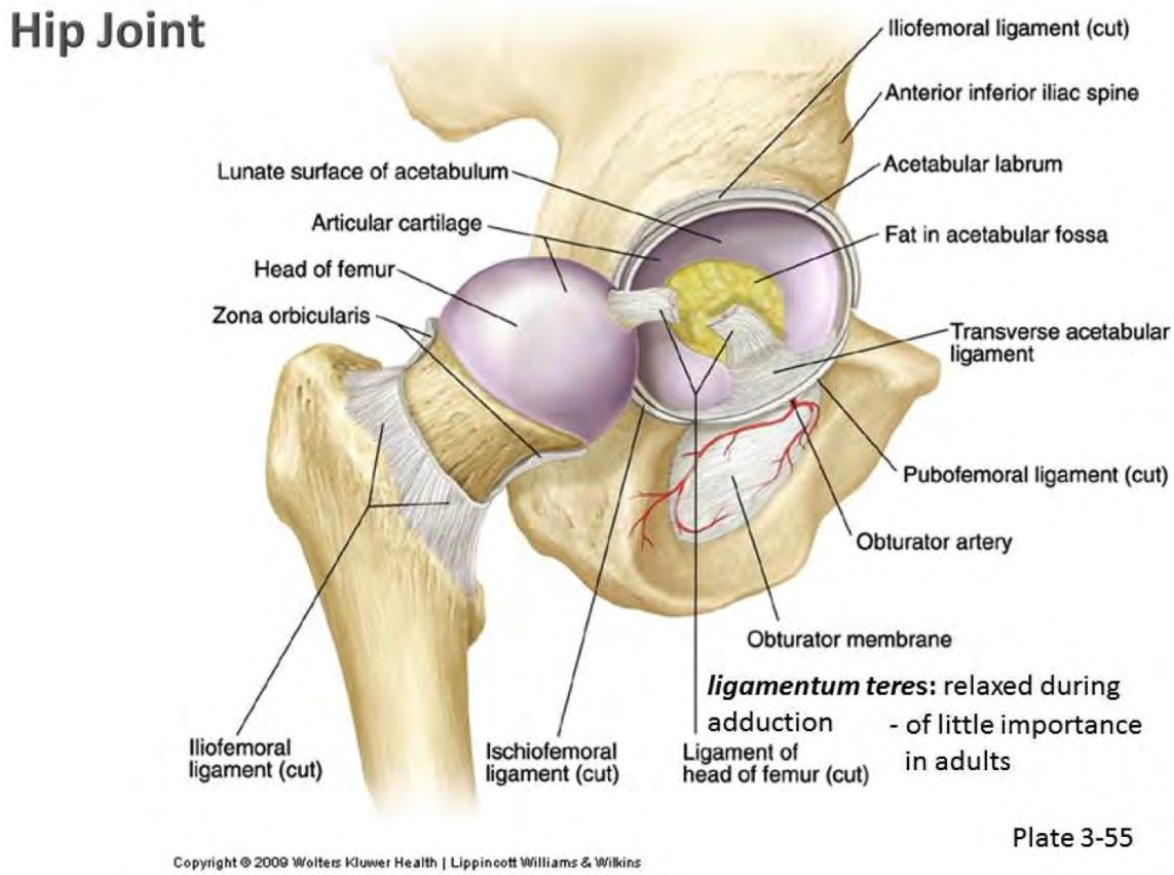

Figure 0-2: Hip joint anatomy with ligament attachment [2].

Biomechanics of the Hip

The hip joint has three degrees of freedom (DOF). The first is the sagittal plane allowing for flexion and extension. The movement in the frontal plane allows for abduction and adduction. Finally, the last DOF in the transverse plane allows for external and internal rotation.

The stability of the hip joint is due to ligaments, the joint capsule, and positioning. Ligaments connect bones to other bones and prevent excessive movement and dislocation. The iliofemoral, pubofemoral and ischiofemoral ligaments and the ligamentum teres all help stabilize the hip joint (Figure 0-2). These ligaments supply the most support anteriorly during hip extension and the least during hip flexion. As a result, most hip dislocations occur because of a proximally directed force with the hip in 90° of

flexion. The joint capsule, which encircles the joint and femoral neck, is very strong. Its strongest aspects are the anterior and superior aspects, reinforced primarily by the two strongest ligaments, the iliofemoral and ischiofemoral ligaments [3]. The positioning of the hip joint is most congruent under high loads and less so under low loads. It is most stable in quadruped (structurally) and in hip extension (owing to ligamentous tautness). Therefore, there is a greater chance of injury during adduction and flexion.

The strong muscles of the hip region also help to hold the hip joint together and prevent dislocation. To produce various movements of the hip joint, many different muscles are involved (Figure 0-3). The extensor muscles include the gluteus maximus, hamstrings (long head of biceps femoris, semitendinosus and semimembranosus). The flexor muscles include the iliopsoas (iliacus and psoas), rectus femoris, tensor fasciae latae, and sartorius. The adductor muscles include the pectineus, adductor brevis, adductor longus, gracilis, and adductor magnus. The abductor muscles include the gluteus medius, gluteus minimus and tensor fasciae latae. The external rotators include obturator internus and externus, gemellus superior and inferior, quadratus femoris, piriformis.

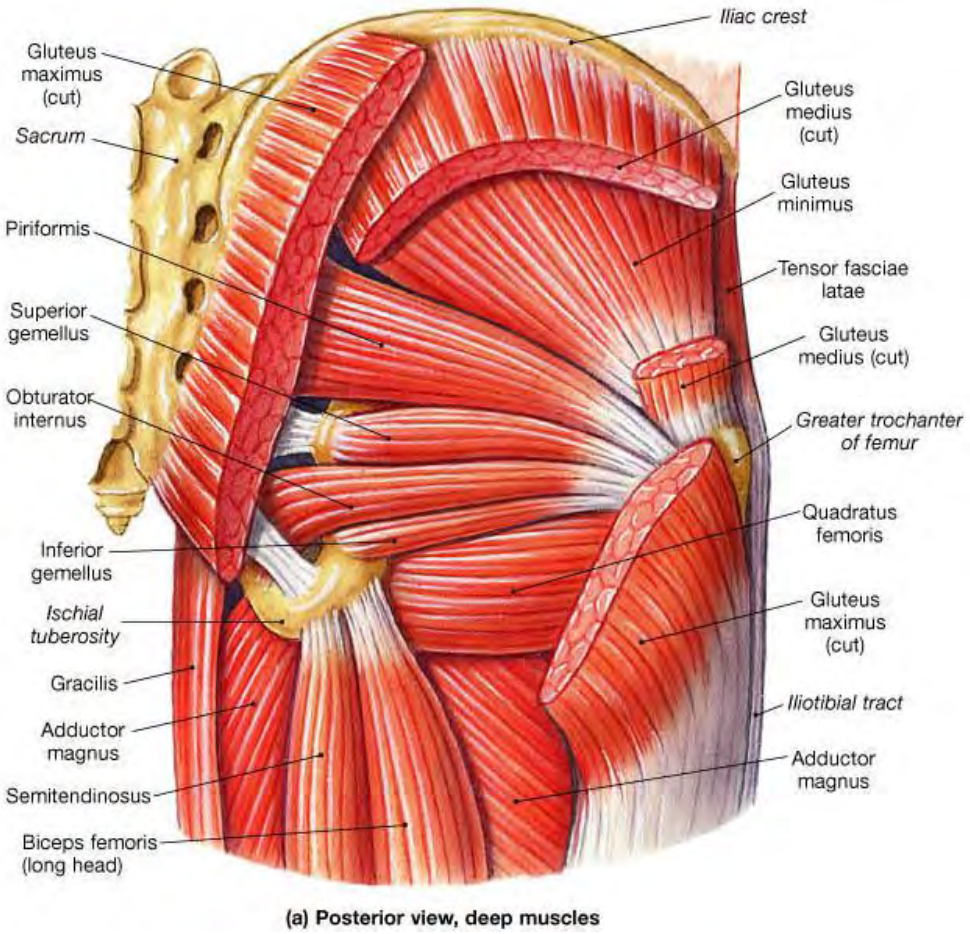

Figure 0-3: The muscles of the hip joint in the posterior view [4].

The internal rotators include the anterior portion of the gluteus medius and the tensor fasciae latae contribute to this action, but no muscle does internal rotation as its primary function.

The acetabulum and head of the femur are both lined by hyaline cartilage, which provides a smooth surface as the two bones glide past one another. During movement, the hyaline cartilage also acts as a shock absorber preventing collision of the bones. Synovial membranes secrete watery synovial fluid to lubricate the joint capsule between the layers of hyaline cartilage.

In the hip joint there are ligaments that prevent dislocation. The hip joint has a ball and socket structure that allows for the femur to circumduct freely through a 360° circle (Figure 0-4).

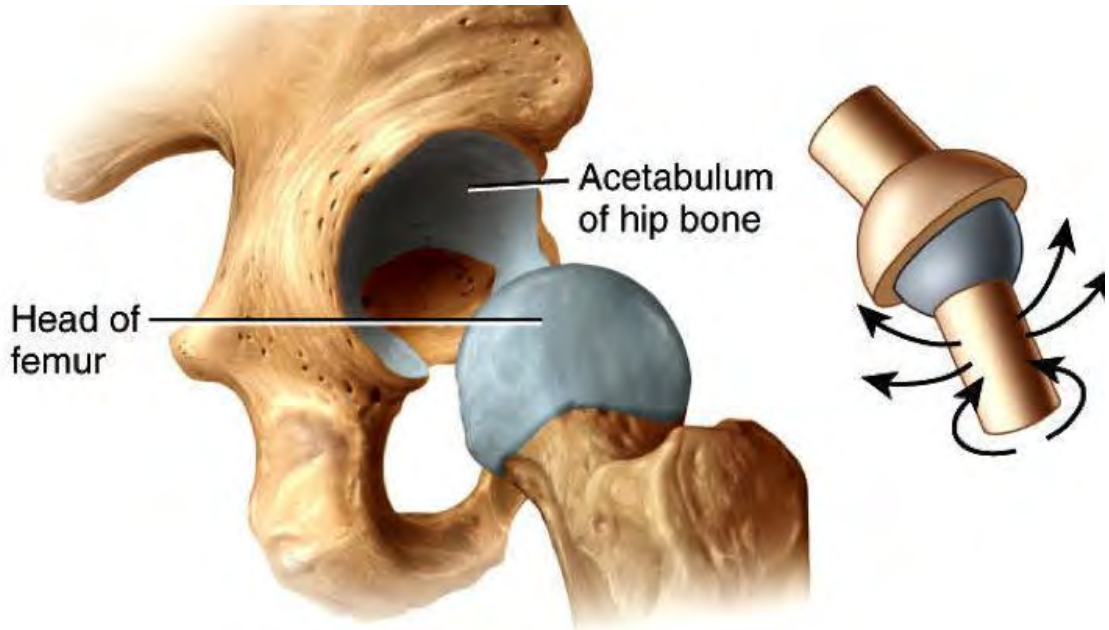

Figure 0-4: The hip joint is a ball and socket type joint, which allows 360 rotation of the femur [5].

Additionally, the femur is able to rotate 90°about its axis at the hip joint. Each hip joint must also be capable of supporting half the body's weight along with any additional forces acting upon the body. During more strenuous activities, such as jumping or running, the movement of the bone results in the forces on the hip joint being many times higher than the normal body weight. The hip joint is able to accommodate these extreme forces that occur due to repeated high intensity physical activities.

Anatomy of the Knee

The knee is the largest human synovial joint, made up of three major bones (femur, tibia and patella) that are joined together by ligaments and muscles (Figure 0-5). It consists of

two articulating joints; the tibiofemoral (TF) and patellofemoral (PF) joints. The tibiofemoral joint is a dual condyloid.

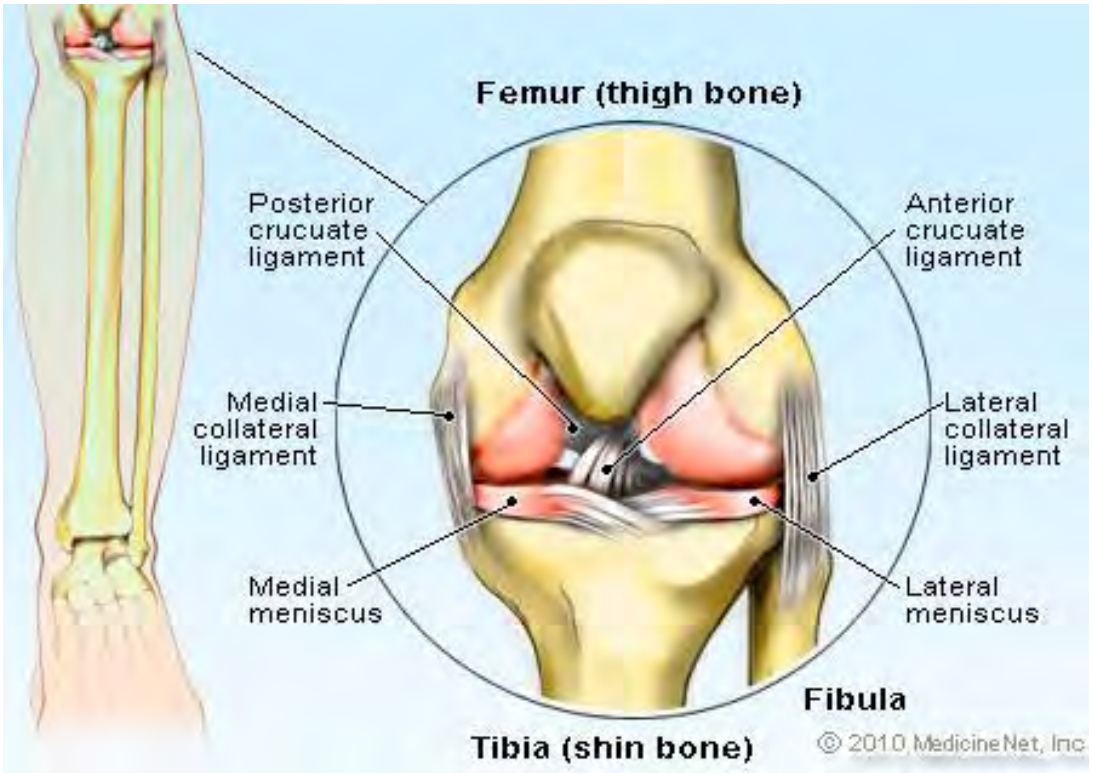

Figure 0-5: Knee joint anatomy [6].

The four major bones that provide the framework for the knee are the femur, fibula, patella and tibia. The frame work for the knee is provided through four major bones: femur, tibia, fibula and patella. The femur, or thigh bone, is the upper part of the leg and largest bone in the body, located proximal to the knee joint. The tibia, or shin bone is distal to the knee joint and second largest bone in the lower leg. The tibia includes major structures such as the intercondyloid eminence (tibial spine), tuberosity, tibial crest, and tibial plafond (Figure 0-6).

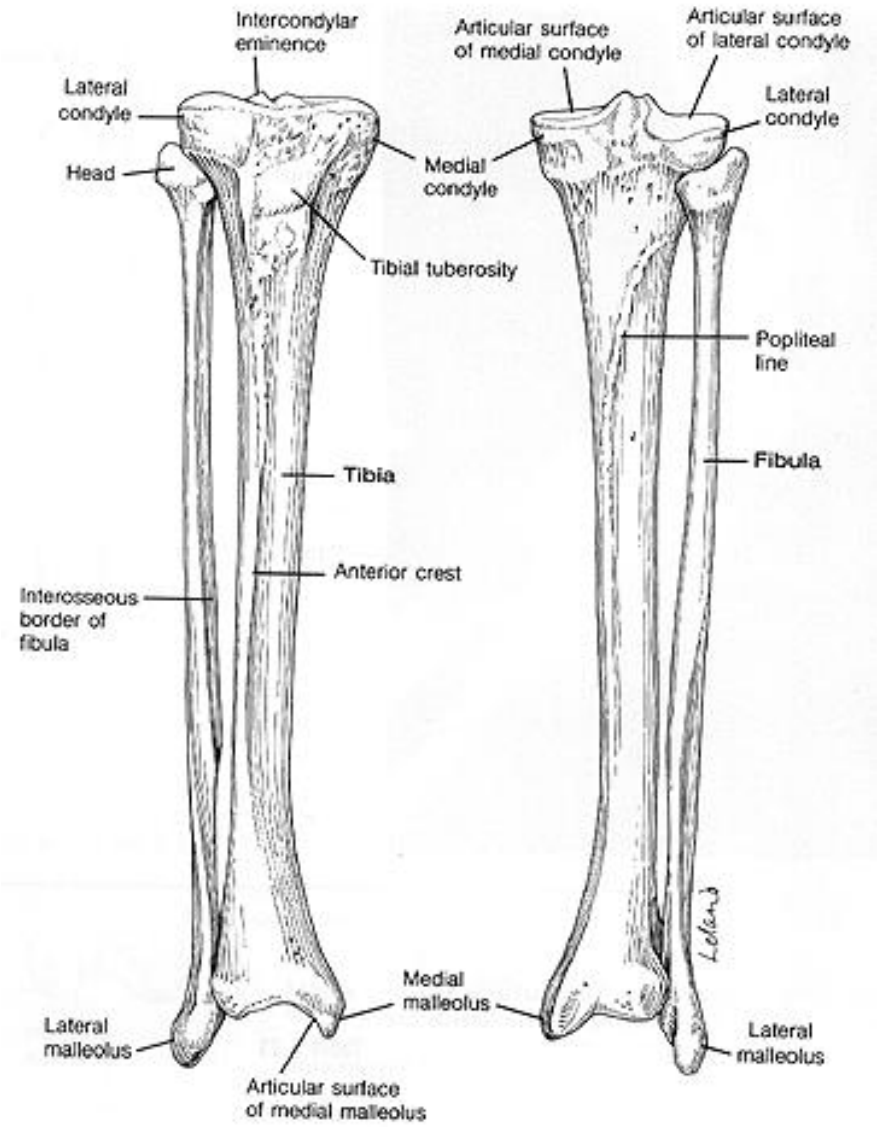

Figure 0-6: Tibia anatomy [7].

The tibial spine is a protuberance of the tibial bone in the proximal direction on the anterior surface of the bone. The tuberosity is the major bone structure on the anterior of the tibia, at the insertion site of the patella tendon. The tibial crest is located on the anterior side of the tibia, where it extends from the tuberosity towards the ankle.
On the distal end of the tibia is the plafond which forms the roof of the ankle joint. In the interior of the bone there is an intramedullary canal that runs the length of the long axis

of the bone. The fibula is the smaller bone located in the lower leg and it runs parallel to the tibia bone. The patella, also called the knee cap is on the front of the leg located at the knee joint (Figure 0-7). The tibiofemoral joint is the main joint of the knee which includes the articulation between the femur and tibia.

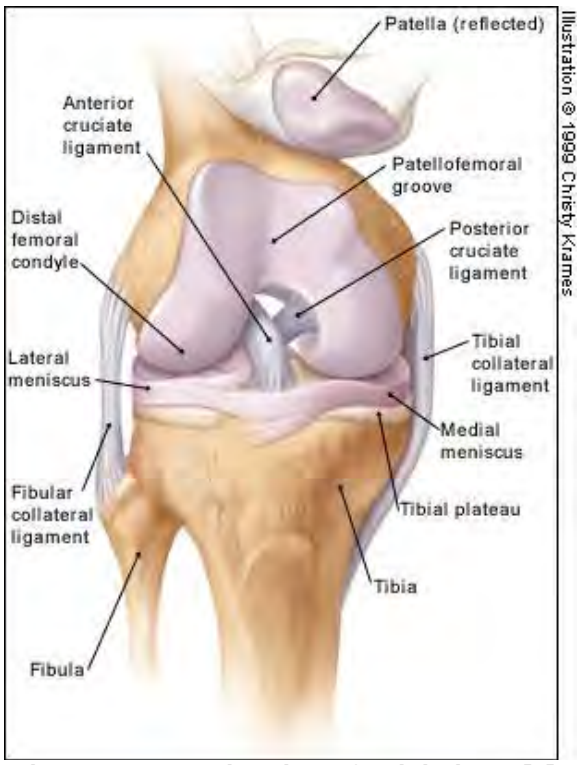

Figure 0-7: Anterior view of a right knee [8].

Biomechanics of the Knee

The knee joint has six degrees of freedom (DOF) for movement (Figure 0-8). The primary movement is flexion and extension which is done in the sagittal plane. The knee movement is restricted mainly to the sagittal plane. The connecting ligaments do allow some lateral movement and rotation.

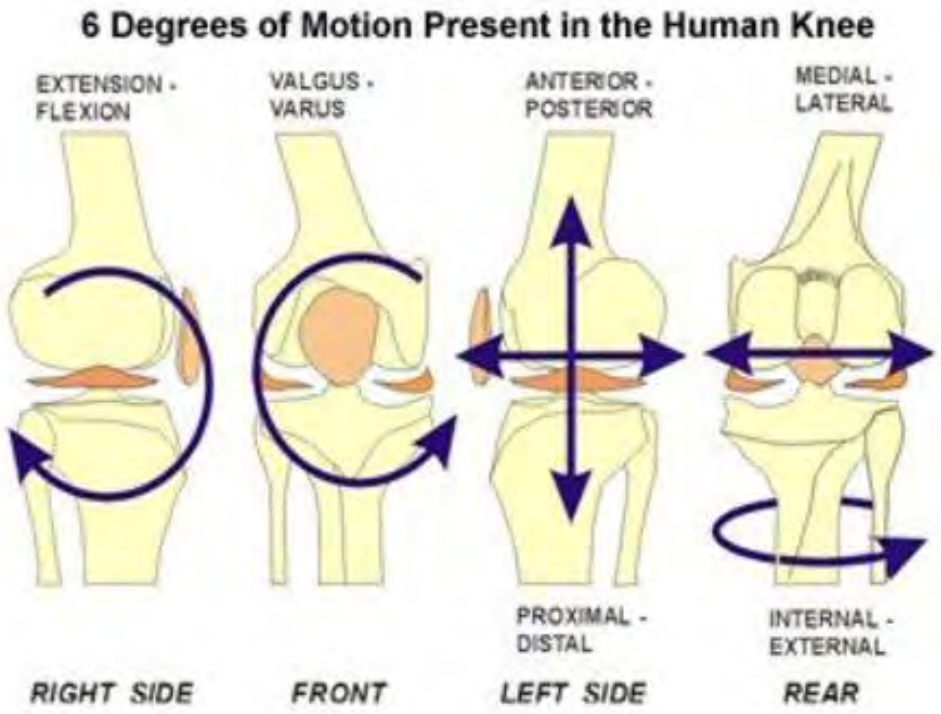

Figure 0-8: The knee point with 6 degrees of freedom [9].

The knee is classified as a modified hinge joint (Figure 0-9). The quadriceps muscles are used to complete extension. Knee flexion is caused by the hamstring muscles and assisted by the gracilis, sartorius gastrocnemius and plantaris. The knee joint can be rotated internally-externally, independently of the flexion/extension movement by the muscles which attach at the sides of the joint.

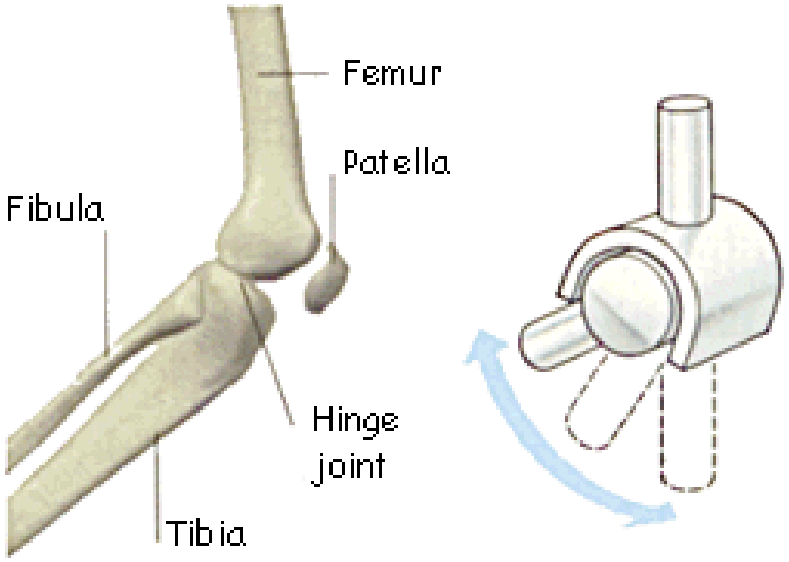

Figure 0-9: The knee joint represented as a modified hinge joint type [10] .

The main external rotation of the tibia is the bicep femoris. The internal rotators of the tibia are the sartorius, gracilis, semitendinosus and semimembranosus. The main joint movement is a combination of rolling, sliding and rotation of the femoral condyles over the tibial plateaus [11].

Bone: Mechanical Properties and Remodeling Processes

Composition and Structure of Bone

Bone is an important dynamic tissue in the human body, which continues to models and remodels due to forces acting on it. The main two critical mechanical functions of bone are: 1) provide a rigid skeletal framework to support and protect the internal organs, 2) forming a system of rigid levers that can be moved by the forces of attached muscles. The major mineral constituents of bone are calcium carbonate, calcium phosphate, collagen and water.

Calcium carbonate and calcium phosphate make up approximately 60-70% of the dry bone and are the primary determinants of the bone stiffness and compressive

strength. Collagen is a protein that provides flexibility while also contributing to the tensile strength of the bone. Water makes up the remaining 25-30% of the bone. Bone tissue is classified into two main categories based on its porosity or percentage of bone volume that is occupied by non-mineralized tissues. Cortical or compact bone has porosity ranging from 5-30%. Cancellous bone (trabecular or spongy bone) has a porosity ranging from 30-90%. Cancellous bone has a honeycomb structure with mineralized horizontal and vertical bars which are called the trabecula. The area between the trabeculae are filled with fat and marrow.

In a long bone, the diaphysis or central port is formed by the cortical bone (Figure 0-10). The cortical bone is roughly cylindrical in shape and relatively thin. The cancellous bone is primarily located in the epiphyses and metaphysis of the long bone and forms in the interior of all other bones.

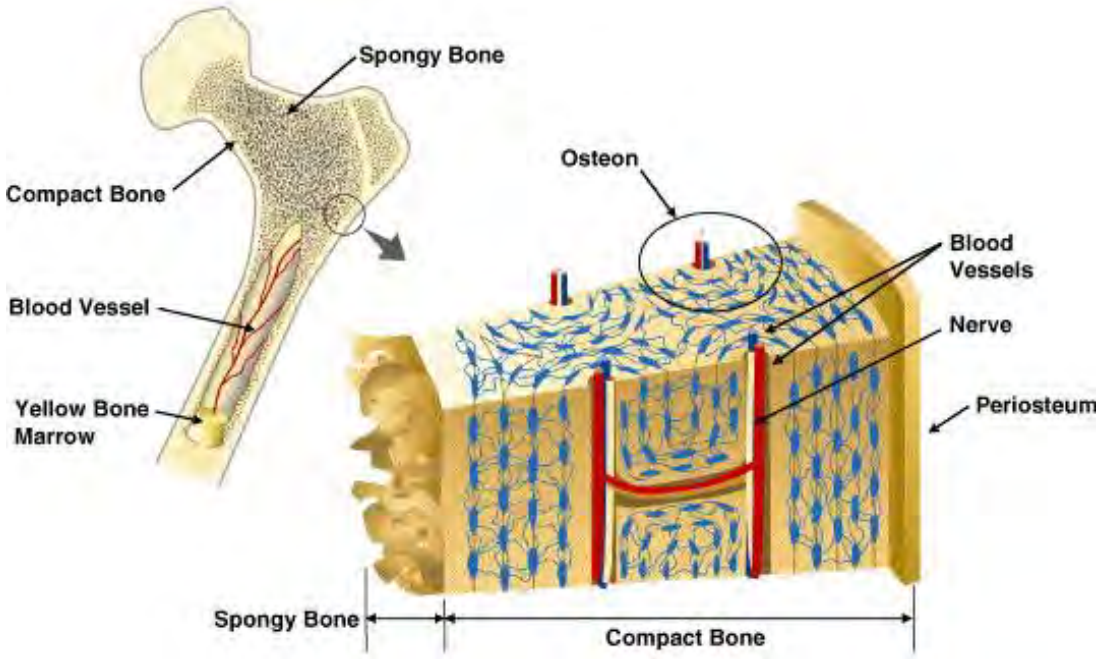

Figure 0-10: Long bone focused on structure of compact bone [12].

The periosteum is a dense connective tissue containing blood vessels and nerves which covers the outer surface of the bone. The endosteum is a thinner connective tissue that lines the inner surface of the medullary cavity (canal). The periosteum and endosteum contain osteoblasts which are responsible for bone growth, repair and remodeling. The endosteum contains osteoclasts which as responsible for bone resorption.

Rho et al. noted the importance of the hierarchical structure of bone in to its mechanical properties [13]. They determined that the mechanical properties of the bone varied at the different levels and structures of the bone.

The levels of the bone collectively are (Figure 0-11):

i. Macrostructure: cortical and cancellous bone,
ii. Microstructure (from 10 to 500 mm): Haversian systems, osteons, single trabecular
iii. Sub-microstructure (1-10 mm): lamellae
iv. Nanostructure (from a few hundred nanometers to 1 mm)
v. Sub-nanostructure (below a few hundred nanometers): molecular structure of constituent elements, mineral, collagen and non-collagenous organic proteins.

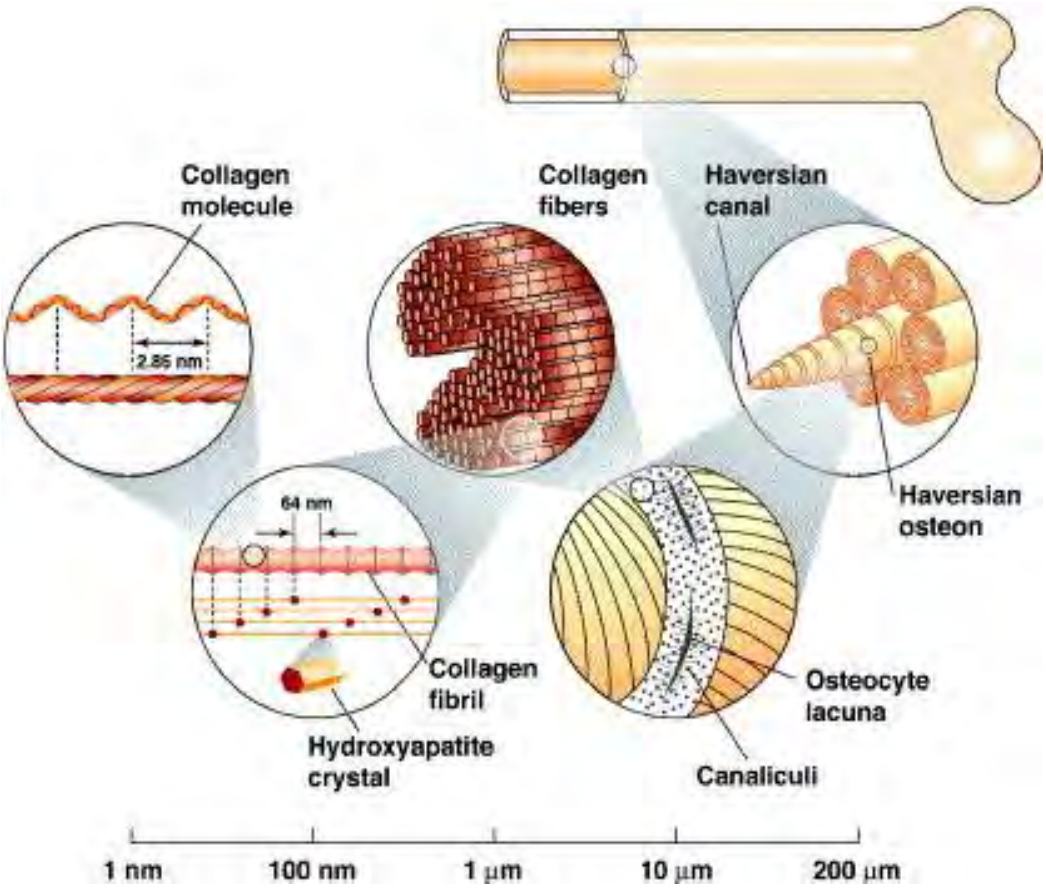

Figure 0-11: Hierarchical structure of human cortical and compact bone [12].

The hierarchically organized structure of bone has an irregular, yet optimized arrangement and orientation of the component which makes it heterogeneous and anisotropic. Osteoporosis and osteoarthritis (degenerative diseases) may be influenced by the microstructures at several different levels [13]. Mechanical studies of bone have focused mainly on the micro and macro structural levels. New research focused on the sub-micro and smaller hierarchical structure may help improve the understanding of bone. Further research could help to identify if certain diseases are contained at specified structure level, thus may allowed for isolated treatment.

Mechanical Properties of Bone

The mechanical behavior of bone is affected by its porosity. Cortical bone with a higher mineral content is stiffer and able to withstand higher stress. Cancellous bone is less dense and has a lower elastic modulus, however it is able to undergo greater strain before failure. Mechanical tests such as uniaxial tensile, compressive test, 2-point bending and torsion test can be used to determine the mechanical properties of bone. Microstructure level properties can be determined through microindentation, nanoindentation and acoustic tests [14].

Anisotropic and Heterogeneous Properties of Bone

The mechanical properties of cortical and cancellous bone are anisotropic in nature [15-17]. The strength and elastic modulus of the bone is dependent on its orientation. For the cortical bone, the properties along the anterior-posterior (AP) and medial-lateral (ML) direction are similar or transverse isotropic. For the cancellous bone, this is not necessarily accurate. The modulus and the strength of the cortical bone are highest along the superior-inferior (SI) direction (0°, longitudinal), lowest at the AP/ML direction (90°, transverse) and intermediate values between 0° to 90°. The cancellous bone is anisotropic based on its trabecular morphology. For the cancellous bone, it is anisotropic based on its trabecular morphology [17, 18]. The human long bone, the apparent modulus of the cancellous bone in the SI direction is about 2.5 times larger than in the AP direction [19]. The apparent modulus in the AP direction is higher than in the ML direction [19]. One study that tested a single human proximal tibial epiphysis found that cancellous bone structure is approximately transversely isotropic (average $E_{transverse,1}$ = 51.0 MPa, $E_{transverse,2}$ = 37.2 MPa and $E_{longitudinal}$ = 227.4 MPa, [16]). The properties are the apparent values for the porous trabecular structure as a whole, not actually the material properties of the bone material of individual trabecula.

Cortical and cancellous regions of the bone are mechanically heterogeneous and their properties are anatomically site dependent. One study of the human proximal tibia showed that the modulus of cancellous bone at different location with the same metaphysis can differ by 100 times [20]. The elastic modulus and strength of bovine cortical bone were highest at the mid-diaphysis and decreased gradually at the epiphyses [21] (Figure 0-12). At the mid-diaphysis, the properties are highly anisotropic. At the epiphyses the properties are isotropic. A survey of published data by Goldstein et al. showed that mechanical properties of bone are largely dependent on anatomical sites [22].

A wide range of elastic modulus and yield strength for cortical and cancellous have been reported. The elastic modulus (5 - 34.4 GPa) and strength (35 - 295 MPa) of cortical bone can vary greatly. The mechanical properties depend on the anatomical site, type of mechanical test and orientation of the test specimens. The cancellous bone modulus and strength are 10 - 1570 MPa and 1.5 - 38 MPa, respectively [23]. Elastic modulus of cortical bone ranges from 17.4 GPa and 9.6 GPa in the longitudinal and transverse directions of the long bone, respectively [24]. One study showed that cancellous bone can vary from 20 - 5000 MPa [17].

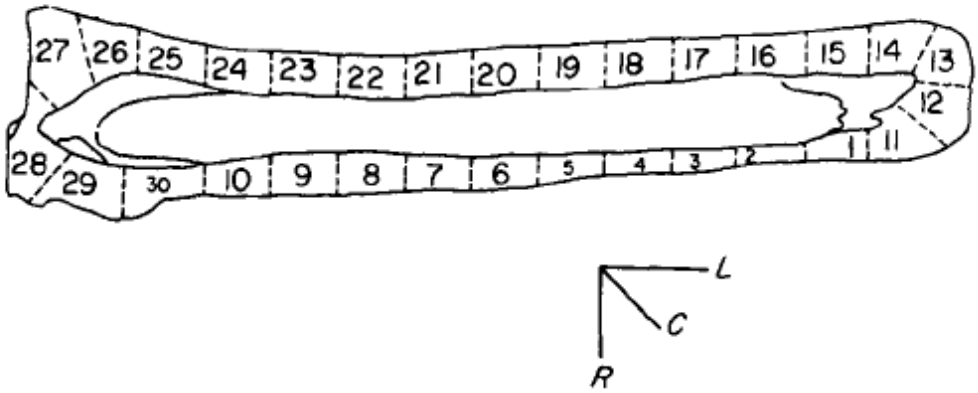

Figure 0-12: Cross-section of typical bovine tibia with zone marked along it longitudinal axis [21].

Stiffness and Strength in Relation to Apparent Density

There is a strong correlation between bone mechanical properties and its apparent density (ρ). In the early 1970s, a linear relationship between the strength and apparent density of cancellous bone was reported [15]. The cortical bone has an average apparent density of approximately 1.8 g/cm^3, and the cancellous bone range from 0.14 - 1.10 g/cm^3 [24].

The apparent density of bone can be derived for Computed Tomography (CT scan data. A linear correlation between the CT number (Hounsfield Units, HU) and apparent density was established for the tibial bone [25] and vertebral bone [26, 27]. Using the apparent density the mechanical properties of the bone can be calculated in a non-invasive way.

Mechanical Properties of Tibia and Femur

The three regions of the bone include the epiphysis, metaphysis and diaphysis. At the distal and proximal end of the long bone is the epiphysis. At birth, the epiphysis is separated from the main bone by a layer of cartilage, known as the growth plate, that eventually ossifies and becomes fused (Figure 0-13). The growth plate is located in the metaphysis and is in between the diaphysis and the epiphysis. The diaphysis is a cylindrical region and is the main section of the long bone. There is also the periosteum and the endosteum. The periosteum is a dense fibrous membrane that covers the outer surface of the bone, except at the joints. It serves as an attachment site for tendons and muscles. It also contains nerves and blood vessels that nourish the bone. The endosteum is a vascular membrane that lines the inner surface of the bone along the intramedullary canal.

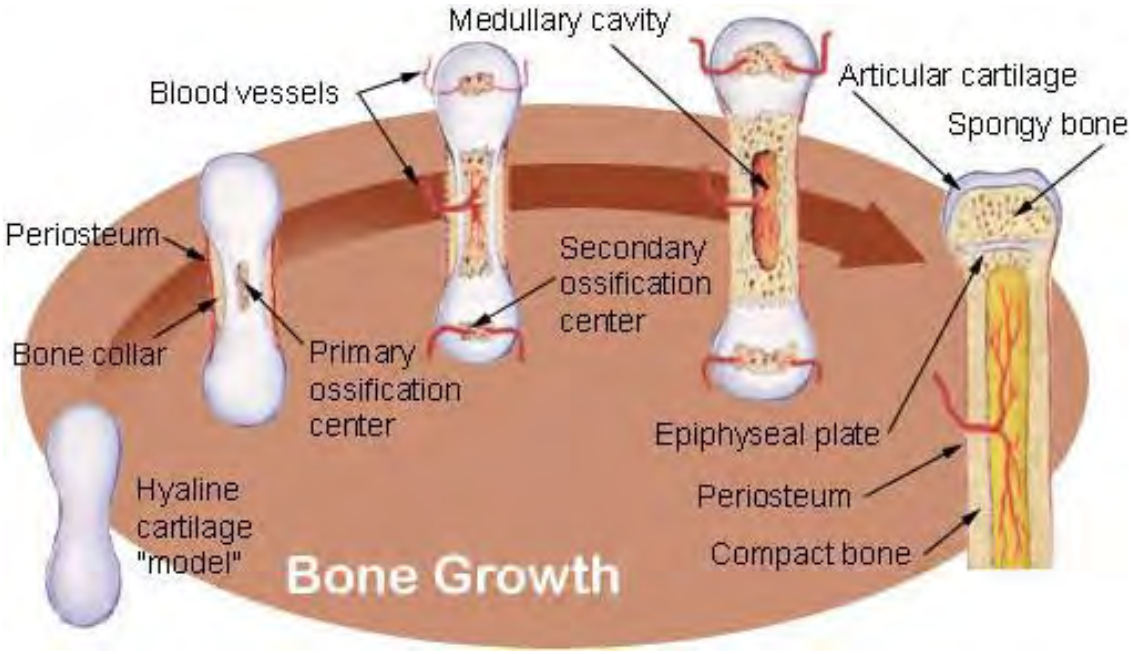

Figure 0-13: The stages of bone growth [28].

The final classification of the bone includes cortical and cancellous bone. Cortical bone is located on the outer surface of the diaphysis and is more dense bone. Cancellous or spongy bone is located in the inner region of the diaphysis and metaphysic region.

Remodeling Processes

In the 19th century, Wolff developed a theory that bone mass will increase or decrease as the forces acting on the bone increase or decrease [29]. The osteocyte directs the bone modeling and remodeling processes. The bone modeling and remodeling involves apposition (bone growth) and resorption (bone loss). Osteocytes are cells that embed themselves into the bone. Osteocytes are sensitive to changes in the interstitial fluid flow through the pores resulting from the strain on the bone. In response to a change in strain, osteocytes will trigger the response of osteoblasts (bone forming cells) and osteoclasts (bone resorbing cells). A dominance of osteoclastic activity will result in an increase in bone mass (hypertrophy). If there is a dominance in osteoclastic activity, there will be a reduction of bone mass (atrophy). When there is a balance between the

two activities, the bone structural integrity will remain unchanged, while the turnover of material continues.

Based on conceptual observations and biological behavior, it was hypothesized that the basic structure and mass of the bone is dependent on its mechanical loading history. Specifically, the amount of strain change in a nonlinear manner. A level of normal bone mass is maintained through normal physiological activities, where the bone is fairly unresponsive to changes in load history. The time when the bone is fairly unresponsive (unchanging) is called the "dead zone." When the strain on the bone exceeds the normal activity range, the bone mass will increase. Limited activity or immobilization can lead to severe bone loss. This suggests that bone mass gain with normal activity will stabilize once bone reaches maturity.

The complex biological process of bone remodeling is dependent on genetic, hormonal, metabolic, age factors and functional requirements. Formulation of several bone remodeling theories have been developed to explain Wolff's law and the functional adaptation of bone quality. Bone remodeling theory is an adaptive feedback control process of the bone [30]. External forces on the bone are converted to an internal load which then induces stresses and strains. Within the control process, the senor will detect mechanical response and then the transducers will convert them into cellular responses resulting in the remodeling potential. This potential will then cause osteoblast and osteoclast activity that will lead to bone formation and resorption. A normal load will result in homeostatic equilibrium where there will be no change in the bone morphology. An abnormal load will result in gradual change of the bone shape and/or density. As such, the stresses and strains in the bone will change, again affecting the remodeling potential.

The process will continue until the structure of the bone has sufficiently adapted. The feedback signal will diminish and change in the shape and density will cease. Mechanical features which are collectively called the stimulus are necessary to model the adaptive process. This stimulus is used to activate the bone. Cowin supported strain as the proper stimulus as it is primary and a measurable physical quantity representing deformation [31]. He further argued that stress is a secondary measurement and must be computed indirectly. Different studies have used different defined stimulus: strain [32], strain energy [33-35], strain rate [36] and damage-based [37, 38].

In bone remodeling theory, site dependence and time dependence also be considered [30]. Different bones provide different mechanical functions and are subject different loads. The tibia is a major load-bearing bone whereas the radius is subjected only to functional loads. The tibia and radius osteoblasts and osteoclasts may have different adaptation response. Hart stated that surfaces of the same bone could be different in terms of the "remodeling equilibrium" values and speed of cell-mediated adaptive response [30]. This would change the approach of the remodeling models as now each specific site would need to be taken into account. Hypothetical bone remodeling curves were drawn, suggesting that no single curve is applicable for all bones or in all regions of single bone [39]. Currently, some degree of site dependence is assumed for most remodeling theories. In terms of time dependence, the times it takes for the bone to decrease or increase by a specific amount of density must be considered. It remains a challenge for the bone remodeling theories to predict whether a change of bone morphology will take place within weeks or months (Figure 0-14).

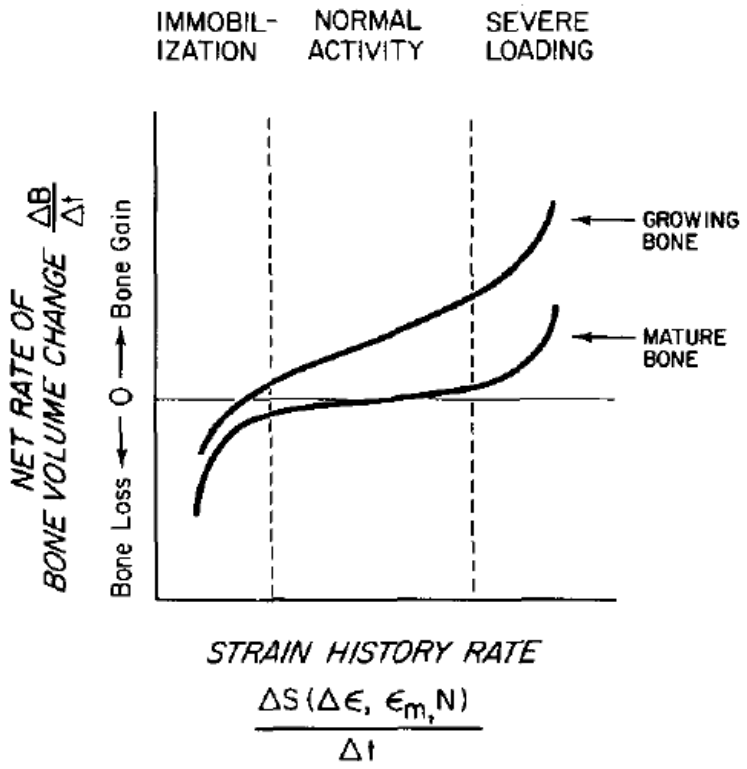

Figure 0-14: Hypothesis of relationship between bone strain history and its remodeling rate [40].

There are many established theories; two of the stain-based theories are described in detail below. These two theories are quasi-static, neglecting the effects of loading rate, viscoelasticity and inertia.

The "Theory of Adaptive Elasticity (AE)" started being developed in 1976 and describes the remodeling behavior of cortical bone where an elastic material adapts its structure to applied loading [41-45]. This phenomenological theory is based on linear elasticity theory and is also enhanced by additional constitutive equations that allows for changes in the density and external shapes of cortical bone. According to Frost (1964), there are two classes of bone remodeling, internal or external (surface) remodeling. The bone is only able to adapt its density or change in volumetric porosity for internal remodeling. The bone can deposit or resorb on the bone surface in external remodeling.

Constitutive remodeling rate equations relate the bone tissue deposition and resorption to the mechanical stimulus [46].

An internal remodeling rate equation specifics the rate of change of bone density ρ at each point “X” in the bone as a function of density at point “X,” therefore the change in bone remodeling stimulus at point “X” is defined as:

$$\frac{\partial \rho}{\delta t}(X) = f(\rho(X), change\ in\ stimulus\ at\ X)$$

$$\text{or} \qquad \frac{\partial \rho}{\delta t}(X) = A[S(X) - S_0(X)]$$

Where A is a remodeling constant, S is the actual stimulus, and S_O is the reference stimulus at homeostatic equilibrium.

The external remodeling rate equation specifies the velocity (V) of the remodeling bone surface at a surface point “X” as a function of the change in bone remodeling stimulus at the surface point “X”:

$$V(X) = f(change\ in\ stimulus\ at\ the\ surface\ X)$$

$$\text{or} \qquad V(X) = B[S(X) - S_0(X)]$$

B is another remodeling constant. The remodeling rate equations can be site specific if they depend on a specific anatomical point (X). For the AE theory, the mechanical stimulus used is a strain tensor. The AE theory can be modified to stimulate cancellous bone remodeling behavior [30], however requires higher complexity. AE theory was used in finite element modeling to study strain-induced remodeling in the long bone [32].

The AE theory neglected the influenced of strain history effect on the cortical boner remodeling rate. Additionally, there is difficulty in applying the AE theory to cancellous bone due to lack of accountability for the adaptation of the bone material. Carter and associates established another theory that focused on the "self-optimization" process of a material [34, 47-49]. Fyhrie & Carter developed a unified theory relating

change in trabecular orientation and apparent density of cancellous bone with applied stress [34]. The chosen mechanical stimulus was strain energy density with the assumption that the bone will optimize its stiffness using the least materials. Assuming the bone to be self-optimizing, the trabecular orientation will align with the principle stress directions. After alignment, the apparent density will be proportional to an "effective stress." Therefore, the bone architecture and change in bone mass can be predicted. This theory is called the Bone Maintenance Theory. A general method for defining the daily load history with the bone maintenance theory was developed [49]. The stimulus required for activation of bone response is a function of the strain energy density, apparent density and loading cycles:

$$S^* \propto \frac{1}{\rho^k} \sum_{day} n_i \, U_i^k$$

Where U is the strain energy density, i is the number of loading conditions, n is the number of loading cycles, and k is a constant. Assuming that the stimulus is constant everywhere, the bone apparent density can be approximated as:

$$\rho \propto \left[\sum n_i \, U_i^k \right]^{1/k}$$

The “load history bone maintenance” theory was expanded into a time-dependent remodeling theory for internal and external remodeling. It was developed to be suitable for both cortical and cancellous bone as it accounts for the bone surface area available for osteoblastic and osteoclastic activities [39, 50].

Bone Diseases or Medical Need

Diseases such as arthritis or osteoporosis cause damage to the joints. An estimated 20% of adults have reported some form of arthritis, which increases to almost 50% with adults 65 years or older [51]. By 2030, it is estimated that 67 million

Americans age 18 years and older will be diagnosed with arthritis [52]. Arthritis in the hip or knee results in worn cartilage and decreased joint space (Figure 0-15). This increases the need for medical treatments and surgical procedures to aid and prevent the effects of these diseases.

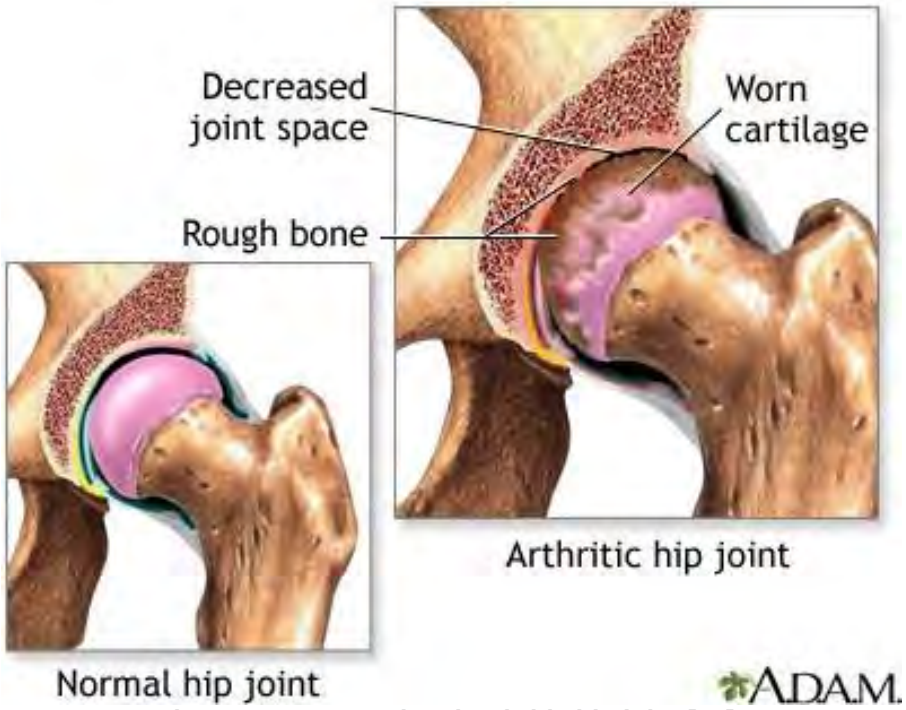

Figure 0-15: Normal and arthritic hip joint [53].

Osteoarthritis results in the ends of the bone rubbing together. This can progress into swollen and inflamed membranes (Figure 0-16).

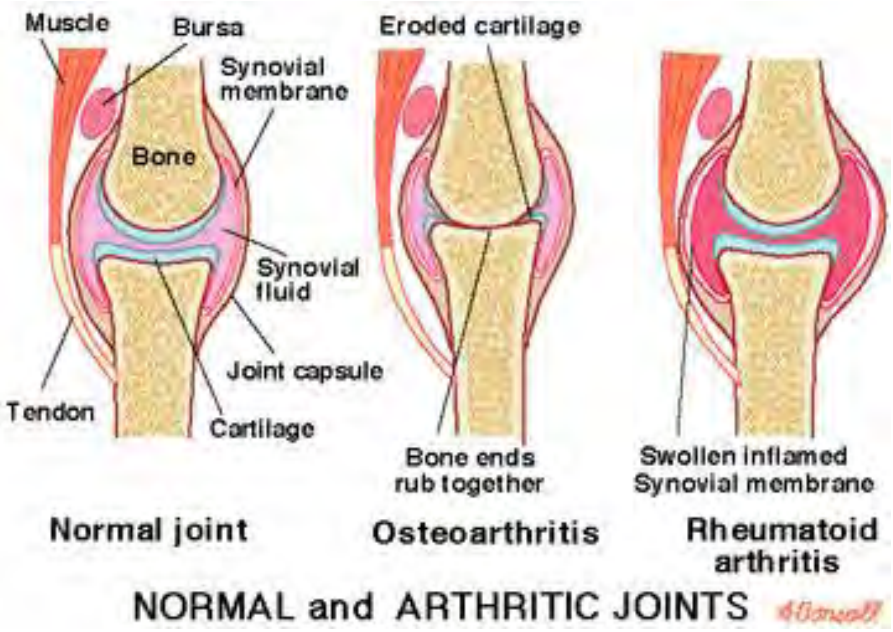

Figure 0-16: The knee joint with normal, osteoarthritis and rheumatoid arthritis [54].

Brief History and Development of Total Joint Replacement

In London in 1822, Anthony White performed the first excision joint arthroplasty. The first surgical principles and techniques for bone fracture treatment were developed in the 18th and 19th century. In 1826, John Rhea Bartonii performed the first osteotomy, where a bone is cut to shorten, lengthen or change its alignment [55]. During this time, artificial joint appeared, however were unsuccessful in most cases mostly due to septic complications. Professor Themistocles Glück implanted the first artificial knee in 1890 [56]. He also implanted the first artificial hip implant in 1891. He is credited for introducing the term arthroplasty in 1902. Glück was also a pioneer in proposing the idea of biocompatibility [56].

In 1925, a surgeon in Boston molded a piece of glass into the shape of a hollow hemisphere which could fit over the ball of the hip joint and provide a new smooth surface for movement [57]. In 1936, a dramatic improvement was made when scientists

manufactured a cobalt-chromium alloy. This cobalt-chromium alloy was both strong and resistant to corrosion and is still used today. In the 1950s, Frederick R. Thompson and Austin T. Moore separately developed replacements for the entire ball of the hip. In 1958 John Charnley introduced the idea replacing the eroded arthritic socket with a Teflon component. When this failed, Charnley used a cemented polyethylene cup to reconstruct the socket. By 1961, he was performing surgery regularly with successful results. Charnley was interested in animal studies and applied these findings to the design of hip replacement. An acrylic implant designed by the brothers Robert and Jean Judet currently holds the world record for implant in vivo durability with 51 years [58].

Some of the early work for knee replacement began by implanting metal spacers between the bones of the knees. In the 1950s, McKeever and McIntosh attempted this procedure but the results were unpredictable. Artificial knees were being developed during the same time period. The reason for inferior results may have been attributed inadequate surgical technique. In 1957, Walldius published his comparison of hinge knee endoprosthesis and resection arthroplasty. During the late 1960s, Frank Gunston developed a metal-on-plastic knee replacement to be secured with cement to the bone. It was not until the mid-1980s that contemporary principles of mechanical axis balance and the importance of joint stability was developed.

In 1974, Insall introduced the first successful total condylar knee replacement. The prosthesis was made of three components for resurfacing all three surfaces of the knee (femur, tibia and patella). Each was fixed with bone cement and the results were promising. The history and development of porous-coated implants is explained in detail in another section.

Bone Biology of Bone Ingrowth in Implants - Healing Process

Peri-implant healing begins when the surgeon prepares the bone to accept the metal implant. Surgical preparation of the bone is important for implant healing because it allows for initial implant stability and causes bleeding leading to formation of a hematoma.

Primary implant stability is a requirement for successful peri-implant healing [59]. It is based on having limited micromotion and a limited gap at the bone-implant interface. Limited micromotion or movement at bone-implant interface is important for a stable implant which allows for successful ingrowth around the implant [60]. Previous studies have shown micromotion ranging 20–50 μm results in bone formation [61-63]. A study by Pillar et al suggests that micromotion greater than 150 μm would lead to fibrous tissue attachment to the implant surface instead of bone [63]. There is a trade-off between stability and contact between the bone and implant [60]. Poor bone formation has been shown when the implant is in too close contact with the adjacent bone [64]. However, gaps less than 500 μm have been shown to improve the quality and rate of bone formation and bone has reduced ability to bridge gaps of greater than 2000 μm [60, 64-66]. Blood is the first tissue that the implant will have contact with when introduced into the bone. The contact with blood result in a series of biological processes: protein deposition, coagulation, inflammation and tissue formation. There is a host response that shows the response that is similar to an infection or an introduction of a foreign material. The implant surface chemistry and topography influence the host body response [67]. Only seconds after blood contacts the implant surface a monolayer of protein is present. The protein layer composition is largely determined by the surface properties of the implant. The type of the proteins adsorbed on the implant surface may determine the response from the host to the material. Fibronectin and vitronectin

contain RGD sequences and may interact with mesenchymal cells through their cell surface integrins [68].

The next step in the healing process is coagulation and platelet activation. Platelets are the first cells to contact the surface of the implant. They have been shown on the implant surface within 5 seconds after contact with blood [67]. The activation of the platelets results in a number of important intracellular processes ([67], Figure 0-17).

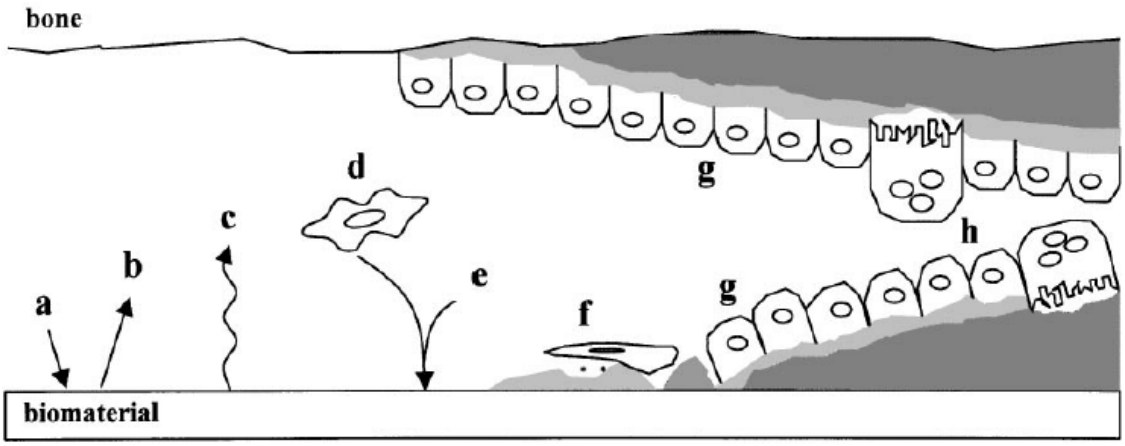

Figure 0-17: A representation of the bone-implant interface events. (a) Protein adsorption from blood and tissue fluids, (b) protein desorption, (c) surface changes and material release, (d) inflammatory and connective tissue cells approach the implant, (e) possible targets release of matrix proteins, (f) adhesion of osteogenic cells, (g) bone deposition on the exposed bone and implant surface, (h) remodeling of newly formed bone [67].

The implant topography can affect the degree of platelet activation. Platelet activation causes a significant change in the shape of the cell. This change is important for coagulation as it allows for the expression of factors tenase and prothrombinase with the cell membrane. Platelets contain membrane-bound adhesion receptors on their surface. Activation of the platelet causes conformational change in the receptor that allow it to bind with the adsorbed proteins on the implant [69]. Once there is activation of multiple platelets, they will aggregate and then form a clot. The formation of a stable clot proves both the biochemical and mechanical components required for osteoconduction. Many

signaling molecules are found within this clot: cytokines, chemoattractants, mitogens and growth factors [70]. The clot acts a biodegradable depot for the previously mentioned chemicals. Activation has been shown to be more influenced by the presence of microtopographical features on the implant surface than by the calcium phosphate. Activation of platelets at the implant surface leads to a natural gradient for the signals molecules. This results in a high concentration near the implant surface and low concentration near the where the host bone was cut. The fibrin clot is essential for mediating osteoconduction and inflammation [71].

The inflammatory response occurs concurrently and also interacts with the coagulation and platelet activation [72]. During the inflammatory response, the important leukocytes are the neutrophils and monocytes. The peak levels of the neutrophils occur in the initial 24 to 48 hours. The monocytes however, rapidly transform into macrophages, becoming the dominant leukocytes after 48 hours [70]. Cytokines released by the platelets cause activation of leukocytes traveling within the capillaries surrounding the implant [73].

Inflammatory cytokines are the first signaling molecules to be expressed and may also be required to initiate bone formation. Beyond the recruitment of the leukocytes, the role of these cytokines in bone formation remains unclear. One study results have suggested that TNF-α may be required for proper mesenchymal cell recruitment and/or differentiation in osteogenic cells [74]. Within 24 hours of injury, members of the tissue growth factor beta (TGF-β) superfamily are expressed [75]. Members of this superfamily include bone morphogenetic proteins (BMPs and growth and differentiation factors (GDFs). These two factors have been shown to promote bone formation at a fracture site. Osteoinductive factors are factors that drive differentiation of osteogenic cells from mesenchymal cells. These factors have shown improved bone formation during peri-implant healing using in vivo animal models [76-79].

Angiogenesis is essential as metabolically active osteogenic cells require a blood supply. Angiogenic factors are released with the degradation of the extracellular matrix. One factor stored in the extracellular matrix is the vascular endothelial growth factor (VEGF) [80]. Within pre-existing capillaries VEGF stimulated endothelial cells, loosening their gap junction to undergo cell division and migrating to form new vessels. VEGF receptors may also modulate osteoblast function as they have been found on osteoblasts [81]. The interaction of the signaling molecules within the peri-implant space results in the recruitment, migration and differentiation of the mesenchymal cells. This involves both osteoinduction and osteoconduction in which the osteogenic cells will participate in the formation of woven bone.

Mesenchymal cells are recruited from the marrow, pericytes and the cambium layer of the periosteum [74]. The mesenchymal cells migrate towards the implant through the preliminary matrix of the fibrin clot. As the mesenchymal cells move, numerous factors released by platelets and leukocytes cause the cells to differentiate into the osteoblastic lineage [82]. Through a porcine models, it has been shown with 24 hours post-implantation, the osteoprogenitor cells colonize the implant surface and being secreting the matrix [83]. This matrix then forms the afibrillar interfacial zone whose thickness varies from 0.2 to 0.5 μm [67]. Davies et al first described this interfacial zone to be analogous to the cement lines that lines the osteons in the lamellar bone [84, 85].The afibrillar interfacial zone forms a non-collagenous, calcified layer on the implant surface. Beyond the afibrillar zone is a collagenous compartment than becomes mineralized after the afibrillar zone [67]. Fully differentiated osteoblasts form the collagen compartment. Osteoblasts move away from the advancing mineralization front, however sometimes they become enveloped and become osteocytes within a bone lacuna. This processes results in immature woven being formed. It proceeds in an appositional fashion from the implant's surfaces to the edges of the cut bone. This

process is known as 'contact osteogenesis' [71]. Bone formation may also occur from the cut bone surface toward the implant. This bone formation is termed 'distance osteogenesis' [71]. During implantation, osteocytes within the bone edges will die due to thermal necrosis. The depth of the dead bone extends 100 to 500 μm and will be reabsorbed by the osteoclasts [67, 86]. Osteoblasts migrate to the surface of the reabsorbed bone and form a non-collagenous cement line similar to that on the surface of the implant [87]. Next, there is a formation of a collagen containing layer by fully differentiated osteoblasts. Fluorochrome labeling of the bone suggests that contact osteogenesis occurs at a rate approximately 30% faster than distance osteogenesis [67, 88].

Distance and contact osteogenesis result in immature woven bone formation around the implant. Within the host bone, this will provide secondary stabilization of the implant. There is a changeover from the primary stabilization that results from a friction fit of the implant to the secondary stabilization. Secondary stabilization results from the formation of the woven bone around the implant [89]. Secondary stability of the implant may result from bone bonding, if the surface of the implant allows for contact osteogenesis. The implants surface topography is complex due to its pores and undercuts, the cement line may interdigitate with the implant surface and bone bonding can occur. [71].

Cementless implant success is dependent on the speed of early peri-implant healing interface and mechanical strength at the bone-implant interface. Surface modifications of the implant may enhance healing and mechanical strength. Improving the surface of the implant is commonly done by: (1) sintering of fibers or metallic beads over the implant surface and (2) plasma spray deposition of ceramics of metal onto the implant surface. Sintered porous-coated implant involves heating which can alter the mechanical properties of the implant. There is evidence that an implant surface becomes

rougher and more complex after implantation. One study of a smooth hydroxyapatite-coated implants had a breakdown at the material grain boundaries and rough surface after implantation in a rat tibia [90]. In addition to the surface characteristics, pore size of the porous-coating is also important for ingrowth surfaces. Studies have shown optimal pore size to be in a range between 50-400 μm [91], and is often preferred to be greater than 100 μm [92].

Remodeling of the bone continues throughout the healing process and continuously in all bones in the body. There is a defined sequence of events for bone remodeling. First there is activation of the osteoclast cutting cones. Then the bone is removed by osteoclasts. Then angiogenesis brings the pericytes where they differentiate into osteoblasts. Finally, the osteoblast form new bone [93]. Remodeling first occurs with the host bone and then within the woven bone formed in the peri-implant gap.

During implantation there is significant damage to the bone. There is microdamage that occurs beyond the site of implantation by 1 to 2 mm [93]. There is an enhanced remodeling within the host bone surrounding the bone that may occur for the next six months [93]. The desired end result is to have lamellar bone around the implant. Woven bone will form rapidly and consists of loosely packed collagen fibers of varying size and random spatial alignment. In contrast, the collagen fibers of lamellar bone are organized in thicker bundles and oriented in the plane of the lamella. The bone in contact with the implant surface will continue to remodel through the lifetime of the implant.

A previous study compared histology with the biomechanical strength of pull-out and torsion of titanium screws in a rat model over time [94]. The results showed that the strength increased with in the first four weeks and related directly to bone quality. There was also a positive correlation between torsional strength and bone contact with the implant.

Remodeling is influenced by the biomechanical stresses within the bone surrounding the implant. In the 19th century, Wolff observed bone adapting to a mechanical load [29]. The law states that bone mass will increase or decrease as the forces acting on the bone increase or decrease. The osteocytes direct the bone modeling and remodeling processes. The osteoclastic and osteoblastic activity is balanced in healthy bone that is subjected to normal loading from everyday activities. When the bone is loaded for a period of time, balance will be load and osteoclastic activity will dominate [95]. This can result in a lower amount bone. In terms of the implant, if the implant has a higher stiffness than the bone, stress-shielding can occur. Stress-shielding is when the bone with lower is stressed less resulting in bone resorption [96].

Total Joint Replacement

Total hip replacement (THA) and total knee replacement (TKA) have been successfully employed for the treatment of end stage arthritis, rheumatoid arthritis and fracture. Total joint replacement is a surgical procedure in which parts of the human joint are replaced by metal, plastic or ceramic components (Figure 0-18).

Figure 0-18: The knee before and after total knee replacement [97].

Fixation Types

There are two main types of fixation for total joint replacement (Figure 0-19). The first type uses cement to provide a mechanical attachment of the prosthesis to the bone. The second type, cementless, relies on a biological attachment of the prosthesis onto bone through osseointegration.

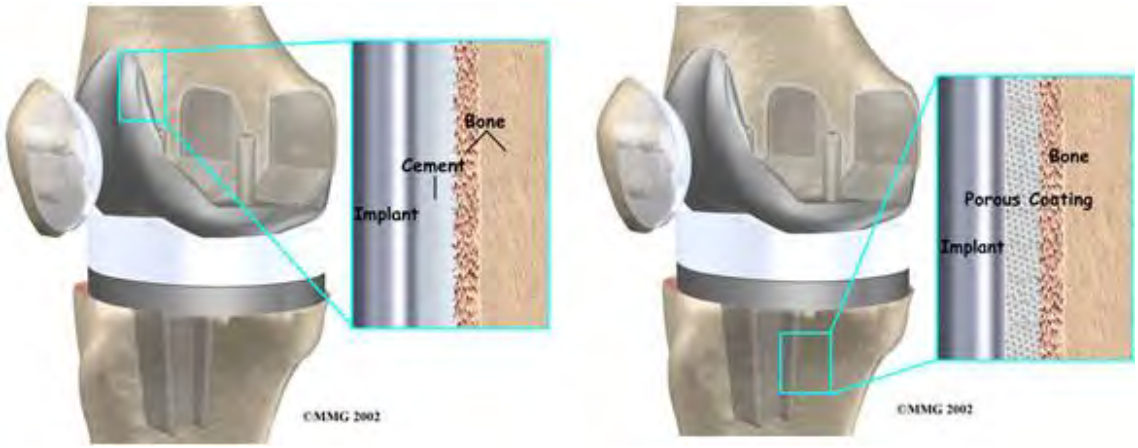

Figure 0-19: Representative image of cemented and cementless fixation [91].

In the 1960s cemented fixation was pioneered by Sir John Charnley. The cemented fixation used a self-curing polymeric material known as polymethylmethacrylate (PMMA). PMMA is formed when a powder component and liquid containing a monomer methacrylate component are combined. The reaction produces a dough-like substance that is then placed in the bone bed. The bone cement then penetrates into the pores of cancellous bone when the implant is pressed into it. Within a short period of time, the bone cement hardens creating intimate interlock with the bone trabecula and with the surface of the implant. Cement fixation works best in compression and cannot sustain much tensile load on the interfaces. The advantage of cement fixation is that it does not require accurate bone preparation and can filling larger cavities in osteoporotic bone. The strength at the bone-cement interface depends greatly on the bone quality and depth of cement penetration surrounding the implant [98]. The strength of the cement layer also relies of the cement porosity which is a result of air being trapped during the mixing process and transfer from the mixing container. The higher the cement porosity, the lower the strength of the cement layer would result. The success of cemented fixation is dependent of the surgical technique, choice of cement and implant design.

For cementless fixation, implants rely of fixation surface having a interacting mechanically with the surrounding bone to provide initial fixation. The first important technique is press-fit between the implant and bone where the implant is hammered in the under-reamed bone. During the surgery the surgeon will cut the bone to fit the implant as closely as possible (Figure 0-20). The initial stability of an implant depends primarily on the tight fit between the implant and bone. The next important step is biological fixation at the bone-implant interface. The implant with a porous-coated surface provides initial fixation through frictional interlock. However, further bone formation into or onto the implant surface is necessary for secondary fixation. In the

early post-surgery period, the fixation is vulnerable and depends on bone growth that starts within a few weeks post implantation.

Figure 0-20: Total knee replacement cutting of bone surface during the surgery [99].

Despite the success of these procedures, there were an estimated 45,000 total hip revisions and 60,000 total knee revisions performed in the United States in 2009 [100].

Reason for Revision

There are several different reasons for revision including infection, instability, dislocation, loosening and pain [101]. Pain can sometimes be linked to other reasons for revision.

Joint replacement infections may occur in the wound or deep around the implants. The lack of blood supply around the implant makes it easier for

microorganisms to attach to the device and infect the surrounding tissues. The surface of the implant are ideal for organisms to adhere, multiply and create a film that acts like a biological shield that protects them from antibiotics. An infection may occur in the wound or deep around the prosthesis and can occur right after the surgery or years later. In 2010, the rate of infection for knee replacement was less than 1%. Due to an infection, the implant may lose its attachment to bone. Even if the implant remains fixed to the bone, pain, swelling and drainage from the infection may make revision surgery necessary. Early infection may occur within 3 months of surgery. Late infections occur more than a year after surgery and are believed to be acquired from another location in the body.

Instability can be due to several reasons: looseness of the joint, inadequate flexion and improper position or alignment. Instability occurs when soft-tissue around the joint is unable to provide stability for adequate function. Dislocation is an acute form instability in which a sudden movement or migration of the implant from its normal position. An example in the hip would be if the femoral head dislocates fully out of the acetabular shell liner. Dislocation is more common in the hip than the knee. In the knee, if the ligaments around the knee become damaged or improperly balance, the knee may become unstable. The risk of dislocation is usually highest during the first months after surgery as the tissues are healing.

Loosening of the implant occurs from weakening of the bond on the bone-cement or bone-implant interface. Patient related factors, such as age, activity level, surgical history and weight can also contribute to implant failure. During the initial surgery, it was either cemented into position or bone was expected to grow into the surface of the implant. In either case, the implant was firmly fixed. Over time, however, an implant may loosen from the underlying bone, causing the knee to become painful.

Hip registries and national samples are used to determine the main reasons for revision after total hip arthroplasty. A recent Nationwide Inpatient Sample (NIS) study that reviewed 51,345 revision THA procedures in the United States showed that the most common reasons for revision were instability/dislocation (22.5%), mechanical loosening (19.7%) and infection (14.8%) [100]. The 2014 Australian Registry showed that the most common reasons for revision of primary total conventional hip replacement are loosening/lysis (28.4%), implant dislocation (25.0%), fracture (17.5%) and infection (17.1%). However, this included cemented and cementless fixation method and all implantation times. For primary total conventional hip replacement with average implantation of 1.5 years, the main reasons for revision were instability (35.0%), infection (22.2%), loosening/lysis (22.2%) and fracture (19.7%). The Swedish Registry showed that the most common reasons for revision after two year follow-up were infection (58.4%) and dislocation (18.3%). Loosening as a reason for revision accounted for 2% of the revisions.

In the knee, infection (25.2%), loosening (16.1%) and implant failure/breakage (9.7%) were the most common reasons for revision in an NIS study that reviewed 60,355 revision procedures [102]. The Australian Registry reported that the most common reason for revision for combined cemented and cementless fixation for TKA was loosening/lysis (29.1%), infection (22.2%), patellofemoral pain (12.1%), pain (9.2%) and instability (6.1%) [103]. The Swedish registry showed that the most common reason for revision for combined cemented and cementless fixation from primary surgery TKA was infection (25.9%), loosening (25.8%) and instability (13.1%) over a ten-year reporting period [104].

History of Porous Coatings

The first patent with the concept of biological fixation was issued before 1910 by Greenfield for an artificial tooth root [105]. However, it was be another 60 years until the concept of bone ingrowth for implant/prosthetic ingrowth reemerged. In the late 1940s, investigations of porous materials as soft tissue substitute materials. The design specification included inertness, resiliency, softness and strength for porous implants in soft tissue [106]. During the 1950s, polyvinyl [106, 107] and polyethylene [108] sponges were initially used for implants for soft tissue were now studied for the reconstruction of bone [109-111]. The first resorbable porous bone cement, Ostamer, was a polyurethane foam and was developed for osteosynthesis [112]. Later investigations focused on the effect of pore size through a polyurethane foam with pore sizes ranging from 280 μm to 3.2 mm [113, 114] and Teflon with smaller pore size range from 5 – 50 μm [115]. In 1963, Cerosium, a porous ceramic-plastic composite, was investigated. This was one of the first porous materials that could be considered for load-bearing orthopaedic applications. Smith was the first to propose a porous material and also that porous material would be biocompatible with bone.[116].

In the 1969, the first reported porous metal was fabricated using powder metallurgy techniques to create a porous cobalt-chromium alloy [117]. They noted the potential advantages in porous metals: (1) promotion of biologic fixation; (2) lower modulus of elasticity and higher damping capacity, closer to natural bone; (3) reduced weight; (4) customizable for specific medical applications. Two years later a group investigated from cobalt-chromium alloy to titanium because of titanium lower modulus of elasticity and density [118]. In 1969, porous stainless steel was used as an implant in bone and bone ingrowth was shown deep into the porous material [119]. However, later investigations showed that porous stainless steel underwent excessive corrosion.

In 1970, Hulbert et al. showed that substantial bone tissue ingrowth was possible with pore sizes that were greater than 100 μm. Furthermore, when the pore sizes were increased to 150 μm and greater, osteon formation was observed [120].

One group suggested that the porous metallic material fabricated by powder metallurgy techniques exhibit poor strength properties when the porosity is large enough for bone ingrowth [121]. Many groups investigated fiber metal composites due to their ability to combine strength with porosity. The specific fiber-metal composite developed by Rostoker and Galante have been studied since 1969 [122-124] and is clinically used in hip [125] and knee implants [126, 127] and segmental replacement of bone [53, 128, 129]. Fiber metal specimens in rabbits showed dense bone ingrowth at 6 weeks and 3 months after implantation [122] (Figure 0-21).

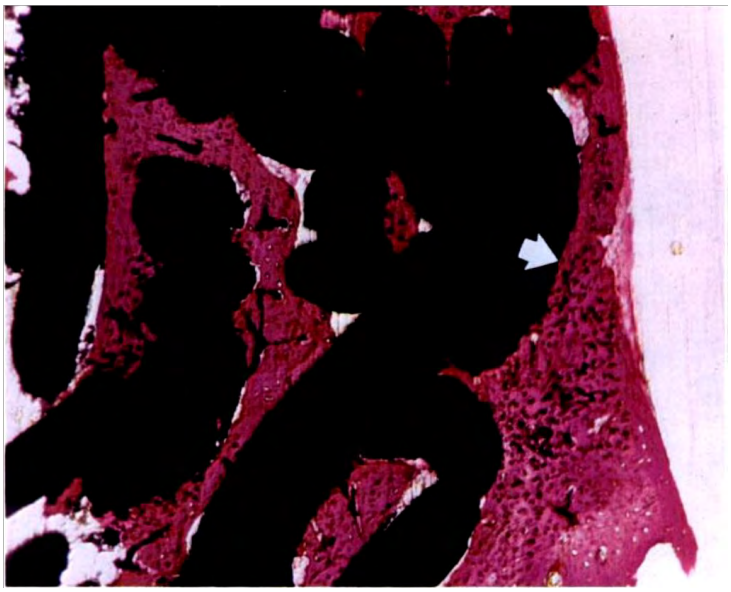

Figure 0-21: Fiber metal implants in rabbits with deep bone ingrowth obtained at 6 weeks and 3 months after implantation [122].

In the early 1970s, a group investigated porous cobalt-chromium because of its inertness and durability. Using mechanical push-out tests placed in cortical bone of

dogs, they were able to show that the small and large pore size materials were efficacious [130] (Figure 0-22).

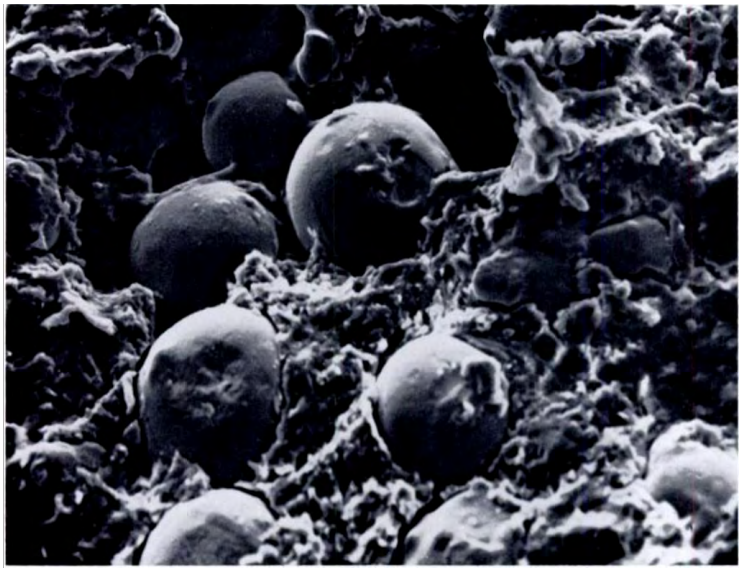

Figure 0-22: Scanning electron micrograph of a porous-coated Vitallium implant showing tissue ingrowth penetrating in the surface coating [130].

This initial research by Pilliar and Cameron [66, 131, 132], which was further developed by Bobyn and others, was the basis for the porous cobalt-chromium alloy coatings that are currently in use [91, 133, 134].

In the early 1970s, Teflon was used as the matrix for the porous material called Proplast, based on the postulate that the porous interface material may approximate those of granulation and fibrous tissue [135]. This new design was employed in hemiarthroplasties [136] and later in total hip replacement femoral stems [137, 138]. However, the polymer coating led to high loosening rates and was abandoned in the 1990s [139].

In the late 1960s investigation of porous ceramic materials began [140, 141]. One study showed that a minimum of 100 um for interconnection size was needed for mineralized bone growth [141]. The authors also noted that interconnected pore size as small as 40 um could have the potential for mineralized bone growth. A potential

difficulty was that the calcium aluminate implants undergo a hydration reaction that hindered mineralization of osteoid tissue. In 1973, Cameron et al. showed that if excessive initial movement occurs at the bone-implant interface, bone formation or ingrowth is inhibited [59], first image. In 1981, Pilliar et al. showed fibrous connective tissue can occur with excessive motion [142]. In the extreme cases, a fibrous encapsulation of the implant can occur with the surrounding tissue appearing much the same as that around a conventional smooth-surfaced implant.

Porous titanium (sintered microspheres) was used to fabricate an artificial tooth roots in 1979 [143]. Porous polymer was studied due to its ability to be carved in the operating room to customize implants [144, 145]. These studies led the way for investigation of porous polysulfone, which is a higher strength thermoplastic [146]. In 1980, Bobyn et al. showed that the optimum size for rapid ingrowth is between 50 to 400 μm [91] (Figure 0-23).

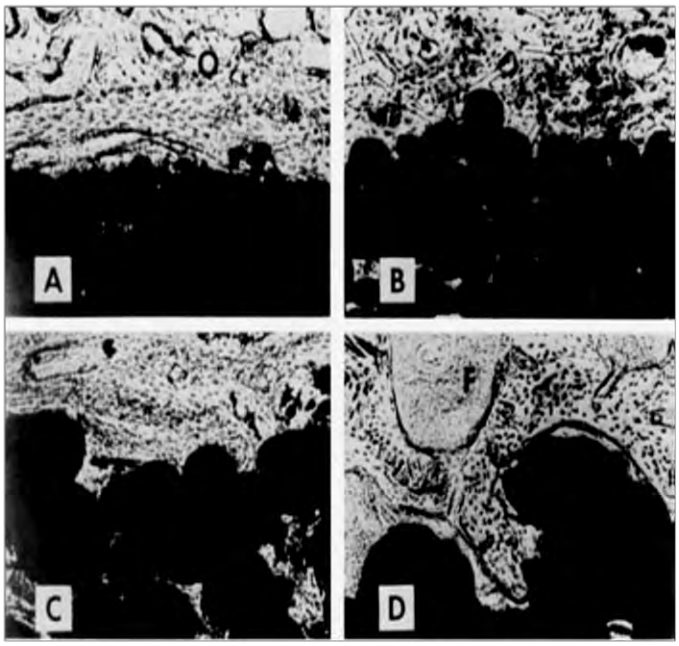

Figure 0-23: Histologic photomicrographs the bone-implant interfaces of porous systems with: A) 20-50 μm pores, B) 50-200 μm pores C) 200-400 μm pores and D) 400-800 μm pores at 12 weeks.

‘‘Osseointegration’’ is described by Albrektsson et al. in 1981 as the attachment of lamellar bone to implants without intervening fibrous tissue based on human retrieval studies [147] (Figure 0-24).

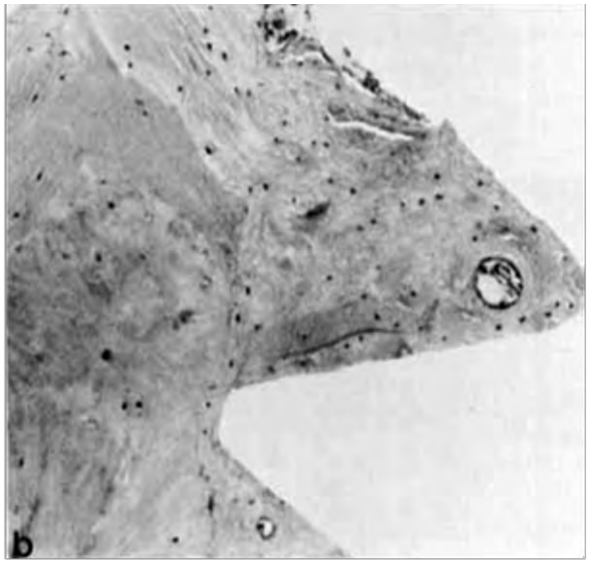

Figure 0-24: Histological section showing the bone tissue well remodeled to the screw thread pattern.

In North America in the mid 1980s cementless acetabular fixation in THA became a predominant method due to concern regarding long-term durability of bone cement and continued evolution of porous coated acetabular shells [148]. In the late 1990s, the first Highly Porous Metals were approved by the FDA [149, 150]. Throughout the 2000s, several manufacturers developed High Porous Metals.

Advancements in Cementless Technologies

While clinical outcomes of the initial cementless technologies (i.e. sintered beads, fiber metal, hydroxyapatite coatings and plasma sprays) have been successful, aseptic loosening remains a leading cause of revision [100, 102]. Highly porous metals

(HPMs) have high volumetric porosity, low modulus of elasticity and high frictional characteristics [151, 152]. These properties are believed to promote initial stability and foster osseous ingrowth. Over the last decade several orthopaedic manufacturers have introduced highly porous metals in total joint arthroplasty [153].

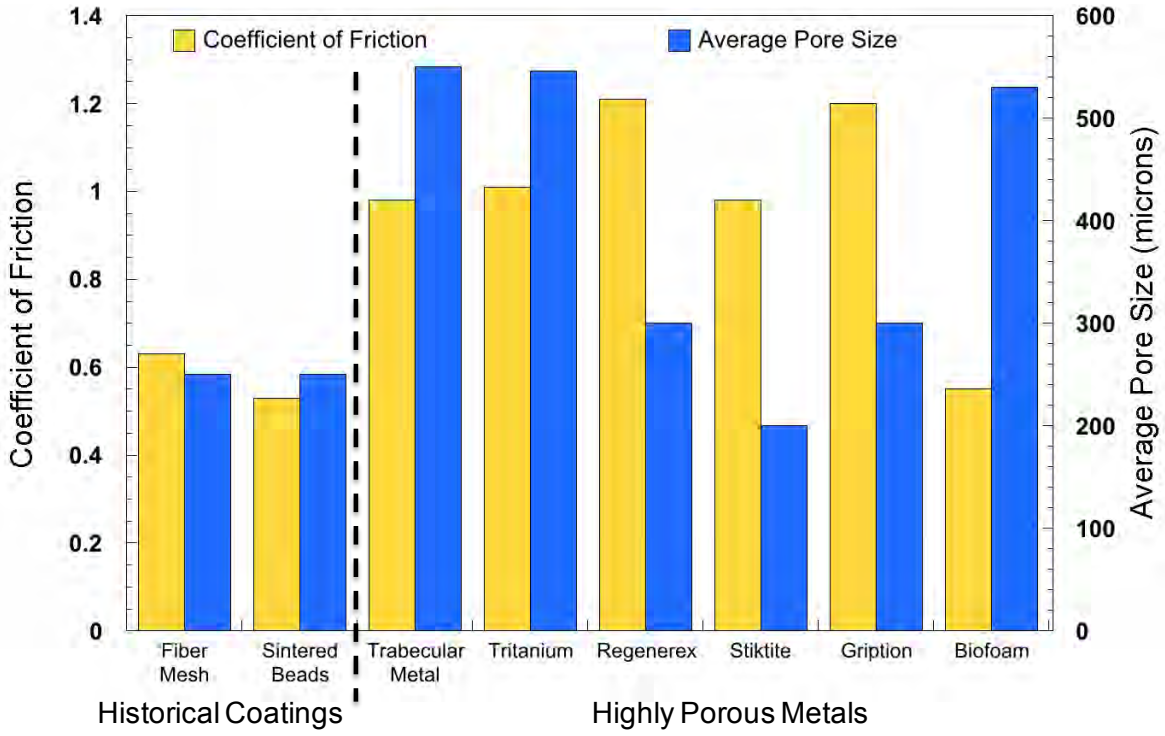

Figure 0-25: Material properties of historical coatings and highly porous metals. Notes: There are two distinct manufacturing processes used for the porous metal component of products marketed as Tritanium® [154].

Porous tantalum (Trabecular Metal™; Zimmer Inc, Warsaw, Indiana) was the first HPM cleared by the FDA in 1997. Other HPMs were cleared between 2006 and 2009, therefore clinical and retrieval studies of other HPMs have been limited. Studies of these HPMs have focused on animal studies and initial short-term clinical studies [155-159]. Each of these HPMs has varying elastic modulus, pore size and coefficient of friction [153].

The newer HPMs include Tritanium®, StikTite™, Gription™, Regenerex®, and Biofoam®. A canine study of Tritanium® has shown significantly higher bone ingrowth, into canine femurs after 12 weeks, than CoCr beaded surfaces [155]. A 36-month follow-up clinical study of 288 Tritanium® acetabular shells showed no revisions for acetabular loosening [156]. Early unpublished reports of StikTite™ have shown an improved coefficient of friction and implant stability at a 9-month follow-up [152]. A clinical study of StikTite™ coated shells reported reduced subsidence measured by RSA compared to a sintered bead coating [157]. Additionally, a clinical study of acetabular shells showed similar results between StikTite™ (Smith and Nephew, TN, USA) and a sintered bead porous surface (Roughcast, Smith and Nephew, TN, USA) for 62 patients with a 2 year follow-up [160]. One clinical study evaluated the 3 year outcomes for the Tri-Lock® femoral stem using the Gription™ porous coating. The 27.3 month mean average follow-up for 101 patients has shown no early complication or loosening [161]. One of the first clinical studies using Regenerex® revision shells showed 28 patients with no reported loosening cases after 25 month average follow-up [162]. Biofoam® when compared to sintered Ti beaded implants through canine femoral implants showed a higher bone ingrowth at 12 weeks [159]. Biofoam® wedge has been used in lateral column lengthening. The results for 26 patients after 14.6 month mean follow-up, showed low nonunion rates and improve radiographic correction [163].

Porous tantalum coatings are designed with several distinct features: increased volume available for tissue in-growth due to high porosity (75-85%) [151, 152, 164], comparable elastic modulus to trabecular bone (2.5–3.9 MPa) to reduce stress shielding and favorable frictional characteristics ($\mu = 0.88$) to reduce micromotion [153]. The high porosity of the porous tantalum can be seen through a Scanning electron microscopy (SEM) image [165] (Figure 0-26).

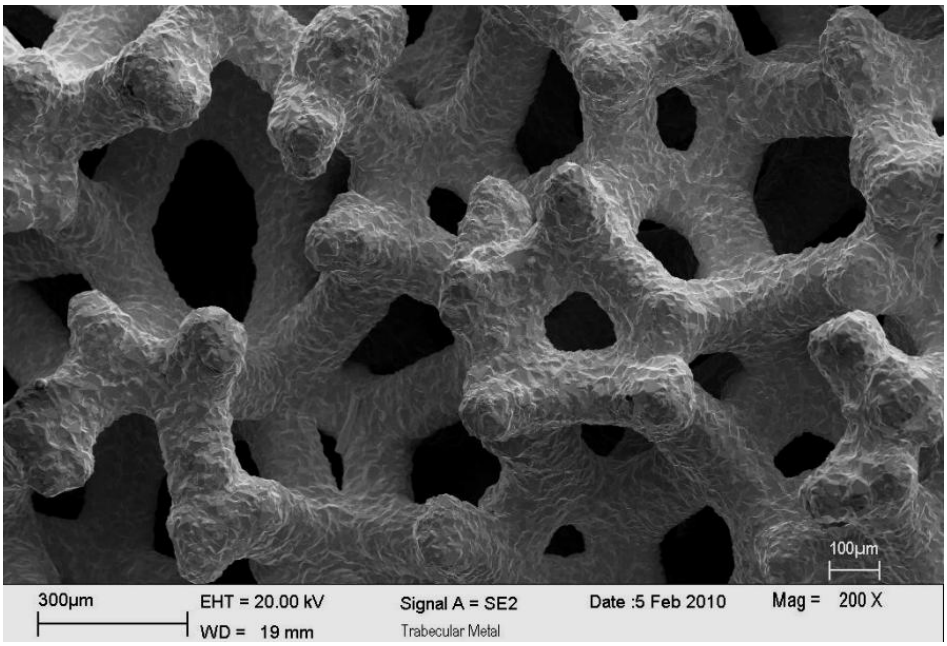

Figure 0-26: Scanning Electron Microscopy (SEM) of porous tantalum [165].

Animal studies using porous tantalum implants have shown bone ingrowth of: 40 – 50% bone ingrowth (dogs, femur implants, 4 weeks implantation time [164]), 8.3% (pigs, intervertebral lumbar arthrodeses, 3 months implantation time [166]) and 35.1% (goats, spinal fusion implants, 6 weeks implantation time [167]).

Several clinical studies of porous tantalum acetabular shells have reported no cases of acetabular loosening [168-170]. In a recent study using the Swedish registry with a 3.3 year follow-up, the risk of reoperation or revision was not significantly different between the TM cup, a press-fit porous-coated cup (Trilogy) and cemented all-polyethylene cup [171]. One clinical study of 45 patients with porous tantalum acetabular shells with minimum of 10 year follow-up have show zero cases of acetabular loosening [172]. A clinical study with mean 3.5 year follow-up of 613 primary total hip arthroplasties showed no revisions due to aseptic loosening of the acetabular shell [168]. Another study with an average of 6.1 years follow-up of 263 porous tantalum acetabular shells had no cases of acetabular loosening [170]. Despite the number of clinical studies

on porous tantalum acetabular shells [168-171, 173], there have been limited retrieval studies of porous tantalum acetabular shells and femoral stems [174].

The porous tantalum patellar implant clinical studies results have been mixed, some with limited cases of loosening, while others having lower survivorship. One case study showed survival of a porous tantalum patellar implant for 8 years [175]. Another study with an average follow-up of 7.7 years showed 83% survivorship (19/23 implants) [176]. A clinical study of 90 porous tantalum patellas with an average follow-up of 4.5 years showed no cases of patellar loosening [177]. Ten porous tantalum augment patellar implants with at least 18 months follow-up. One patient developed loosening, however this patient had previously undergone patellectomy [178].

Several clinical studies and one registry study of the porous tantalum tibial tray have shown no cases of tibial loosening [177, 179-181]. In a recent study using the Finnish registry with seven year follow up there were no reported revisions due to aseptic loosening in 1143 patients with a monoblock porous tantalum tibial tray [181]. Studies of porous tantalum tibial trays have shown stabilization of components at 2 and 5-year follow-ups despite initial migration [177, 179, 180]. However, a recent study presented subsidence as a major concern for porous tantalum tibial trays, in which the failures correlated to specific patient factors (tall, heavy, male) [182]. There has been one case study of a porous tantalum tibial tray, which showed preferential bone ingrowth in the peg region [183]. No study has compared the bone ingrowth performance between modular and monoblock porous tantalum tibial trays.

Although clinical studies of porous tantalum implants have been generally promising with well-fixed implants and limited loosening incidents [184-191], information gleamed from retrieval analysis may yield more information about the bone-implant interface. To date, retrieval analysis of porous tantalum implants has been limited [174, 183].

Factors Affecting Bone-Implant Fixation

The factors affecting bone-implant fixation can be organized into three main categories: implant design, surgery factors and patient factors. A previous study defined an ideal bone implant material as having a biocompatible chemical composition to avoid adverse tissue reaction, high corrosion resistance, acceptable strength, resistance to wear and a modulus of elasticity similar to that of bone to minimize bone resorption around the implant [192].

An implant surface with a high coefficient of friction will enhance primary stability and reduce micromotions generated at the interface. Previous studies have shown micromotion ranging 20–50 μm results in bone formation [61-63], while micromotion exceeding 150 μm will result in fibrous tissue formation [62, 193, 194]. Small micromotions are important for adequate bone ingrowth and subsequent secondary fixation [195, 196]. In addition, bone ingrowth is also influenced by the biocompatibility and surface geometry characteristics of the implant [197].

Determination of the coefficient of friction between the bone and porous coating or substrate can be completed with mechanical testing. ASTM standard D4518-91 outlines the procedure to determine the coefficient of friction by using an inclined plane.

The coefficient of friction for porous tantalum was determined using an inclined plane apparatus based on ASTM Specification D4518-91 [198]. The substrate block (cancellous bone or porous tantalum) was secured to the inclined plated with a smaller slide block (cortical bone or porous tantalum). The substrate title angle is gradually increased and the angle and coefficient of friction are calculated. Porous tantalum has a high coefficient of friction (0.88) compared to historical porous-coated implants (0.5-0.66). This may be due to the spicules on the surface of the porous tantalum that can snag the rough bone.

Surface geometry characteristics that may affect bone ingrowth are pore size, porosity and pore interconnectivity. There is still debate about the optimum pore size [199]. Bobyn et al. showed that 50 – 400 μm as the desired range [91]. Implants having coatings with porosities of 50% have show good survival rates [200]. Implants with porosity of 75-80% have shown substantial increase in fixation strength [164]. There is an upper limit to allowed porosity as too much porosity can reduce the mechanical strength of the implant surface [199]. For pore interconnectivity, the number of interconnections may be a more important factor than the size of the interconnections [201]. Bone ingrowth into a porous substrate will increase the bone-implant interface strength. However, bone ingrowth beyond a certain depth does not additionally enhance the bone-implant interface strength in porous substrates [202] or cement-bone interfaces [203].

The bone-implant fixation progression starts from the day of surgery continuing to the stage of bone remodeling (greater than 6 months). During surgery a congruent surface enhances initial implant stability, while the bleeding surface provides vascular access. The initial implant is attained by achieving a congruent fit (“fit and fill”) between the implant and bone while minimizing micromotion [65, 158]. The initial implant-bone gap is preferably less than 500 μm [64, 66]. Gaps larger than 2.0 mm have shown reduced ability for the bone to bridge the gap [65].

The potential for bone ingrowth depends upon the success of the primary stability at the bone-implant interface. The primary stability is achieved by press-fit implantation and depends on friction at the bone-implant interface, surgical technique, implant size, implant shape, implant material properties, surface roughness and the patient bone quality [193, 204].

After primary implant stability is achieved, bone ingrowth will continue. Implant properties, patient activity and patient bone quality can play a role in long-term bone remodeling.

Retrieval Analysis

Implant retrieval analysis is a technique that can be used to determine how the device functions, as it provides unique information related to in vivo device mechanics, kinematics, and material performance. The FDA has developed a National Medical Device Post market Surveillance Plan with the mission of monitoring the safety and effectiveness of the medical devices [205]. The NIH has supported implant retrieval analysis as it provides input into future implant technology and development [206]. ASTM F561-13 is the current standard for retrieval analysis of medical devices. This standard covers the recommendations for retrieval, handling and analysis of implanted medical devices and specimens that are removed from patients during revision surgery, postmortem or as part of animal studies. The protocols are divided into three main stages: Stage I is minimum non-destructive analysis, Stage II is more complete nondestructive analysis and Stage III is destructive analysis.

Retrieval analysis of porous-coated implants allows for characterization of the amount of bone ingrowth. Assessment of implanted from humans can be from retrieved implants of living patients or from post-mortem samples from deceased patients. Analysis of postmortem implants allows for investigation of well-functioned implants. However, the cost of postmortem samples and procuring the specified type of implant can limit the number analyzed in each study.

At Drexel University, the Implant Research Center focuses on retrieval analysis of medical devices. The goal of the lab is to pursue clinically and societally relevant studies related to implant performance through a collaborative research. Through the

Implant Retrieval Center, retrieved medical devices with accompanying clinical and patient information is collected and analyzed.

Finite Element Modeling

Finite element modeling has been widely used in the engineering field for the investigation and understanding of engineering problems. In Orthopaedic biomechanics, FEM has been employed to study stress/strain behavior in bone surrounding an implant [207-209], periprosthetic bone remodeling [33, 210-212] and bone-implant interface micromotion [213-215]. Clinical follow-up of at least 10-15 years is necessary for long-term results of an implant design or modified surgical technique. Potential early failure modes may begin to surface within a few years after surgery. Retrieval analysis, previously described, will provide initial information on the failure modes. FEM may be used as assessment tool for further evaluation into the effect of implant design or clinical factors on implant integration. If the FEM models can successfully simulate the response of the bone to the implant, implant design features and surgical techniques can be evaluated and studied parametrically. The response of the bone to the implant includes stress/strain response, bone mineral density and interface micromotion. The surgical techniques may include amount of bone resected, varus/valgus deformity correction, cemented/cementless, varus/valgus malalignment, etc). The implant design features include stem length/diameter, material properties, monoblock vs modular design).

The results from the retrieval analysis of porous tantalum implants may be further analyzed using finite element modeling. The knowledge gained from FEM models may be used to improve prosthesis' design or to evaluate the effect of surgical placement. The long-term survival of a cementless implant relies on the fixation strength of the biological attachment at the bone-implant interface.

This biological attachment depends on the initial stability of the fixation. Excessive bone-implant motion can inhibit the osseointegration process. Previous studies have shown micromotion ranging 20–50 μm results in bone formation [61-63]. A study by Pillar et al suggests that micromotion greater than 150 μm would lead to fibrous tissue attachment to the implant surface instead of bone [63]. However, when micromotion exceeds the 50-150 um range, fibrous tissue growth results whereby the strength may be compromised, leading to possible implant loosening [197, 216]

Existing FE models of porous tantalum implants have been limited to a two-dimensional (2D) glenoid implant ingrowth model [217], microstructural model of the porous tantalum-UHMWPE (Ultra High Molecular Weight Polyethylene) construct [218] and a femoral stem ingrowth model [210]. The 2D glenoid study focused on how the primary fixation, elastic properties and coefficient of friction affect the ingrowth process. The results of the study showed that the implant material properties which resulted in a good distribution of load reduced the peak micromotion [217]. The microstructural model of porous tantalum-UHMWPE determined that porous tantalum porosity and UHMWPE thickness were the most significant design parameters [218]. The femoral porous tantalum study focused on investigating material properties of a composite femoral stem that would produce the best ingrowth results. The porous tantalum with an inner CoCrMo core femoral stem performed slightly better with respect to the Epoch (PEEK, polyetheretherketone core) stem and considerably better with respect to a Ti-alloy stem [210].

The goal of this dissertation is to investigate the reasons for revision of porous tantalum implants and also investigate factors affecting implant fixation through retrieval analysis and FE modeling. Implant selection and design can be improved by determining the effect of various factors by which highly porous metals are integrated into the body.

Chapter 1 Effect of number of previous revisions and fixation type on reason for revision

Abstract

The first objective of this study was to determine the reasons for revision of retrieved porous tantalum implants. The second objective was to determine, within our retrieval cohort, if the proportion of implants revised for aseptic loosening was different based on surgery history (primary or revision), fixation method (cementless or cemented) and coating type (porous tantalum or historical coating). The main reasons for revision of the retrieved porous tantalum hip and knee implants were infection (n=74, 31.9%), instability (n=58, 31.9%), acetabular loosening (9.0%, n=19) and pain (n=15, 6.5%). Our results showed that porous tantalum acetabular shells from primary surgeries (n=2, 2.3%) had a lower proportion of implants revised for acetabular loosening compared to acetabular shells from revision surgeries (n=19, 25.7%, $p<0.001$). porous tantalum acetabular shells (n=1) had a lower proportion of implants revised for acetabular loosening compared to fiber metal implants (n=6, $p = 0.047$). Our results showed that porous tantalum (n=1) had a lower proportion of tibial implants revised for tibial loosening compared to cemented (NexGen®, n=10).

Introduction

Total hip replacement (THA) and total knee replacement (TKA) have been successfully employed for the treatment of end stage arthritis, rheumatoid arthritis and fracture. Despite their success, there were an estimated 45,000 total hip revisions and 60,000 total knee revisions performed in the United States in 2009 [100]. A recent Nationwide Inpatient Sample (NIS) study that reviewed 51,345 revision THA procedures in the United States showed that the most common reasons for revision were

instability/dislocation (22.5%), mechanical loosening (19.7%) and infection (14.8%) [100]. Infection (25.2%), loosening (16.1%) and implant failure/breakage (9.7%) were the most common reasons for revision in an NIS study that reviewed 60,355 revision TKA procedures [102]. Thus, implant loosening remains an important concern both in THA and TKA. In an effort to reduce loosening rates caused by long-term breakdown of the cement mantle, manufacturers introduced cementless technologies to provide for biological fixation by tissue ingrowth or ongrowth (osseointegration) at the bone-implant interface. Historically used porous coatings include cobalt-chrome-alloy sintered beads, Fiber Metal™, Cancellous-Structured Titanium™ and titanium plasma spray [153]. Even though these materials have had excellent clinical results further improvement may be possible [164].

Orthopaedic manufacturers have introduced various highly porous metals (HPMs), to address aseptic loosening of hip and knee components [153]. Porous tantalum coatings are designed with several distinct features: increased volume of tissue ingrowth due to high porosity (75-85%) [151, 152, 164], comparable elastic modulus to trabecular bone (2.5–3.9 MPa) to reduce stress shielding and favorable frictional characteristics ($\mu = 0.88$) to reduce micromotion [153]. Animal studies using porous tantalum implants have shown bone ingrowth of: 40 – 50% bone ingrowth (dogs, femur implants, 4 weeks implantation time [164]), 8.3% (pigs, intervertebral lumbar arthrodeses, 3 months implantation time [166]) and 35.1% (goats, spinal fusion implants, 6 weeks implantation time [167]).

Initial large-scale clinical studies have been generally promising with well-fixed implants and a low incidence of loosening focusing on radiographic review after short-to-intermediate term implantation [184-191]. One recent clinical study of 56 porous tantalum acetabular shells showed 100% survivorship at 12 year mean follow-up [172].

Despite the number of clinical studies on porous tantalum, there have been limited studies focused on retrieval analysis of these implants. The first objective of this study was to determine the reasons for revision of retrieved porous tantalum implants. The second objective was to determine, within our retrieval cohort, if the proportion of implants revised for aseptic loosening was different based on surgery history (primary or revision), fixation method (cementless or cemented) and coating type (porous tantalum or historical coating).

Porous tantalum implants were designed with a high porosity, low elastic modulus and increased friction which may provide a favorable environment for bone ingrowth. The resulting increased bone ingrowth could increase the quality of fixation and thus may decrease the proportion of porous tantalum implants revised for aseptic loosening. Comparing primary and revision surgeries, there is a decrease in available bone stock which may result in increased revision rate due to aseptic loosening. We hypothesized that the proportion of implants revised for aseptic loosening would be lower in implants from primary surgeries compared to implants from revision surgeries. We also hypothesized that the proportion of implants revised for aseptic loosening would be lower in porous tantalum implants compared to historical coating implants. Finally, we hypothesized that the proportion of implants revised for aseptic loosening would be lower in the porous tantalum implants compared to cemented implants.

Methods

Under an IRB-approved multicenter retrieval program, 232 porous tantalum implants (Trabecular Metal™; Zimmer Inc, Warsaw, Indiana, Figure 1-1) were retrieved during revision surgeries.

Figure 1-1: Representative sampling of retrieved cementless implants collected through the multicenter retrieval program. Image courtesy of Christina Arnholt.

Between 2003 and 2015, 160 acetabular shells, 7 femoral stems, 11 patellas and 54 Nexgen tibial trays were retrieved (Figure 1-2).

Figure 1-2: Porous tantalum implants: acetabular shell (top left), femoral stem (top right), tibial trays (bottom left) and patellar implants (bottom right) [219].

Acetabular shells consisted of 86 primary surgery implants and 74 revision surgery implants, based on available clinical data. Three femoral stems were retrieved after primary surgeries. The patellas consisted of 5 implants from primary surgeries and 4 implants from revision surgeries. Except for one modular and one monoblock implant, all of the tibial trays were revised following primary surgeries. Clinical data consisting of age, primary/revision surgery, implantation time, UCLA Activity Score and reason for revision were obtained for each implant. The UCLA Activity Score indicates a patient's activity (range: 1 to 10). Each reason for implant revision and whether it was a primary or revision surgery was confirmed through the operative notes.

The average implantation time was shortest in the femoral stems (0.3±0.3 years) and highest in the tibial trays (2.2±2.4 years, Table 1-1). The average patient age was lowest in the tibial trays (55±9 years) and highest in the patellas (61±9 years). The average patient weight was lowest in the acetabular shells (196±51 lbs) and highest for

the tibial trays (215±49 lbs). On average, the patients in this study had a mildly to moderately active lifestyle (Table 1-1).

Table 1-1: Clinical data for porous tantalum implant collection.

Cohort	n	Age (Y)	Weight (Lbs)	Implantation Time (Y)	UCLA Activity Score
Acetabular Shells	160	59±13 (26-88)	196±51 (95-328)	1.5±2.2 (0.0-12.5)	5±2 (1-10)
Femoral Stems	7	60±15 (38-85)	204±36 (157 - 250)	0.3±0.3 (0.0 -0.8)	N/A
Patellas	11	61±9 (48-77)	206±50 (128 - 315)	1.4±2.0 (0.3 – 7.3)	5±2 (2-10)
Tibial Trays	54	55±9 (36-78)	215±49 (122-330)	2.2±2.4 (0.0-12.8)	5±2 (2-10)

Values are expressed as mean±SD, with range in parentheses.
*Data only available for two femoral stems.

Through the same multicenter retrieval program, cohorts of cementless components were selected to match the porous tantalum cohorts based on several clinical factors.

Acetabular shells from primary surgeries cohorts based on comparing porous tantalum (n=86, primary) to fiber metal (n=94, primary) and porous-beads (n=134, primary). The cohorts were matched based on implantation time (short-term criteria), gender [220], UCLA Activity Score [220], age and BMI. For an implant to be considered, it needed to be from a primary surgery, no metal-on-metal or ceramic bearing and have no use of cement. For each porous tantalum implant, a fiber metal implant was first matched by implantation time and next gender. Next it was then matched based on activity level. Finally, if possible, it was also matched for age and BMI. During the selection process, the reviewer was blinded to the reason for revision column remove selection bias. If implantation time and gender could not be matched, the implant was removed from the study. After the cohorts were matched, statistical tests were run to verify that implantation time, gender, activity, age and BMI are similar between groups.

Primary porous tantalum tibial trays were matched to primary Nexgen cemented (n=396) and porous-beads/fiber metal (n=25). The cohorts were matched based on

implantation time (short-term criteria), gender [220], UCLA activity score [220], Age and BMI. Only implants from primary surgeries with polyethylene used as the bearing surface were considered. For each porous tantalum implant, a fiber metal implant would first be matched by implantation time and next gender. The implant was then matched based on activity level. Finally, if possible, it was also matched for age and BMI. If implantation time and gender could not be matched, the implant was removed from the study. After the cohorts are matched, statistical tests were run to verify that implantation time, gender, activity, age and BMI are similar between groups.

Pearson's Chi-squared test was used to assess the differences in proportion of implants revised for aseptic loosening based on surgical history (primary or revision), coating type (porous tantalum or historical coating) and fixation type (cemented or cementless) on implants from our retrieval cohort. All statistical tests ($p<0.05$) were performed using SPSS Statistics package (Version 22.0; IBM, Chicago, IL, USA).

Results

Reasons for revision based on implant type

The main reasons for revision of the retrieved porous tantalum implants were infection (n=74, 31.9%), instability (n=58, 31.9%), acetabular loosening (9.0%, n=19) and pain (n=15, 6.5%). Acetabular shells from primary surgeries were mostly revised for infection (n=24, 27.9%), instability (n=27, 31.4%), hematoma (n=12, 14.0%), pain (n=4, 4.7%, Figure 1-3). Acetabular shells from revision surgeries were revised primarily for infection (n=40, 54.1%), acetabular loosening (n=19, 25.7%) and instability (n=7, 9.5%, Figure 1-3). The main reason for revision of the femoral stems was infection (n=3, 42.9%).

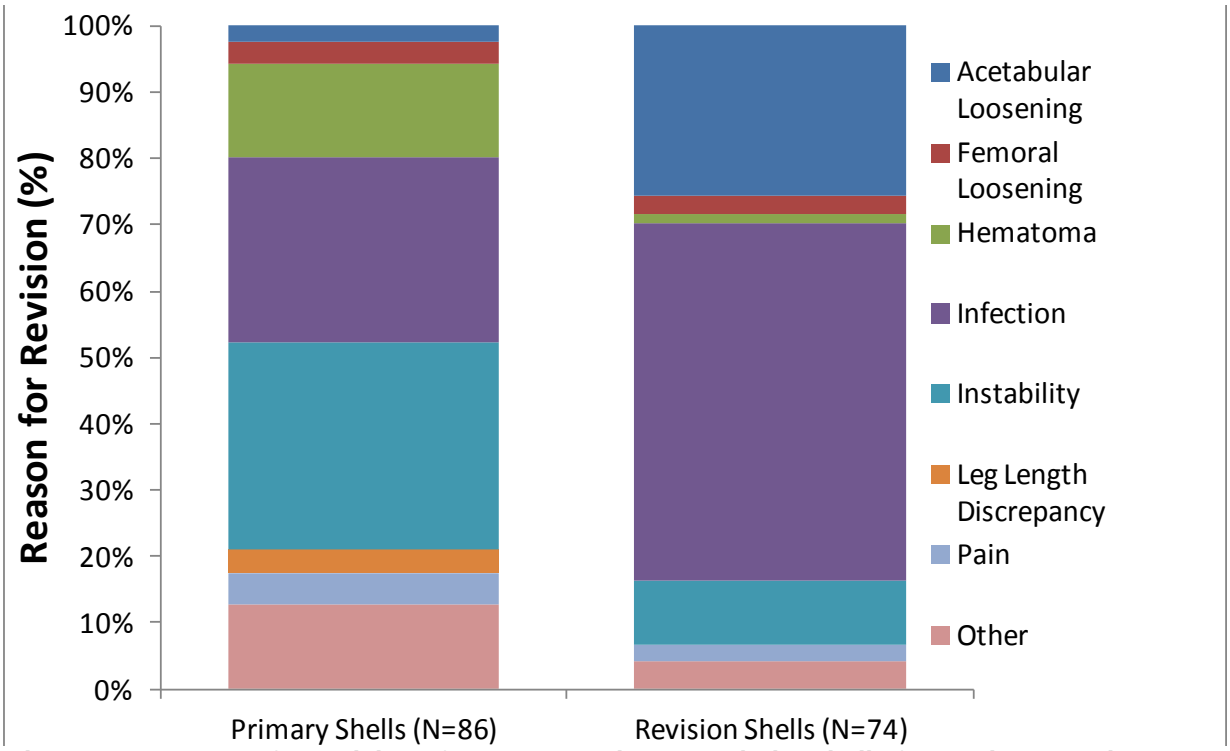

Figure 1-3: Reasons for revision of porous tantalum acetabular shells from primary and revision surgery.

The main reasons for revision of the patellas were patellar loosening (n=4, 36.4%) and instability (n=2, 18%). The primary tibial trays were mainly revised for instability (n=22, 42.3%), pain (n=9, 17.3%) and infection (n=6, 11.5%). The modular CR-Flex tibial trays were revised for tibial loosening (n=1, 50%) and unresurfaced patella (n=1, 50%). The modular LPS-Flex tibial trays were revised for femoral loosening (n=1, 20%), infection (n=1, 20%), instability (n=1, 20%), pain (n=1, 20%) and stiffness (n=1, 20%). The monoblock CR-Flex components were revised for instability (n=3, 37.5%), malalignment (n=2, 25%), arthrofibrosis (n=1, 12.5%), infection (n=1, 12.5%) and internal rotation of tibial component (n=1, 12.5%). The reasons for revision of the monoblock LPS-Flex components were instability (n=18, 46.2%), pain (n=6, 15.4%), infection (n=5, 12.8%), femoral loosening (n=3, 7.7%), periprosthetic fracture (n=2, 5.1%), tibial subsidence

(n=2, 5.1%), arthrofibrosis (n=1, 2.6%), femoral component overhang (n=1, 2.6%) and tibial loosening (n=1, 2.6%, Figure 1-4).

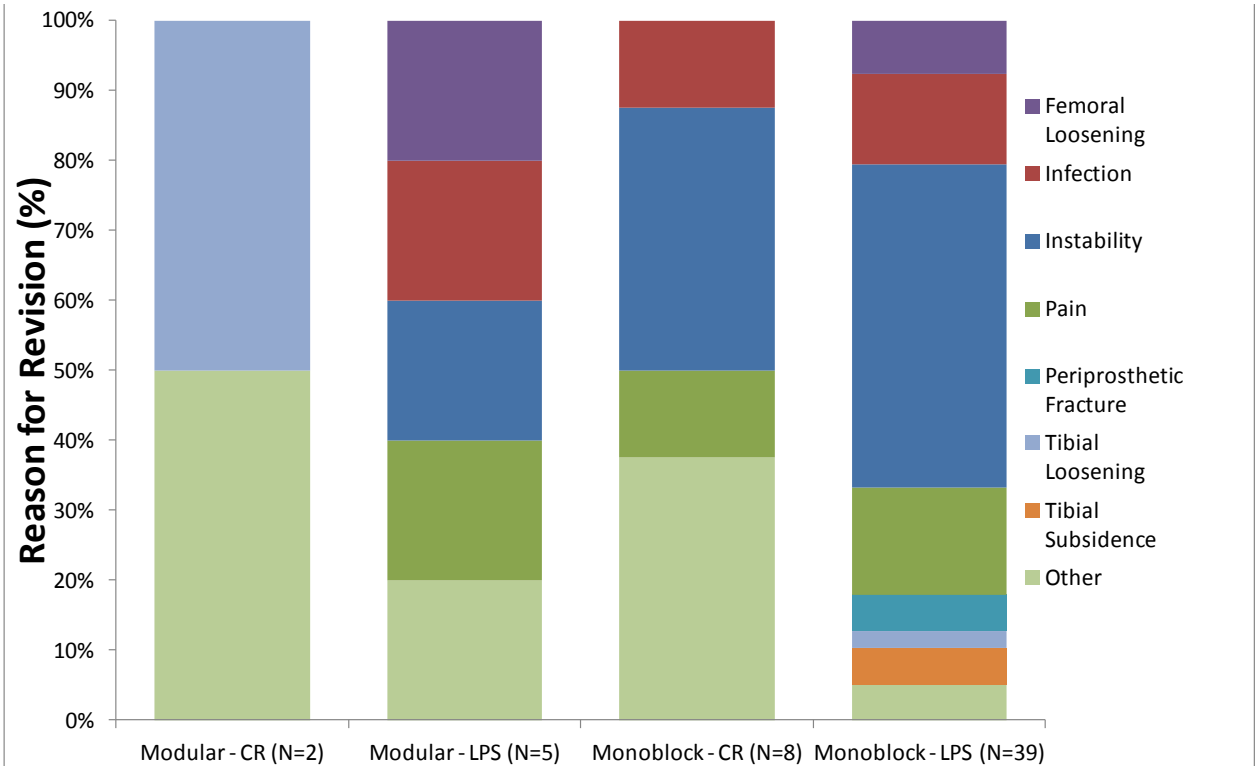

Figure 1-4: Reasons for revision of tibial implants based on implant design.

Association of loosening based on number of previous surgeries

The primary and acetabular shells had similar implantation time (p=0.891), age (p=0.289) and BMI (p=0.605). However, the patients with primary acetabular shells (p=0.004) had a significantly higher UCLA Activity Score than the patients from revision surgery. Our study showed that porous tantalum acetabular shells from primary surgeries (n=2, 2.3%) had a lower proportion of implants revised for acetabular loosening compared to acetabular shells from revision surgeries (n=19, 25.7%, p<0.001, Figure 1-5).

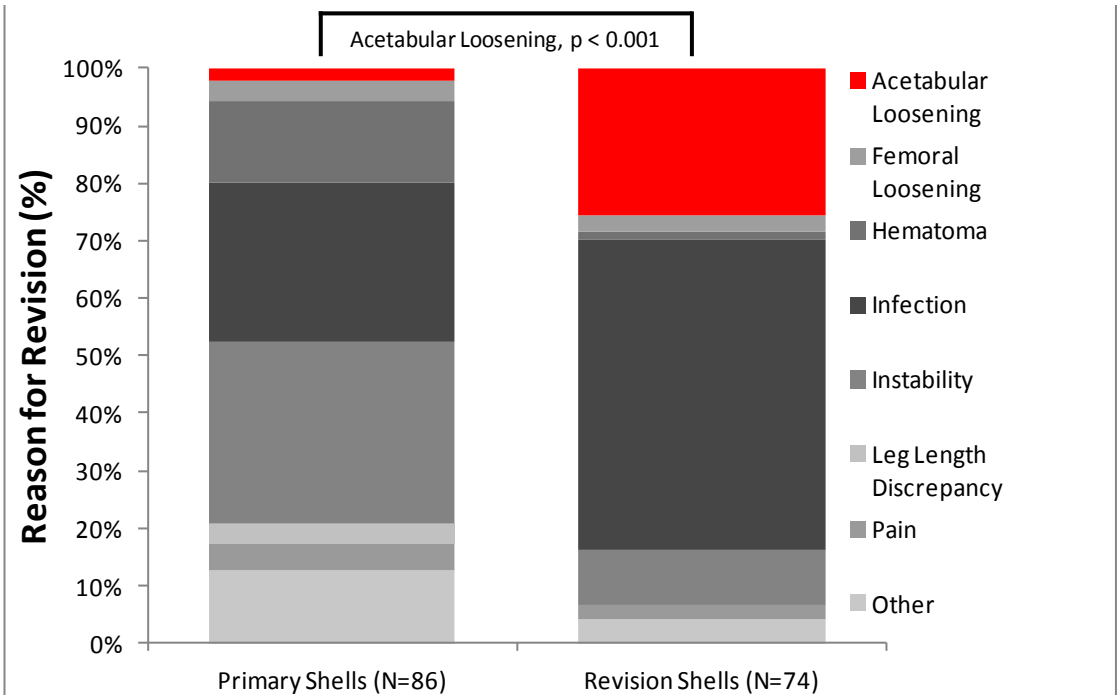

Figure 1-5: Reason for revision based on previous number of surgeries for retrieved porous tantalum acetabular shells.

Association of acetabular loosening based on surface type

Primary porous tantalum acetabular shells showed a lower proportion of implants revised for acetabular loosening compared to fiber-metal implants. Primary porous tantalum acetabular shells (n=36) were matched to primary fiber-metal acetabular shells (n=36). Primary porous tantalum acetabular shells were mainly revised for infection (n=13, 36.1%), instability (n=8, 22.2%) and pain (n=3, 8.3%). Primary fiber metal shells were mainly revised for infection (n=8, 22.2%), instability (n=8, 22.2%), acetabular loosening (n=6, 16.7%) and femoral loosening (n=6, 16.7%, Figure 1-6).

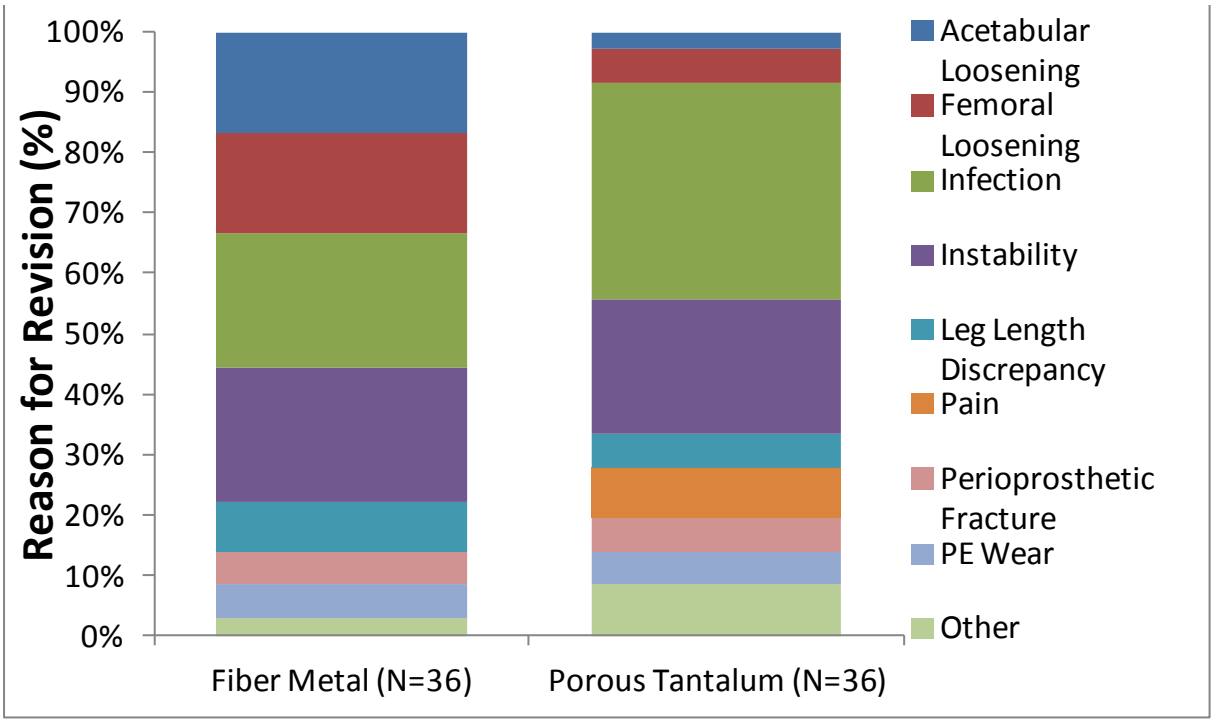

Figure 1-6: Reason for revision for acetabular shells based on coating type.

The two cohorts had similar clinical factors: implantation time (p=0.727), gender (p=1.00), UCLA Activity Score (p=0.188), age (p=0.264) and BMI (p=0.647). Our results showed that porous tantalum (n=1) had a lower proportion of acetabular shells revised for acetabular loosening compared to fiber metal (n=6, p = 0.047, Figure 1-7).

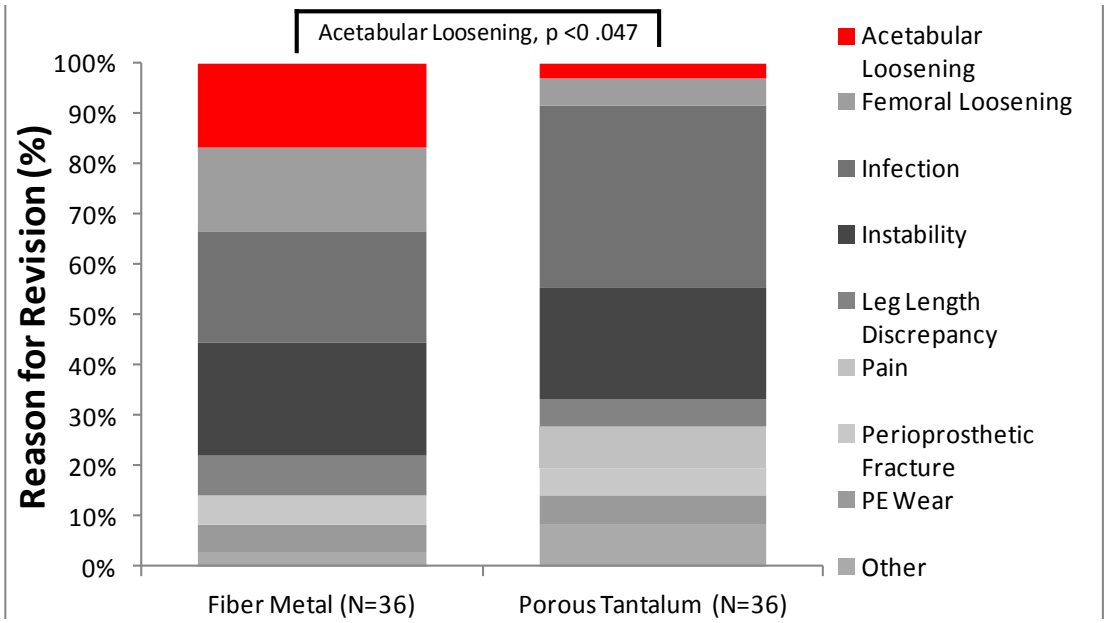

Figure 1-7: Acetabular loosening as reason for revision based on porous coating type.

Primary porous tantalum acetabular shells (n=26) were matched to primary bead acetabular shells (n=26). The two cohorts had similar clinical factors: implantation time (p=0.855), gender (p=1.00), UCLA Activity Score (p=0.844), age (p=0.895) and BMI (p=0.969). Our results showed that porous tantalum (n=1) had a similar proportion of acetabular shells revised for acetabular loosening compared to porous beads (n=4, p = 0.158, Figure 1-8).

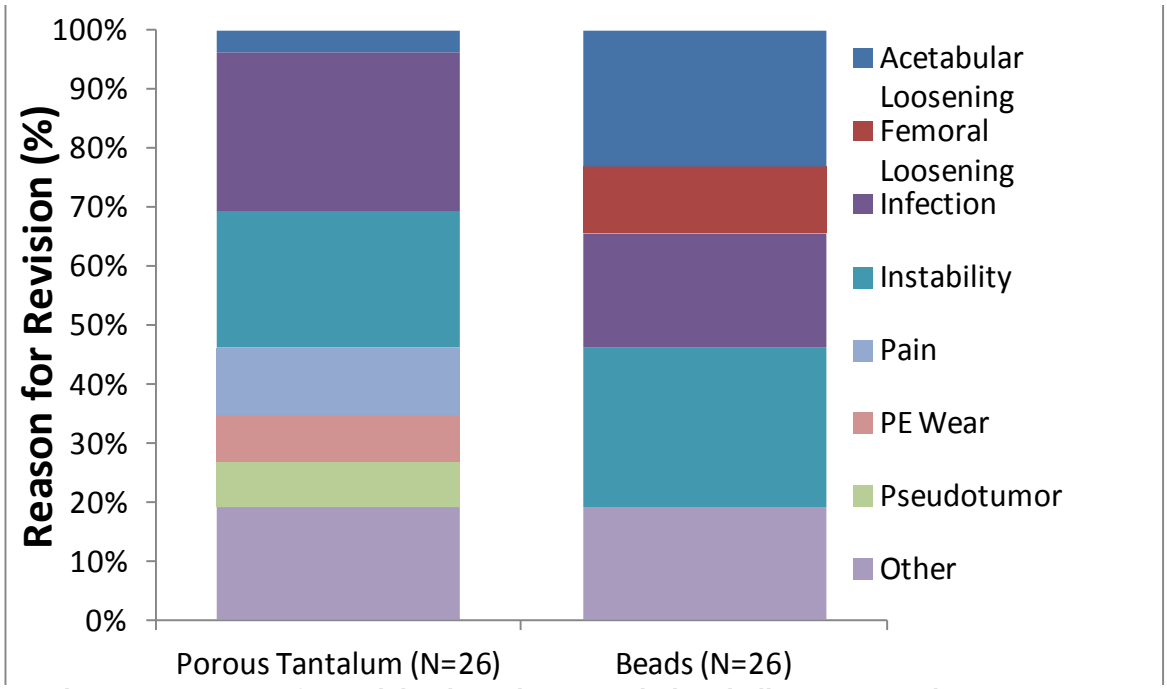

Figure 1-8: Reason for revision based on acetabular shell porous coating type.

Association of loosening based on tibial fixation method

Primary porous tantalum (n=49) tibial trays were matched to primary cemented NexGen® (n=49) tibial trays. The porous tantalum implants for this comparison were mainly revised for instability (n=22, 44.9%), pain (n=7, 14.3%) and infection (n=6, 12.2%). The cemented NexGen® tibial implants for this comparison were mainly revised for instability (n=20, 40.8%), tibial loosening (n=11, 22.4%) and infection (n=9, 18.4%, Figure 1-9).

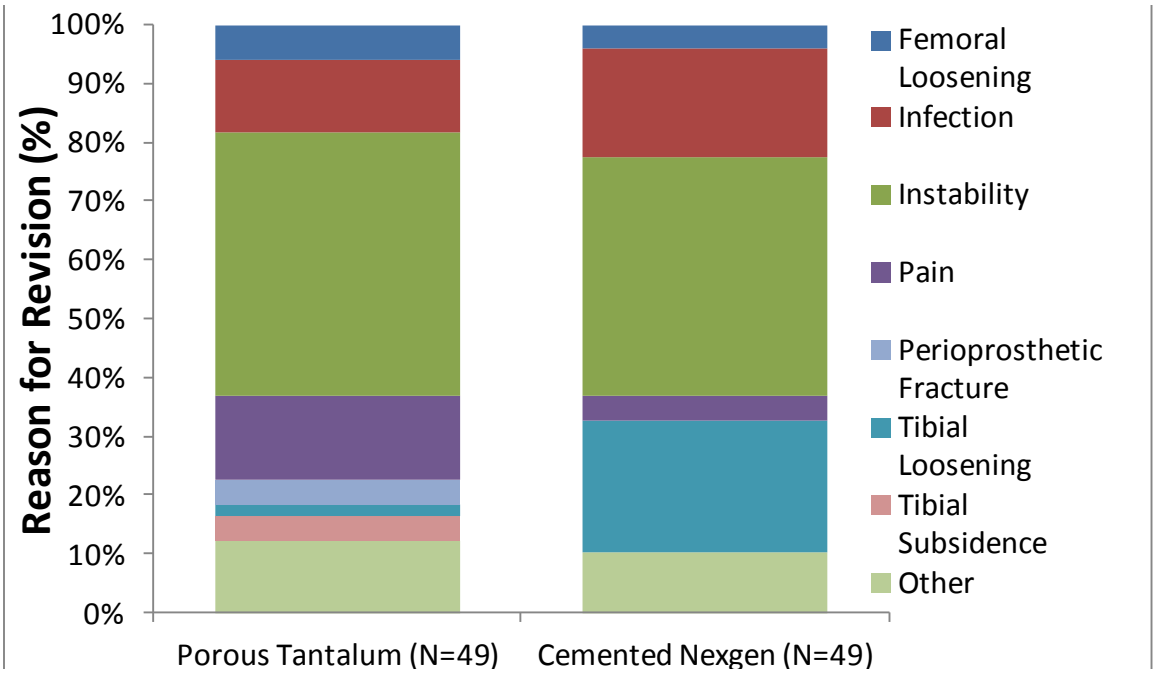

Figure 1-9: Reason for revision based on tibial tray implant fixation method.

The two cohorts had similar clinical factors: implantation time (p=0.771), gender (p=1.00), UCLA Activity Score (p=0.232), age (p=0.665) and BMI (p=0.170). Our results showed that porous tantalum (n=1) had a lower proportion of tibial implants revised for tibial loosening compared to cemented (NexGen®, n=10, Figure 1-10).

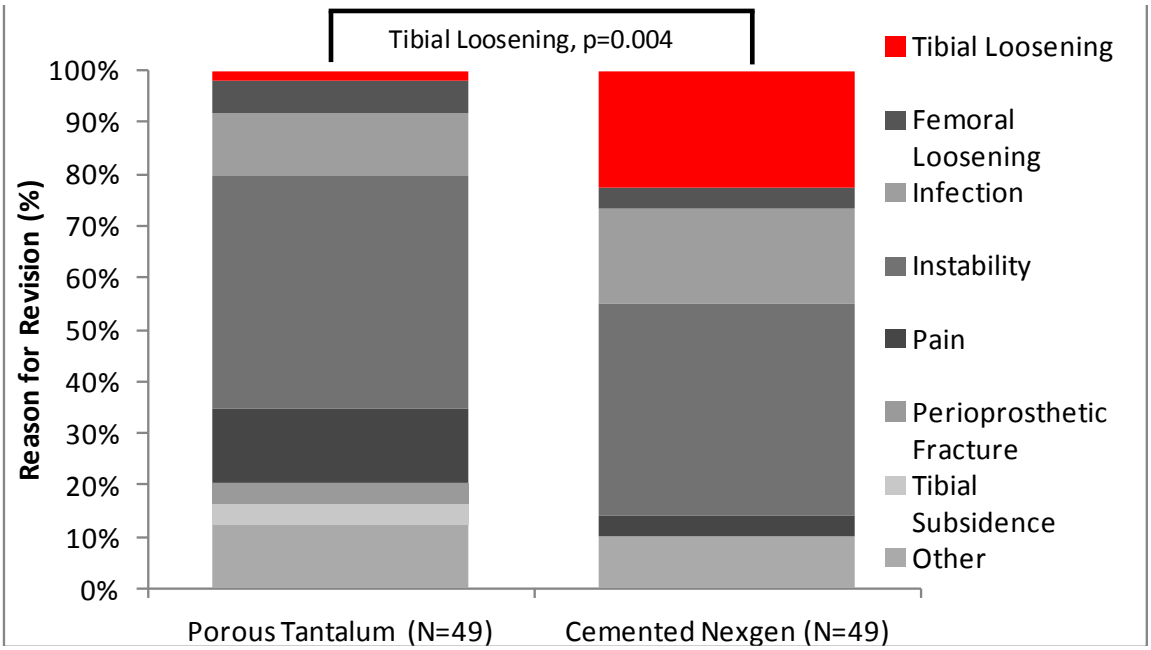

Figure 1-10: Reason for revision based on tibial tray fixation type.

Primary porous tantalum (n=9) tibial trays were matched to primary combined fiber metal/porous-beads (n=9) tibial trays. The porous tantalum implants for this comparison were mainly revised for instability (n=5, 55.6%) and infection (n=2, 22.2%). The fiber metal/porous-beads tibial implants for this comparison were mainly revised for instability (n=2, 22.2%), stiffness (n=2, 22.2%) and tibial loosening (n=2, 22.2%, Figure 1-11).

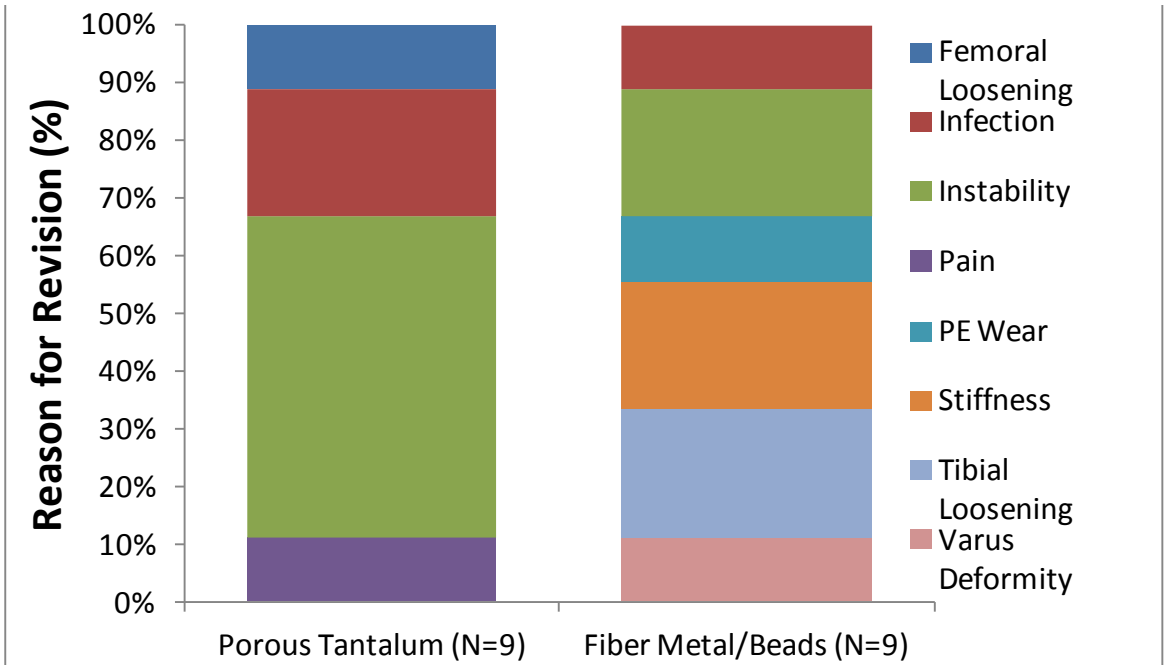

Figure 1-11: Reason for revision based tibial tray coating design.

The two cohorts had similar clinical factors: implantation time (p=1.00), gender (p=1.00), UCLA Activity Score (p=0.955), age (p=0.236) and BMI (p=0.541). Our results showed that porous tantalum implants (n=0) had a similar proportion of tibial implants revised for tibial loosening compared to fiber metal/beads (n=2, p = 0.132).

Discussion

Our results showed that porous tantalum acetabular shells from primary surgeries had a lower proportion of implants revised for acetabular loosening compared to implant from revision surgeries. The porous tantalum acetabular shells had a lower proportion of implants revised for acetabular loosening compared to fiber metal implants. The porous tantalum tibial implants had a lower proportion of implants revised for tibial loosening compared to cemented implants.

There were several limitations to this study. The first limitation is the limited number of implants collected for each cohort. There was a limited amount of fiber metal

and porous bead tibial trays for the comparison study. The second limitation is the difference in implantation time between the porous tantalum acetabular shells and other porous-coated implants. The historical porous-coated implants were introduced decades before the porous tantalum implants, allowing for implants with a longer implantation time. Despite long-term implants, the comparisons were made such that implantation time was similar between groups. However, it should also be noted that the polyethylene liners that are used in porous tantalum implants are different than the historical porous-coated shells.

Our results showed that the most prevalent reasons for revision of primary surgery porous tantalum acetabular shells were infection (n=24, 27.9%) and instability (n=27, 31.4%) and hematoma (n=12, 14.0%). These results are similar to the Swedish Hip Registry, which shows that short-term retrievals (0-3 years) have a higher revision rate (21.7%), due to infection, when compared to long-term implants (4-6 years (5.0%), 7-10 years (2.6%) and >10 years (1.5%)) [221]. In our study, aseptic loosening was dependent on surgical history (primary or revision), which is similar to the Australian Registry with aseptic loosening for primary surgeries at 31.3% and 54.1% for all surgeries [222]. Acetabular loosening (2.5%) was not a prevalent reason for revision for the primary porous tantalum acetabular shells. One recent clinical study of 56 porous tantalum acetabular shells showed 100% survivorship at 12 year mean follow-up [172].

Similar to the NIS results [223], main reasons for revision for primary porous tantalum acetabular shells were dislocation/instability and infection. However, the porous tantalum (2.3%) cohort had a smaller proportion of implants revised for acetabular loosening compared to an NIS study (19.7%). Similar to the Swedish Registry results, main reasons for revision for the primary porous tantalum acetabular shells were dislocation/instability and infection [224]. However, the porous tantalum (2.3%) group had a higher amount of acetabular loosening compared to the Swedish Registry (2%).

This registry may report more than one complication for each type of complication. For the reporting purposes, the occurrence of a complication divided by the total complication number is reported.

From the Australian Registry study, the most common reasons for revision of primary total conventional hip replacement are loosening/lysis (28.4%), implant dislocation (25.0%), fracture (17.5%) and infection (17.1%) [103]. However, this included cemented and cementless fixation method and all implantation times. For primary total conventional hip replacement with average implantation of 1.5 years, the main reasons for revision were instability (35.0%), infection (22.2%), loosening/lysis (22.2%) and fracture (19.7%). Similar to the Australian Registry results, main reasons for revision were primary porous tantalum acetabular shells, dislocation/instability and infection. However, the porous tantalum (2.5%) group had a lower amount of loosening compared to the Australian Registry (22.2%). The Australian registry combine loosening/lysis into one category. The reason they state is because when lysis occurs it may be in association with loosening.

Our results showed that the most prevalent reasons for revision of primary porous tantalum tibial trays were mainly revised for instability (n=22, 42.3%), pain (n=9, 17.3%) and infection (n=6, 11.5%). This is similar to a previous NIS study that showed the main reasons for revision of implants revised before 5 years were infection (38%, 105/279 components) and instability (27%, 74/279 components) [225]. Earlier uncemented tibial components showed a higher loosening rate than our study: 19% (21/108 components, porous-beads, 64 month follow-up [226]) and 7% (8/108 components, Fiber Mesh™, 11 years average follow-up [227]). Previous studies of porous tantalum tibial trays with short-term follow-up showed few to no cases of tibial loosening [184, 228, 229].

Infection (25.2%), loosening (16.1%) and implant failure/breakage (9.7%) were the most common reasons for revision in an NIS study that reviewed 60,355 revision TKA procedures [102]. Similar to the NIS results, main reasons for revision for primary porous tantalum tibial trays were pain, instability and infection. However, the porous tantalum (2.0%) cohort had a lower amount of loosening compared to the NIS (16.1%).

The Swedish Registry reported the most common reason for revision for combined cemented and cementless fixation from primary surgery TKA was infection (25.9%), loosening (25.8%) and instability (13.1%) over a ten year reporting period [104]. Similar to the Swedish Registry, one of the main reasons for revision was infection. However, the porous tantalum had a higher prevalence of instability (43.1%) compared to Swedish Registry (13.1%). However, the porous tantalum (2.0%) cohort had a lower amount of loosening compared to the Swedish Registry (25.8%).

The Australian registry reported the most common reason for revision for combined cemented and cementless fixation for TKA was loosening/lysis (29.1%), infection (22.2%), patellofemoral pain (12.1%), pain (9.2%) and instability (6.1%) [103]. Similar to the Australian Registry, one of the main reasons for revision was infection. However, the porous tantalum had a higher prevalence of instability (43.1%) compared to Australian Registry (6.1%). However, the porous tantalum (2.0%) cohort had a lower amount of loosening compared to the Australian Registry (29.1%).The most common reasons for revision of the primary porous tantalum were instability (43.1%), pain (15.7%) and infection (11.8%). Tibial loosening (2.0%) was not a prevalent reason for revision.

Our retrieval results showed that the proportion of retrieved implants revised for tibial loosening was significantly lower in the porous tantalum cohort compared to the NexGen® cemented cohort. The proportion of NexGen® cemented tibial trays revised for aseptic loosening in the matched cohort was 20%, which is less than the Australian

Registry which showed 50% [103]. The difference may be due to the combining of lysis and loosening in the Australian Registry.

Our study showed that primary porous tantalum implants showed a lower proportion of implants revised for acetabular loosening compared fiber metal implants. However, it remains unclear if higher amount of bone ingrowth is causing the lower amount of loosening. Retrieval analysis of porous tantalum implants to determine the amount of bone ingrowth may yield further insight into the new biomaterial. Additionally, clinical analysis of long-term implants, especially the tibial trays will help to determine if loosening has decreased over the life of the implant.

Chapter 2 Characterizing bone ingrowth in retrieved porous tantalum implants.

Part 1: Determine Factors Affecting Bone Ingrowth in Retrieved Porous Tantalum Hip Implants

Abstract

The objective of this study was to investigate the effect of clinical factors, location within an implant and implant type on bone ingrowth. Twenty well-fixed acetabular shells and seven femoral stems were evaluated for bone ingrowth. Nonparametric statistical tests were used to investigate differences in bone ingrowth related to implant type, spatial location within an implant, substrate depth and clinical factors. Bone ingrowth in both implants was highest in the superficial 500 μm from the bone-implant interface. Bone ingrowth was not significantly different between acetabular shells and femoral stems.

Introduction

Total hip arthroplasty restores function and reduces pain in patients with arthritis and fracture. A variety of porous coatings and surface treatments have been used to obtain fixation through bone ingrowth or ongrowth [148, 153]. Historical porous coatings include sintered titanium mesh, cancellous-structured titanium and sintered beads [153]. Failure of first generation cementless acetabular components has been attributed to aseptic loosening [230], particle migration through screw holes [231], locking mechanism failure [232] and PE wear [233]. In order to further improve on the clinical success of these coatings in hip components [234], manufacturers have developed new highly porous metals. These newly developed materials are thought to have favorable material properties to increase fixation at the bone-implant interface [153].

Porous tantalum, a highly porous metal, has favorable characteristics including a low elastic modulus (2.5–3.9 MPa) to reduce stress shielding, high porosity (75-85%) to promote bone ingrowth and a favorable coefficient of friction (μ = 0.88) to reduce micromotion [153, 164]. Animal models of porous tantalum have been promising with high amounts of bone ingrowth [164, 235]. The Trabecular Metal™ modular cup (Zimmer, Inc., Warsaw, IN) consists of a porous tantalum ingrowth surface metallurgically bonded onto a titanium alloy acetabular shell [236]. The Trabecular Metal™ primary hip prosthesis (Zimmer, Inc.) is femoral stem with porous tantalum on the proximal half of a titanium alloy stem.

Several clinical studies of porous tantalum acetabular shells have reported no cases of aseptic loosening [168-170]. In a recent study using the Swedish registry with a 3.3 year follow-up, the unadjusted and adjusted risk of reoperation or revision was not significantly different between the TM cup, a press-fit porous-coated cup (Trilogy) and cemented all-polyethylene cup [171]. A clinical study with mean 3.5 year follow-up of 613 primary total hip arthroplasties showed no revisions due to aseptic loosening of the acetabular shell [168]. One clinical study of 45 patients with porous tantalum acetabular shells with minimum of 10 year follow-up have show zero cases of acetabular loosening [172]. Another study with an average of 6.1 years follow-up of 263 porous tantalum acetabular shells had no cases of acetabular loosening [170]. Despite the number of clinical studies on porous tantalum acetabular shells [168-171, 173], there have been limited retrieval studies of porous tantalum acetabular shells and femoral stems [174].

The clinical and design factors affecting bone ingrowth into porous tantalum acetabular shells and femoral stems remain unknown. Therefore, the purpose of this study was to investigate the effect of implant type, anatomic location and patient factors on bone ingrowth in retrieved porous tantalum hip implants. We hypothesized that there would be differences in bone ingrowth between anatomic location within each implant.

Additionally, we hypothesized that clinical factors would correlate with the amount of bone ingrowth.

Methods

A total of 126 acetabular shells and 7 femoral stem porous tantalum implants were retrieved under an IRB-approved multicenter retrieval program between 2003 and 2013 (Figure 2-1).

Figure 2-1: A retrieved porous tantalum acetabular shell (left) and femoral stem (right).

Clinical data consisting of age, primary/revision surgery, implantation time, reason for revision and revision operative reports was obtained. The acetabular shells were implanted for an average of 1.6±2.0 years (Range: 0.0-12.5). The average patient age was highest for the femoral stems with 60 ± 15 years (Range: 38-85, Table 1). Primary acetabular shells were revised for infection (n=19, 33.3%), instability (n=15, 26.3%), hematoma (n=5, 8.8%), pain (n=3, 5.3%) and femoral loosening (n=3, 5.3%). Acetabular shells with previous revisions were revised primarily for infection (n=32, 55.2%), acetabular loosening (n=15, 25.9%) and instability (n=4, 6.9%). The femoral stems were revised for infection (n=3, 42.9%), femoral loosening (n=1, 14.3%), periprosthetic fracture (n=1, 14.3%) and recurrent instability (n=1, 14.3%)

Twenty acetabular shells and all seven femoral stems were chosen for bone ingrowth analysis.

Acetabular shells were excluded based on the following criteria: gross loosening, presence of bone cement, previous complex revision surgeries or fibrous fixation. The implantation time, patient age, weight and UCLA score were similar between the overall collection and analyzed acetabular shells (Table 2-1).

Table 2-1: Summary of patient demographics for the total collection of acetabular shells and components analyzed for bone ingrowth.

Cohort	n	Age (Y)	Weight (Lbs)	Implantation Time (Y)	UCLA Score
Acetabular Shells	126	59±11 (36-88)	194±50 (95-328)	1.6±2.0 (0.0-12.5)	5±2 (2-10)
Acetabular Shells	20	59±9 (45-78)	194±50 (116-292)	2.3±1.6 (0.3-6.8)	6±3 (2-10)
Femoral Stems	7	60 ± 15 (38-85)	188±31 (157-218)	0.3±0.3(0-0.8)	N/A

Values are expressed as mean±SD, with range in parentheses.
*Data only available for two femoral stems.

The acetabular shells analyzed for bone ingrowth were revised for infection (n=10, 50%), instability (n=4, 20%), femoral loosening (n=3, 15%), pain (n=2, 10%) and periprosthetic fracture (n=1, 5%). The reasons for revision of the femoral stems were infection (n=3, 42.9%), femoral loosening (n=1, 14.3%), instability (n=1, 14.3%) and periprosthetic fracture (n=1, 14.3%). The reason for revision for one stem was not reported.

Bone ingrowth analysis starts with dehydrating implants to image analysis of representative slices of each implant (Figure 2-2).

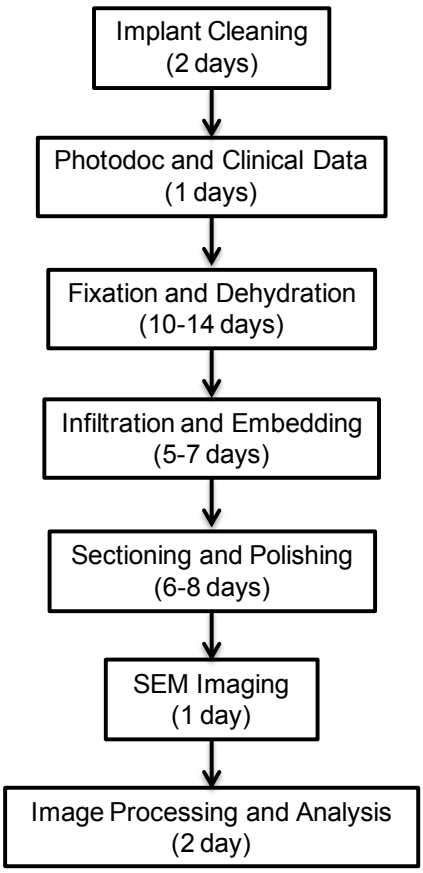

Figure 2-2: Bone ingrowth analysis processing for one implant.

Each implant was dehydrated using increasing graded alcohols (40% ethanol to 100% acetone). Specimens were infiltrated and embedded using Osteo-bed resin and catalyst (Polysciences and Sigma-Aldrich). Specimens were cut into 3–4 mm sections using a diamond cut-off saw (Isomet 1000, Buehler, Lake Bluff, Illinois). Each section was ground flat, polished and sputter-coated with platinum–palladium to facilitate imaging. The sections from each implant were imaged at 22X magnification using a scanning electron microscope (SEM, XL30 ESEM FEG, FEI, Hillsboro, Oregon and Supra 50 VP, Zeiss Peabody, Massachusetts) equipped with a BSE detector to facilitate bone–implant imaging. Four sections per acetabular shell and 5-7 sections per femoral stem were analyzed (Figure 2-3).

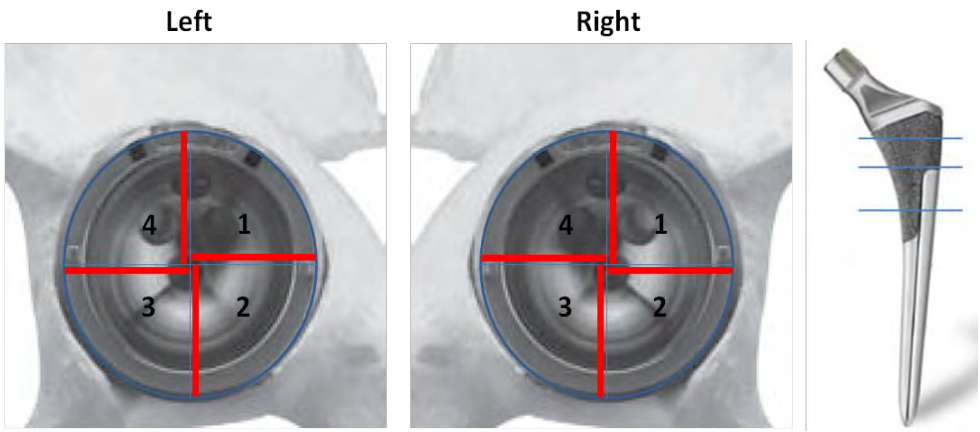

Figure 2-3: Component sectioning based on anatomic location for acetabular shells (left) and femoral stems (right).

The anatomic orientation was determined using radiographs and the locations of the screw holes, when available. Individual images from BSE were stitched to create a montage for each individual section. Image processing of each montage consisted of thresholding the montage image to identify areas of tantalum and bone followed by manual correction for areas of false signal (e.g., residual polishing media) prior to analysis (Figure 2-4).

Figure 2-4: Representative BSE montage image of an acetabular shell.

Bone ingrowth measurements consisted of Bone Area/Pore Area (BA/PA), BA/PA depth analysis, extent of ingrowth and maximum depth of ingrowth. The BA/PA represents the fraction of available pore space within the porous coating that was occupied by bone. The entire process was validated by comparing the results against a manual point counting analysis conducted by two operators (Figure 2-5).

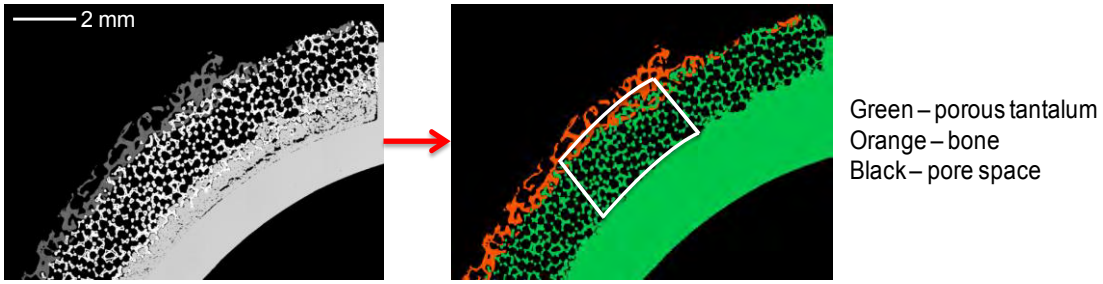

Figure 2-5: Acetabular shell image illustrating an example of segmentation for calculation.

The zones for BA/PA depth analysis were defined as: zone 1 (0-500μm), zone 2 (500-1000μm) and zone 3 (1000μm - full depth) (Figure 2-6).

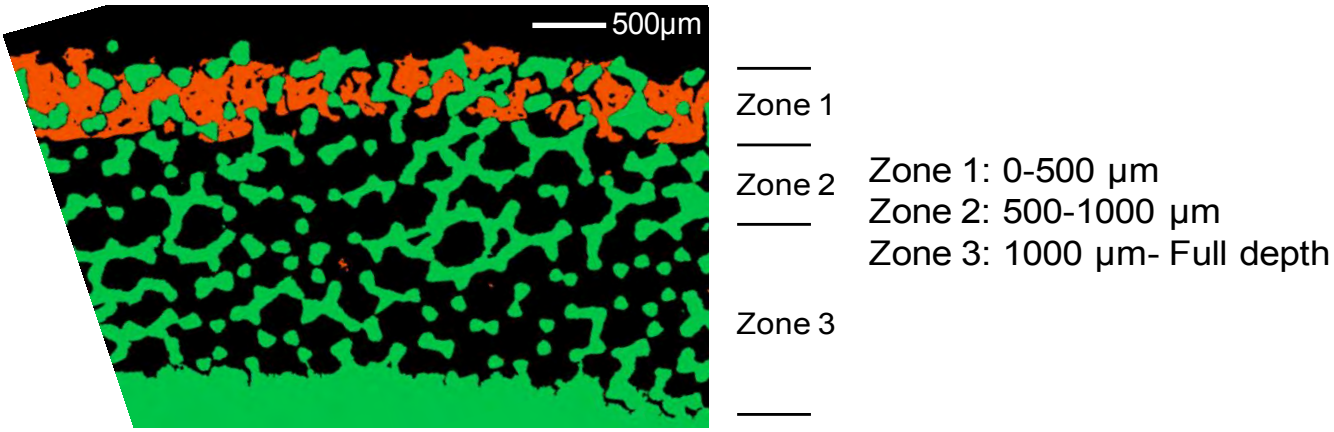

Figure 2-6: BA/PA depth analysis showing the three different zones.

The extent of bone ingrowth provides a topological indication of the distribution of bone ingrowth across the surface of the implant. The extent of ingrowth was calculated as the number of 1 mm sectors exhibiting ingrowth divided by the total number of sectors. An example image of a femoral stem shows 2 sectors out of 3 with bone, which is 2/3=66% extent of bone ingrowth (Figure 2-7).

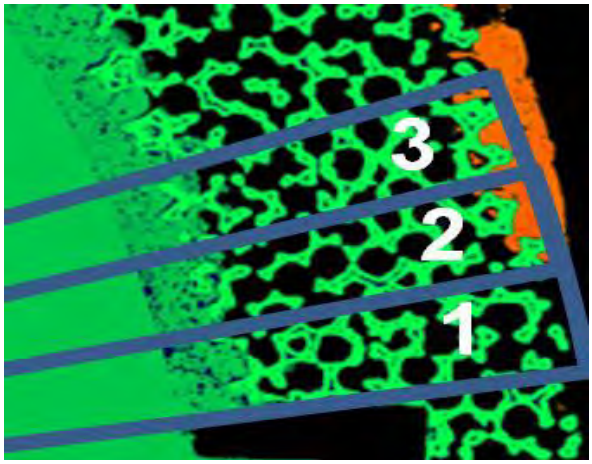

Figure 2-7: Representative image of an acetabular shell illustrating the calculation for extent of ingrowth.

The maximum depth was evaluated using two metrics. One is the actual maximum depth the bone grew into the substrate, measured in mm. The second measurement is the deepest point where bone was present in the substrate and was expressed as a percentage of the total available depth (Figure 2-8).

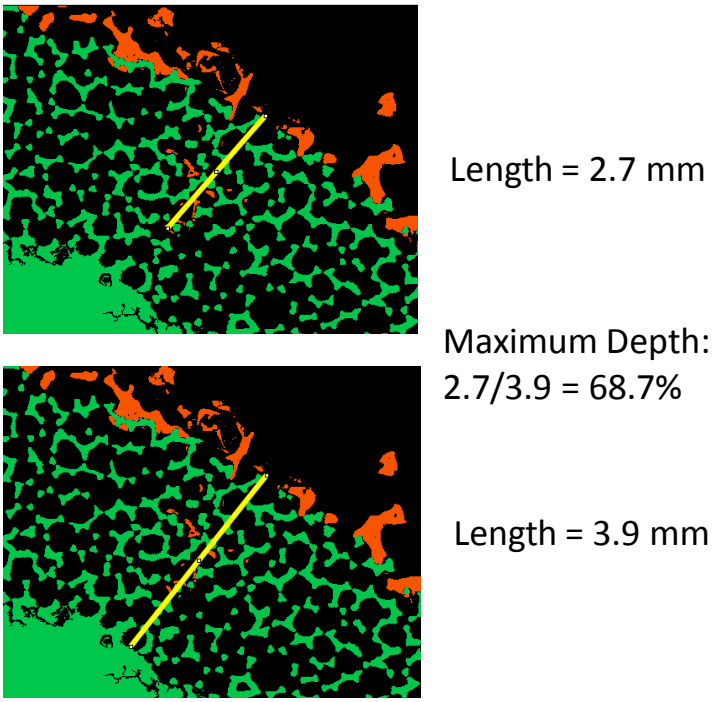

Figure 2-8: Representative images of acetabular shell illustrating maximum bone ingrowth depth calculation.

Nonparametric statistical tests were used to investigate differences in bone measurements by implant type (acetabular shell vs. femoral stem), location within the implant and depth (Related: Friedman's, Non-related: Kruskal-Wallis). The acetabular shell locations were compared based on quadrant (anterior, inferior, posterior, superior) and Gruen zone (I, II, III). For the femoral stem, comparisons were made between location within the implant (proximal, central, distal, anterior, lateral, medial and posterior). Post-hoc Dunn tests were completed for subsequent pairwise comparisons. Spearman's rank order correlation was used to identify correlations between continuous variables (implantation time, age, height, weight, UCLA Activity Score and bone measurements). All statistical tests ($p<0.05$) were performed using PASW Statistics package (Version 22.0; IBM, Chicago, IL).

Results

Bone ingrowth was present in the porous tantalum layer for each of the 20 analyzed acetabular shells and 7 femoral stems. The average BA/PA was 3.6 ± 3.3% (Range: 1.2% to 9.1%) for the acetabular shells and 5.8 ± 3.9% (Range: 2.7% to 10.4%) for the femoral stems. The average extent of ingrowth was 42 ± 28% (Range: 20% to 83%) for the acetabular shells and 47 ± 26% (Range: 15% to 77%) for the femoral stems. The average maximum depth of ingrowth was 3.0 mm (76%) for the acetabular shells and 1.1 mm (82%) for the femoral stems. In regions where the bone did not bridge the entire depth of the porous layer, a superficial layer of dense trabecular bone that was integrated with the porous layer was often observed (Figure 2-9).

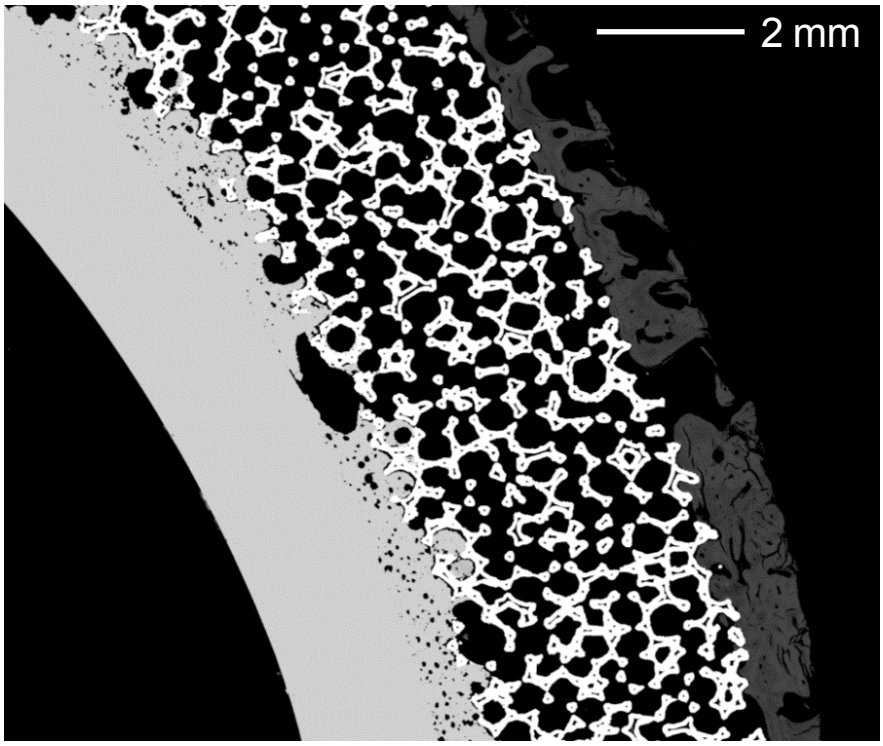

Figure 2-9: A superficial layer of dense trabecular bone was integrated with the porous tantalum layer on a shell that was implanted in a 56 year old male for 2.2 years.

In areas with limited or no bone ingrowth, dense fibrous tissue was noted. Localized regions of increased ingrowth were also observed around screw holes in the acetabular shells (Figure 2-10).

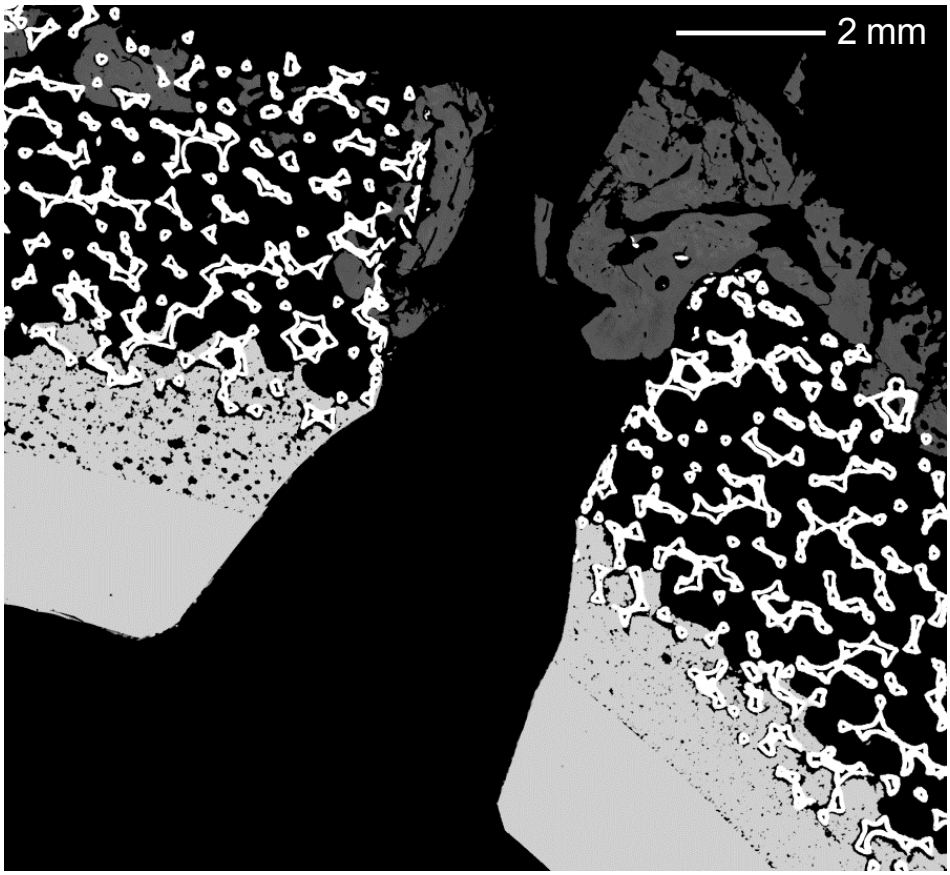

Figure 2-10: Localized increased density around a screw hole.

Bone ingrowth varied based on regional location in femoral stem but not the acetabular shell. The BA/PA was similar for all quadrants of the acetabular shells ($p=0.064$, Friedman's). There was no significant difference between acetabular Gruen zones (I, II, III) for BA/PA ($p=0.291$, Friedman's). There was no significant difference in bone ingrowth measurements between the proximal, central and distal location in the femoral stem (BA/PA: $p=0.368$, Extent: $p=0.368$ and Depth: $p=0.311$, Friedman's).

BA/PA was significantly higher in the medial region (8.8%) of the femoral stem compared to the anterior region (2.7%), p=0.011, Friedman's).

Bone ingrowth varied based on the depth into the porous tantalum substrate for both types of implants (Figure 2-11). For the acetabular shells, there was a significantly higher amount of bone in the superficial zone 1 (10.8%) compared to deeper zones 2 (4.9%, p=0.013) and 3 (1.6%, p<0.001, Friedman's). For the femoral stems, there was a higher amount of bone ingrowth in zone 1 (10.8%) compared to zone 3 (2.3%, p=0.043, Friedman's, Figure 2-11).

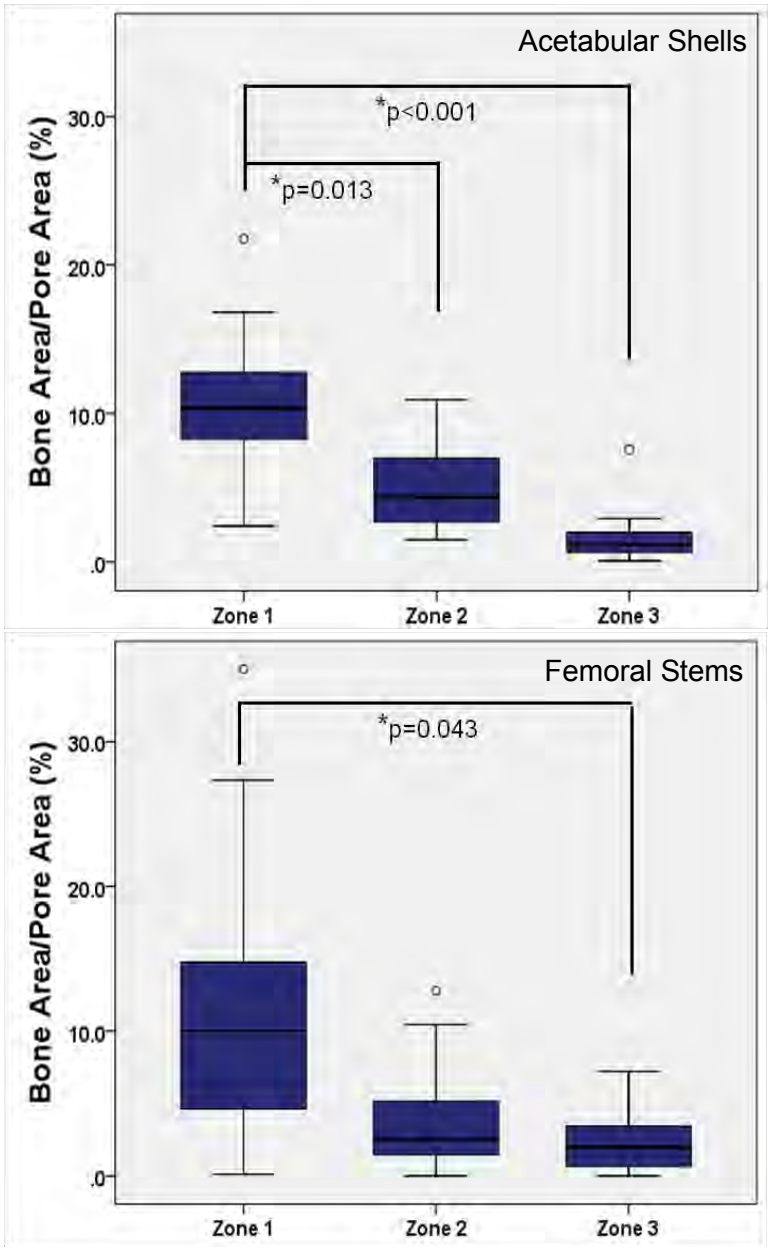

Figure 2-11: Comparison of bone area/pore area depth analysis for the acetabular shells and femoral stems.

There were 9 (45%) acetabular shells and 2 (29%) femoral stems that had bone fully bridge the porous tantalum layer in local areas (Figure 2-12).

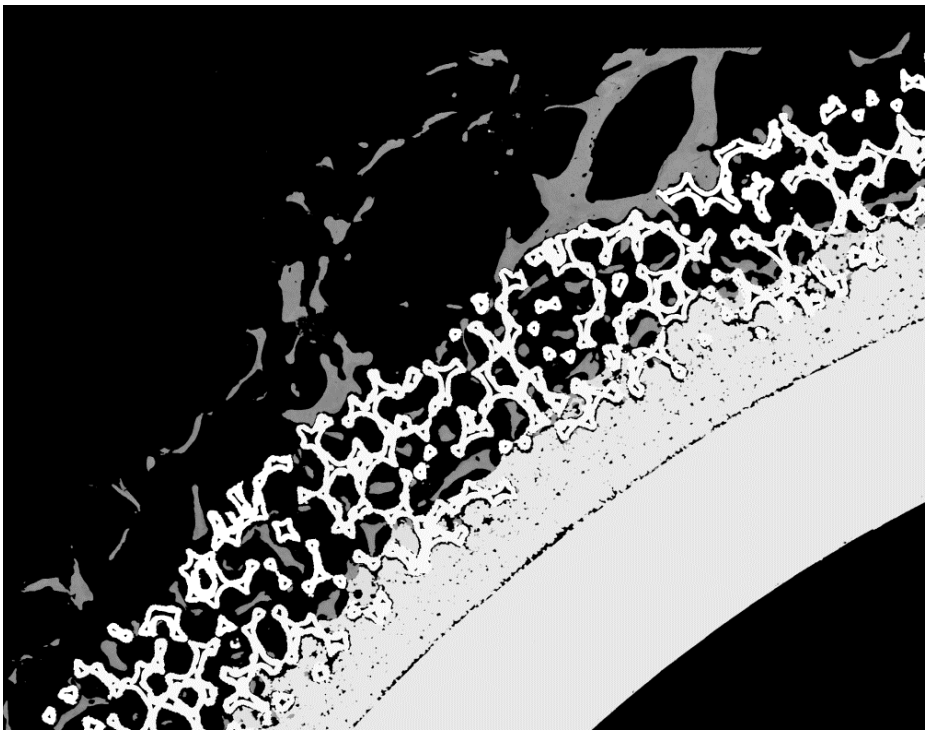

Figure 2-12: Bone bridging entire depth of the porous tantalum layer on the superior surface. This shell was implanted in a 57 year old female for 4.0 years.

For acetabular shells with screw holes, bone ingrowth was observed surrounding the screw holes in 22/33 sections. Bone ingrowth was primarily located in the curved medial and lateral portions of the femoral stem (Figure 2-13).

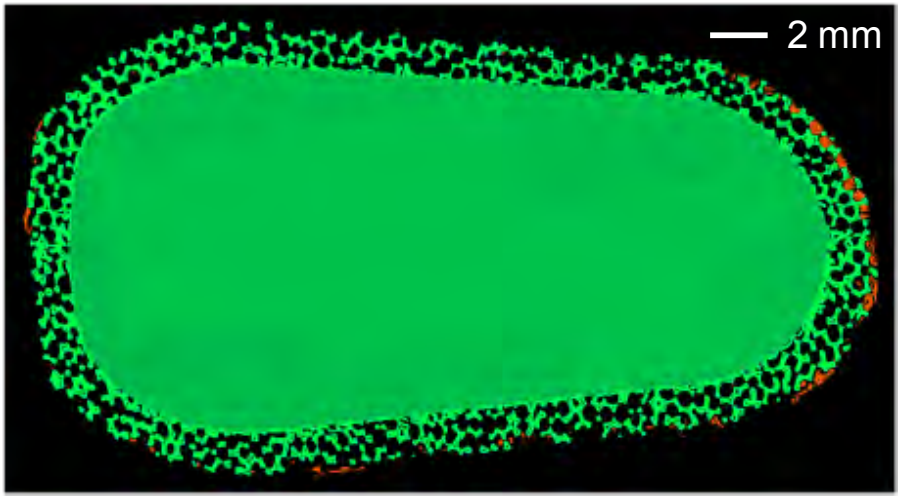

Figure 2-13: Fixation was preferentially located in the curved medial and lateral portions of the stem. This component was implanted in a 61 year old female for 0.1 years.

Immature woven bone formation was observed in multiple femoral stem implants (Figure 2-14). Although indicative of continuing integration of the component, this material was not included in the analysis of ingrowth unless it exhibited a degree of mineralization that was comparable to the regions of mature bone.

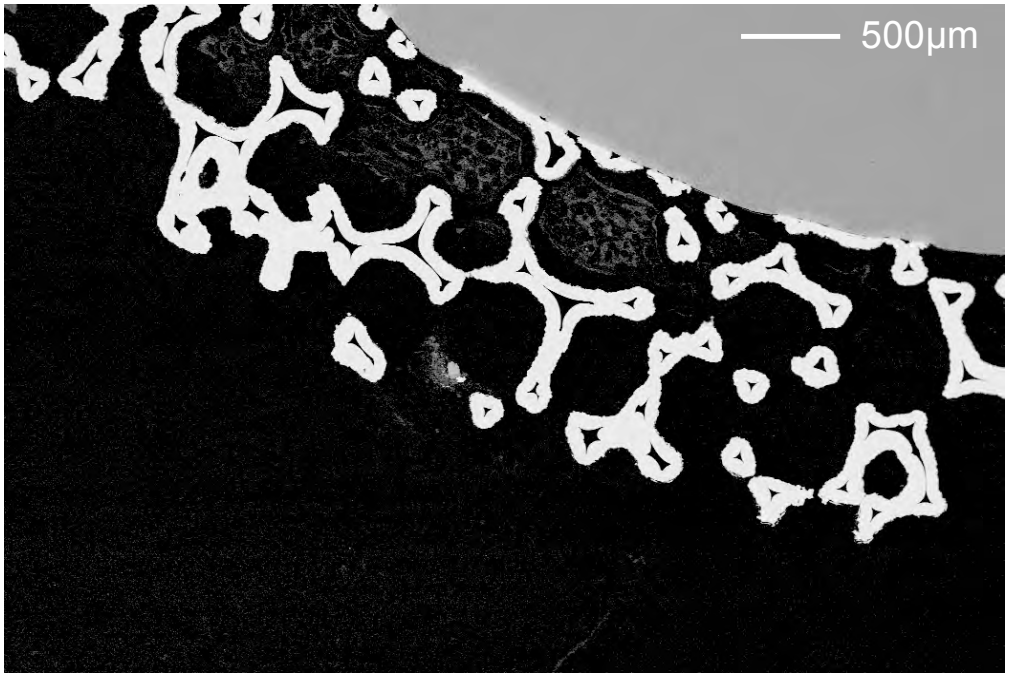

Figure 2-14: Immature woven bone was observed in multiple locations and implants.

None of the investigated clinical or patient factors correlated with bone ingrowth. All bone analysis measurements were similar between acetabular shells from primary surgeries and revision surgeries. For the acetabular shells, there was no significant relation between implantation time, patient weight, patient height and activity level and bone ingrowth. The femoral stem bone ingrowth was not significantly associated with any clinical or patient factors.

Discussion

This multi-center study evaluated implant and clinical factors affecting bone ingrowth into porous tantalum acetabular shells and femoral stems. There have been many clinical studies on porous tantalum acetabular shells [168-171, 173], however none of femoral stems. The clinical results of the porous tantalum acetabular shells have been promising with limited revisions due to acetabular loosening. There have been only a few retrieval analysis studies on porous tantalum acetabular shells and femoral stems. Our results show that implant type (acetabular shell vs femoral stem) and clinical factors were not significantly associated with the amount of bone ingrowth in retrieved porous tantalum hip implants. We did show that the bone ingrowth depth could vary within the coating as bone growth was highest in the superficial 500 μm of the porous tantalum for both implants.

This study had several limitations. We were only able to collect a limited number of femoral stems (n=7). Only 40% (8/20) of the acetabular shells analyzed for bone ingrowth had implantation times greater than 2 years and, thus, we were limited to observation of short-term implants. The implants analyzed were not postmortem retrievals and may not be representative of well-functioning implants. Additionally, the implant removal procedure can negatively affect the amount of adhered bone through mechanical damage.

We compared our acetabular shell and femoral stem bone ingrowth results to historical porous coating surfaces. Our acetabular BA/PA (3.6 ± 3.3%) was similar to a previous retrieval study of sintered titanium mesh (3.8 ± 8%) [231], however it was lower compared to postmortem studies that investigated cancellous-structure titanium (12 ± 6%) [237] and sintered beads (13%) [1]. Differences in BA/PA between porous tantalum and historical porous coatings may be due to porosity of the coating, implantation time, measurement techniques, or other factors. To account for differences in porosity, the BA/PA can be scaled or multiplied by its porosity to calculate the bone per unit of total area. After the adjustment, the bone in the porous tantalum acetabular shells (2.7%) is higher than the sintered titanium mesh (1.9%), however, still lower than cancellous-structured titanium (6.1%) and sintered beads (5.2%).

We also compared our femoral stem results to historical porous coatings. Our femoral stem BA/PA was significantly lower (5.8 ± 3.9%) than two previous studies of sintered titanium mesh (26.9 ± 17.6%) [6] and plasma coating with Hydroxyapatite (HA), which had BA/PA of (29.1 ± 2.0%) [28]. Even when the BA/PA was adjusted for the pore area, the bone ingrowth into the porous tantalum (4.4%) femoral stems was still lower than the sintered titanium mesh (13.5%) and plasma coating with HA (13.1%). The average implantation time for the sintered titanium mesh (3.8 years) [6] and plasma coating with HA (4.5 years) [28] were higher than the tantalum stems (0.3 years). The available depth for bone ingrowth in the tantalum (1.8 mm) is significantly higher than the sintered titanium mesh (1.7 mm) [6] and plasma coating (0.5 mm) [28].

Bone ingrowth into the porous tantalum acetabular shells differed based on location. Bone ingrowth in zone 1, the superficial 500 μm of the porous tantalum was significantly higher than zone 3. Bone ingrowth was particularity dense in regions adjacent to screw holes, similar to a previous study [231].

There was no significant relation between location and bone ingrowth into the femoral stems when the comparing proximal, central and distal regions, which is similar to a previous study of sintered titanium mesh coated femoral stems [6]. However, a different study of hydroxyapatite plasma sprayed femoral stems showed a higher amount of bone ingrowth in the distal region compared to the proximal and central regions [28].This may be due to the porous tantalum coating which is limited to proximal region of the overall stem and that we were only able to analyze seven stems. The higher amount of bone in the medial may be due to the higher loading and contact at the bone-implant interface. The bone concentrated in the curved regions of the femoral stem may also be to the increase in stress on the bone due to the curvature of the stem.

In our study, bone ingrowth measurements for both the acetabular shells and femoral stems did not correlate with available patient factors, however results from previous studies of other porous-coated implants have been mixed [6, 28, 231]. Bone ingrowth into the acetabular shells and femoral stems was not significantly related to the available clinical data: implantation time, age, height, weight, UCLA Activity Score. Bone ingrowth in our study may have not correlated with patient factors due to the limited number of implants analyzed and patient variability. In order to account for patient variability, a larger number of implant would need to be analyzed. One of the limitations of retrieval analysis is the number of implants to be analyzed due to resources and costs. A previous study of sintered titanium mesh acetabular shells showed that BA/PA ($r=0.86$, $p<0.001$) and extent ($r=0.80$, $p<0.001$) increased with implantation time in acetabular shells [231]. Our femoral stem bone ingrowth did not correlate with implantation time, similar to a previous study of 21 plasma coating with HA femoral stems [28]. The lack of correlation between implantation time and bone ingrowth measurements for the porous tantalum stems may be due to their short-term implantation time of 0.3 years. A different study of femoral stems with plasma coating

with HA that implantation time and BA/PA correlated with implantation time (r=0.48, p=0.02) [6].

In conclusion, our study showed that bone ingrowth was primarily observed in the superficial 500 μm (zone 1) of short-term porous tantalum acetabular shells and femoral stems. BA/PA was highest in the superficial 500 μm (zone 1) for both implants. This may provide the opportunity to reduce the thickness of the porous substrate in future designs. The findings of our study are specific to porous tantalum acetabular shells and femoral stems. Future studies that analyze long-term results will yield further insight into the clinical performance of porous tantalum hip implants.

Part 2: Determine Factors Affecting Bone Ingrowth in Retrieved Porous Tantalum Knee Implants

Abstract

There are two different porous tantalum tibial trays designs, one monoblock (UHMWPE backed) and one metal (Titanium) backed. This study investigated effect of implant design, spatial location and clinical factors on bone ingrowth. Six patellas and twenty-four porous tantalum tibial trays (three modular and twenty-one monoblock) were evaluated for bone ingrowth. Nonparametric statistical tests were used to investigate differences in bone ingrowth by implant design, tray spatial location, substrate depth and clinical factors. Modular trays (5.3 ± 3.2%) exhibited higher bone ingrowth than monoblock trays (1.6 ± 1.9%, $p = 0.032$). Bone ingrowth in both designs was highest in the initial 500 μm from the surface. Implantation time was positively correlated with bone ingrowth for monoblock trays.

Introduction

Although cemented fixation is considered the gold standard for total knee arthroplasty (TKA) [97, 99], some cementless tibial components have been clinically successful [238-243]. Revision reasons of first generation cementless tibial components include tibial loosening, particle migration through screw holes, and particle induced osteolysis [227, 244-247]. New materials and cementless designs have been proposed to address loosening due to stress shielding and breakdown of the cement mantle [152]. One of these coatings, made of tantalum, is designed with a high porosity (75-85%), with potential for increased bone ingrowth. It has favorable frictional properties ($\mu = 0.88$) to reduce micromotion between the bone and tray, and a low elastic modulus (2.5–3.9 MPa) to reduce stress shielding [151, 153, 164].

There are two types of NexGen® ® (Zimmer, Inc., Warsaw, IN) porous tantalum tibial trays that are currently clinically available. The monoblock design consists of a porous tantalum ingrowth surface with an ultra-high molecular weight (UHMWPE) bearing surface compression molded into it and two hexagonal porous tantalum pegs for initial stability. This monoblock design was intended to prevent backside wear, which may reduce long-term UHMWPE particle burden [181, 248]. An alternate design, the porous tantalum modular component, consists of a titanium alloy modular tray with a porous tantalum layer that also includes two hexagonal pegs. This design includes a central boss (small circular peg) in the central posterior of the tray that is used with a lock down screw.

Several clinical studies and one registry study of the porous tantalum tibial tray have shown no cases of tibial loosening [177, 179-181]. In a recent study using the Finnish registry with seven year follow-up there were no reported revisions due to aseptic loosening in 1143 patients with a monoblock porous tantalum tibial tray [181]. Studies of porous tantalum tibial trays have shown stabilization of components at 2 and 5-year follow-ups despite initial migration [177, 179, 180]. The initial studies of lower cases of aseptic loosening may be due to increased bone ingrowth. However, there has been one case study of a porous tantalum tibial tray, which showed preferential bone ingrowth in the peg region [183]. Additionally, no study has compared the bone ingrowth performance between the modular and monoblock porous tantalum tibial trays. Finally, there has been no retrieval study characterizing the amount of bone ingrowth in porous tantalum patellar implants.

The effect of implant design (patella vs tibial tray, modular vs monoblock), spatial location within an implant and implantation time or other clinical factors on bone ingrowth into porous tantalum tibial knee implants remain unknown. Therefore, the goal of this study was to investigate in vivo bone ingrowth in retrieved monoblock and modular

porous tantalum tibial tray implants. The first objective of this study was to determine the effect of implant design and spatial location within a porous tantalum tibial tray on bone ingrowth. The second objective was to determine if implantation time or patient factors correlated with bone ingrowth. We hypothesized that bone ingrowth will be different in the two tibial tray designs due to differences in elastic modulus of the two designs. We also hypothesized that bone ingrowth would not grow into the full depth of the substrate. Finally, we hypothesized that bone ingrowth would correlate with clinical or patient factors.

Methods

Porous tantalum tibial trays (NexGen® ® Trabecular Metal™; Zimmer Inc, Warsaw, Indiana) were retrieved during revision surgery under an IRB-approved multicenter retrieval program. Between 2003 and 2014, 11 patellar implants, 4 modular tibial trays (2 CR-Flex and 2 LPS-Flex) and 41 monoblock tibial trays (8 CR-Flex and 33 LPS-Flex) were collected (Figure 2-15). Six of the patellas were from primary surgeries. All of the tibial trays were revised following primary surgeries, except for one modular and one monoblock tibial. Clinical data consisting of age, height, weight, implantation time and reason for revision were obtained for each patient (Table 2-2).

Table 2-2: Summary of patient demographics for the patellas and tibial trays.

Implant Type	Implantation Time (Y)	Patient Age (Y)	Weight (Lbs)	UCLA Activity Score
Patella (N=11)	1.4 ± 2.0 (0.3 – 7.3)	61±9 (48-77)	206±50 (128 - 315)	5±2 (2-10)
Modular (N=4)	1.9±1.2 (0.3-3.2)	59±4 (55-63)	169±18 (144-185)	4±2 (3-6)
Monoblock CR-Flex (N= 8)	1.0±0.3 (0.6-1.4)	53±6 (46-63)	210±32 (162-270)	3±1 (2-4)
Monoblock LPS-Flex (N=33)	2.5±2.7 (0.2-12.8)	57±10 (36-78)	227±53 (122-330)	5±2 (2-10)

Values are expressed as mean±SD, with range in parentheses.

Revision operative reports were reviewed to verify the reason for revision and if loosening was noted by the revising surgeon.

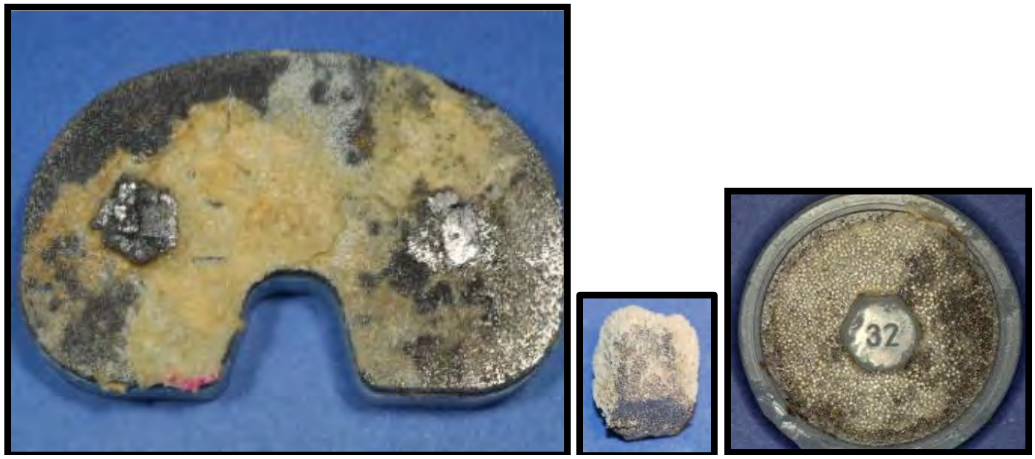

Figure 2-15: A retrieved tibial tray (left), tibial tray peg (center) and patellar implant (right).

The patellas were implanted for 1.4±2.0 years. The tibial trays were implanted for 1.9±1.2 years (modular), 1.0±0.3 years (monoblock: CR-Flex) and 2.5±2.7 years (monoblock: LPS-Flex). The average age of patients at implantation was highest in the modular tibial trays (59±4 years) and lowest in the monoblock: CR-Flex (53±6 years). The average weight of the patients was highest in the monoblock: LPS-Flex tibial trays (227±53 lbs) and lowest in the modular tibial trays (169±18 lbs). The patients in this study on average had a mildly to moderately active lifestyle as determined by UCLA Activity Score (Table 2-2).

The patellas were primarily revised for patellar loosening (45.5%, n=5), instability (18.2%, n=2) and femoral loosening (18.2%, n=2). The modular CR-Flex tibial trays were revised for tibial loosening (n=1, 50%) and unresurfaced patella (n=1, 50%). The modular LPS-Flex tibial trays were revised for infection (n=1, 50%) and stiffness (n=1, 50%). The monoblock CR-Flex components were revised for instability (n=3, 37.5%), malalignment (n=2, 25%), arthrofibrosis (n=1, 12.5%), infection (n=1, 12.5%) and internal rotation of tibial component (n=1, 12.5%). The reasons for revision of the monoblock LPS-Flex components were instability (n=15, 45.5%), infection (n=5, 15.2%),

femoral loosening (n=4, 12.11%), pain (n=2, 6.1%), periprosthetic fracture (n=2, 6.1 %), tibial subsidence (n=2, 6.1 %), arthrofibrosis (n=1, 3.0%) femoral component overhang (n=1, 3.0%) and tibial loosening (n=1, 3.0%).

Out of the collection, 6 patellas, 3 modular (1 CR-Flex and 2 LPS-Flex) and 21 monoblock (3 CR-Flex and 18 LPS-Flex) implants were selected to be analyzed for bone ingrowth. Patellas from revision surgeries and cemented patellas were excluded. One modular tray was excluded as it was collected after a fourth revision surgery. The selected tibial trays were implants from primary surgeries with favor given to the trays that were retrieved together with their pegs (in some cases, the pegs are left in the patient). Seven of the monoblock tibial trays with associated pegs were analyzed and reported in a previous study [249]. The original study lacked power (p=0.28) to investigate differences in bone ingrowth due to spatial location (central, lateral, medial and peg). The current study increased the power (p=0.82) for the spatial location analysis and also allowed for comparison of design (modular vs monoblock). Analyzed patellas were implanted for 0.9±0.5 years. Analyzed trays were implanted for 1.8±1.5 years (modular), 1.3±0.2 years (monoblock: CR-Flex) and 1.9±1.5 years (monoblock: LPS-Flex). The implantation time, patient age, weight and UCLA score were not different between the overall collection and the analyzed implants.

The analyzed patellas were revised for instability (n=2, 33.3%), femoral loosening (n=2, 33.3%), infection (n=1, 16.7%) and arthrofibrosis (n=1, 16.7%). The three analyzed modular components were revised for infection, pain and stiffness. The analyzed monoblock CR-Flex components were revised for instability (n=2, 66.6%) and malalignment (n=1, 33.3%). The reasons for revision of the analyzed monoblock LPS-Flex were instability (n=9, 50%), infection (n=3, 16.7%), femoral loosening (n=2, 11.1%), pain (n=2, 11.1%), femoral component overhang (n=1, 5.6%) and periprosthetic fracture (n=1, 5.6%).

The process for sample preparation and bone ingrowth measurement were previously described (Chapter 2: Part 1, [249]). Briefly, each implant was dehydrated using increasing graded alcohols, embedded in polymethylmethacrylate (Polysciences and Sigma-Aldrich) and sectioned using a diamond wafering saw (Isomet 1000, Buehler, Lake Bluff, Illinois). Each section was ground flat, polished, sputter-coated and imaged using a scanning electron microscope (SEM, XL30 ESEM FEG, FEI, Hillsboro, Oregon and Supra 50 VP, Zeiss Peabody, Massachusetts) in backscattered electron mode. Three sections were analyzed from each patella (Figure 2-16). Six sections were analyzed from each tibial tray (2 medial, 2 central and 2 lateral) in addition to one central section for each available peg (Figure 2-16).

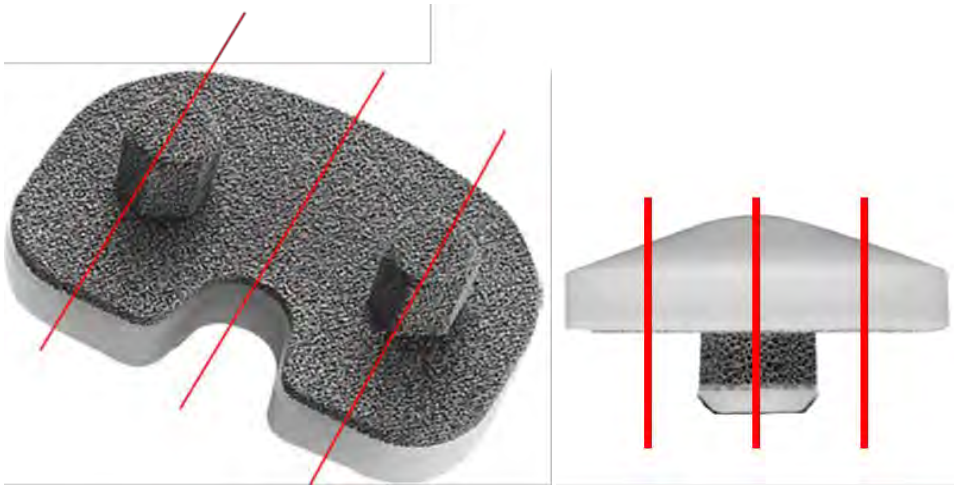

Figure 2-16: Location of serial cutting for tibial trays (left) and patellar implants (right)

The bone ingrowth analysis consisted of four major measurements: the bone area/pore area (BA/PA), extent of ingrowth, maximum depth of ingrowth and evaluation of the BA/PA by zone. BA/PA was defined as the fraction of available pore space within the porous coating that was occupied by bone. It is calculated by dividing the bone area (BA) divided by the pore area (PA) (Figure 2-17).

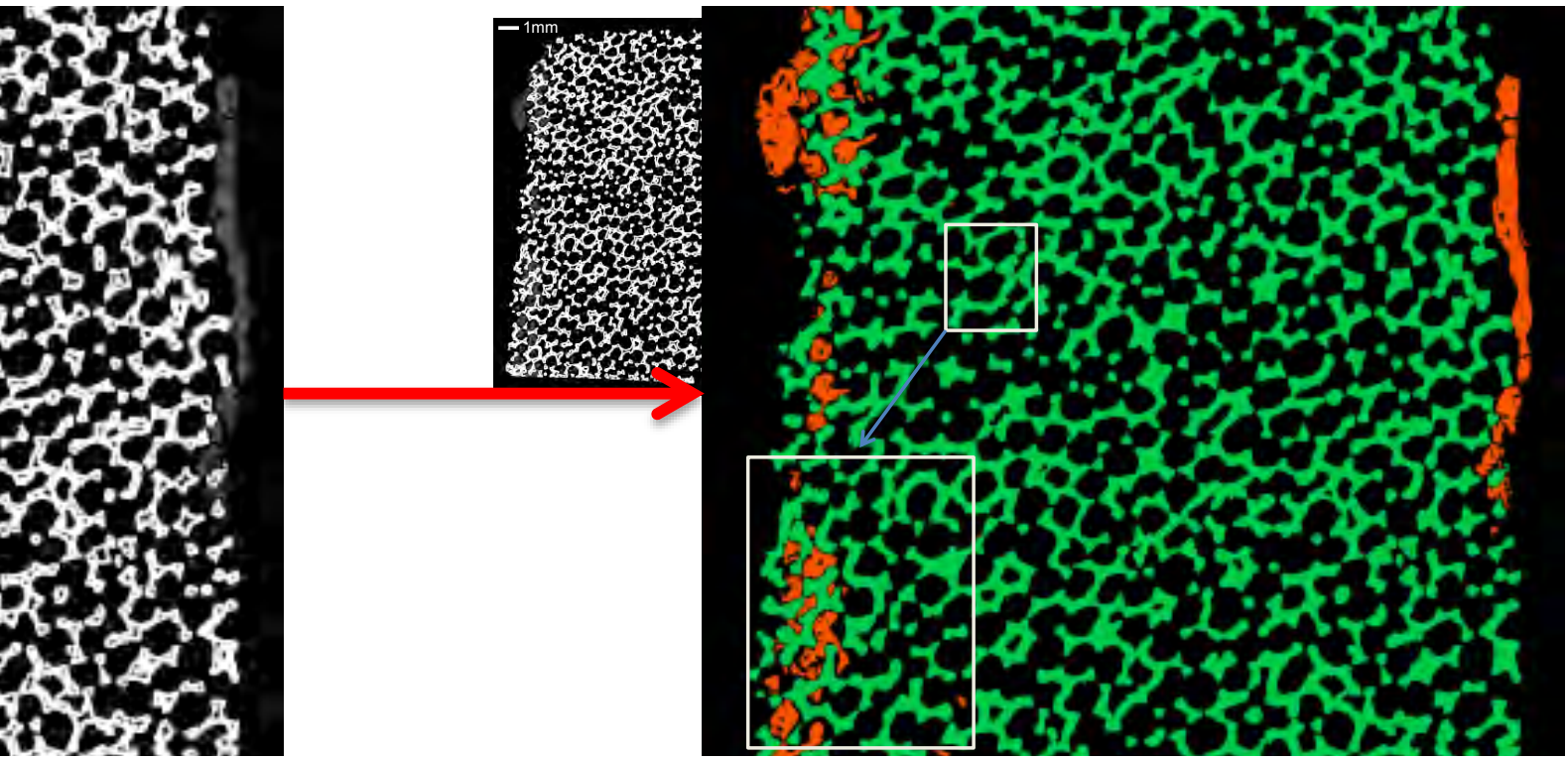

Figure 2-17: Representative image of Bone Area/Pore Area measurement for a tibial tray peg slice. The tantalum is green, bone is orange and black is available pore space.

The extent of bone ingrowth is a topological quantification of the distribution of bone ingrowth across the surface of the implant. The surface of the implant was divided into 1mm increments, in which each section was assessed for evidence of bone ingrowth penetrating into the surface of the implant. The extent of ingrowth was calculated as the number of sections with ingrowth divided by the total number of sections and expressed as a percentage (Figure 2-18).

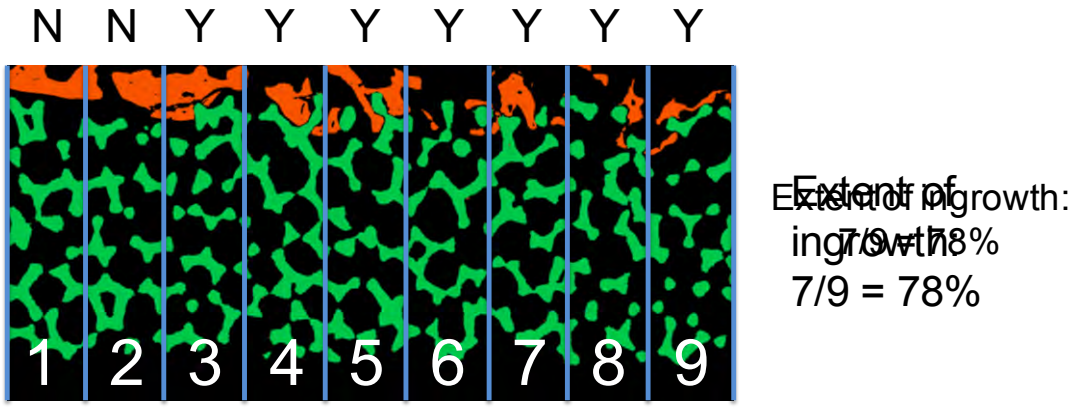

Figure 2-18: Representative image of extent of ingrowth measurement.

The maximum depth of ingrowth was defined at the deepest point where bone was observed in the porous tantalum substrate. The maximum depth was evaluated using two metrics. One is the actual maximum depth the bone grew into the substrate, measured in mm. The second measurement is the deepest point where bone was present in the substrate and was expressed as a percentage of the total available depth (Figure 2-19).

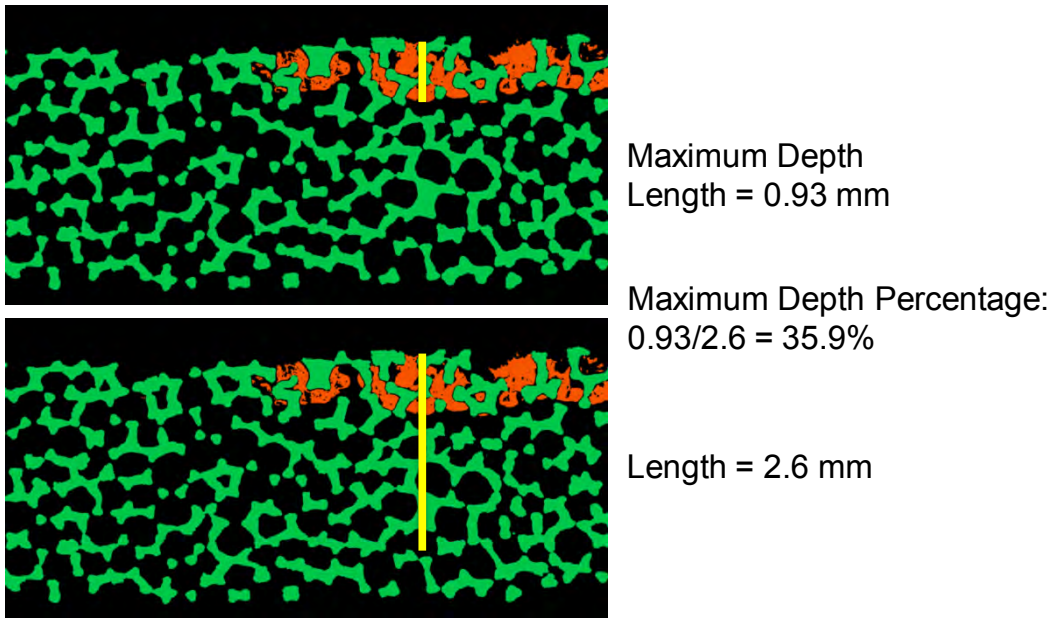

Figure 2-19: Representative image of maximum depth measurement.

The zones for BA/PA depth analysis were defined by depth as: zone 1 (0-500μm, superficial zone), zone 2 (500-1000μm) and zone 3 (1000μm - full depth) (Figure 2-20).

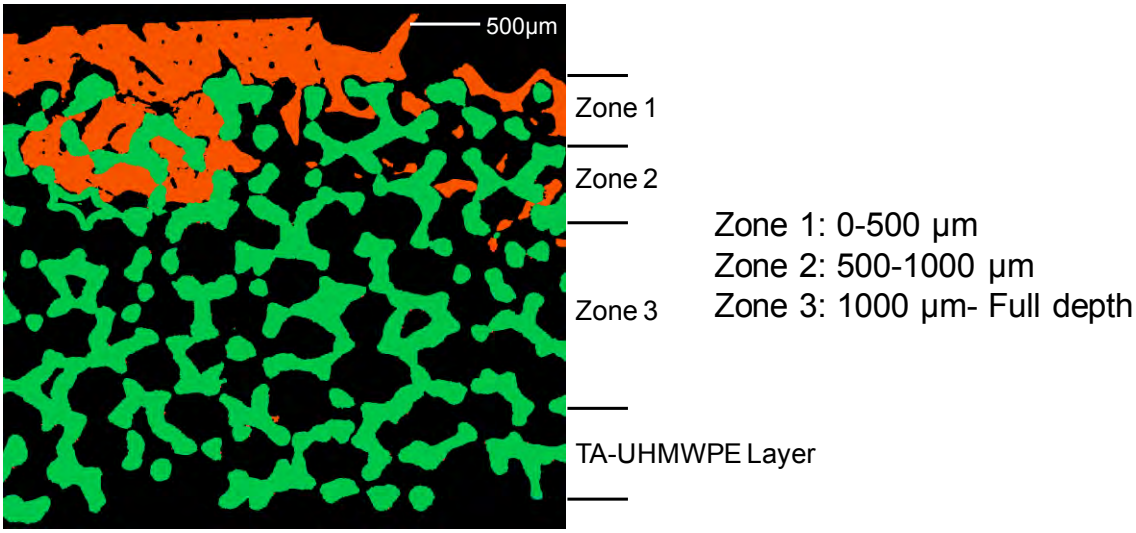

Figure 2-20: Representative image of BA/PA zonal analysis.

Following bone ingrowth analyses, five of the monoblock tibial trays were randomly chosen and histologically analyzed for presence of fibrous and bone tissue. For each implant, one central, lateral and medial section was histologically analyzed. Sections were ground down to 20 - 30 μm, polished and stained using Toluidine Blue and imaged under transmitted light microscopy at 5 and 10X using a Zeiss Axioplan (Zeiss, Oberkochen, Germany) microscope camera. Sections were analyzed to note location of regions with fibrous tissue or bone ingrowth.

Nonparametric statistical tests were used to investigate differences in BA/PA, extent of ingrowth and maximum depth by design (modular versus monoblock), spatial location within the implant (central, lateral, medial and peg) and depth (Related – Friedman's Analysis of Variance by Ranks, Independent – Kruskal-Wallis Test). Post-hoc Dunn tests were completed for subsequent pairwise comparisons. Spearman's rank order correlation was used to identify correlations between continuous variables

(implantation time, patient age, height, weight, UCLA Activity Score, BA/PA, extent of ingrowth and maximum depth). The level of significance chosen for all statistical analyses was $p<0.05$. All statistical tests were performed using PASW Statistics package (Version 22.0; IBM, Chicago, IL).

Results

Bone ingrowth measurements differed between the patellar implants and tibial trays. BA/PA was similar between the patellas (3.4 ± 4.0%) and tibial trays (2.0 ± 3.0%, p=0.240). Extent of ingrowth was significantly different between the patellas (40 ± 32%) and tibial trays (21 ± 21%, p=0.03). Maximum depth of ingrowth was similar between the patellas (1.1 mm, 45%) and tibial trays (1.6 mm, 61%, p=0.217).

BA/PA was different between for the modular and monoblock implants. The total BA/PA from the modular tray sections (5.3 ± 3.2%) was higher when compared to the monoblock tray (1.6 ± 1.9%, p=0.032, Figure 2-21). However, for the other bone measurements there was no difference between the modular and monoblock tray (extent: p=0.239 and maximum depth: p=0.127). The pegs of the modular and monoblock components were not different for bone ingrowth measurements (BA/PA: p=0.766, extent: p=0.655 and maximum depth: p=0.456, Figure 2-21).

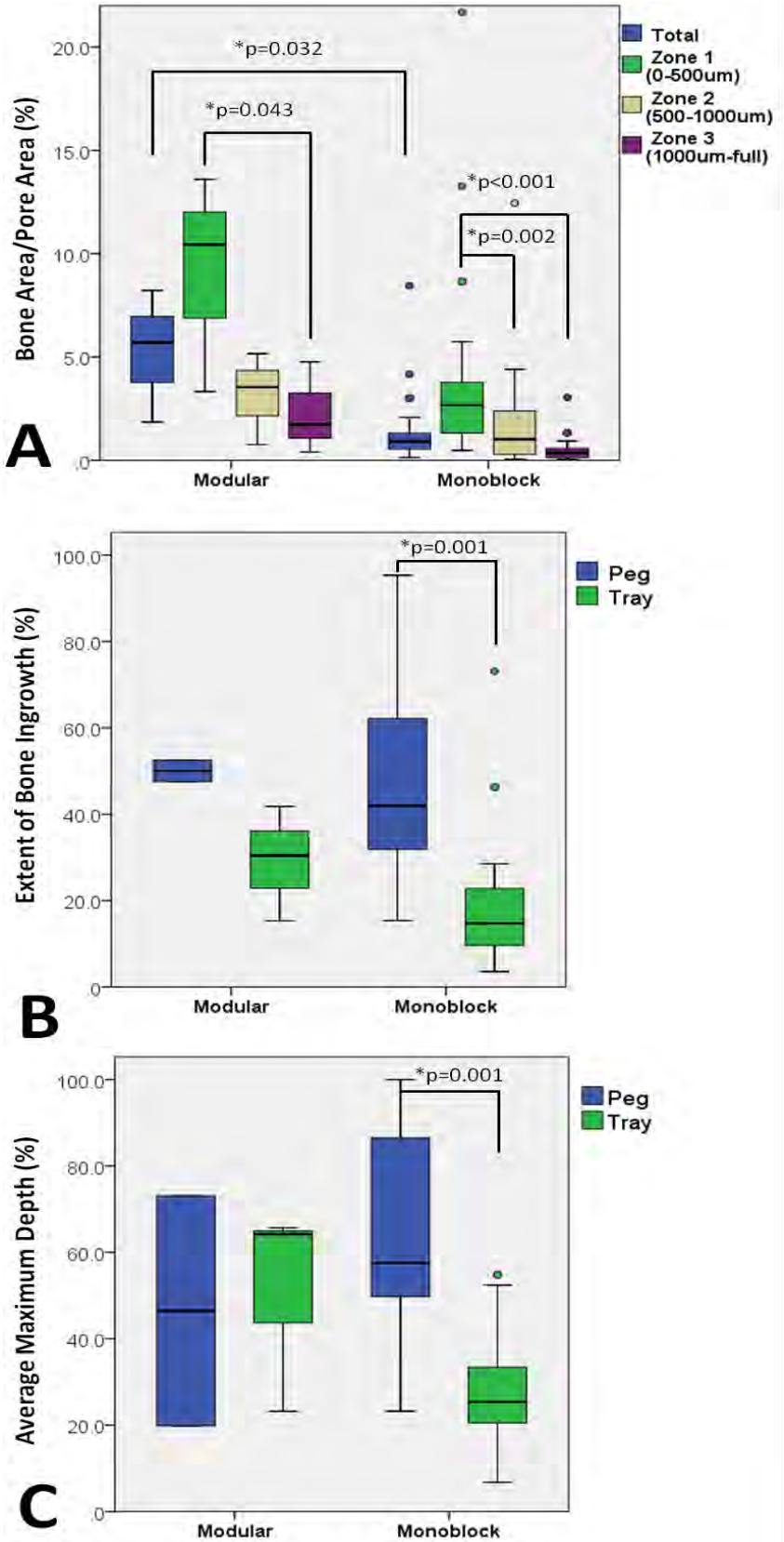

Figure 2-21: Comparison of modular tibial tray sections to monoblock tibial tray sections for (A) Bone area/Pore area, (B) extent of ingrowth and (C) average maximum depth.

Bone ingrowth into the porous tantalum tibial trays differed based on location. The bone ingrowth in the modular and monoblock tibial trays was highest in zone 1 (0-500 μm) of the tray sections. For example, BA/PA in the modular component trays was higher in zone 1 (9.1 ± 5.3%) compared to zone 3 (2.3 ± 2.2%, p=0.043) (Figure 2-21, Table 2-3). For the modular trays, there was no difference between the tray and pegs for total BA/PA (p=0.896), extent (p=0.145) and maximum depth (p=0.241). Total BA/PA was higher in the pegs (2.8 ± 2.5%) than the central tray (1.0 ± 1.3%, p=0.019) for the monoblock components. The monoblock peg had a higher extent of bone ingrowth and maximum depth than all the tray locations (Table 2-4). BA/PA in monoblock trays was higher in zone 1 (4.6 ± 5.4%) compared to zone 2 (2.0 ± 2.7%, p=0.002) and zone 3 (0.5 ± 0.7%, p<0.001, Table 2-4).

Table 2-3: Bone ingrowth measurements for modular tibial trays.

Modular Implants				
Location	BA/PA Total (%)	Extent (%)	Maximum Depth (%)	Maximum Depth (mm)
Central	4.1±3.1 (1.4-7.5)	37±16 (19-48)	41±35 (14-80)	0.5±0.4 (0.2-1.0)
Lateral	5.3±2.7 (2.2-6.9)	25±14 (9-34)	69±26 (41-91)	0.8±0.3 (0.5-1.1)
Medial	6.4±7.0 (2.0-14.5)	26±15 (16-43)	43±43 (15-93)	0.5±0.5 (0.2-1.1)
Peg	2.1±0.4 (1.9-2.4)	50±4 (48-53)	47±38 (20-73)	0.6±0.5 (0.2-0.9)

Values are expressed as mean±SD, with range in parentheses.
There were no differences between tray locations and the peg.
Bone area/pore area is denoted as BA/PA.

Table 2-4: Bone ingrowth measurements for monoblock tibial trays.

Monoblock Implants				
Location	BA/PA Total (%)	Extent (%)	Maximum Depth (%)	Maximum Depth (mm)
Central	1.0±1.3[c] (0.1-5.0)	20±23[a] (0-87)	22±21[b] (0-72)	0.6±0.5[b] (0.0-1.9)
Lateral	1.8±1.9 (0.1-6.3)	25±22[a] (0-76)	35±23[c] (0-90)	0.9±0.6[c] (0.0-2.3)
Medial	2.1±3.2 (0.1-14.1)	21±21[a] (0-88)	33±22[c] (0-71)	0.9±0.6[c] (0.0-1.8)
Peg	**2.8±2.5[c] (0.3-10.0)**	**51±25[a] (15-95)**	**62±24[b,c] (23-100)**	**1.6±0.6[b,c] (0.6-2.6)**

Values are expressed as mean±SD, with range in parentheses.
Bone measurements in bold were significantly higher than others and are denoted by the following:
a = p < 0.001, b = p < 0.01, c = p < 0.05.
Comparison a, b and c were made between implant locations (central, lateral and medial and peg).
Bone area/pore area is denoted as BA/PA.

All six analyzed patellas showed bone ingrowth. One patellar component was implanted in a 48-year old male for 0.7 years and showed full depth of ingrowth (Figure 2-22).

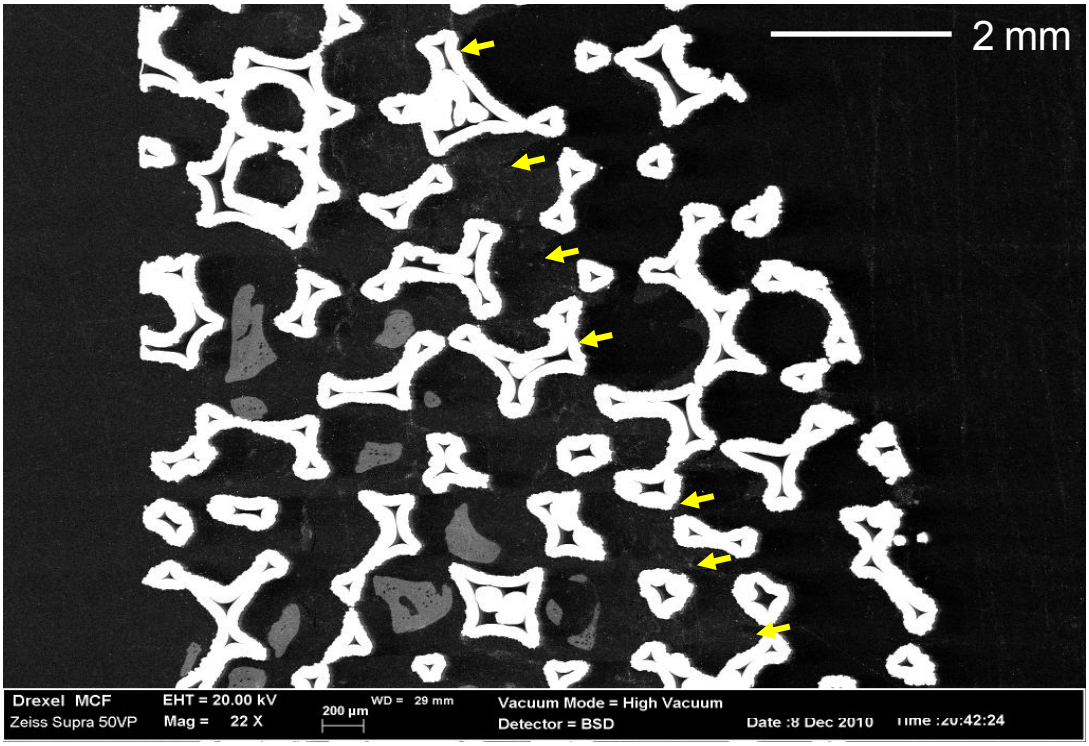

Figure 2-22: Localized bone bridging entire depth of the porous tantalum layer of a patella implant. The edge of the polyethylene layer is indicated by arrows.

In two of the patellar implants, there was dense superficial ingrowth into the peripheral region of the implant. One of these implants was implanted in a 54-year old male for 1.4 years showing a dense superficial layer of bone growth (Figure 2-23). One implant had limited ingrowth and was noted to have been used in conjunction with a femoral component that displayed fibrous fixation at revision.

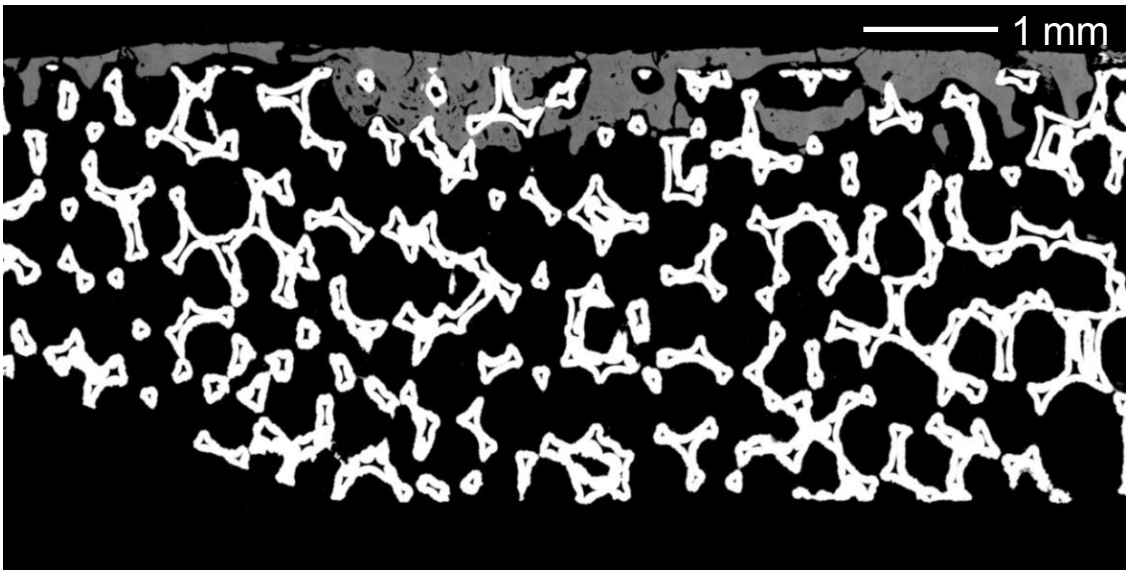

Figure 2-23: Superficial layer of dense trabecular bone integrated with the porous tantalum layer on the anterior surface.

One modular tray component had bone ingrowth spanning the full depth of the porous tantalum substrate (Figure 2-24). However, none of the monoblock components had bone spanning the full depth of the tray. There were 4 monoblock implants that had tibial tray sections that did not have any bone ingrowth while only one peg section had no bone ingrowth. Bone growth in the pegs was predominantly seen on the periphery (Figure 2-24).

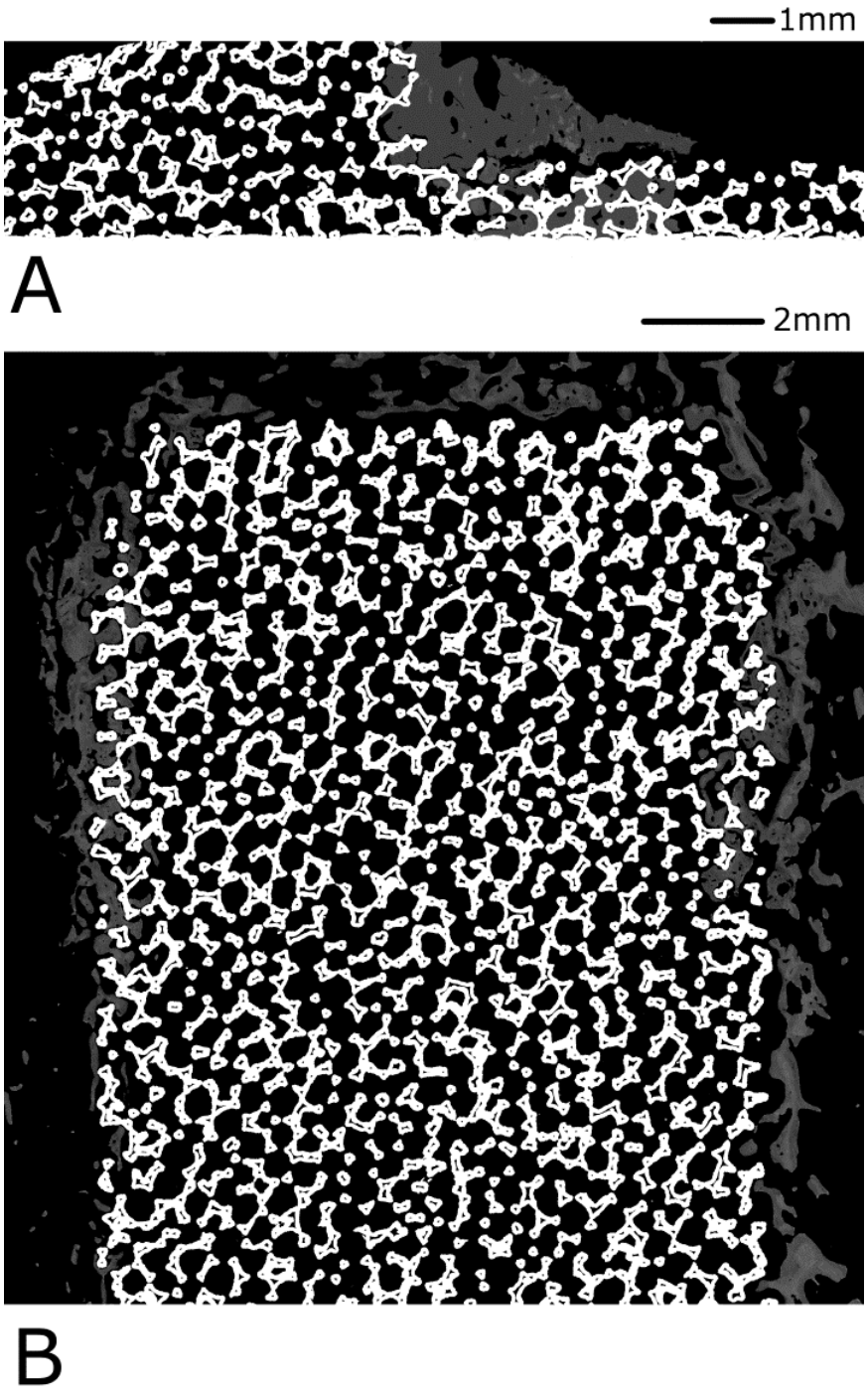

Figure 2-24: Back-scattered electron SEM images of (A) a modular tibial tray section and (B) a porous tantalum peg. Note: Bone ingrowth is located on the periphery of the peg and full ingrowth into the modular tray section. The porous tantalum substrate is white, the bone is gray and the black is the pore area.

There was evidence of bone being pulled away from the porous tantalum substrate during revision surgery (Figure 2-25).

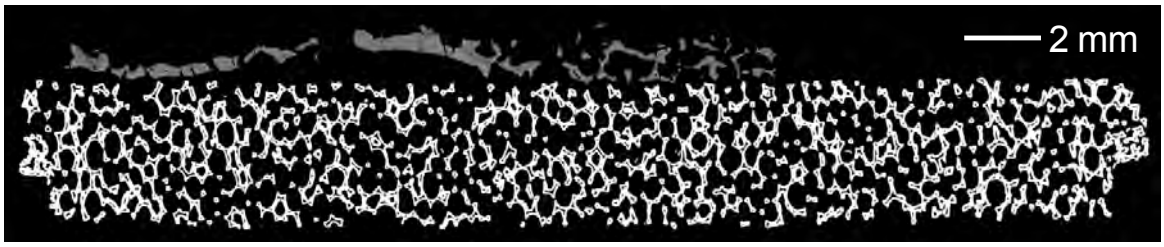

Figure 2-25: A tibial tray implant showing a superficial ongrowth layer. Note: Possible bone pulled from the substrate layer during removal surgery.

Histological assessment of a tibial tray

Although only one sample was fixed in formalin, non-formalin fixed tibial tray and peg slices were used to develop the histological protocols. There was evidence of bone being pulled away from the porous tantalum substrate during revision surgery. Fibrous tissue was seen throughout the tibial tray (Figure 2-26).

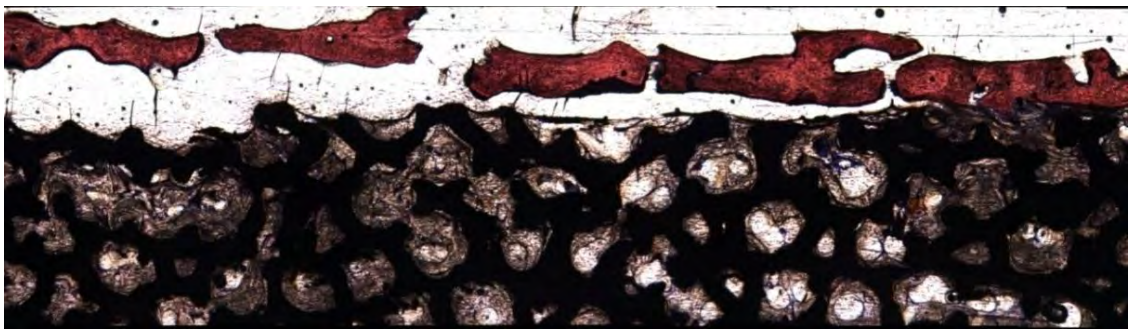

Figure 2-26: Histological images of a tibial tray slice. Note: Bone disrupted from implant and fibrous tissue.

The histologically assessed monoblock implant showed dense fibrous tissue in the center of the peg and in the tray slices where bone was limited (Figure 2-27).

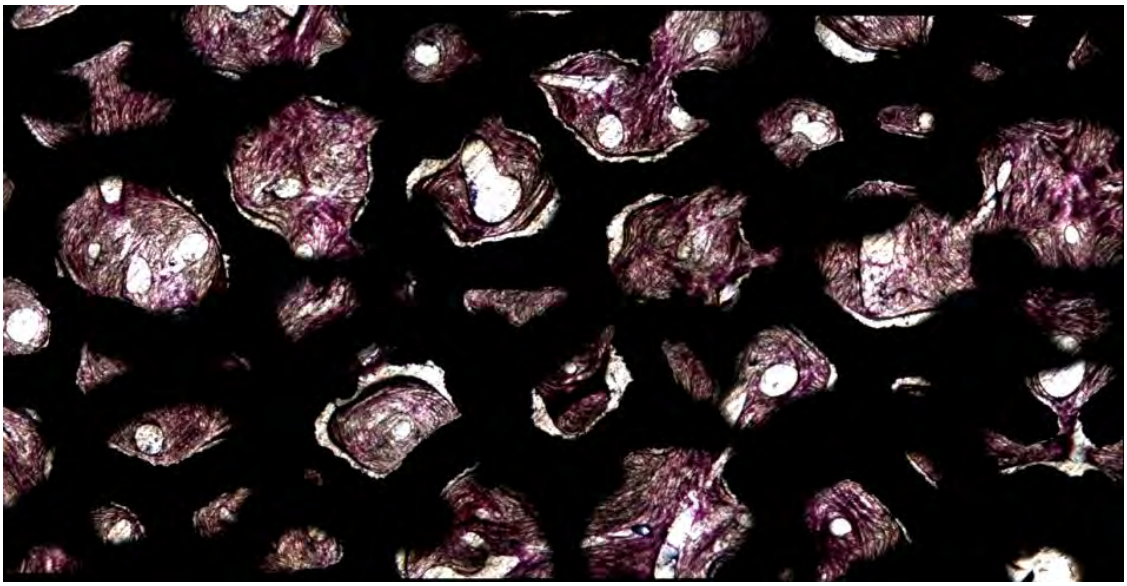

Figure 2-27: Fibrous tissue present in the center of porous tantalum peg.

For the pegs, bone was located on the outer periphery and fibrous tissue was prevalent throughout the center region (Figure 2-28).

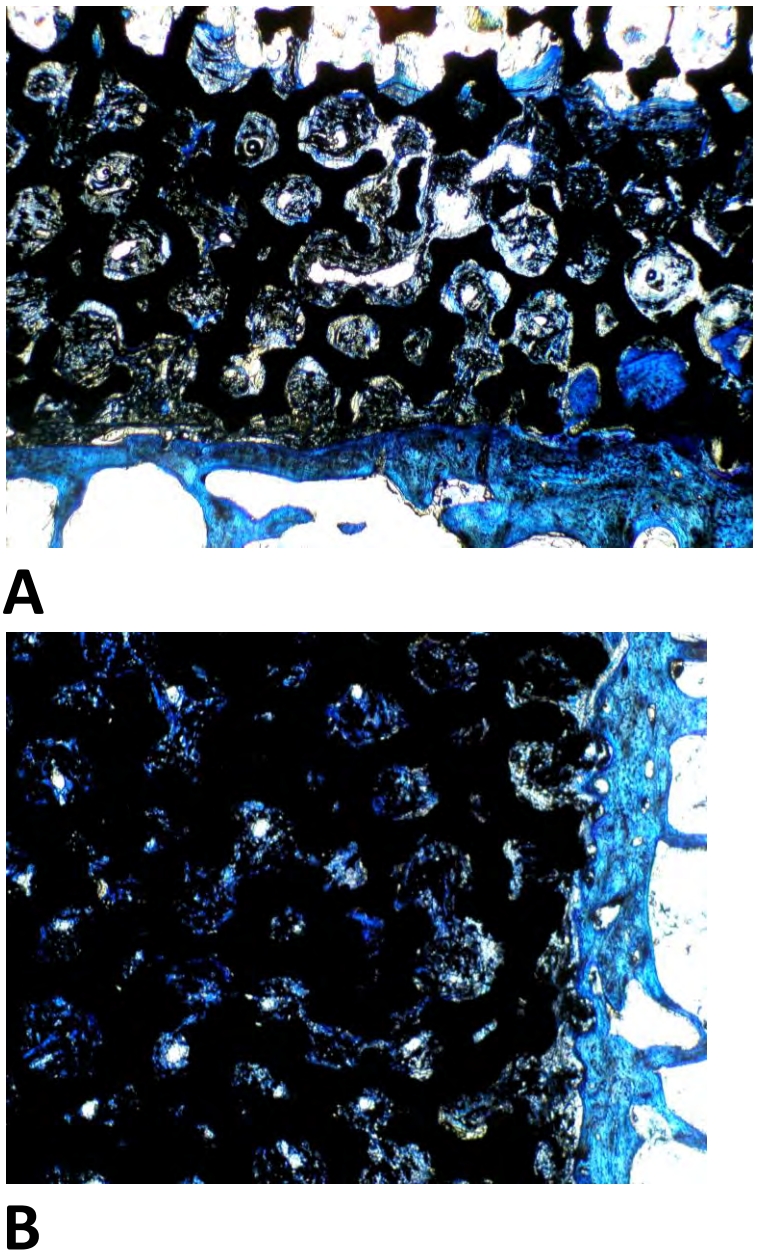

Figure 2-28: Light microscopy images of A) tibial tray with fibrous tissue ingrowth into the full depth of the substrate (5X) B) peg with dense fibrous tissue in the center and bone on the periphery (10X).

There was a high amount of bone at the corners of the pegs. The bone was replaced by the fibrous tissue fixation moving further into the porous tantalum substrate (Figure 2-29).

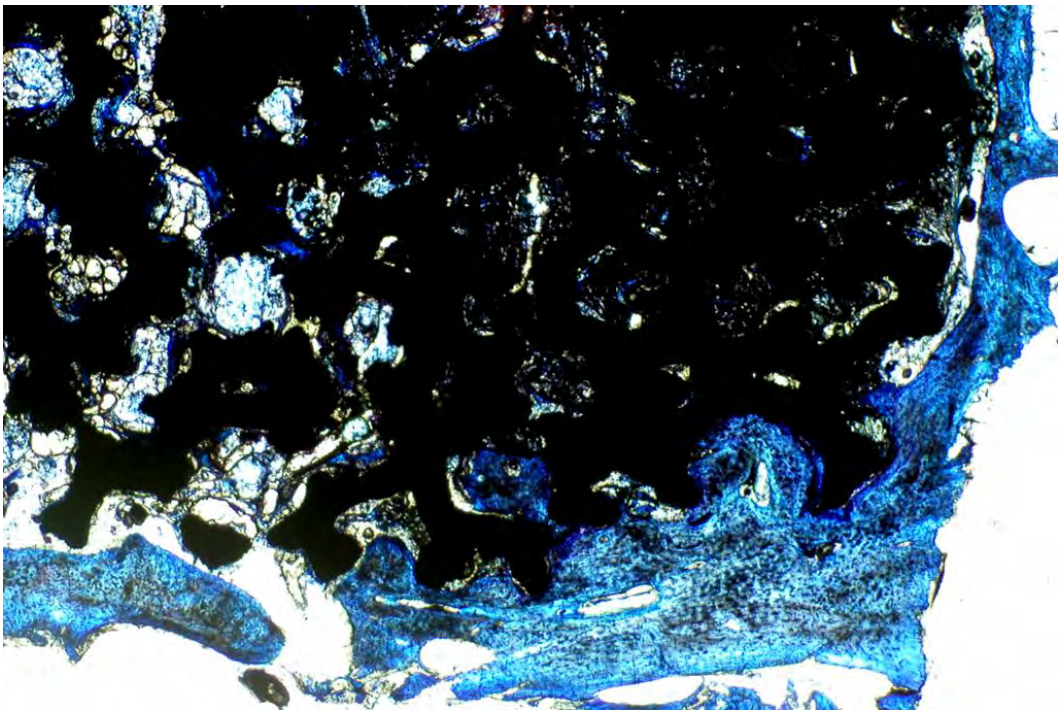

Figure 2-29: Concentrated bone ingrowth on the corner of the pegs with fibrous tissue present in the center.

Vascularized bone was seen at the corner of the pegs (Figure 2-30).

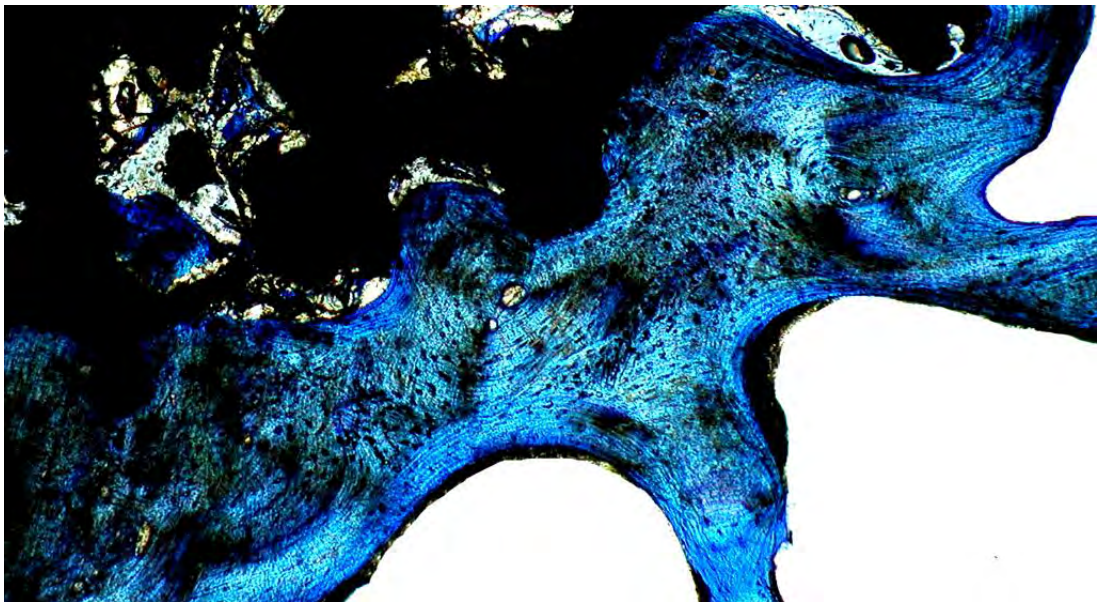

Figure 2-30: Vascularized bone around the corner of the peg.

For the monoblock tibial tray, implantation time was correlated to total BA/PA (Spearman's Rho=0.547, p=0.01), extent of ingrowth (Spearman's Rho=0.488, p=0.025) and maximum depth (Spearman's Rho=0.497, p=0.022). There were no correlations between clinical or patient factors and bone ingrowth measurements for the monoblock tibial trays [age (ρ=0.256, p=0.263), BMI (ρ=0.137, p=0.173), gender (p=0.385), weight (ρ=0.301, p=0.185) and UCLA (ρ=0.074, p=0.762)]. For the modular tibial trays, bone ingrowth did not correlate with implantation time and clinical factors.

Discussion

Highly porous metallic surfaces have been used to support biological fixation of implants. The potential advantages of porous tantalum include enhanced initial fixation and retention of bone stock through reduced stress shielding. Porous tantalum is used in cementless fixation due to its increased porosity, coefficient of friction and decreased elastic modulus. Retrieval analysis studies of porous tantalum tibial trays have been limited [183, 249]. The aim of this study was to examine some possible factors that may affect bone ingrowth in retrieved porous tantalum tibial trays. We found that retrieved modular tibial trays had a higher percentage of bone area/pore area (BA/PA) than the monoblock trays. We also found that BA/PA was highest in the superficial layer (zone 1) of the tibial tray implants. Bone ingrowth measurements correlated with implantation time for monoblock tibial trays but not the modular tibial trays.

This study had several limitations. We were able to collect a large number (n=41) of monoblock tibial trays; but only a small number (n=4) of modular tibial trays. Our retrievals were not retrieved post-mortem and therefore may not be representative of a well-functioning component. The revision procedure can potentially affect the amount of observed ingrown bone in the substrate due to mechanical damage. Finally, the time of implantation for these cohorts of retrieved implants is short-term where only 5 implants

analyzed for bone ingrowth were implanted greater than 3 years. The strengths of our study include a high number of monoblock tibial trays were analyzed. This allowed us to investigate the effect of spatial location within the implant (central, lateral, medial and peg) and clinical factors on bone ingrowth.

Our reported BA/PA (3.5± 4.1%) and extent of bone ingrowth (41± 30%) for the patellas was lower than a previous postmortem study of well functioning cancellous-structured titanium patellar implants (BA/PA, 13± 9% and extent of ingrowth, 86 ±12%) [250]. The lower amount of bone ingrowth may be due to the difference in stiffness between the two designs. The porous tantalum patella implants are monoblock designs, while the cancellous-structured titanium is a metal-backed design.

Our reported BA/PA (5.3 ± 3.2%) for modular tibial trays was lower than a previously reported retrieval study of sintered titanium mesh (9.5%) [251], but similar to two postmortem studies that investigated cancellous-structured titanium (6% ± 2) [244] and sintered cobalt-chromium beads (6%) [252]. Additionally, one study that evaluated 34 cementless tibial components from various manufacturers reported an average of 3% BA/PA [253], which was lower than our reported BA/PA.

The BA/PA for the monoblock tibial trays was lower than these studies [244, 251, 253]. We found the tibial tray extent of bone ingrowth (modular: 29 ± 13% and monoblock: 22 ± 18%) to be similar to a retrieval study of sintered titanium mesh (27 ± 16%) [251], but lower than previous postmortem studies that evaluated cancellous-structured titanium (73 ± 17%) [244]. Differences in BA/PA between porous tantalum and historical porous coatings may be due to porosity, substrate depth and measurement techniques. To account for differences in porosity, each BA/PA can be scaled or multiplied by its porosity (ex: modular BA/PA*porosity = 5.3*0.75). After scaling, the amount of bone in the porous tantalum modular trays (4.0%) is lower than the sintered titanium mesh (4.3%), but higher than the cancellous-structured titanium (3.1%) and

sintered beads (2.4%). The scaled BA/PA for the porous tantalum monoblock (1.2%) is lower than the three historical coatings (sintered titanium mesh, cancellous-structure titanium and cobalt chromium beads). Measured bone ingrowth for tibial trays was lower than three historical porous coatings; however this also reflects the greater substrate porosity and depth.

BA/PA in the modular tibial trays was higher than the monoblock tibial trays. This is an initial finding as only 3 modular components were available for analysis. The difference in the number of modular compared to the monoblock components may be due to the market introduction date. The monoblock market introduction year was 2002, while the modular tibial trays market introduction year was 2007. The depth of the modular coating is 1.2 mm versus the monoblock coating which is 2.6 mm. BA/PA in Zone 1 was not different ($p=0.106$) between modular and monoblock trays. There could also be differences in tray stiffness between these two designs that could affect bone ingrowth.

Patient factors did not correlate with bone ingrowth for the patellas or the modular tibial tray implants. The monoblock tibial tray slices did correlate with implantation time. This may be due to the higher amount of monoblock tibial trays implants ($n=21$) compared to the modular tibial trays ($n=3$) and patellar implants ($n=6$).

Bone ingrowth into the porous tantalum tibial trays differed based on location. BA/PA in the modular and monoblock tibial trays was highest in the superficial layer of the tray sections (zone 1; 0-500 μm). This may be due to the BA/PA was higher in the pegs than the central monoblock tray sections. A previous study of sintered titanium mesh [251] showed higher BA/PA in the fixation pegs than the tray, similar to our monoblock tray findings. A case study of a porous tantalum tibial tray also showed a higher amount of bone ingrowth into the pegs compared to the tray sections [183]. The higher amount of bone ingrowth in the pegs compared to the central tray regions may be

to lower initial amount of bone in the central region of the tibial. This may be due to preferential initial apposition between the bone and pegs due to press-fit of the pegs. Taken together, these findings suggest that future porous tantalum coatings may not need to be as thick, as bone was preferentially located in the superficial layer (zone 1).

Bone ingrowth into the porous tantalum tibial trays did not correlate with patient factors, similar to a previous study [251], though bone ingrowth into the monoblock porous tantalum tibial trays was positively correlated with implantation time. In a previous study of sintered titanium mesh shells, implantation time was shown to be a significant factor of bone ingrowth [231]. This trend was not seen when the same group analyzed bone ingrowth into sintered titanium mesh tibial trays [251]. Similar to previous studies [231, 251], available patient factors did not correlate with the amount of bone ingrowth. However, one clinical study of porous tantalum tibial trays has shown cases of subsidence associated with specific patient factors (tall, heavy, male) [254]. Bone ingrowth was not correlated with implantation time for the modular trays. This may be due to the limited number available for analysis.

In conclusion, our study supports that the bone ingrowth focused primarily in superficial 500 μm (zone 1) of short-term porous tantalum tibial trays is suitable for solid fixation. The BA/PA highest in the superficial 500 μm (zone 1) may provide the opportunity to reduce the thickness of the porous layer thus conserving more bone in future designs. We present the amount of bone ingrowth necessary for solid fixation from 24 short-term porous tantalum tibial trays, in which none were revised for tibial loosening. Instability was the most common reason for revision for the monoblock components. A known limitation of the monoblock component is that the insert thickness cannot be modified after implantation. The findings of our study are specific to porous tantalum tibial trays and may not be representative of other cementless designs. One clinical trial (NCT01637051) is underway that may provide further information on the

comparative performance between the monoblock and modular components. Although retrospective studies and registry data have been positive for porous tantalum components, there have been no randomized controlled trials comparing outcomes after uncemented porous tantalum to cemented components. This may be difficult as a large number of knees may be necessary to power this study. Determination of the amount of bone ingrowth necessary for long-term (> 10 years) fixation of implants will yield further insight into the clinical performance of porous tantalum implants.

Summary

Highly porous metals have been developed to address aseptic loosening of hip and knee components. The potential advantages of porous tantalum are initial fixation and retention of bone stock. Porous tantalum is used in cementless fixation due to its increased porosity, coefficient of friction and decreased elastic modulus for bone-implant fixation. This multi-center study evaluated the clinical, patients and design factors affecting bone ingrowth into porous tantalum acetabular shells, femoral stems, patellas and tibial trays. There have been many clinical studies on porous tantalum implants, with limited cases due to loosening. The limited amount of cases of aseptic loosening in our retrieval studies (Chapter 1) and other clinical studies may be due to high amount of bone ingrowth. There have been only a few retrieval analysis studies on porous tantalum implants. We hypothesized that there will be differences in bone ingrowth between implant type and anatomic location within each implant. Additionally, we hypothesized that clinical and patient factors will affect the amount of bone ingrowth. For all implant types, the highest amount of bone ingrowth was seen in the upper 500 μm (Zone 1) of the porous tantalum substrate. Bone grew into the full depth of the substrate for all implant types and there were differences between implants. BA/PA was lowest in the tibial trays (2.0 ± 3.0%) and highest in the femoral stems (5.8 ± 3.9%). Overall, the tibial

trays had significantly lower bone ingrowth measurements compared to acetabular shells and femoral stems. Despite the increase porosity, low elastic modulus and high coefficient of friction, the porous tantalum retrievals did not show a higher amount of bone ingrowth compared to historical porous-coated implants. The limited number of tibial trays histological analyzed showed that fibrous tissue was present into the depth of the porous tantalum substrate in the tray and pegs regions. This work suggests that a higher amount of bone ingrowth was not the reason for lower cases of aseptic loosening.

Chapter 3 Determine the Effect of Implant Design, Bone Quality and Activity on Initial Implant Stability and Bone Stress through FEM

Abstract

The objective of this study was to investigate the effect of implant design (modular vs monoblock), implant properties, bone quality and patient activity on micromotion for tibial tray implants. A case-specific FE model of a tibia bone with either a modular or monoblock porous tantalum implant was created. The micromotion at the bone-implant interface was tracked during a full gait cycle. The effect of implant design (modular vs monoblock), implant properties (coefficient of friction and elastic modulus), patient activity (walking, standing up and descending stairs) and bone quality on micromotion were assessed. A modular porous tantalum model was developed to assess the effect of implant design on tibial bone stress. The modular porous tantalum tibial tray showed lower micromotion than the monoblock design. Higher coefficient of friction and elastic modulus resulted in lower micromotion. As bone quality increased, micromotion decreased. Standing up and descending stairs showed lower micromotion than walking.

Introduction

The long-term stability of a cementless implant depends on bone growth into the prosthetic surface [197]. Micromotion at the bone-implant interface can affect bone ingrowth. Thus, the magnitude of interface micromotions can be used as an indicator of implant stability and ingrowth potential. Micromotions at the bone-implant interface between 20-50 μm have been reported to allow bone to form, while micromotion exceeding 150 μm will result in fibrous tissue formation [62, 193, 194]. Small

micromotions are important for adequate bone ingrowth and subsequent secondary fixation [195, 196].

There are two types of NexGen® ® (Zimmer, Inc., Warsaw, IN) porous tantalum tibial trays that are currently clinically available. The monoblock design consists of a porous tantalum ingrowth surface with an ultra-high molecular weight (UHMWPE) bearing surface compression molded into it and two hexagonal porous tantalum pegs for initial stability. An alternate design, the porous tantalum modular component, consists of a titanium alloy modular tray with a porous tantalum layer that also includes two hexagonal pegs. This design includes a central boss (small circular peg) in the central posterior of the tray that is used with a lock down screw.

The first objective of this study was to investigate the effect of implant design (modular vs monoblock) and implant properties on micromotion. The second objective was to investigate the effect of bone quality and patient activity on micromotion. We hypothesized the modular porous tantalum tibial tray model would have lower micromotion than the monoblock porous tantalum model. We hypothesized that activity type would affect the amount of micromotion. We also hypothesized that lower bone quality would result in higher micromotions.

Methods

Model Creation

Our case-specific FE model of bone was created from CT data of a human leg (68 year-old female, right tibia). The bone was CT scanned along with a calibration phantom (solid, 0, 50, 100, 200 mg/ml calcium hydroxyapatite, Image Analysis, Columbia, KY, USA); subsequently the data was processed using a medical imaging software package (MIMICS 11.0, Materialise, Leuven, Belgium). Based on the tibia size, a porous tantalum tibia tray implant was chosen from our retrieval collection. This

retrieved UHMWPE insert was micro-CT scanned allowing for a 3D reconstruction to be completed. The bottom outline of the UHMWPE insert was then extruded to create the UHMWPE-TA portion and porous tantalum (TA) portion. Retrieved implants were measured to determine the dimensions and placements based on design type. A monoblock porous tantalum implant model was created with an UHMWPE bearing surface and a tantalum surface with two hexagonal porous tantalum pegs. A model of the modular porous tantalum tibial tray was developed following the same protocol as the remodeling work. The modular porous tantalum implant consisted of a titanium alloy modular tray with a porous tantalum layer that also includes two hexagonal pegs. This design includes a central boss (small circular peg) in the central posterior of the tray that is used with a lock down screw. The porous tantalum monoblock model and modular models were used to assess how material properties of the implant and patient bone affect the amount of bone ingrowth.

The tibia was then resected based on surgeon guidelines. For each type of implant, holes in the tibia were created. Each model was created such that the tibia bone and implant contact surfaces were matched node-to-node. A plastic mold of the femoral component matching the retrieved porous tantalum tibial tray was made and scanned in a micro-CT. The micro-CT data was then converted into a 3D geometry. The use of multiple point loads, individual point loads or surfaces was considered but a 3-D femoral component was determined to be the most reasonable (Appendix B). The solid models of the implants and tibial bone were subsequently imported into the bone surface models using an FEM software package and combined (MSC.MARC-Mentat 2013, MSC Software Corporation, Santa Ana, CA, USA) (Figure 3-1).

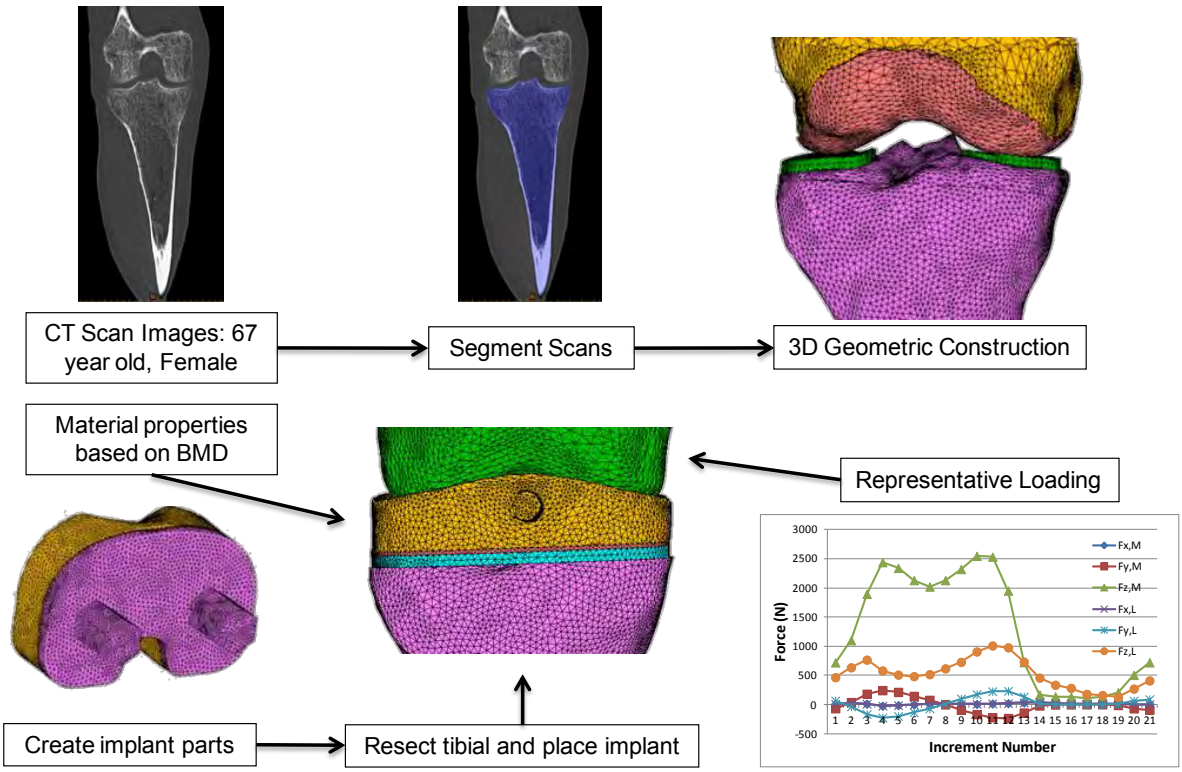

Figure 3-1: The process of creating the finite element model.

The FE models were created from four-noded tetrahedral elements (average of 250,000 elements for each entire model). The number of elements for each model was based on previous studies, which showed suitable results compared to clinical studies [202, 210]. The isotropic properties of cortical and trabecular bone were derived from the calibrated CT data [255]. Bone material properties were assigned based on the local ash density [256]. The calibration phantom was used to convert Hounsfield Units (HU) to calcium equivalent densities (ρ_{CHA}). An in-house software package (DCMTK MFC 10.8) was used to assign a calcium equivalent density (ρ_{CHA}) to each element, based on the average ρ_{CHA} value of all pixels in the element volume. The ash density was computed using relationships specific to the type of phantom used ($\rho_{ash} = 0.0633 + 0.887\rho_{CHA}$). The elastic modulus (E, MPa) was computed for each element from ash density (ρ_{ash}) using correlations for trabecular and cortical bone. The elastic modulus (E, MPa) was

computed for each element from ash density (ρ_{ash}) using correlations for trabecular and cortical bone [256] (Figure 3-2). In the present study we used ash to apparent density ratio (ρ_{ash}/ρ_{app}) equal to 0.6 over the whole density range [257].

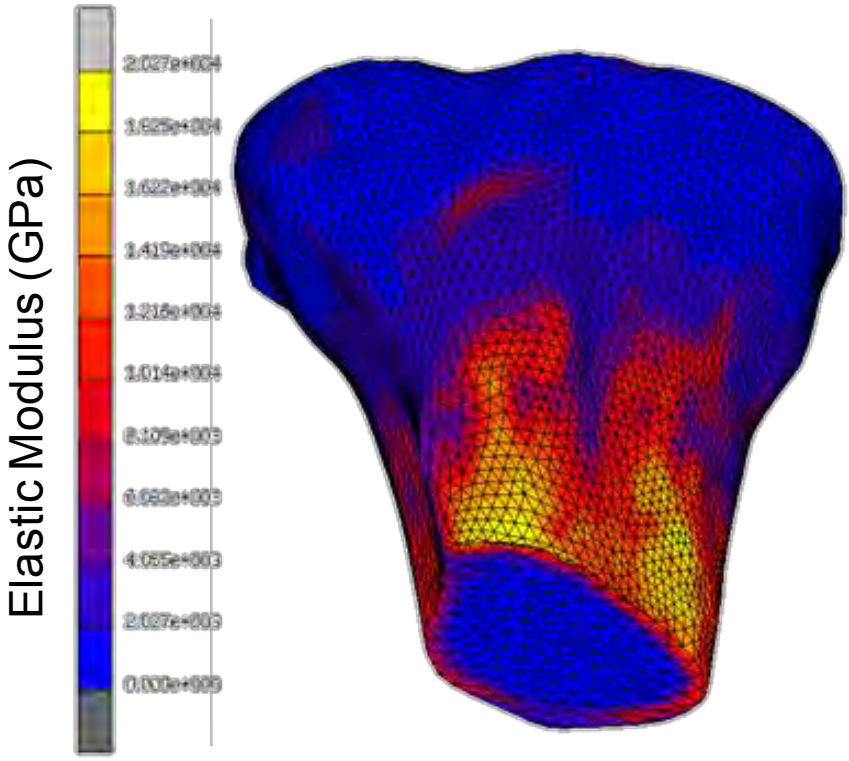

Figure 3-2: The mapped isotropic properties of the tibial bone.

Frictional contact was simulated at the implant-bone interface using a node-to surface contact algorithm (MSC.MARC-Mentat 2013, MSC Software Corporation, Santa Ana, CA, USA). The bone-implant interface and the UHMWPE insert-femoral condyle were defined as touching modeled as contact surfaces using Coulomb Friction (Table 3-2). The material properties for the implant and bone-implant contact were based on previous studies [152, 217] (Table 3-1).

Table 3-1. Material properties used in FE models.

Material	Young's Modulus (GPa)	Poisson's Ratio	Bone-Implant Friction Coefficient
UHMWPE	1.174	0.4	N/A
Porous Tantalum w/UHWMPE	4.26	0.35	N/A
Porous Tantalum	3.3	0.31	0.88

We modified the Orthoload data to fit our implant design [258]. Orthoload is a free public database of forces and moments acting in orthopaedic implants during activities [259]. The implant used in the Orthoload measurements and our finite element models are not of the same design. The coordinate system of the model was defined with the x-axis in the lateral to medial direction, the y-axis in the anterior to posterior direction and z-axis in the superior to inferior direction (Figure 3-3).

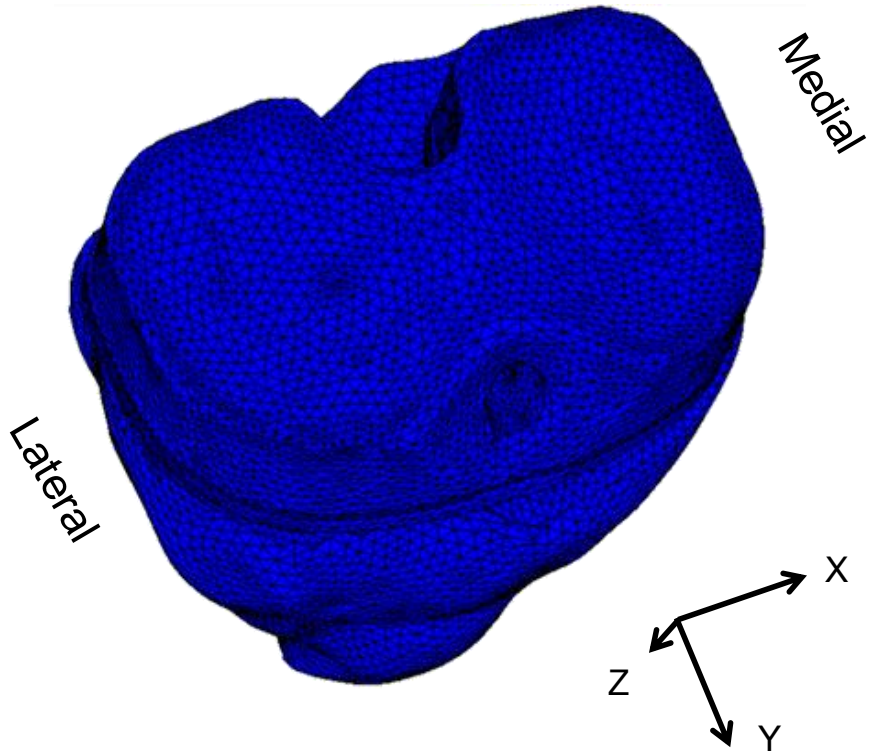

Figure 3-3: The coordinate system for the model.

The forces in the x, y and z-direction were applied at the top center of each condyle. For the intact case, we applied the Fx, Fy and Fz force at the maximum Fz during walking. Forces due to muscles and ligaments were not included in the loading history. Similarly, we calculated the maximum force for standing up and descending stairs. The other parts of the implant were defined as bonded (Table 3-2).

Table 3-2: Contact definition for the porous tantalum monoblock model.

Material	Bone	Pegs	Tray	TA-UHMWPE	UHMWPE	Femoral
Bone	-	Touching*	Touching*	-	-	-
Pegs	Touching*	-	Bonded	-	-	-
Tray	Touching*	Bonded	-	Bonded		-
TA-UHMWPE	-	-	Bonded	-	Bonded	-
UHMWPE	-	-	-	Bonded	-	Touching^
Femoral	-	-	-	-	Touching^	-

*μ=0.88, ^=0.05

The forces in the x, y and z-direction were applied at the top center of each condyle. The Orthoload gait cycle was broken down into 20 steps or increments. Each node corresponds to an increment in which forces are applied in the x, y and z direction.

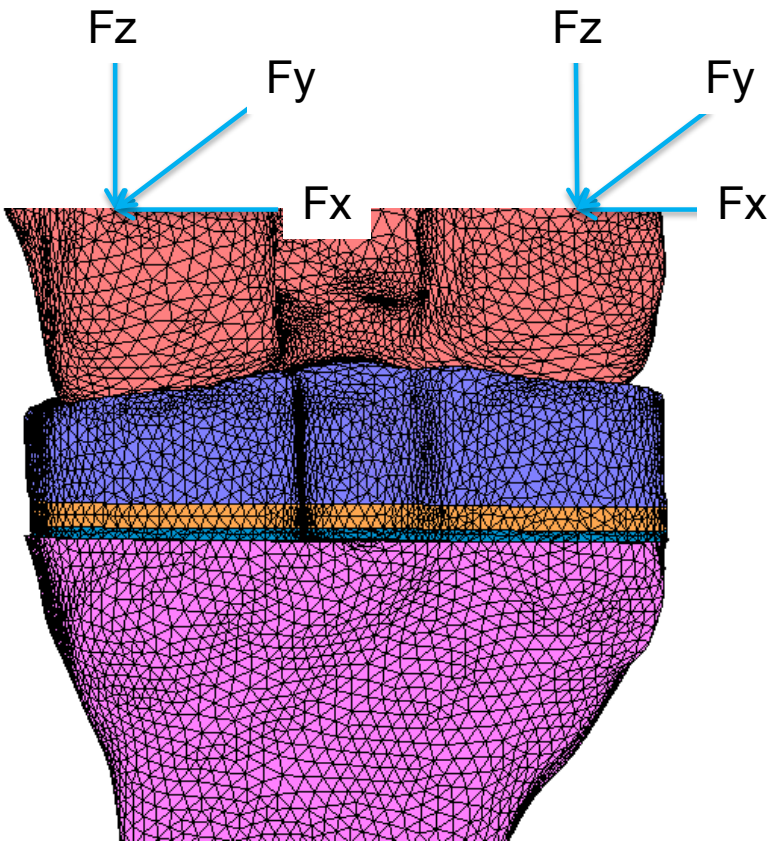

Figure 3-4: Application of loads on the femoral condyle.

For each type of activity, walking, standing up and descending stairs, incremental loading curves were created (Figure 3-5).

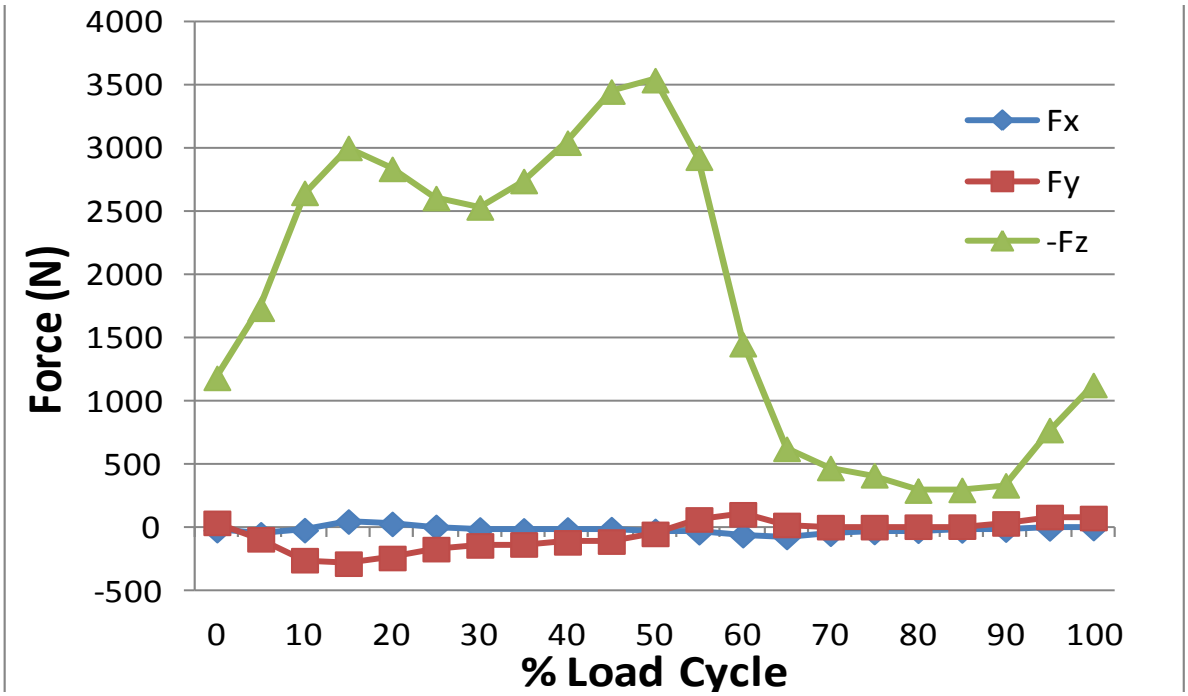

Figure 3-5: Loading cycle used for walking.

Implant design effect was assessed by changing the values of substrate effective modulus and coefficient of friction. The materials properties of the cementless modular implant were chosen specifically to mimic other highly porous metals currently on the market (Appendix B). The substrate elastic modulus (GPa) used were 210, 110, 50 and 3. The coefficient of frictions used were 0.5, 0.75. 1.0 and 1.25. The monoblock implant geometry was used for the stimulations.

For each model, contact nodes on the implant surface were specified. On the bone surface, contact faces were specified to allow (Figure 3-6).

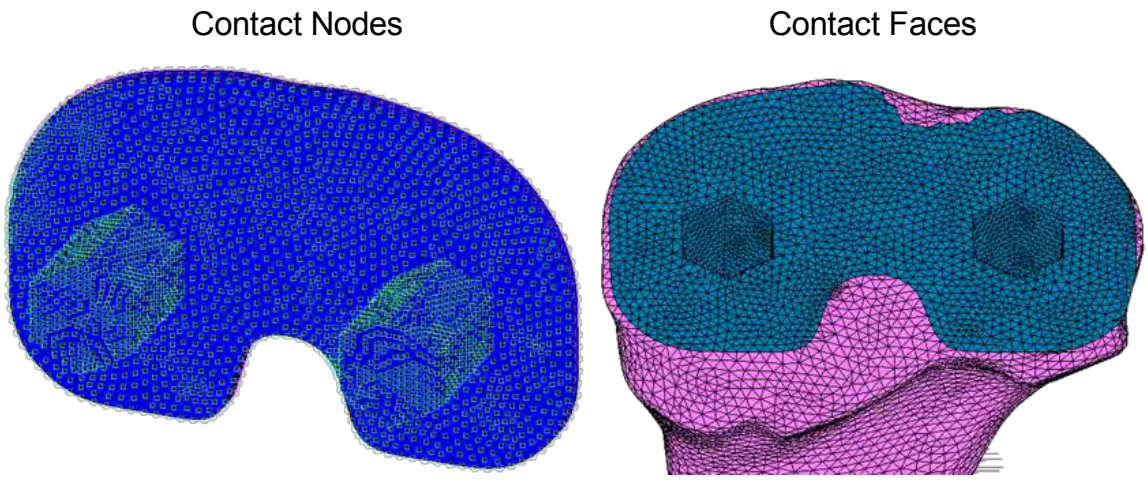

Figure 3-6: Specification of contact nodes and contact faces for the monoblock model.

Peri-prosthetic micromotion was defined as the relative displacement of the implant stem with respect to the adjacent endosteal surface of the bone. An in-house algorithm [260] was used to track micromotion development over time. For every time increment, the position of the stem node was projected on the corresponding contact face, which allowed quantification of the magnitude and direction of micromotions (Figure 3-7).

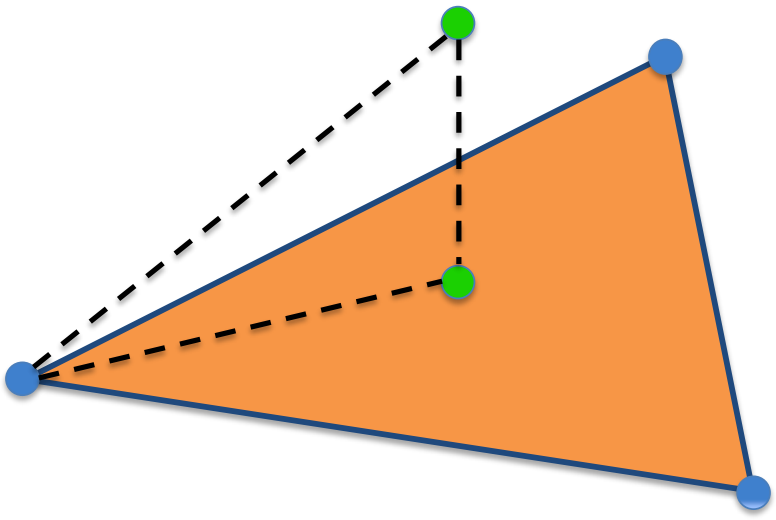

Figure 3-7: Projection of the node onto the contact face.

Incremental micromotions were defined as the distances between subsequent nodal projections onto the bony surface, whereas maximal micromotion was defined as the greatest distance between these projections (Figure 3-8).

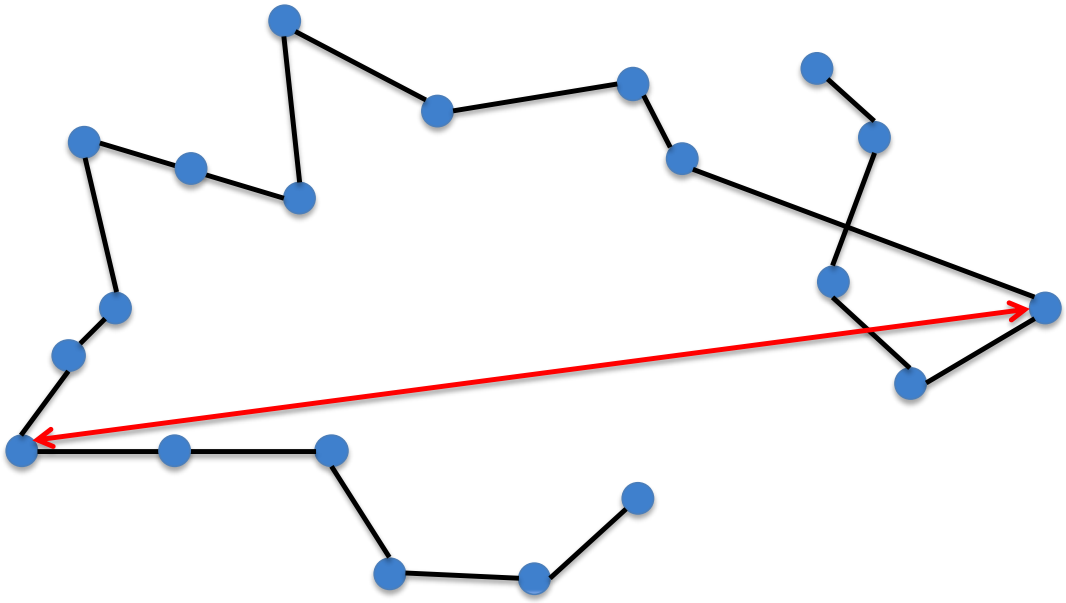

Figure 3-8: Example of incremental nodal projections and maximal micromotion definition (large red arrow).

There are two micromotions calculated, one in parallel to the implant surface (shear micromotion). The second micromotion is the distance between the implant and bone, perpendicular to the implant surface (tensile micromotion). We report the maximum (resultant) micromotion that occurs during the gait cycle of activity. For each model, the activity cycle would be applied four times. This was completed to remove any affects of implant or model settling (Figure 3-9).

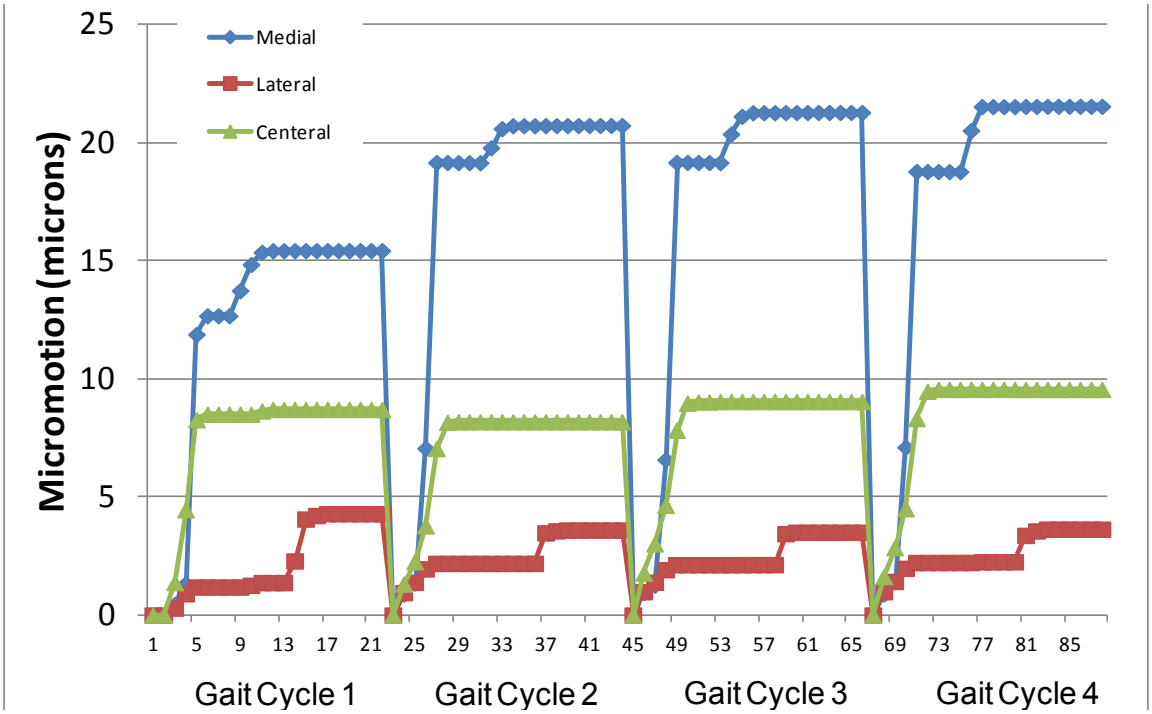

Figure 3-9: Settling in effect for a porous tantalum monoblock tibial component during walking.

The patient bone properties were changed to represent an increase or decrease in BMD. The lower BMD was normal BMD decreased by 30%. The higher BMD was normal BMD increased by 30%. The effect of the change of elastic modulus and coefficient of friction on the stress on the bone and implant was also assessed.

Results

Micromotion Results

The FE models showed that design type affected the amount of micromotion when compared for a walking gait cycle. The modular tibial tray showed lower micromotion than the monoblock design for the shear micromotion (Figure 3-10).

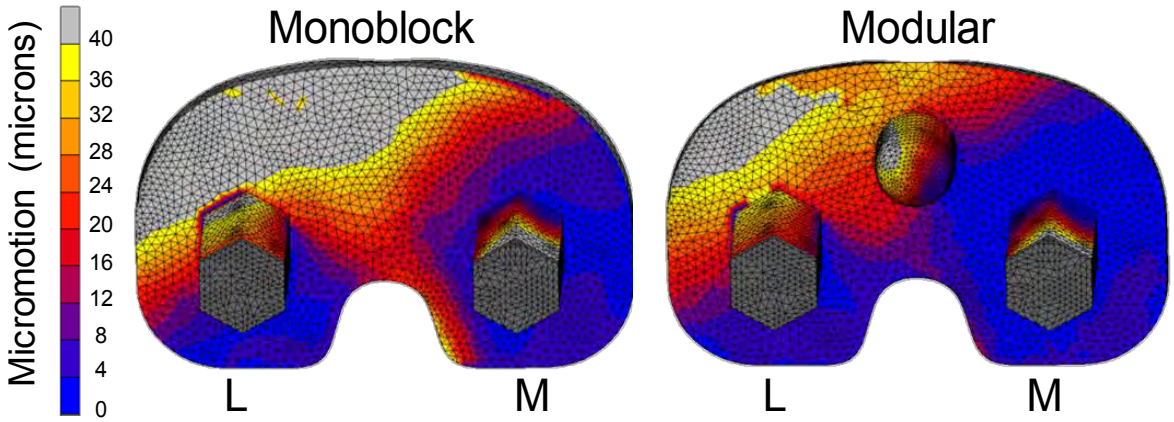

Figure 3-10: Micromotion (shear) results based on tibial tray implant type. Note: Scale adjusted to highlight favorable micromotion.

For the tensile micromotion, the modular and monoblock were not substantially different (Figure 3-11).

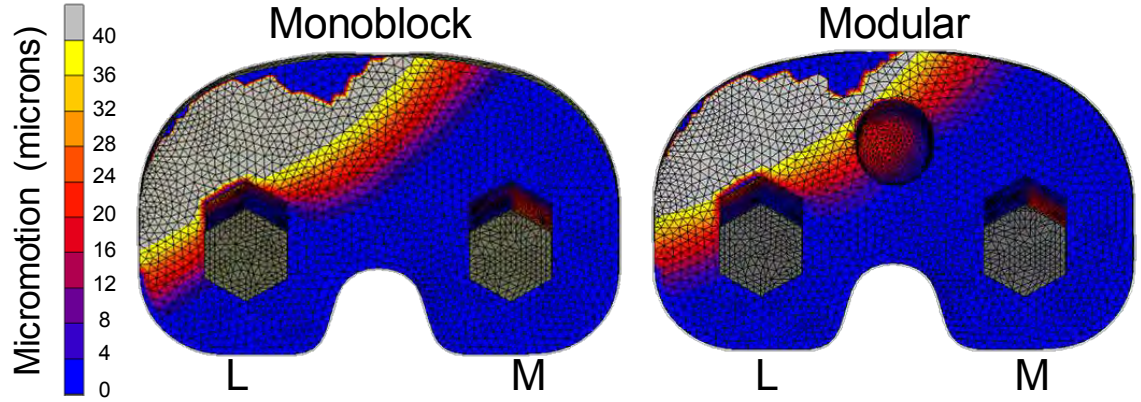

Figure 3-11: Micromotion (tensile) results based on tibial tray implant type. Note: Scale adjusted to highlight favorable micromotion.

Type of activity affected micromotion. For the modular tibial tray design, standing up and descending stairs showed lower micromotion than walking for both the tensile and shear micromotion (Figure 3-12).

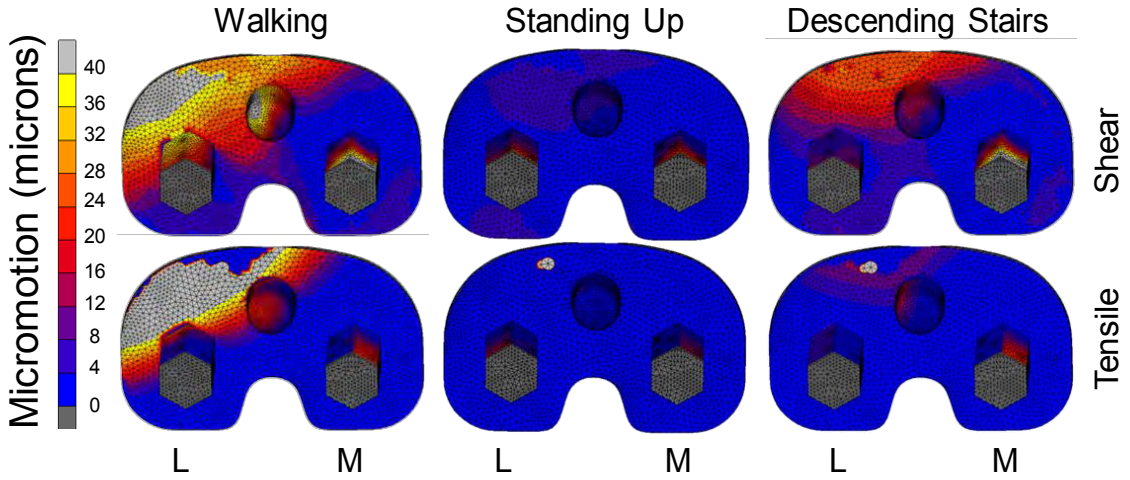

Figure 3-12: Micromotion for the modular tibial tray design based on activity type. Note: Scale adjusted to highlight favorable micromotion.

For the monoblock tibial tray design, standing up and descending stairs showed lower micromotion than walking for both the tensile and shear micromotion (Figure 3-13).

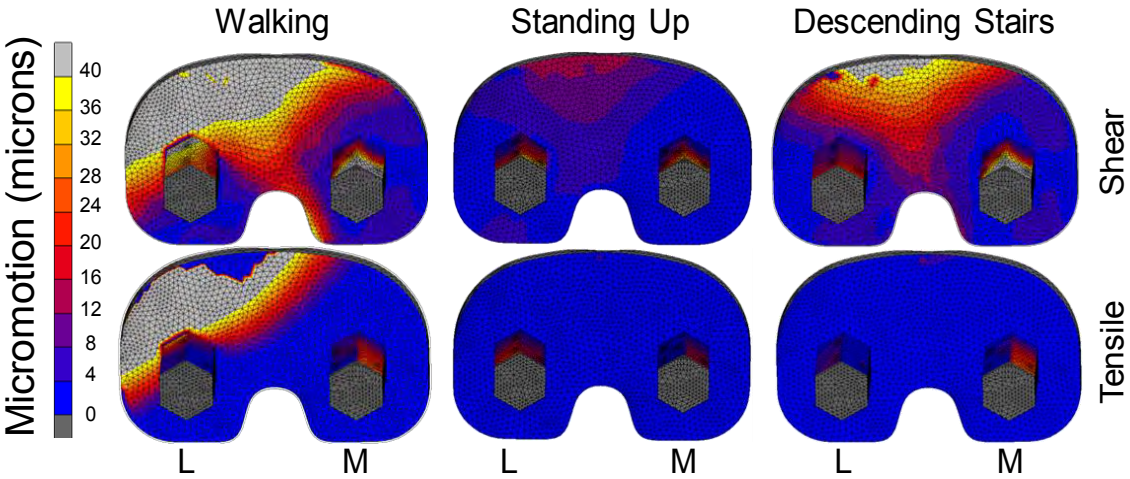

Figure 3-13: Micromotion for the monoblock tibial tray design based on activity type. Note: Scale adjusted to highlight favorable micromotion.

Lower bone quality resulted in higher micromotion for the modular and monoblock tibial tray designs. For the modular tibial tray design, as the bone quality increased, the micromotion decreased (Figure 3-14).

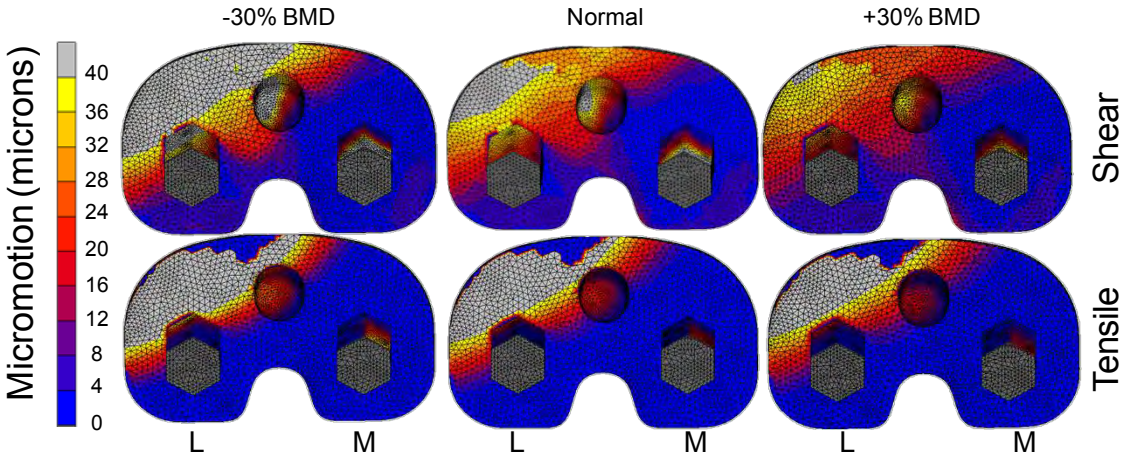

Figure 3-14: Micromotion for the modular porous tantalum tibial tray based on bone quality.

For the monoblock tibial tray design, as the bone quality increased, the micromotion (shear) decreased (Figure 3-15). There was minimal effect of micromotion (tensile) on the bone quality.

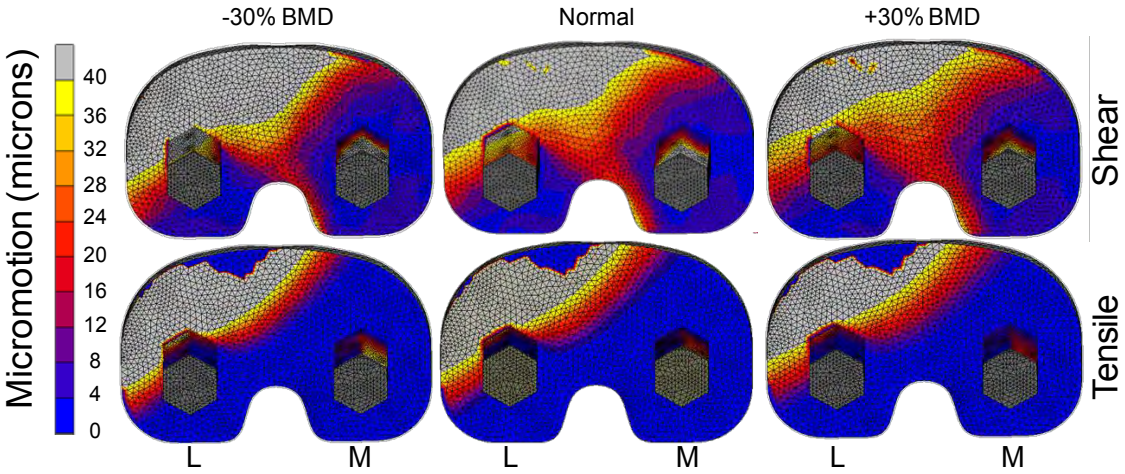

Figure 3-15: Micromotion for the monoblock porous tantalum tibial tray based on bone quality. Note: Scale adjusted to highlight favorable micromotion.

The monoblock model with porous tantalum for walking with normal bone was further evaluated for location within the implant. The medial region of the implant had less micromotion compared to the other regions (Figure 3-16).

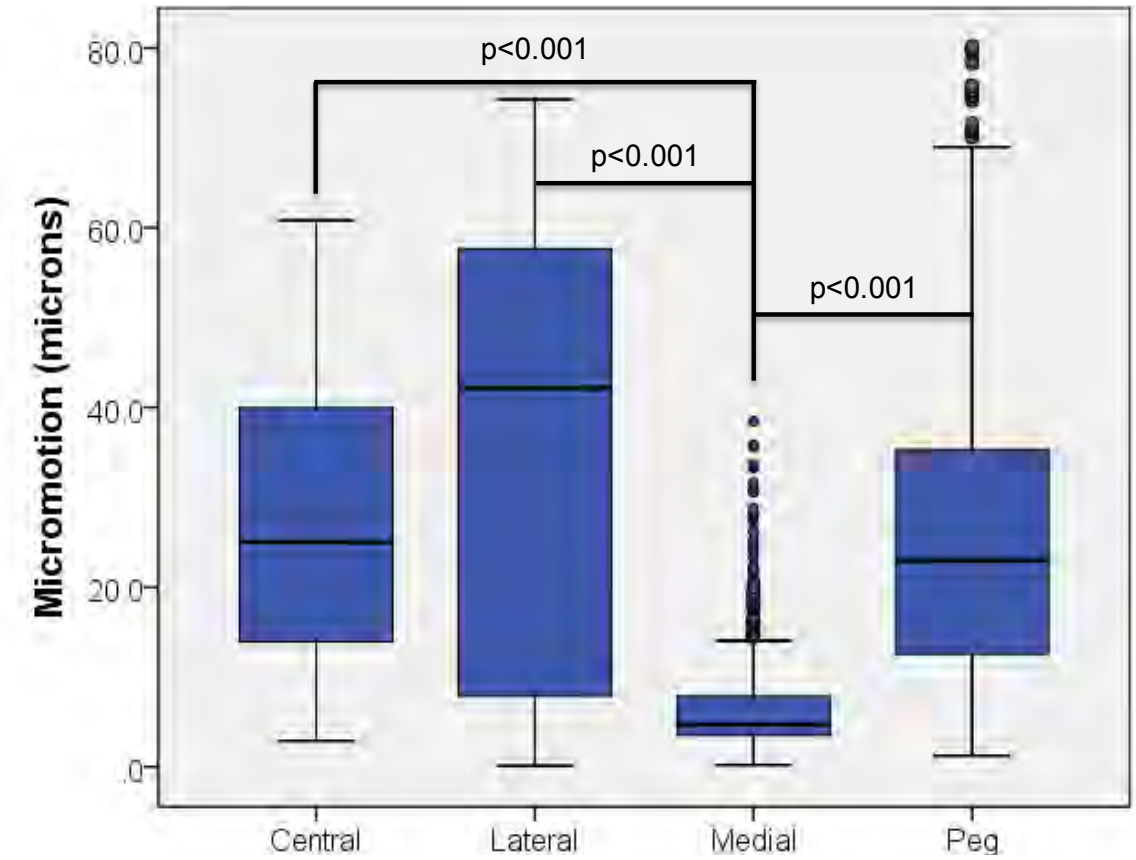

Figure 3-16: Micromotion for the monoblock porous tantalum based on implant location.

Below shows the effect of elastic modulus and coefficient of friction on the micromotion. Comparing the high elastic modulus (210 GPa) to the low elastic modulus (3GPa), there is a clear increase in micromotion (Figure 3-17).

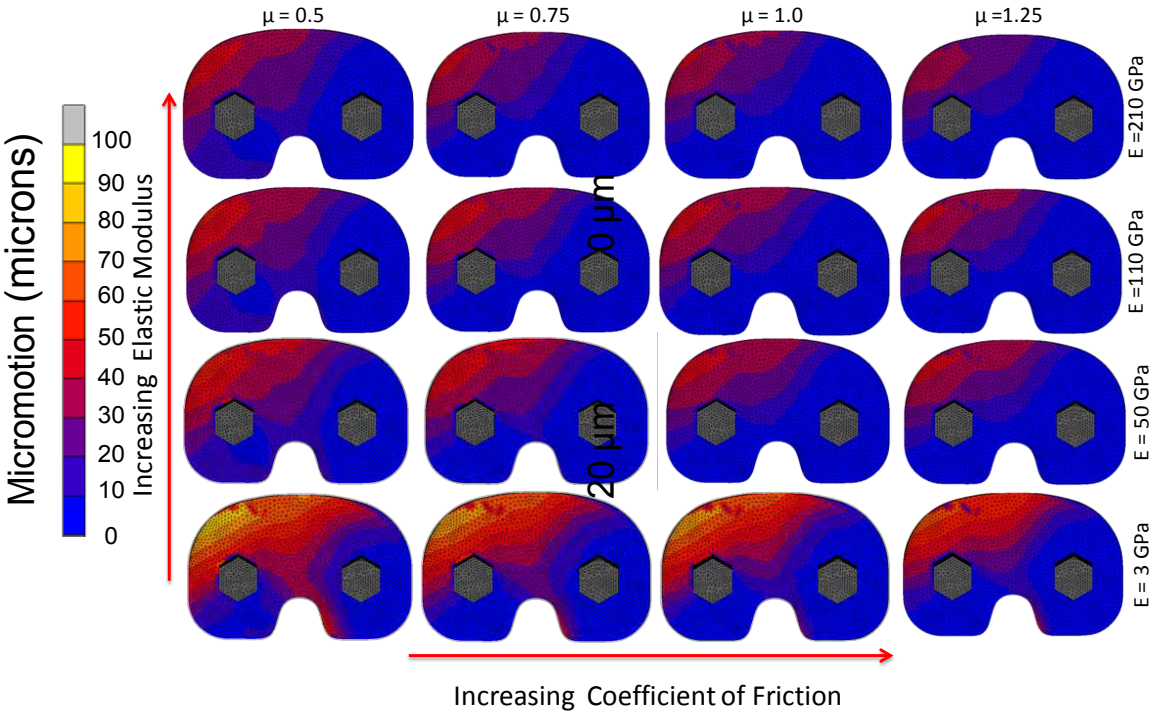

Figure 3-17: Micromotion (shear) for the monoblock tibial tray design based on coefficient of friction and elastic modulus.

The scale for the micromotion is changed to show when the micromotion is above the 40 um range. Micromotions at the bone-implant interface below 40 μm have reported bone ingrowth, while micromotion exceeding 150 μm will result in fibrous tissue formation [62, 193, 194] (Figure 3-18).

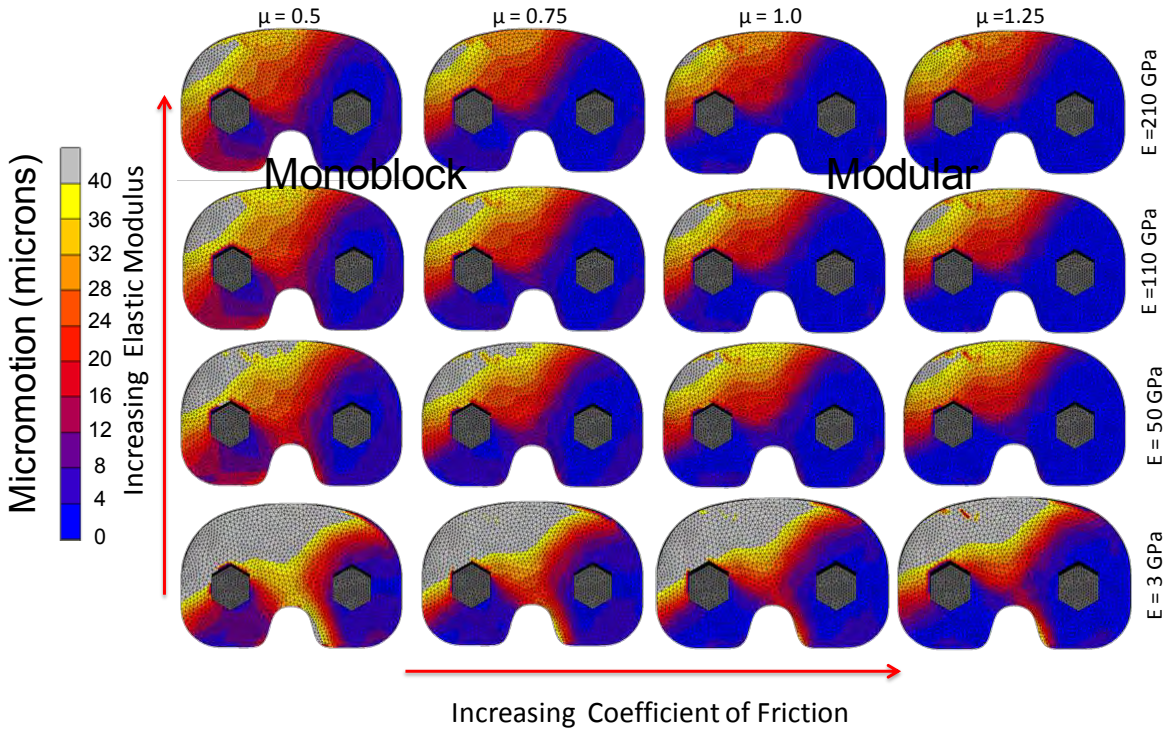

Figure 3-18: Micromotion (shear) for the monoblock tibial tray design based on coefficient of friction and elastic modulus.

Below is a graph of the average micromotion for the tray nodes based on elastic modulus and coefficient of friction. Decreasing the elastic modulus resulted in an increase in micromotion. The effect of increase in coefficient of friction is more substantial in the lower elastic modulus (3 GPa, Figure 3-19).

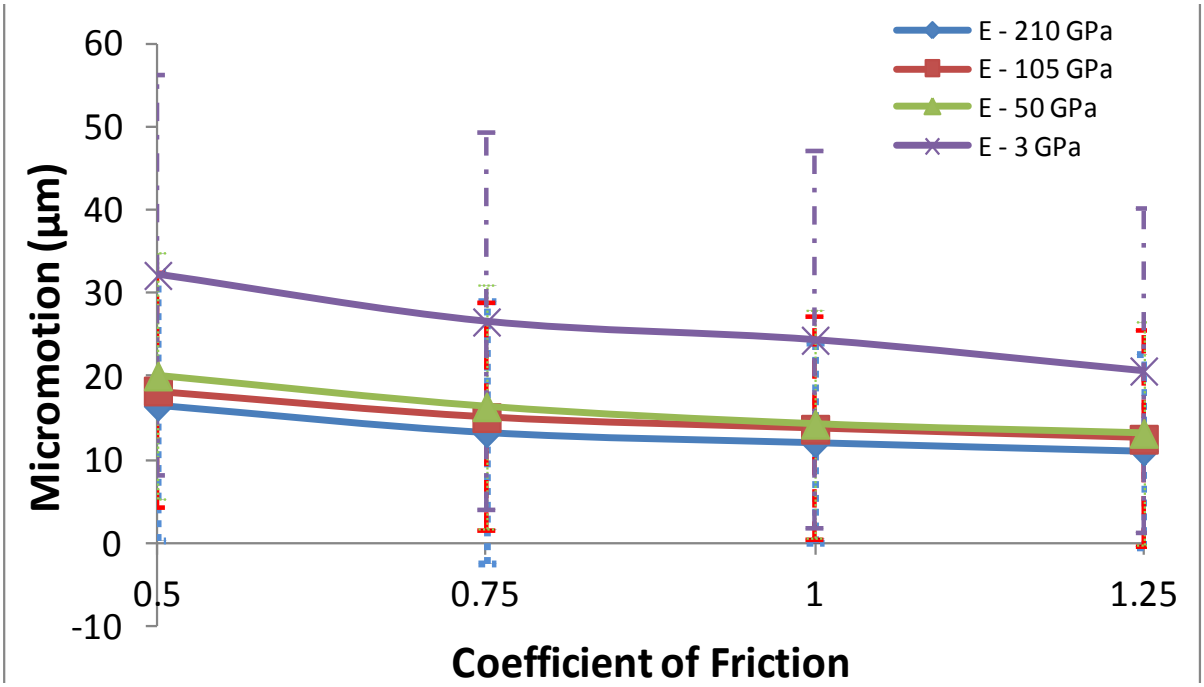

Figure 3-19: Micromotion (shear) for the monoblock tibial tray design based on coefficient of friction and elastic modulus at the bone-tray interface.

Below is a graph of the average micromotion for the peg nodes based on elastic modulus and coefficient of friction. Decreasing the elastic modulus resulted in an increase in micromotion. The effect of increase in coefficient of friction is more substantial in the lower elastic modulus (3 GPa, Figure 3-20).

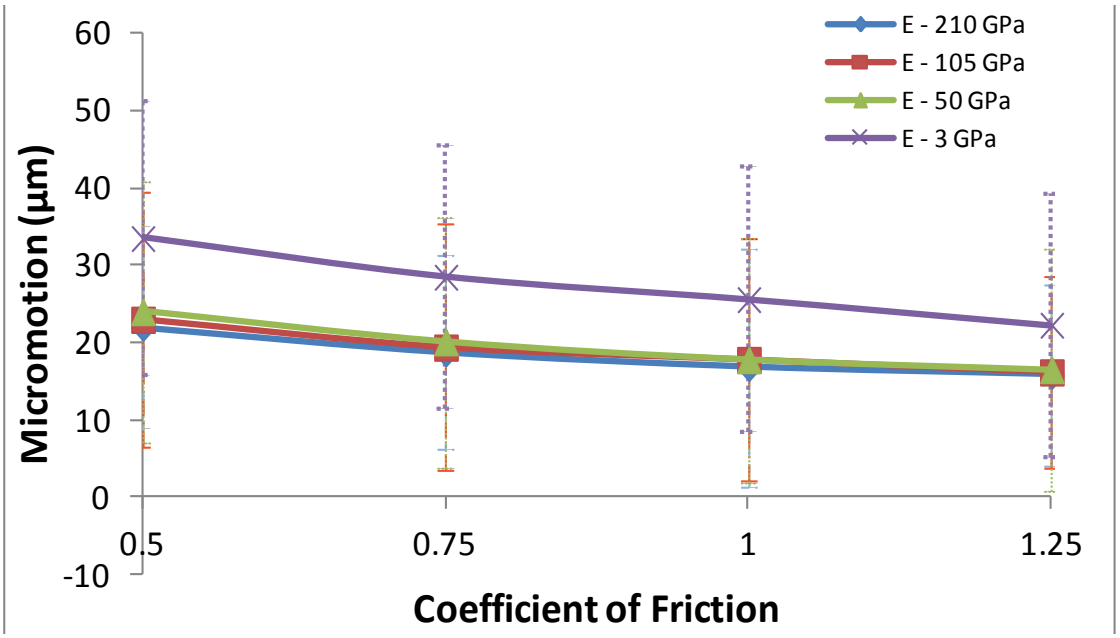

Figure 3-20: Micromotion (shear) for the monoblock tibial tray design based on coefficient of friction and elastic modulus at the bone-peg interface.

Bone and Implant Stress Results

The Von Mises Stress was lower in the modular tibial tray compared to the monoblock tibial tray (Figure 3-21).

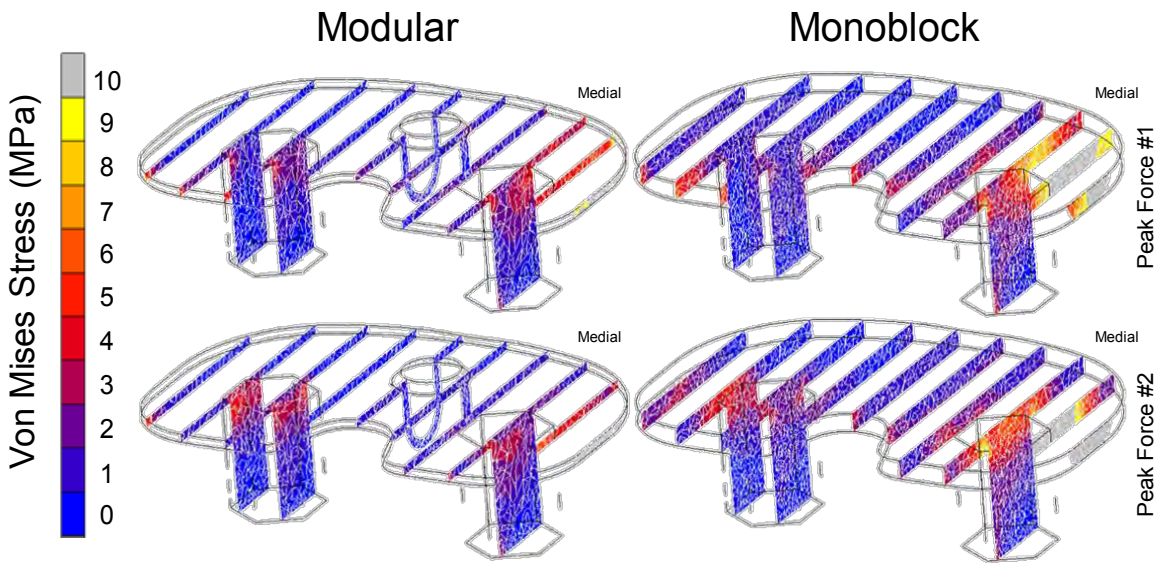

Figure 3-21: Von Mises Stress based on tibial tray design. Note: Modular shows lower stress than the monoblock design.

The stress on the tibial bone was higher in the modular design for both peak loads during gait cycle (Figure 3-22).

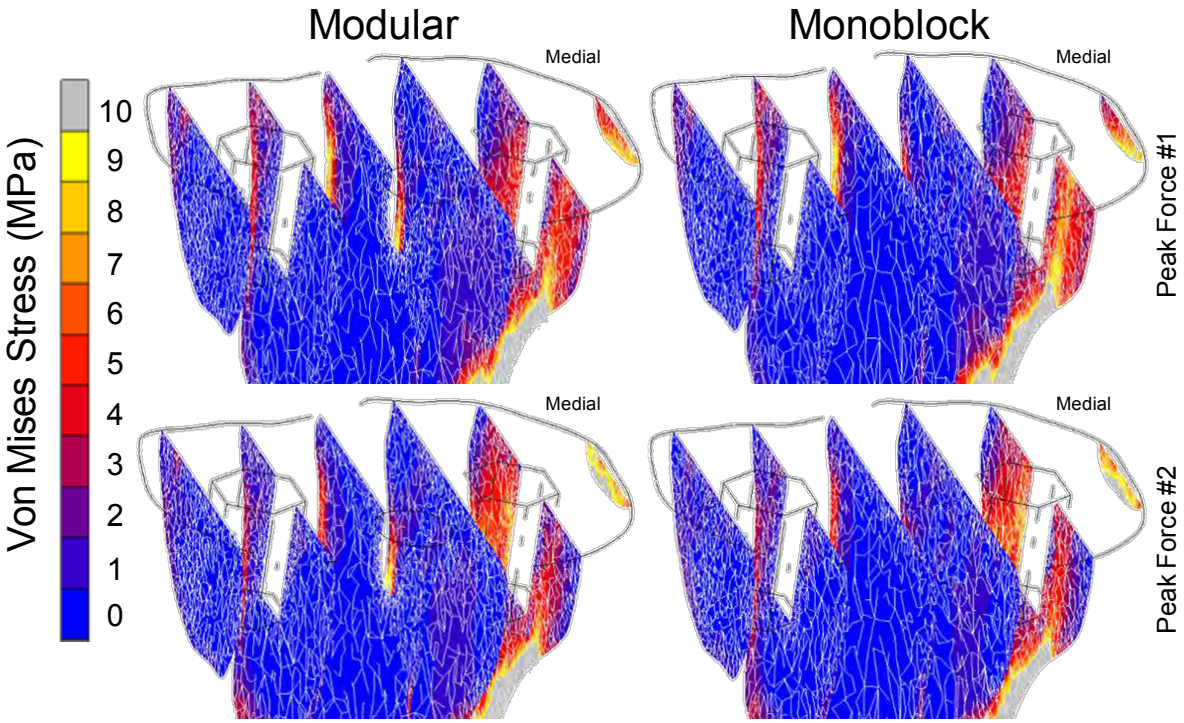

Figure 3-22: Von Mises Stress on the tibia bone based on implant design and peak forces during walking.

Focusing on the first peak load during gait cycle, the tibia bone from the modular model shows higher bone stress in the central and medial sections (Figure 3-23).

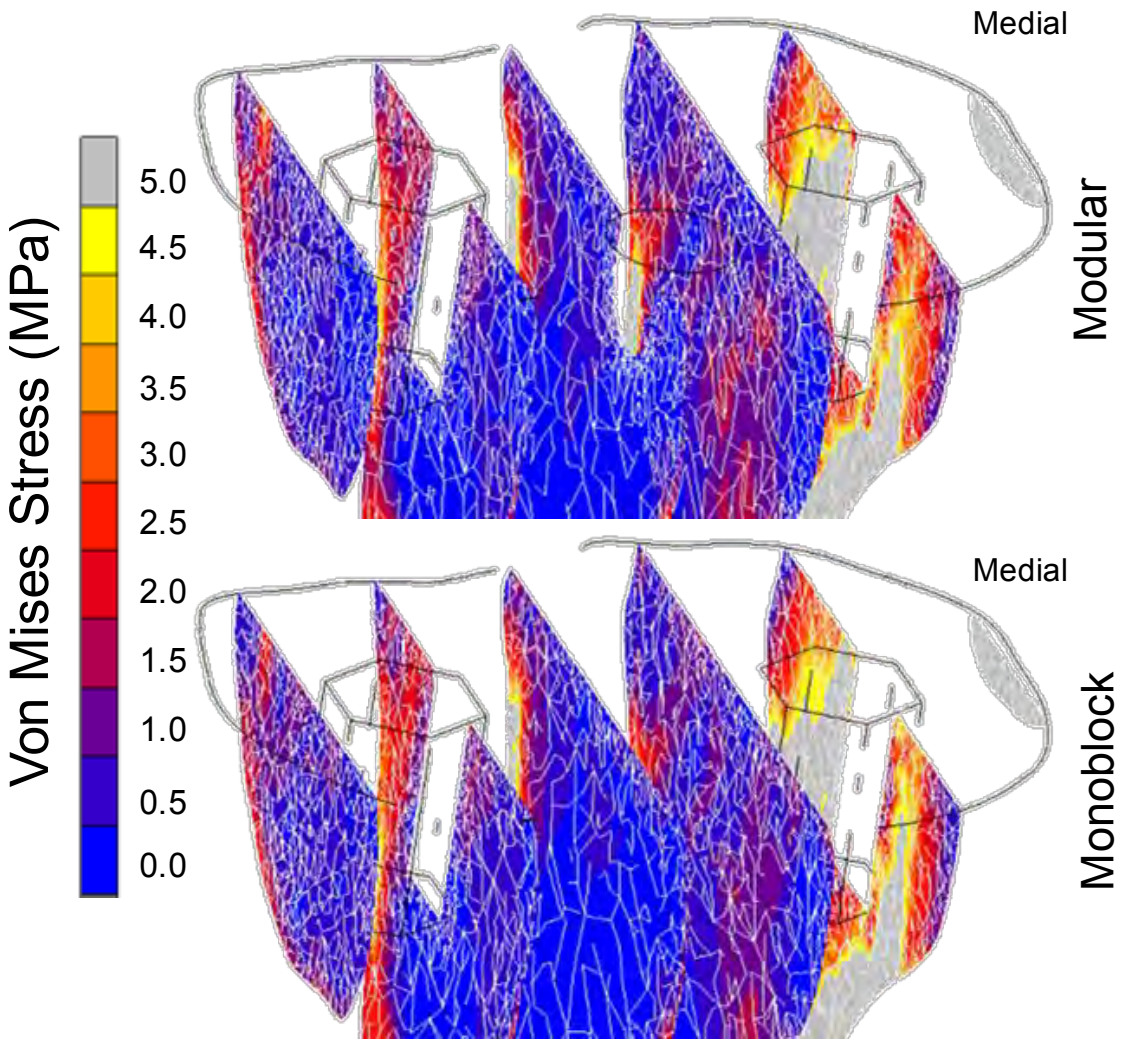

Figure 3-23: Von Mises Stress on the tibia bone based on implant design for first peak force during walking.

Focusing on the second peak load during gait cycle, the tibia bone from the modular model shows higher bone stress in the central and medial sections (Figure 3-24).

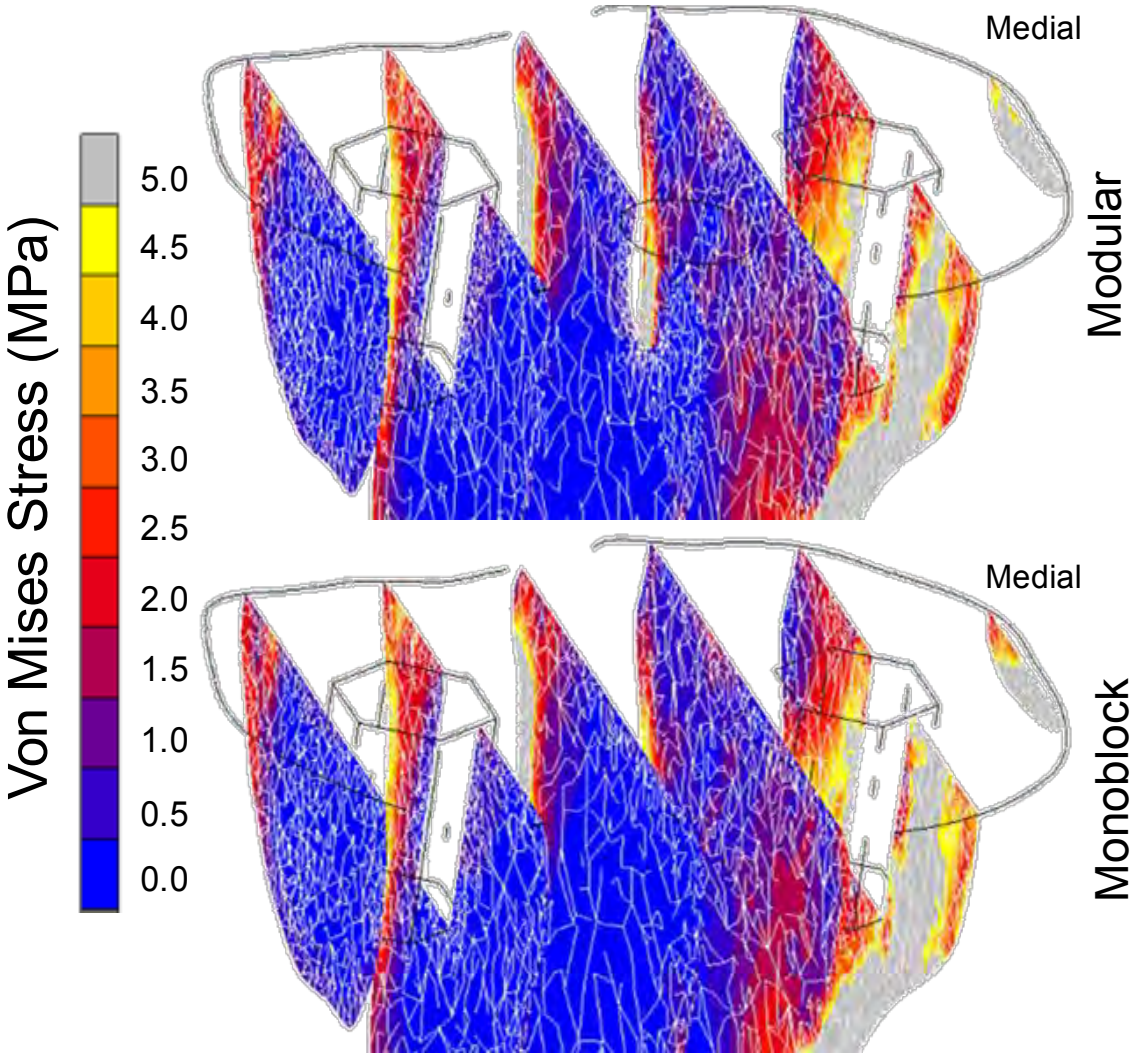

Figure 3-24: Von Mises Stress on the tibia bone based on implant design for second peak force during walking.

Comparing the effect of elastic modulus on the stress on the bone for the highest elastic modulus and lowest, there is no difference (Figure 3-25).

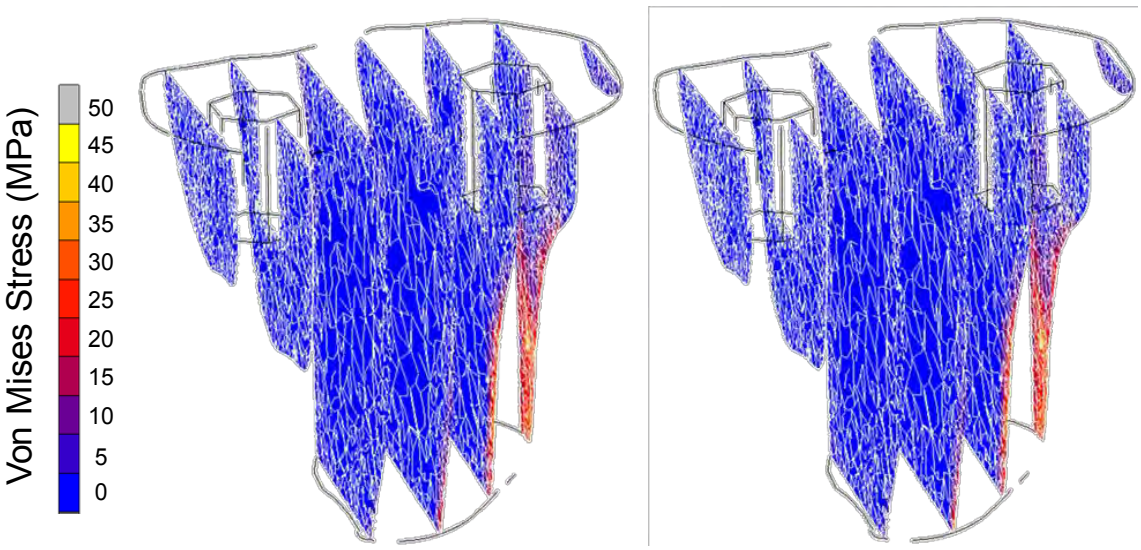

Figure 3-25: The effect of substrate modulus on bone stress.

For a peak load during walking, the modular tibial tray shows lower strain in the porous tantalum region compared to the monoblock design (Figure 3-26).

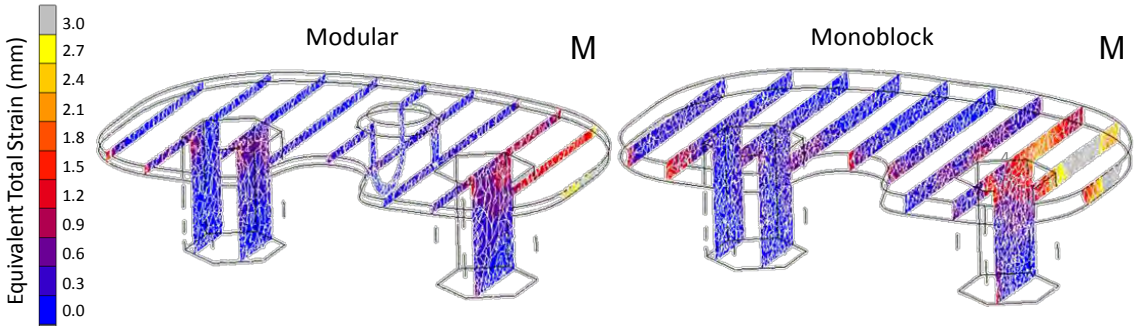

Figure 3-26: The total strain based on implant design at a peak load during walking.

Discussion

FE models were developed to determine the effect of implant design (modular vs monoblock), activity type and patient bone quality on the micromotion at the bone-implant interface of porous tantalum tibial implants. Additionally, the effect of implant properties (elastic modulus and coefficient of friction) on micromotion was assessed. Our

results showed that activity type had the highest effect on micromotion. There was a limited effect seen due to implant design (modular vs monoblock), bone quality and implant properties.

This study had several limitations. For the comparison of the implant properties, the same geometry was used for all modular and monoblock models. For our study, this allowed us to isolate the material properties to investigate their effect. However, implants from different manufacturers will have different geometric designs. The effect of different geometries was not investigated in this current study. Another limitation is that all of our models are based on one cadaveric tibia. We also made several assumptions to calculate the loading cycles based on the data from Orthoload as our implant was not the same. Additionally for the loading, muscles and ligament forces were neglected. The loading is idealized and does not take into account the full range of motion for the femoral component. Finally, the bone-implant is modeled line-to-line with no gaps. There is also no interference fit at the bone-peg interface.

The modular porous tantalum tibial design showed lower micromotion than the monoblock. This is similar to our retrieval work which showed a higher amount of bone ingrowth. This may be due to the differences in stiffness due to the metal-backing of the modular design resulting in a higher stiffness compared to the monoblock design. However, micromotion is an evaluation of the primary fixation and there are many other factors besides design that could have affected the bone ingrowth. It is unclear if the central boss peg plays a role in the fixation of the implant.

When comparing the modular and monoblock porous tantalum designs, we saw higher stress on the tibial bone for the modular design. The higher stress may result in higher bone ingrowth. Our previous retrieval work in Aim 2 showed that modular implants had a higher amount of bone ingrowth monoblock implants.

Using this idealized model, activity type was shown to have an effect on the implant stability which is similar to a previous study [261]. Our results showed significantly lower micromotion than the previous study, however different coefficient of frictions may be one possible reason for this (current study, μ=0.88 and previous study μ=0.4-0.6).

Conclusion

This dissertation investigated retrieved porous tantalum implants for bone ingrowth. Overall, retrieved porous tantalum implants showed the highest amount of bone ingrowth in the upper 500 μm of the substrate. Additionally, tibial trays exhibited significantly lower bone ingrowth compared to the acetabular shells and femoral stems.

The studies in Chapter 1 showed that the main reasons for revision of the retrieved porous tantalum implants were infection, instability, acetabular loosening and pain. The results of the retrieval work and the short-term clinical studies have shown limited cases of loosening of the porous tantalum tibial trays. Retrieval analysis allowed for characterization of bone ingrowth into retrieved porous tantalum implants.

In Chapter 2, the retrieved porous tantalum implants were assessed to determine factors affecting bone ingrowth. For all implant types, the highest amount of bone ingrowth was seen in the upper 500 μm (Zone 1) of the porous tantalum substrate. Bone grew into the full depth of the substrate for all implant types and there were differences between implants. BA/PA was lowest in the tibial trays (2.0% ± 3.0) and highest in the femoral stems (5.8%±3.9). Overall, the tibial trays had significantly lower bone ingrowth measurements compared to acetabular shells and femoral stems. Despite the lower proportion of porous tantalum implants revised for aseptic loosening from Chapter 1 and clinical studies, the retrieval results did not show a higher amount of bone ingrowth compared to historical porous-coated implants. Finite element modeling allowed for further exploration of certain factors potentially influencing the lower proportion of porous tantalum implants revised for aseptic loosening.

In Chapter 3, finite element models were used to determine if implant design, patient activity and bone quality affect bone remodeling and micromotion at the bone-implant interface. FE models for a cemented and monoblock porous tantalum implant were developed to simulate bone remodeling. The micromotion at the bone-implant

interface was sensitive to implant design (modular vs monoblock), patient bone and activity type. The micromotion was relatively insensitive to change of elastic modulus and coefficient of friction. The modeling results were most sensitive to type of simulated activity. From the FE results, the initial implant stability (micromotion) did not appear to be the main factor affecting bone ingrowth. However, this finding may be due to assumptions and limitations of this current model which are discussed in Chapter 3.

The contributions of this dissertation are: (1) completion of a clinical data analysis of a large number of retrieved components to determine the effect of fixation type and/coating type on aseptic loosening as a reason for revision; (2) discovery that bone ingrowth was lower than expected in retrieved porous tantalum implants; (3) development of a semi-automated method for bone ingrowth analysis; and (4) assessment of factors potentially affecting initial implant stability of porous tantalum implants through FE models.

Histological analysis of additional implants may yield further insight into the amount of fibrous tissue ingrowth. Mechanical testing of postmortem implants may help determine the strength of fixation at the bone-implant interface. Although the results from the retrieval work showed limited amount of bone, the amount of bone may be sufficient for fixation. The increased porosity may result in increased fibrous tissue growth which is also increasing the strength at the interface.

The FE models focused on initial implant stability, which was not shown as the main reason why the porous tantalum has limited cases of loosening. Future work could further develop the FE models to assess the sensitivity of the results to surgical variability, additional patient activities, variation in implant/peg geometries, and variation in the loading distribution (lateral/medial). In the model, there was no interference fit between the bone and pegs. In our model, we assumed that there was no gap at the bone-implant interface. In the clinical setting, there may be variation in seating of the

device. FE models that are more representative of the clinical setting may yield further insight into the variability of progression of bone ingrowth into porous tantalum implants.

An initial pilot of bone remodeling was completed (Appendix C). The porous tantalum monoblock predicted the amount of bone loss in the central region, however for the medial and lateral regions did not. Factors that could be investigated through the remodeling models include: pre/post surgery loading, implant properties, implant design (modular vs monoblock) and patient bone quality. Finally, additional models from other patients would need to be developed so that the results could better represent the patient population.

Future designs of implants may include bimodal porosity or porosity gradients [262]. This type of design may help mitigate stress shielding or overstraining of the bone. The bone ingrowth in the porous tantalum implant was concentrated in the upper 500 μm of the porous substrate. The optimal stimulus for bone ingrowth may be concentrated at 0 to 500 μm zone of the porous substrate. The stimulus further into the porous tantalum substrate may be stress shielded, causing tissue fixation. Increasing the elastic modulus of the implant at that location by altering the porosity may yield increased bone ingrowth. Additionally, a porosity gradient may also be a future type of implant design. This would allow lower elastic modulus near the bone and higher away from the bone. This may help decrease the higher strain that was shown in the monoblock tibial tray design.

References

1. Engh CA, Zettl-Schaffer KF, Kukita Y, Sweet D, Jasty M, Bragdon C. Histological and radiographic assessment of well functioning porous-coated acetabular components. A human postmortem retrieval study. The Journal of bone and joint surgery American volume 75(6): 814, 1993

2. Brief Anatomy of Hip Joint. In: Joint BAoH, ed. http://probecurecom/b/brief-anatomy-of-hip-joint/. 2015

3. Norkin CC, Levangie PK. Joint Structure & Function: A Comprehensive Analysis: F.A. Davis, 1983

4. The muscles of the hip joint. In: joint. Tmoth, ed. http://droualbfacultymjcedu/Lecture%20Notes/Unit%203/external_rotators_of_the_hip_jointjpg.

5. Hip Joint: Ball and Socket. In: http://krankbrooklyncom/krankcontent/uploads/2014/04/hip-ball-and-socket-joint1jpg. 2015

6. Urban RM, Jacobs JJ, Sumner DR, Peters CL, Voss FR, Galante JO. The bone-implant interface of femoral stems with non-circumferential porous coating. J Bone Joint Surg Am 78(7): 1068, 1996

7. Tibial Landmarks. In: https://classconnections3amazonawscom/726/flashcards/444726/gif/tibial_landmarks1348545227765gif. 2015

8. Anatomy of the knee: anterior view. In: view. Aotka, ed. 2000

9. 6 Degrees of Motion Present in the Human Knee. In: http://imagewikifoundrycom/image/1/XWkjnfsS1GWsyejsPEdu_Q22613/GW438H344. 2015

10. Hinge Joint. In: Knee HJ-, ed. http://wwwpreventdiseasecom/images/bookhingegif. 2015

11. Kapandji IA. The physiology of the joints: lower limb: Elsevier Health Sciences, 1987

12. Nalla RK, Kruzic JJ, Kinney JH, Balooch M, Ager Iii JW, Ritchie RO. Role of microstructure in the aging-related deterioration of the toughness of human cortical bone. Materials Science and Engineering: C 26(8): 1251, 2006

13. Rho JY, Kuhn-Spearing L, Zioupos P. Mechanical properties and the hierarchical structure of bone. Medical engineering & physics 20(2): 92, 1998

14. Turner CH, Wang T, Burr DB. Shear strength and fatigue properties of human cortical bone determined from pure shear tests. Calcified tissue international 69(6): 373, 2001

15. Galante J, Rostoker W, Ray RD. Physical properties of trabecular bone. Calc Tis Res 5(1): 236, 1970

16. Williams JL, Lewis JL. Properties and an Anisotropic Model of Cancellous Bone From the Proximal Tibial Epiphysis. Journal of Biomechanical Engineering 104(1): 50, 1982

17. Keaveny TM, Hayes WC. A 20-Year Perspective on the Mechanical Properties of Trabecular Bone. Journal of Biomechanical Engineering 115(4B): 534, 1993

18. van Rietbergen B, Weinans H, Huiskes R, Odgaard A. A new method to determine trabecular bone elastic properties and loading using micromechanical finite-element models. Journal of biomechanics 28(1): 69, 1995

19. Ciarelli MJ, Goldstein SA, Kuhn JL, Cody DD, Brown MB. Evaluation of orthogonal mechanical properties and density of human trabecular bone from the major metaphyseal regions with materials testing and computed tomography. Journal of Orthopaedic Research 9(5): 674, 1991

20. Goldstein SA, Wilson DL, Sonstegard DA, Matthews LS. The mechanical properties of human tibial trabecular bone as a function of metaphyseal location. Journal of biomechanics 16(12): 965, 1983

21. Pope MH, Outwater JO. Mechanical properties of bone as a function of position and orientation. Journal of biomechanics 7(1): 61, 1974

22. Goldstein SA. The mechanical properties of trabecular bone: Dependence on anatomic location and function. Journal of biomechanics 20(11–12): 1055, 1987

23. A. AYHaDR. Mechanical Testing of Bone and the Bone–Implant Interface. New York, Ny: CRC Press, 2000

24. Mechanical Testing of Bone and the Bone-Implant Interface: CRC Press, 1999

25. Hvid I, Bentzen SM, Linde F, Mosekilde L, Pongsoipetch B. X-ray quantitative computed tomography: the relations to physical properties of proximal tibial trabecular bone specimens. Journal of biomechanics 22(8-9): 837, 1989

26. Cann CE, Genant HK. Precise measurement of vertebral mineral content using computed tomography. Journal of computer assisted tomography 4(4): 493, 1980

27. McBroom RJ, Hayes WC, Edwards WT, Goldberg RP, White AA, 3rd. Prediction of vertebral body compressive fracture using quantitative computed tomography. The Journal of bone and joint surgery American volume 67(8): 1206, 1985

28. Coathup MJ, Blunn GW, Flynn N, Williams C, Thomas NP. A comparison of bone remodelling around hydroxyapatite-coated, porous-coated and grit-blasted hip replacements retrieved at post-mortem. J Bone Joint Surg Br 83(1): 118, 2001

29. Wolff J. Concept of the Law of Bone Remodelling. In: The Law of Bone Remodelling. Springer Berlin Heidelberg. 1. 1986

30. Hart RT. Bone Modeling Remodeling: Theories and Computation. In: Cowin SC, ed. Bone Mechanics Handbook. Boca Raton: CRC Press. 1. 2001

31. Cowin SC. Mechanical modeling of the stress adaptation process in bone. Calcified tissue international 36 Suppl 1: S98, 1984

32. Hart RT, Davy DT, Heiple KG. A computational method for stress analysis of adaptive elastic materials with a view toward applications in strain-induced bone remodeling. J Biomech Eng 106(4): 342, 1984

33. Huiskes R, Weinans H, Grootenboer HJ, Dalstra M, Fudala B, Slooff TJ. Adaptive bone-remodeling theory applied to prosthetic-design analysis. Journal of biomechanics 20(11-12): 1135, 1987

34. Fyhrie DP, Carter DR. A unifying principle relating stress to trabecular bone morphology. Journal of orthopaedic research : official publication of the Orthopaedic Research Society 4(3): 304, 1986

35. Harrigan TP, Hamilton JJ. An analytical and numerical study of the stability of bone remodelling theories: dependence on microstructural stimulus. Journal of biomechanics 25(5): 477, 1992

36. Lanyon LE, Rubin CT. Static vs dynamic loads as an influence on bone remodelling. Journal of biomechanics 17(12): 897, 1984

37. Prendergast PJ, Taylor D. Prediction of bone adaptation using damage accumulation. Journal of biomechanics 27(8): 1067, 1994

38. Doblar M, Garc a M. Application of an anisotropic bone-remodelling model based on a damage-repair theory to the analysis of the proximal femur before and after total hip replacement. Journal of biomechanics 34(9): 1157, 2001

39. Beaupre GS, Orr TE, Carter DR. An approach for time-dependent bone modeling and remodeling--theoretical development. Journal of orthopaedic research : official publication of the Orthopaedic Research Society 8(5): 651, 1990

40. Carter DR. Mechanical loading histories and cortical bone remodeling. Calcified tissue international 36 Suppl 1: S19, 1984

41. Cowin SC, Hegedus DH. Bone remodeling I: theory of adaptive elasticity. J Elasticity 6(3): 313, 1976

42. Hegedus DH, Cowin SC. Bone remodeling II: small strain adaptive elasticity. J Elasticity 6(4): 337, 1976

43. Cowin SC, Van Buskirk WC. Internal bone remodeling induced by a medullary pin. Journal of biomechanics 11(5): 269, 1978

44. Cowin SC, Nachlinger RR. Bone remodeling III: uniqueness and stability in adaptive elasticity theory. J Elasticity 8(3): 285, 1978

45. Cowin SC, Firoozbakhsh K. Bone remodeling of diaphysial surfaces under constant load: theoretical predictions. Journal of biomechanics 14(7): 471, 1981

46. Cowin SC. Bone stress adaptation models. J Biomech Eng 115(4b): 528, 1993

47. Carter DR, Fyhrie DP, Whalen RT. Trabecular bone density and loading history: regulation of connective tissue biology by mechanical energy. Journal of biomechanics 20(8): 785, 1987

48. Carter DR, Orr TE, Fyhrie DP, Schurman DJ. Influences of mechanical stress on prenatal and postnatal skeletal development. Clinical orthopaedics and related research (219): 237, 1987

49. Carter DR. Mechanical loading history and skeletal biology. Journal of biomechanics 20(11-12): 1095, 1987

50. Beaupre GS, Orr TE, Carter DR. An approach for time-dependent bone modeling and remodeling-application: a preliminary remodeling simulation. Journal of orthopaedic research : official publication of the Orthopaedic Research Society 8(5): 662, 1990

51. Centers for Disease C, Prevention. Prevalence of doctor-diagnosed arthritis and arthritis-attributable activity limitation--United States, 2010-2012. MMWR Morbidity and mortality weekly report 62(44): 869, 2013

52. Hootman JM, Helmick CG. Projections of US prevalence of arthritis and associated activity limitations. Arthritis and rheumatism 54(1): 226, 2006

53. Kuo KN, Gitelis S, Sim FH, Pritchard D, Chao E, Rostoker W, Galante JO, McDonald P. Segmental replacement of long bones using titanium fiber metal composite following tumor resection. Clinical orthopaedics and related research (176): 108, 1983

54. Tips MH. Natural Home Remedies For Arthritis. In.:

55. Di Matteo B, Tarabella V, Filardo G, Vigano A, Tomba P, Marcacci M. John Rhea Barton: the birth of osteotomy. Knee surgery, sports traumatology, arthroscopy : official journal of the ESSKA 21(9): 1957, 2013

56. Brand RA, Mont MA, Manring MM. Biographical sketch: Themistocles Gluck (1853-1942). Clinical orthopaedics and related research 469(6): 1525, 2011

57. Hernigou P. Smith-Petersen and early development of hip arthroplasty. International orthopaedics 38(1): 193, 2014

58. Kovac S, Pisot V, Trebse R, Rotter A. Fifty-one-year survival of a Judet polymethylmethacrylate hip prosthesis. The Journal of arthroplasty 19(5): 664, 2004

59. Cameron HU, Pilliar RM, MacNab I. The effect of movement on the bonding of porous metal to bone. J Biomed Mater Res 7(4): 301, 1973

60. Franchi M, Fini M, Martini D, Orsini E, Leonardi L, Ruggeri A, Giavaresi G, Ottani V. Biological fixation of endosseous implants. Micron 36(7-8): 665, 2005

61. Burke R, Bragdon CR, Lowenstein JD. Mechanical aspects of the bone-porous surface interface under known amounts of implant motion,. In: Transactions of the 39th Annual Meeting Orthopaedic Research. 1993

62. Jasty M, Bragdon C, Burke D, O'Connor D, Lowenstein J, Harris WH. In vivo skeletal responses to porous-surfaced implants subjected to small induced motions. The Journal of bone and joint surgery American volume 79(5): 707, 1997

63. Pilliar RM, Lee JM, Maniatopoulos C. Observations on the effect of movement on bone ingrowth into porous-surfaced implants. Clinical orthopaedics and related research (208): 108, 1986

64. Futami T, Fujii N, Ohnishi H, Taguchi N, Kusakari H, Ohshima H, Maeda T. Tissue response to titanium implants in the rat maxilla: ultrastructural and histochemical observations of the bone-titanium interface. Journal of periodontology 71(2): 287, 2000

65. Sandborn PM, Cook SD, Spires WP, Kester MA. Tissue response to porous-coated implants lacking initial bone apposition. J Arthroplasty 3(4): 337, 1988

66. Cameron HU, Pilliar RM, Macnab I. The rate of bone ingrowth into porous metal. Journal of biomedical materials research 10(2): 295, 1976

67. Puleo DA, Nanci A. Understanding and controlling the bone-implant interface. Biomaterials 20(23-24): 2311, 1999

68. Kieswetter K, Schwartz Z, Dean DD, Boyan BD. The role of implant surface characteristics in the healing of bone. Critical reviews in oral biology and medicine : an official publication of the American Association of Oral Biologists 7(4): 329, 1996

69. SR H. Biomaterials Science, 2005

70. Anderson J. Biomaterial Sciences. In: Ratner BD HA, Schoen F, Lemons J., ed. San Diego, CA. 2005

71. Davies JE. Understanding peri-implant endosseous healing. Journal of dental education 67(8): 932, 2003

72. Gorbet MB, Sefton MV. Biomaterial-associated thrombosis: roles of coagulation factors, complement, platelets and leukocytes. Biomaterials 25(26): 5681, 2004

73. Bazzoni G, Dejana E, Del Maschio A. Platelet-dependent modulation of neutrophil function. Pharmacological research : the official journal of the Italian Pharmacological Society 26(3): 269, 1992

74. Gerstenfeld LC, Cho TJ, Kon T, Aizawa T, Cruceta J, Graves BD, Einhorn TA. Impaired intramembranous bone formation during bone repair in the absence of tumor necrosis factor-alpha signaling. Cells, tissues, organs 169(3): 285, 2001

75. Einhorn TA. The science of fracture healing. Journal of orthopaedic trauma 19(10 Suppl): S4, 2005

76. Sumner DR, Turner TM, Purchio AF, Gombotz WR, Urban RM, Galante JO. Enhancement of bone ingrowth by transforming growth factor-beta. The Journal of bone and joint surgery American volume 77(8): 1135, 1995

77. Lin M, Overgaard S, Glerup H, Soballe K, Bunger C. Transforming growth factor-beta1 adsorbed to tricalciumphosphate coated implants increases peri-implant bone remodeling. Biomaterials 22(3): 189, 2001

78. Liu Y, Huse RO, de Groot K, Buser D, Hunziker EB. Delivery mode and efficacy of BMP-2 in association with implants. Journal of dental research 86(1): 84, 2007

79. Park J, Lutz R, Felszeghy E, Wiltfang J, Nkenke E, Neukam FW, Schlegel KA. The effect on bone regeneration of a liposomal vector to deliver BMP-2 gene to bone grafts in peri-implant bone defects. Biomaterials 28(17): 2772, 2007

80. Ferrara N, Davis-Smyth T. The biology of vascular endothelial growth factor. Endocrine reviews 18(1): 4, 1997

81. Fischbach C, Mooney D. Polymeric Systems for Bioinspired Delivery of Angiogenic Molecules. In: Werner C, ed. Polymers for Regenerative Medicine. Springer Berlin Heidelberg. 191. 2006

82. Gruber R, Karreth F, Kandler B, Fuerst G, Rot A, Fischer MB, Watzek G. Platelet-released supernatants increase migration and proliferation, and decrease osteogenic differentiation of bone marrow-derived mesenchymal progenitor cells under in vitro conditions. Platelets 15(1): 29, 2004

83. Meyer U, Joos U, Mythili J, Stamm T, Hohoff A, Fillies T, Stratmann U, Wiesmann HP. Ultrastructural characterization of the implant/bone interface of immediately loaded dental implants. Biomaterials 25(10): 1959, 2004

84. Davies JE CR, Lowenberg B, Shiga A. . Deposition and resorption of calcified matrix in vitro by rat bone marrow cells. Cells Mater 1: 3, 1991

85. Davies JE NN, Takeshita N, Smith DC. Deposition of cement-like matrix on implant materials. In: The Bone-Biomaterial Interface. Toronto: University of Toronto Press. 285. 1991

86. Listgarten MA. Soft and hard tissue response to endosseous dental implants. The Anatomical record 245(2): 410, 1996

87. Marco F, Milena F, Gianluca G, Vittoria O. Peri-implant osteogenesis in health and osteoporosis. Micron 36(7-8): 630, 2005

88. Davies JE HMHM. Histodynamics of endosseous wound healing. In: JE D, ed. Bone Engineering. Toronto, ON: Em squared inc. 1. 2000

89. Raghavendra S, Wood MC, Taylor TD. Early wound healing around endosseous implants: a review of the literature. The International journal of oral & maxillofacial implants 20(3): 425, 2005

90. Edwards JT, Brunski JB, Higuchi HW. Mechanical and morphologic investigation of the tensile strength of a bone-hydroxyapatite interface. J Biomed Mater Res 36(4): 454, 1997

91. Bobyn JD, Pilliar RM, Cameron HU, Weatherly GC. The optimum pore size for the fixation of porous-surfaced metal implants by the ingrowth of bone. Clinical orthopaedics and related research (150): 263, 1980

92. Pilliar RM. Cementless implant fixation--toward improved reliability. The Orthopedic clinics of North America 36(1): 113, 2005

93. Brunski JB. In vivo bone response to biomechanical loading at the bone/dental-implant interface. Advances in dental research 13: 99, 1999

94. Branemark R, Ohrnell LO, Nilsson P, Thomsen P. Biomechanical characterization of osseointegration during healing: an experimental in vivo study in the rat. Biomaterials 18(14): 969, 1997

95. Frost HM. The Utah paradigm of skeletal physiology: an overview of its insights for bone, cartilage and collagenous tissue organs. Journal of bone and mineral metabolism 18(6): 305, 2000

96. Glassman AH, Bobyn JD, Tanzer M. New femoral designs: do they influence stress shielding? Clinical orthopaedics and related research 453: 64, 2006

97. Attar FG, Khaw FM, Kirk LM, Gregg PJ. Survivorship analysis at 15 years of cemented press-fit condylar total knee arthroplasty. J Arthroplasty 23(3): 344, 2008

98. Schlegel UJ, Knifka J, Rollinghoff M, Koebke J, Eysel P, Morlock MM. Effects of impaction on cement mantle and trabecular bone in hip resurfacing. Archives of orthopaedic and trauma surgery 131(4): 459, 2011

99. Font-Rodriguez DE, Scuderi GR, Insall JN. Survivorship of cemented total knee arthroplasty. Clinical orthopaedics and related research (345): 79, 1997

100. Kurtz SM, Lau E, Ong K, Zhao K, Kelly M, Bozic KJ. Future young patient demand for primary and revision joint replacement: national projections from 2010 to 2030. Clinical orthopaedics and related research 467(10): 2606, 2009

101. Surgeons AAO. Joint Revision Surgery - When Do I Need It? In.:

102. Bozic KJ, Kurtz SM, Lau E, Ong K, Chiu V, Vail TP, Rubash HE, Berry DJ. The epidemiology of revision total knee arthroplasty in the United States. Clinical orthopaedics and related research 468(1): 45, 2010

103. Association AO. National Joint Replacement Registry Report. In: Hip and Knee Arthoplasty Annual Report. 2014

104. Register SKA. Annual Report 2014. In. 2014

105. Greenfield E. Mounting for Artificial Teeth. In: Office USP, ed. United States. 1909

106. Grindlay JH, Clagett OT. A plastic sponge prosthesis for use after pneumonectomy; preliminary report of an experimental study. Mayo Clin Proc 24(21): 538, 1949

107. Waugh JGaJ. Plastic sponge which acts as a framework for living tissue. Arch Surg 63: 288, 1951

108. Newman Z. The use of the non-absorbable polyethylene sponge, “Polystan sponge” as a subcutaneous prostheses. . Br Plast Surg 9: 195, 1952

109. RS Bryan HJaJG. The effect of polyvinyl-formal (Ivalon) sponge on cortical bone healing. Proc Staff Mtg Mayo Clin 33: 453, 1958

110. Popovici AF. Polyvinyl plastic sponge in experimental orthopedic surgery; a preliminary report. Bull Georgetown Univ Med Cent 7(5): 177, 1954

111. Struthers AM. An experimental study of polyvinyl sponge as a substitute for bone. Plast Reconstr Surg (1946) 15(4): 274, 1955

112. Mandarino MP, Salvatore JE. Polyurethane polymer (ostamer): its use in fractured and diseased bones; experimental results. Surg Forum 9: 762, 1958

113. Gilmer WS, Jr., Tooms RE, Salvatore JE. An experimental study of the influence of implanted polyurethane sponges upon subsequent bone formation. Surg Gynecol Obstet 113: 143, 1961

114. Sadr B, Arden GP. A comparison of the stability of proplast-coated and cemented Thompson prostheses in the treatment of subcapital femoral fractures. Injury 8(3): 234, 1977

115. Simon AFaW. Bone ingrowth in Teflon sponge. Surg Gynecol Obstet 116: 588, 1963

116. Smith L. Ceramic-Plastic Material as a Bone Substitute. Arch Surg 87: 653, 1963

117. Hirschhorn J. Powder metallurgy fabrication of cobalt alloy surgical implant materials. Research in Dental and Medical Materials: 137, 1969

118. HS Hirshhorn AMaMD. Porous titanium surgical implant materials. Journal of Biomedical Materials Research 5(6): 49, 1971

119. CD Petersen JMaCS, et al. Union between bone and implants of open pore ceramic and stainless steel: a histologic study. J Bone Joint Surg 51A: 805, 1969

120. Hulbert SF, Young FA, Mathews RS, Klawitter JJ, Talbert CD, Stelling FH. Potential of ceramic materials as permanently implantable skeletal prostheses. J Biomed Mater Res 4(3): 433, 1970

121. Lueck RA, Galante J, Rostoker W, Ray RD. Development of an open pore metallic implant to permit attachment to bone. Surg Forum 20: 456, 1969

122. Galante J, Rostoker W, Lueck R, Ray RD. Sintered fiber metal composites as a basis for attachment of implants to bone. The Journal of bone and joint surgery American volume 53(1): 101, 1971

123. Lembert E, Galante J, Rostoker W. Fixation of skeletal replacement by fiber metal composites. Clinical orthopaedics and related research 87: 303, 1972

124. H Ronningen JGaWR. Fixation of total hip prostheses in dogs using fiber metal composites. In: Transactions of the 26th Annual Meeting of the Orthopaedic Research Society. 1980

125. Gustilo RKaR. Bias ingrowth prosthesis with bone grafting in failed femoral stem total hip arthroplasty. Phoenix: Harrington Arthritis Research Center, 1984

126. Galante J. Tissue ingrowth-total knee. Phoenix: Harrington Arthritis Research Center, 1984

127. Landon GC, Galante JO, Maley MM. Noncemented total knee arthroplasty. Clinical orthopaedics and related research (205): 49, 1986

128. Andersson GB, Gaechter A, Galante JO, Rostoker W. Segmental replacement of long bones in baboons using a fiber titanium implant. The Journal of bone and joint surgery American volume 60(1): 31, 1978

129. Heck DA, Chao EY, Sim FH, Pritchard DJ, Shives TC. Titanium fibermetal segmental replacement prostheses. A radiographic analysis and review of current status. Clinical orthopaedics and related research (204): 266, 1986

130. Welsh RP, Pilliar RM, Macnab I. Surgical implants. The role of surface porosity in fixation to bone and acrylic. The Journal of bone and joint surgery American volume 53(5): 963, 1971

131. Cameron HU, Macnab I, Pilliar RM. A porous metal system for joint replacement surgery. Int J Artif Organs 1(2): 104, 1978

132. Pilliar RM, Cameron HU, Macnab I. Porous surface layered prosthetic devices. Biomed Eng 10(4): 126, 1975

133. Bobyn JD, Pilliar RM, Cameron HU, Weatherly GC. Osteogenic phenomena across endosteal bone-implant spaces with porous surfaced intramedullary implants. Acta Orthop Scand 52(2): 145, 1981

134. Bobyn JD, Pilliar RM, Cameron HU, Weatherly GC, Kent GM. The effect of porous surface configuration on the tensile strength of fixation of implants by bone ingrowth. Clinical orthopaedics and related research (149): 291, 1980

135. Homsy CA, Cain TE, Kessler FB, Anderson MS, King JW. Porous implant systems for prosthesis stabilization. Clinical orthopaedics and related research 89: 220, 1972

136. Bryan WJ, McCaskill BL, Tullos HS. Hip endoprosthesis stabilization with a porous low modulus stem coating: factors influencing stabilization. Clinical orthopaedics and related research (157): 125, 1981

137. Tullos HS, McCaskill BL, Dickey R, Davidson J. Total hip arthroplasty with a low-modulus porous-coated femoral component. J Bone Joint Surg Am 66(6): 888, 1984

138. Maathuis PG, Visser JD. High failure rate of soft-interface stem coating for fixation of femoral endoprostheses. J Arthroplasty 11(5): 548, 1996

139. Goosen JH, Castelein RM, Runne WC, Dartee DA, Verheyen CC. Long-term results of a soft interface- (Proplast-) coated femoral stem. Acta orthopaedica 77(4): 585, 2006

140. Klawitter J. Application of porous ceramics for the attachment of high load internal orthopedic applications. In: Engineering Conference on Bioceramics: Engineering in MedicineHenniker. Henniker, NH. 1970

141. Klawitter JJaH, S. F. Application of porous ceramics for the attachment of load-bearing internal orthopaedic applications. J Biomed Mater Res 2: 161, 1971

142. Pilliar RM, Cameron HU, Welsh RP, Binnington AG. Radiographic and morphologic studies of load-bearing porous-surfaced structured implants. Clinical orthopaedics and related research (156): 249, 1981

143. Young FA, Spector M, Kresch CH. Porous titanium endosseous dental implants in Rhesus monkeys: microradiography and histological evaluation. J Biomed Mater Res 13(6): 843, 1979

144. Sauer BW, Weinstein AM, Klawitter JJ, Hulbert SF, Leonard RB, Bagwell JG. The role of porous polymeric materials in prosthesis attachment. J Biomed Mater Res 8(3): 145, 1974

145. Spector M, Flemming WR, Kreutner A. Bone growth into porous high-density polyethylene. J Biomed Mater Res 10(4): 595, 1976

146. Spector M, Michno MJ, Smarook WH, Kwiatkowski GT. A high-modulus polymer for porous orthopedic implants: biomechanical compatibility of porous implants. J Biomed Mater Res 12(5): 665, 1978

147. Albrektsson T, Branemark PI, Hansson HA, Lindstrom J. Osseointegrated titanium implants. Requirements for ensuring a long-lasting, direct bone-to-implant anchorage in man. Acta Orthop Scand 52(2): 155, 1981

148. Spector M. Historical review of porous-coated implants. The Journal of arthroplasty 2(2): 163, 1987

149. Corporation I. 510(k) Summary. k962468. In. 1997

150. Kostakos AT, Macheras GA, Frangakis CE, Stafilas KS, Baltas D, Xenakis TA. Migration of the trabecular metal monoblock acetabular cup system. The Journal of arthroplasty 25(1): 35, 2010

151. Levine BR, Sporer S, Poggie RA, Della Valle CJ, Jacobs JJ. Experimental and clinical performance of porous tantalum in orthopedic surgery. Biomaterials 27(27): 4671, 2006

152. Levine B. A New Era in Porous Metals: Applications in Orthopaedics. Advanced Engineering Materials 10(9): 788, 2008

153. Levine BR, Fabi DW. Porous metals in orthopedic applications – A review. Poröse Metalle in orthopädischen Anwendungen – Eine Übersicht. Materialwissenschaft und Werkstofftechnik 41(12): 1001, 2010

154. Day J HJ, Klein GR, Levine HB, Hartzband MA, Parvizi J, Kraay MJ,, Rimnac CM KS. Porous Coatings. In: 79th Annual Meeting of the American Academy of Orthopaedic Surgeons,. San Francisco,CA. 2012

155. Frenkel SR, Jaffe WL, Dimaano F, Iesaka K, Hua T. Bone response to a novel highly porous surface in a canine implantable chamber. J Biomed Mater Res B Appl Biomater 71(2): 387, 2004

156. Naziri Q, Issa K, Pivec R, Harwin SF, Delanois RE, Mont MA. Excellent results of primary THA using a highly porous titanium cup. Orthopedics 36(4): e390, 2013

157. Bourne RB, McCalden RW, Naudie D, Charron KD, Yuan X, Holdsworth DW. The next generation of acetabular shell design and bearing surfaces. Orthopedics 31(12 Suppl 2), 2008

158. Bertollo N, Matsubara M, Shinoda T, Chen D, Kumar M, Walsh WR. Effect of Surgical Fit on Integration of Cancellous Bone and Implant Cortical Bone Shear Strength for a Porous Titanium. The Journal of arthroplasty, 2011

159. Brownhill . BIOFOAM™ CANCELLOUS TITANIUM ™ fixation for orthopaedic implant applications. In. Wright Medial Poster:

160. Naudie DD, Somerville L, Korczak A, Yuan X, McCalden RW, Holdsworth D, Bourne RB. A randomized trial comparing acetabular component fixation of two porous ingrowth surfaces using RSA. The Journal of arthroplasty 28(8 Suppl): 48, 2013

161. Sperati G, Ceri L. Total hip arthroplasty using TRI-LOCK(R) DePuy bone preservation femoral stem: our experience. Acta bio-medica : Atenei Parmensis 85(2): 66, 2014

162. Bonicoli E, Piolanti N, Andreani L, Parchi P, Lisanti M. Preliminary report with the Regenerex™ revision shell: clinical, functional, and radiologic evaluations with a mean follow-up of 25 months. Eur Orthop Traumatol 4(1): 9, 2013

163. Gross CE, Huh J, Gray J, Demetracopoulos C, Nunley JA. Radiographic Outcomes Following Lateral Column Lengthening With a Porous Titanium Wedge. Foot & ankle international, 2015

164. Bobyn JD, Stackpool GJ, Hacking SA, Tanzer M, Krygier JJ. Characteristics of bone ingrowth and interface mechanics of a new porous tantalum biomaterial. J Bone Joint Surg Br 81(5): 907, 1999

165. Zimmer. Trabecular Metal SEM Image.

166. Zou X, Li H, Bunger M, Egund N, Lind M, Bunger C. Bone ingrowth characteristics of porous tantalum and carbon fiber interbody devices: an experimental study in pigs. Spine J 4(1): 99, 2004

167. Sinclair SK, Konz GJ, Dawson JM, Epperson RT, Bloebaum RD. Host bone response to polyetheretherketone versus porous tantalum implants for cervical spinal fusion in a goat model. Spine (Phila Pa 1976) 37(10): E571, 2012

168. Noiseux NO, Long WJ, Mabry TM, Hanssen AD, Lewallen DG. Uncemented porous tantalum acetabular components: early follow-up and failures in 613 primary total hip arthroplasties. The Journal of arthroplasty 29(3): 617, 2014

169. Moen TC, Ghate R, Salaz N, Ghodasra J, Stulberg SD. A Monoblock Porous Tantalum Acetabular Cup Has No Osteolysis on CT at 10 Years. Clinical orthopaedics and related research 469(2): 382, 2011

170. Fernandez-Fairen M, Murcia A, Blanco A, Merono A, Murcia A, Jr., Ballester J. Revision of failed total hip arthroplasty acetabular cups to porous tantalum components: a 5-year follow-up study. The Journal of arthroplasty 25(6): 865, 2010

171. Mohaddes M, Rolfson O, Karrholm J. Short-term survival of the trabecular metal cup is similar to that of standard cups used in acetabular revision surgery. Acta orthopaedica: 1, 2014

172. Wegrzyn J, Kaufman KR, Hanssen AD, Lewallen DG. Performance of Porous Tantalum vs. Titanium Cup in Total Hip Arthroplasty: Randomized Trial with Minimum 10-Year Follow-Up. The Journal of arthroplasty 30(6): 1008, 2015

173. Macheras GA, Kateros K, Koutsostathis SD, Tsakotos G, Galanakos S, Papadakis SA. The Trabecular Metal Monoblock acetabular component in patients with high congenital hip dislocation: a prospective study. J Bone Joint Surg Br 92(5): 624, 2010

174. D'Angelo F, Murena L, Campagnolo M, Zatti G, Cherubino P. Analysis of bone ingrowth on a tantalum cup. Indian journal of orthopaedics 42(3): 275, 2008

175. Kumar Nanjayan S, Wilton T. Trabecular metal patella--is it really doomed to fail in the totally patellar-deficient knee? A case report of patellar reconstruction with a novel technique. The Knee 21(3): 779, 2014

176. Kamath AF, Gee AO, Nelson CL, Garino JP, Lotke PA, Lee GC. Porous tantalum patellar components in revision total knee arthroplasty minimum 5-year follow-up. The Journal of arthroplasty 27(1): 82, 2012

177. Unger AS, Duggan JP. Midterm results of a porous tantalum monoblock tibia component clinical and radiographic results of 108 knees. The Journal of arthroplasty 26(6): 855, 2011

178. Tigani D, Trentani P, Trentani F, Andreoli I, Sabbioni G, Del Piccolo N. Trabecular metal patella in total knee arthroplasty with patella bone deficiency. The Knee 16(1): 46, 2009

179. Wilson DA, Richardson G, Hennigar AW, Dunbar MJ. Continued stabilization of trabecular metal tibial monoblock total knee arthroplasty components at 5 years-measured with radiostereometric analysis. Acta orthopaedica 83(1): 36, 2012

180. Henricson A, Rosmark D, Nilsson KG. Trabecular metal tibia still stable at 5 years: an RSA study of 36 patients aged less than 60 years. Acta orthopaedica 84(4): 398, 2013

181. Niemelainen M, Skytta ET, Remes V, Makela K, Eskelinen A. Total knee arthroplasty with an uncemented trabecular metal tibial component: a registry-based analysis. The Journal of arthroplasty 29(1): 57, 2014

182. Meneghini RM, de Beaubien BC. Early Failure of Cementless Porous Tantalum Monoblock Tibial Components. The Journal of arthroplasty, 2013

183. Sambaziotis C, Lovy AJ, Koller KE, Bloebaum RD, Hirsh DM, Kim SJ. Histologic retrieval analysis of a porous tantalum metal implant in an infected primary total knee arthroplasty. The Journal of arthroplasty 27(7): 1413 e5, 2012

184. Tigani D, Sabbioni G, Raimondi A. Early aseptic loosening of a porous tantalum knee prosthesis. La Chirurgia degli organi di movimento 93(3): 187, 2009

185. Helm AT, Kerin C, Ghalayini SR, McLauchlan GJ. Preliminary results of an uncemented trabecular metal tibial component in total knee arthroplasty. The Journal of arthroplasty 24(6): 941, 2009

186. Wilson DA, Astephen JL, Hennigar AW, Dunbar MJ. Inducible displacement of a trabecular metal tibial monoblock component. The Journal of arthroplasty 25(6): 893, 2010

187. Minoda Y, Kobayashi A, Iwaki H, Ikebuchi M, Inori F, Takaoka K. Comparison of bone mineral density between porous tantalum and cemented tibial total knee arthroplasty components. The Journal of bone and joint surgery American volume 92(3): 700, 2010

188. Komarasamy B, Vadivelu R, Bruce A, Kershaw C, Davison J. Clinical and radiological outcome following total hip arthroplasty with an uncemented trabecular metal monoblock acetabular cup. Acta Orthop Belg 72(3): 320, 2006

189. Macheras GA, Papagelopoulos PJ, Kateros K, Kostakos AT, Baltas D, Karachalios TS. Radiological evaluation of the metal-bone interface of a porous tantalum monoblock acetabular component. J Bone Joint Surg Br 88(3): 304, 2006

190. Xenakis TA, Macheras GA, Stafilas KS, Kostakos AT, Bargiotas K, Malizos KN. Multicentre use of a porous tantalum monoblock acetabular component. International orthopaedics 33(4): 911, 2009

191. Simon JP, Bellemans J. Clinical and radiological evaluation of modular trabecular metal acetabular cups. Short-term results in 64 hips. Acta Orthop Belg 75(5): 623, 2009

192. Schmidt C, Ignatius AA, Claes LE. Proliferation and differentiation parameters of human osteoblasts on titanium and steel surfaces. J Biomed Mater Res 54(2): 209, 2001

193. Ramamurti BS, Orr TE, Bragdon CR, Lowenstein JD, Jasty M, Harris WH. Factors influencing stability at the interface between a porous surface and cancellous bone: a finite element analysis of a canine in vivo micromotion experiment. J Biomed Mater Res 36(2): 274, 1997

194. Dammak M, Shirazi-Adl A, Schwartz M, Jr., Gustavson L. Friction properties at the bone-metal interface: comparison of four different porous metal surfaces. J Biomed Mater Res 35(3): 329, 1997

195. Soballe K, Brockstedt-Rasmussen H, Hansen ES, Bunger C. Hydroxyapatite coating modifies implant membrane formation. Controlled micromotion studied in dogs. Acta Orthop Scand 63(2): 128, 1992

196. Szmukler-Moncler S, Salama H, Reingewirtz Y, Dubruille JH. Timing of loading and effect of micromotion on bone-dental implant interface: review of experimental literature. J Biomed Mater Res 43(2): 192, 1998

197. Kienapfel H, Sprey C, Wilke A, Griss P. Implant fixation by bone ingrowth. The Journal of arthroplasty 14(3): 355, 1999

198. Zhang Y, Ahn PB, Fitzpatrick DC, Heiner AD, Poggie RA, Brown TD. INTERFACIAL FRICTIONAL BEHAVIOR: CANCELLOUS BONE, CORTICAL BONE, AND A NOVEL POROUS TANTALUM BIOMATERIAL. Journal of Musculoskeletal Research 03(04): 245, 1999

199. Karageorgiou V, Kaplan D. Porosity of 3D biomaterial scaffolds and osteogenesis. Biomaterials 26(27): 5474, 2005

200. Petersilge WJ, D'Lima DD, Walker RH, Colwell CW, Jr. Prospective study of 100 consecutive Harris-Galante porous total hip arthroplasties. 4- to 8-year follow-up study. The Journal of arthroplasty 12(2): 185, 1997

201. Otsuki B, Takemoto M, Fujibayashi S, Neo M, Kokubo T, Nakamura T. Pore throat size and connectivity determine bone and tissue ingrowth into porous implants: three-dimensional micro-CT based structural analyses of porous bioactive titanium implants. Biomaterials 27(35): 5892, 2006

202. Tarala M, Waanders D, Biemond JE, Hannink G, Janssen D, Buma P, Verdonschot N. The effect of bone ingrowth depth on the tensile and shear strength of the implant-bone e-beam produced interface. Journal of materials science Materials in medicine 22(10): 2339, 2011

203. Majkowski RS, Bannister GC, Miles AW. The effect of bleeding on the cement-bone interface. An experimental study. Clinical orthopaedics and related research (299): 293, 1994

204. Adler E, Stuchin SA, Kummer FJ. Stability of press-fit acetabular cups. The Journal of arthroplasty 7(3): 295, 1992

205. Agency FD. National Medical Device Postmarket Surveillance Plan. In. 2013

206. Health NIo. Improving Medical Implant Performance Through Retrieval Information: Challenges and Opportunities. In: National Institutes of Health Technology Assessment Statement. 2003

207. Au AG, Liggins AB, Raso VJ, Amirfazli A. A parametric analysis of fixation post shape in tibial knee prostheses. Medical engineering & physics 27(2): 123, 2005

208. Tissakht M, Ahmed AM, Chan KC. Calculated stress-shielding in the distal femur after total knee replacement corresponds to the reported location of bone loss. Journal of orthopaedic research : official publication of the Orthopaedic Research Society 14(5): 778, 1996

209. Swider P, Pedrono A, Mouzin O, Soballe K, Bechtold JE. Biomechanical analysis of the shear behaviour adjacent to an axially loaded implant. Journal of biomechanics 39(10): 1873, 2006

210. Tarala M, Janssen D, Verdonschot N. Balancing incompatible endoprosthetic design goals: a combined ingrowth and bone remodeling simulation. Medical engineering & physics 33(3): 374, 2011

211. Behrens BA, Nolte I, Wefstaedt P, Stukenborg-Colsman C, Bouguecha A. Numerical investigations on the strain-adaptive bone remodelling in the periprosthetic femur: influence of the boundary conditions. Biomedical engineering online 8: 7, 2009

212. Gillies RM, Hogg MC, Kohan L, Cordingley RL. Adaptive bone remodelling of all polyethylene unicompartmental tibial bearings. ANZ journal of surgery 77(1-2): 69, 2007

213. Fitzpatrick CK, Hemelaar P, Taylor M. Computationally efficient prediction of bone-implant interface micromotion of a cementless tibial tray during gait. Journal of biomechanics 47(7): 1718, 2014

214. van der Ploeg B, Tarala M, Homminga J, Janssen D, Buma P, Verdonschot N. Toward a more realistic prediction of peri-prosthetic micromotions. Journal of orthopaedic research : official publication of the Orthopaedic Research Society 30(7): 1147, 2012

215. Chong DY, Hansen UN, Amis AA. Analysis of bone-prosthesis interface micromotion for cementless tibial prosthesis fixation and the influence of loading conditions. Journal of biomechanics 43(6): 1074, 2010

216. Jasty M, Bragdon CR, Zalenski E, O'Connor D, Page A, Harris WH. Enhanced stability of uncemented canine femoral components by bone ingrowth into the porous coatings. The Journal of arthroplasty 12(1): 106, 1997

217. Andreykiv A, Prendergast PJ, van Keulen F, Swieszkowski W, Rozing PM. Bone ingrowth simulation for a concept glenoid component design. Journal of biomechanics 38(5): 1023, 2005

218. Vivanco J, Fang Z, Levine D, Ploeg HL. Evaluation of the mechanical behavior of a direct compression molded porous tantalum-UHMWPE construct: a microstructural model. Journal of applied biomaterials & biomechanics : JABB 7(1): 34, 2009

219. Zimmer. Trabecular Metal™ Technology. In.:

220. Cherian JJ, Jauregui JJ, Banerjee S, Pierce T, Mont MA. What Host Factors Affect Aseptic Loosening After THA and TKA? Clinical orthopaedics and related research, 2015

221. Register SHA. Annual Report 2010. In. 2010

222. Registery AH. Annual Report 2011. In. 2011

223. Bozic KJ, Kurtz SM, Lau E, Ong K, Vail TP, Berry DJ. The epidemiology of revision total hip arthroplasty in the United States. The Journal of bone and joint surgery American volume 91(1): 128, 2009

224. Register SHA. Annual Report 2013. In. 2013

225. Fehring TK, Odum S, Griffin WL, Mason JB, Nadaud M. Early failures in total knee arthroplasty. Clinical orthopaedics and related research (392): 315, 2001

226. Moran CG, Pinder IM, Lees TA, Midwinter MJ. Survivorship analysis of the uncemented porous-coated anatomic knee replacement. The Journal of bone and joint surgery American volume 73(6): 848, 1991

227. Berger RA, Lyon JH, Jacobs JJ, Barden RM, Berkson EM, Sheinkop MB, Rosenberg AG, Galante JO. Problems with cementless total knee arthroplasty at 11 years followup. Clinical orthopaedics and related research (392): 196, 2001

228. Bobyn JD, Poggie RA, Krygier JJ, Lewallen DG, Hanssen AD, Lewis RJ, Unger AS, O'Keefe TJ, Christie MJ, Nasser S, Wood JE, Stulberg SD, Tanzer M. Clinical validation of a structural porous tantalum biomaterial for adult reconstruction. The Journal of bone and joint surgery American volume 86-A Suppl 2: 123, 2004

229. Dunbar MJ, Wilson DA, Hennigar AW, Amirault JD, Gross M, Reardon GP. Fixation of a trabecular metal knee arthroplasty component. A prospective randomized study. The Journal of bone and joint surgery American volume 91(7): 1578, 2009

230. Dorr LD, Lewonowski K, Lucero M, Harris M, Wan Z. Failure mechanisms of anatomic porous replacement I cementless total hip replacement. Clinical orthopaedics and related research (334): 157, 1997

231. Sumner DR, Jasty M, Jacobs JJ, Urban RM, Bragdon CR, Harris WH, Galante JO. Histology of porous-coated acetabular components. 25 cementless cups retrieved after arthroplasty. Acta Orthop Scand 64(6): 619, 1993

232. Gonzalez della Valle A, Ruzo PS, Li S, Pellicci P, Sculco TP, Salvati EA. Dislodgment of polyethylene liners in first and second-generation Harris-Galante acetabular components. A report of eighteen cases. The Journal of bone and joint surgery American volume 83-a(4): 553, 2001

233. Tompkins GS, Jacobs JJ, Kull LR, Rosenberg AG, Galante JO. Primary total hip arthroplasty with a porous-coated acetabular component. Seven-to-ten-year results. The Journal of bone and joint surgery American volume 79(2): 169, 1997

234. Klika AK, Murray TG, Darwiche H, Barsoum WK. Options for acetabular fixation surfaces. J Long Term Eff Med Implants 17(3): 187, 2007

235. Hacking SA, Bobyn JD, Toh K, Tanzer M, Krygier JJ. Fibrous tissue ingrowth and attachment to porous tantalum. J Biomed Mater Res 52(4): 631, 2000

236. Administration USFaD. 510(k) Premarket Notification: K021891. In. September 5th, 2001. 1

237. Bloebaum RD, Mihalopoulus NL, Jensen JW, Dorr LD. Postmortem analysis of bone growth into porous-coated acetabular components. The Journal of bone and joint surgery American volume 79(7): 1013, 1997

238. Sorrells RB, Voorhorst PE, Murphy JA, Bauschka MP, Greenwald AS. Uncemented rotating-platform total knee replacement: a five to twelve-year follow-up study. The Journal of bone and joint surgery American volume 86-A(10): 2156, 2004

239. Akizuki S, Takizawa T, Horiuchi H. Fixation of a hydroxyapatite-tricalcium phosphate-coated cementless knee prosthesis. Clinical and radiographic evaluation seven years after surgery. J Bone Joint Surg Br 85(8): 1123, 2003

240. Berger RA, Rosenberg AG, Barden RM, Sheinkop MB, Jacobs JJ, Galante JO. Long-term followup of the Miller-Galante total knee replacement. Clinical orthopaedics and related research (388): 58, 2001

241. Goldberg VM, Kraay M. The outcome of the cementless tibial component: a minimum 14-year clinical evaluation. Clinical orthopaedics and related research (428): 214, 2004

242. Ritter MA, Meneghini RM. Twenty-Year Survivorship of Cementless Anatomic Graduated Component Total Knee Arthroplasty. The Journal of arthroplasty 25(4): 507, 2010

243. Melton JT, Mayahi R, Baxter SE, Facek M, Glezos C. Long-term outcome in an uncemented, hydroxyapatite-coated total knee replacement: a 15- to 18-year survivorship analysis. J Bone Joint Surg Br 94(8): 1067, 2012

244. Bloebaum RD, Bachus KN, Jensen JW, Hofmann AA. Postmortem analysis of consecutively retrieved asymmetric porous-coated tibial components. The Journal of arthroplasty 12(8): 920, 1997

245. Engh GA, Bobyn JD, Petersen TL. Radiographic and histologic study of porous coated tibial component fixation in cementless total knee arthroplasty. Orthopedics 11(5): 725, 1988

246. Engh GA, Parks NL, Ammeen DJ. Tibial osteolysis in cementless total knee arthroplasty. A review of 25 cases treated with and without tibial component revision. Clinical orthopaedics and related research (309): 33, 1994

247. Kim YH, Oh JH, Oh SH. Osteolysis around cementless porous-coated anatomic knee prostheses. J Bone Joint Surg Br 77(2): 236, 1995

248. Scott N. Knee Wear. In: Insall & Scott Surgery of the Knee. Elservier. 175. 2012

249. Kurtz SM, Kocagoz SB, Hanzlik JA, Underwood RJ, Gilbert JL, MacDonald DW, Lee GC, Mont MA, Kraay MJ, Klein GR, Parvizi J, Rimnac CM. Do ceramic femoral heads reduce taper fretting corrosion in hip arthroplasty? A retrieval study. Clinical orthopaedics and related research 471(10): 3270, 2013

250. Bloebaum RD, Bachus KN, Jensen JW, Scott DF, Hofmann AA. Porous-coated metal-backed patellar components in total knee replacement. A postmortem retrieval analysis. The Journal of bone and joint surgery American volume 80(4): 518, 1998

251. Sumner DR, Kienapfel H, Jacobs JJ, Urban RM, Turner TM, Galante JO. Bone ingrowth and wear debris in well-fixed cementless porous-coated tibial components removed from patients. The Journal of arthroplasty 10(2): 157, 1995

252. Vigorita VJ, Minkowitz B, Dichiara JF, Higham PA. A histomorphometric and histologic analysis of the implant interface in five successful, autopsy-retrieved, noncemented porous-coated knee arthroplasties. Clinical orthopaedics and related research (293): 211, 1993

253. Cook SD, Barrack RL, Thomas KA, Haddad RJ, Jr. Quantitative histologic analysis of tissue growth into porous total knee components. The Journal of arthroplasty 4 Suppl: S33, 1989

254. Meneghini RM, de Beaubien BC. Early failure of cementless porous tantalum monoblock tibial components. J Arthroplasty 28(9): 1505, 2013

255. Keyak JH, Kaneko TS, Tehranzadeh J, Skinner HB. Predicting proximal femoral strength using structural engineering models. Clinical orthopaedics and related research (437): 219, 2005

256. Keyak JH, Falkinstein Y. Comparison of in situ and in vitro CT scan-based finite element model predictions of proximal femoral fracture load. Medical engineering & physics 25(9): 781, 2003

257. Schileo E, Dall'ara E, Taddei F, Malandrino A, Schotkamp T, Baleani M, Viceconti M. An accurate estimation of bone density improves the accuracy of subject-specific finite element models. Journal of biomechanics 41(11): 2483, 2008

258. Bergmann G, Bender A, Graichen F, Dymke J, Rohlmann A, Trepczynski A, Heller MO, Kutzner I. Standardized loads acting in knee implants. PloS one 9(1): e86035, 2014

259. Orthoload. In.:

260. Waanders D, Janssen D, Miller MA, Mann KA, Verdonschot N. Fatigue creep damage at the cement-bone interface: an experimental and a micro-mechanical finite element study. Journal of biomechanics 42(15): 2513, 2009

261. Taylor M, Barrett DS, Deffenbaugh D. Influence of loading and activity on the primary stability of cementless tibial trays. Journal of orthopaedic research : official publication of the Orthopaedic Research Society 30(9): 1362, 2012

262. Miao X, Sun D. Graded/Gradient Porous Biomaterials. Materials 3(1): 26, 2009

263. Kováčik . Correlation between Young's modulus and porosity in porous materials. Journal of Materials Science Letters 18(13): 1007, 1999

264. Tarala M, Janssen D, Verdonschot N. Toward a method to simulate the process of bone ingrowth in cementless THA using finite element method. Medical engineering & physics 35(4): 543, 2013

265. Lonner JH, Klotz M, Levitz C, Lotke PA. Changes in bone density after cemented total knee arthroplasty: influence of stem design. The Journal of arthroplasty 16(1): 107, 2001

266. Davis AM, Damani M, White LM, Wunder JS, Griffin AM, Bell RS. Periprosthetic bone remodeling around a prosthesis for distal femoral tumors: longitudinal follow-up. The Journal of arthroplasty 20(2): 219, 2005

267. Minoda Y, Kobayashi A, Ikebuchi M, Iwaki H, Inori F, Nakamura H. Porous tantalum tibial component prevents periprosthetic loss of bone mineral density after total knee arthroplasty for five years-a matched cohort study. The Journal of arthroplasty 28(10): 1760, 2013

268. Huiskes R, Weinans H, van Rietbergen B. The relationship between stress shielding and bone resorption around total hip stems and the effects of flexible materials. Clinical orthopaedics and related research (274): 124, 1992

269. Martin RB. Porosity and specific surface of bone. Critical reviews in biomedical engineering 10(3): 179, 1984

270. Janssen D, Aquarius R, Stolk J, Verdonschot N. Finite-element analysis of failure of the Capital Hip designs. J Bone Joint Surg Br 87(11): 1561, 2005

271. Morlock M, Schneider E, Bluhm A, Vollmer M, Bergmann G, Muller V, Honl M. Duration and frequency of every day activities in total hip patients. Journal of biomechanics 34(7): 873, 2001

272. Heller MO, Bergmann G, Deuretzbacher G, Durselen L, Pohl M, Claes L, Haas NP, Duda GN. Musculo-skeletal loading conditions at the hip during walking and stair climbing. Journal of biomechanics 34(7): 883, 2001

273. Janssen D, Mann KA, Verdonschot N. Micro-mechanical modeling of the cement-bone interface: the effect of friction, morphology and material properties on the micromechanical response. Journal of biomechanics 41(15): 3158, 2008

274. Pérez MA, García JM, Doblaré M. Analysis of the debonding of the stem–cement interface in intramedullary fixation using a non-linear fracture mechanics approach. Engineering Fracture Mechanics 72(8): 1125, 2005

275. Nuño N, Groppetti R, Senin N. Static coefficient of friction between stainless steel and PMMA used in cemented hip and knee implants. Clinical Biomechanics 21(9): 956, 2006

Appendix A Additional Bone Ingrowth Results

For all implant types, bone ingrowth was highest in the upper 500 μm of the porous tantalum substrate (Table A-1).

Table A-1: Bone area/pore area depth analysis based on implant type.

Porous Coating	BA/PA Zone 1	BA/PA Zone 2	BA/PA Zone 3
Acetabular Shell	Higher	Lower	Lower
Femoral Stem	Higher	-	Lower
Tibial Tray	Higher	-	Lower
Tibial Tray Peg	Higher	Lower	Lower
Patella	Higher	Lower	Lower

The high and knee porous tantalum implants are each different geometrically, the thickness of the porous tantalum substrate and loaded differently. A comparison between the bone measurements for the different implants want completed. Acetabular shells and femoral stems had a higher amount of bone ingrowth than the tibial trays (Table A-2).

Table A-2: Bone measurements based on implant type.

Porous Coating	BA/PA (%)	Extent of Ingrowth (%)	Maximum Depth (%)
Acetabular Shell	Higher	Higher	Higher
Femoral Stem	Higher	-	Higher
Tibial Tray	**Lower**	**Lower**	**Lower**
Tibial Tray Peg	-	Higher	Higher
Patella	-	-	-

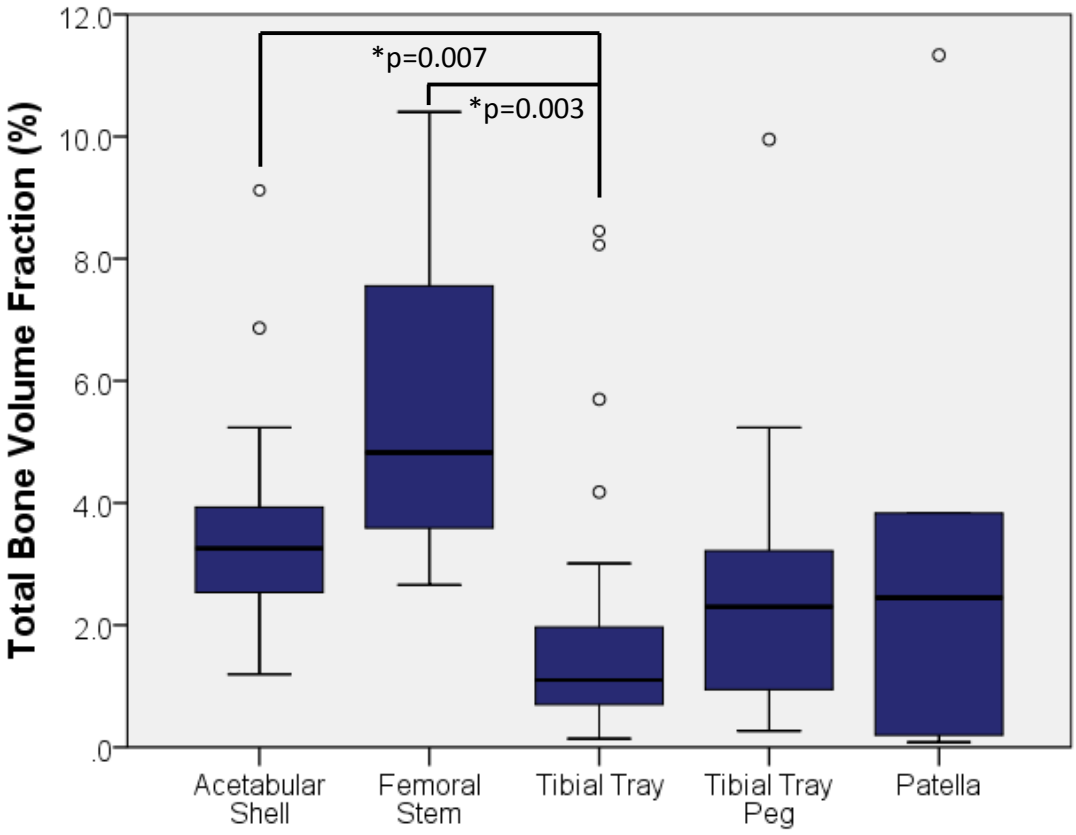

Figure A-1: Bone area/pore area (BA/PA) based on implant type.

The average extent of bone ingrowth was lowest in the tibial trays (21% ±21) and highest in the femoral stems (47% ± 26) (Figure A-2).

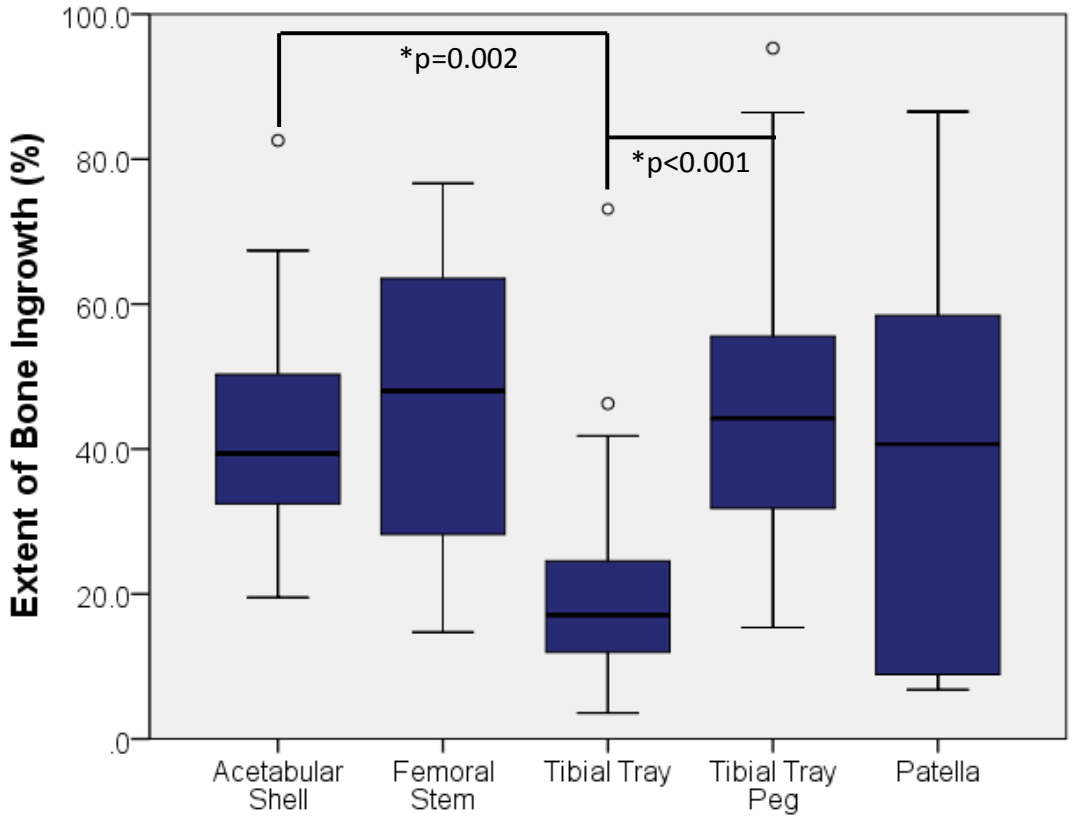

Figure A-2: Extent of ingrowth based on implant type.

The average maximum depth expressed as a length shows that most of the implants show some instances where the bone grew into the full depth of the porous tantalum substrate. However, the tibial tray still shows lower ingrowth depth (Figure A-3).

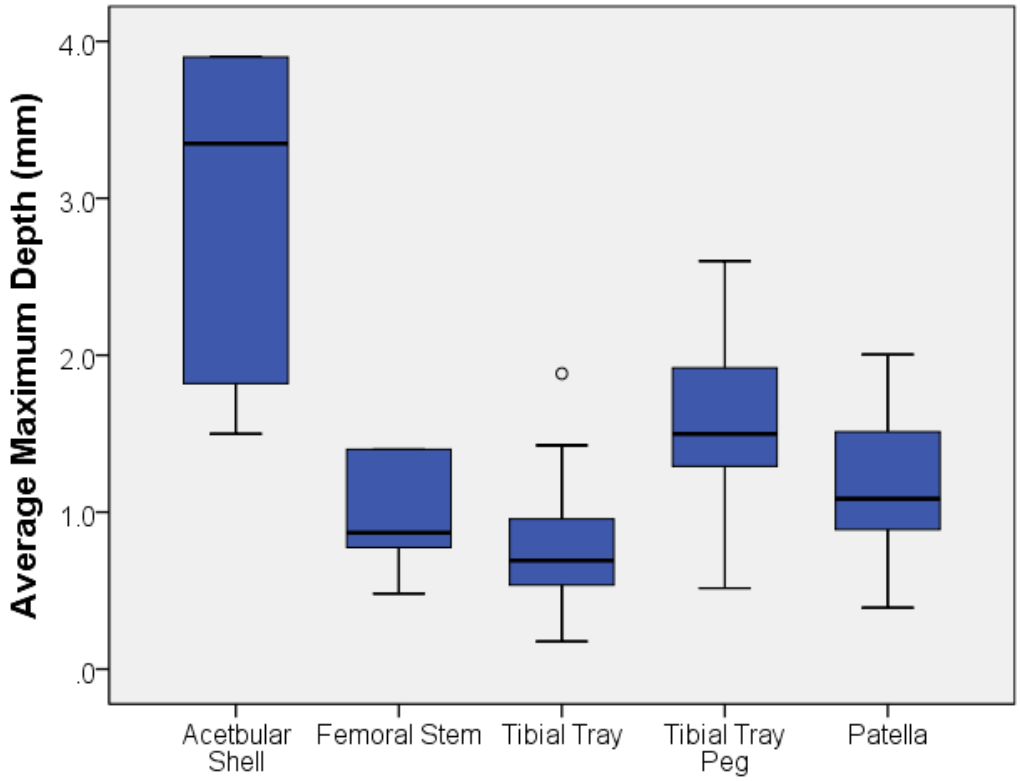

Figure A-3: Average maximum depth based on implant type, expressed as length (mm).

The average maximum depth of bone ingrowth was lowest for the tibial trays (61%± 22) and highest in the femoral stems (82%±23) (Figure A-4). The femoral stems were implanted for a short duration and immature woven bone formation was seen in several implants. Bone ingrowth was primarily located in curved medial and lateral portions of the stem.

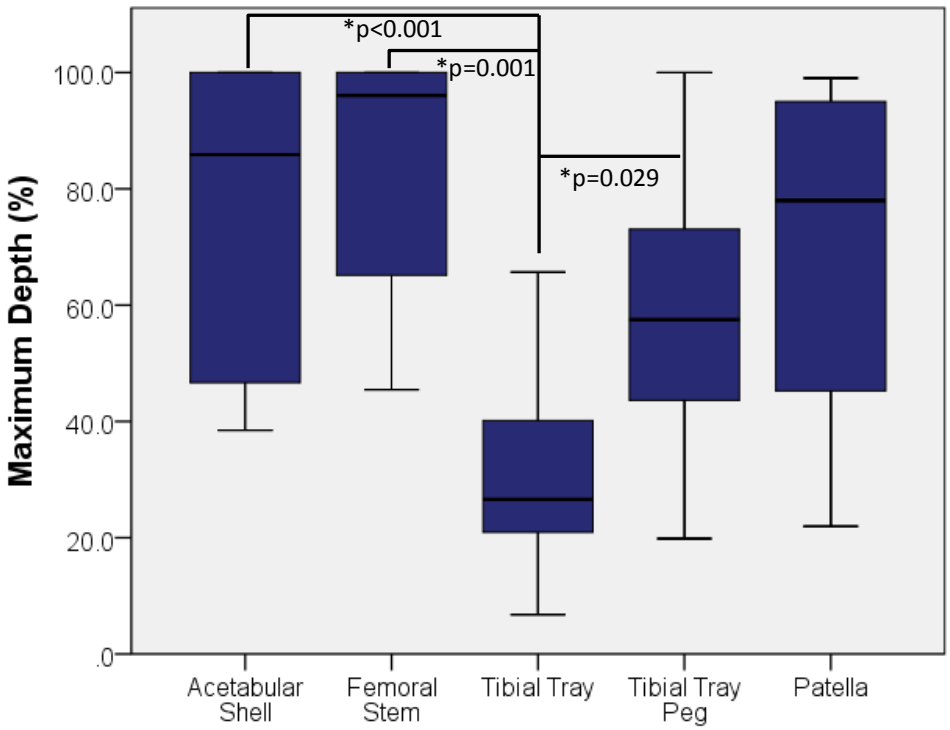

Figure A-4: Maximum depth of ingrowth expressed as a percentage based on anatomic location.

Appendix B Micromotion Model Development

For the development of the models, different options for applying to load on the UHMWPE insert were explored. The first two methods involved using point loads on the tibial insert directly. The first point load showed that the stress did not distribute properly through the UHMWPE insert (Figure B-1).

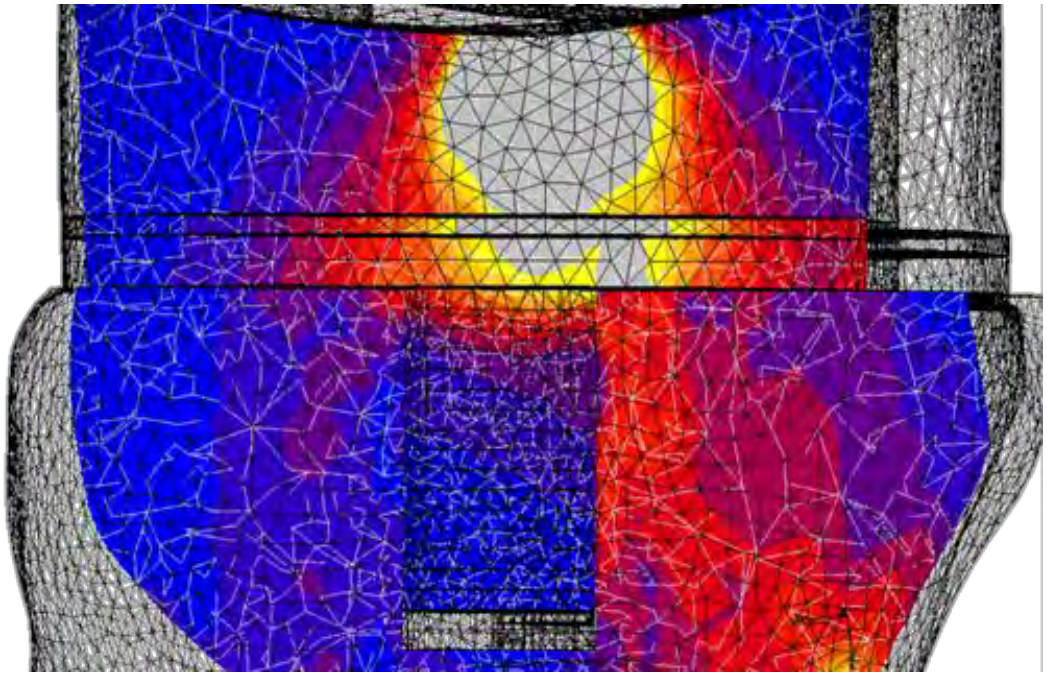

Figure B-1: Distribution of stress into the monoblock implant model when using one point loads

Using a five point loads (equivalent load in the center point) still did not allow the stress to distribute properly through the UHMWPE insert (Figure B-2).

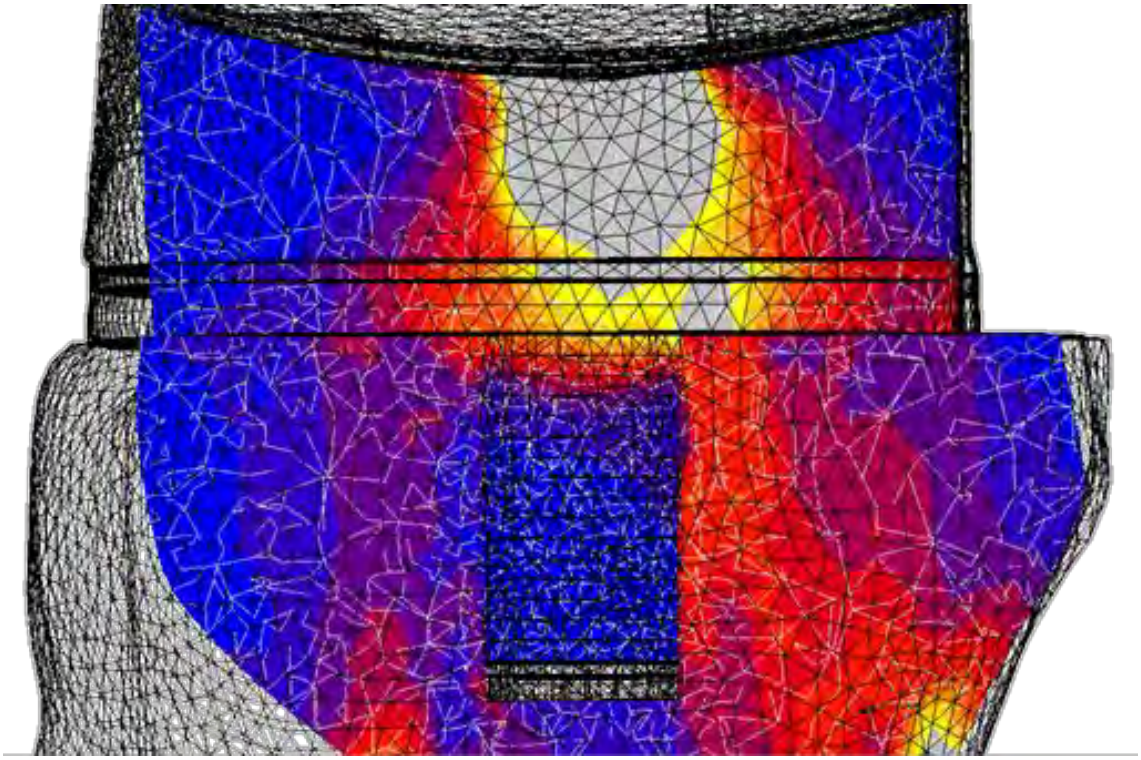

Figure B-2: Distribution of stress into the monoblock implant model when using five point loads

The use of a femoral component showed a more realistic distribution of the loading through the UHMWPE insert and into the next layer of the implant (Figure B-3).

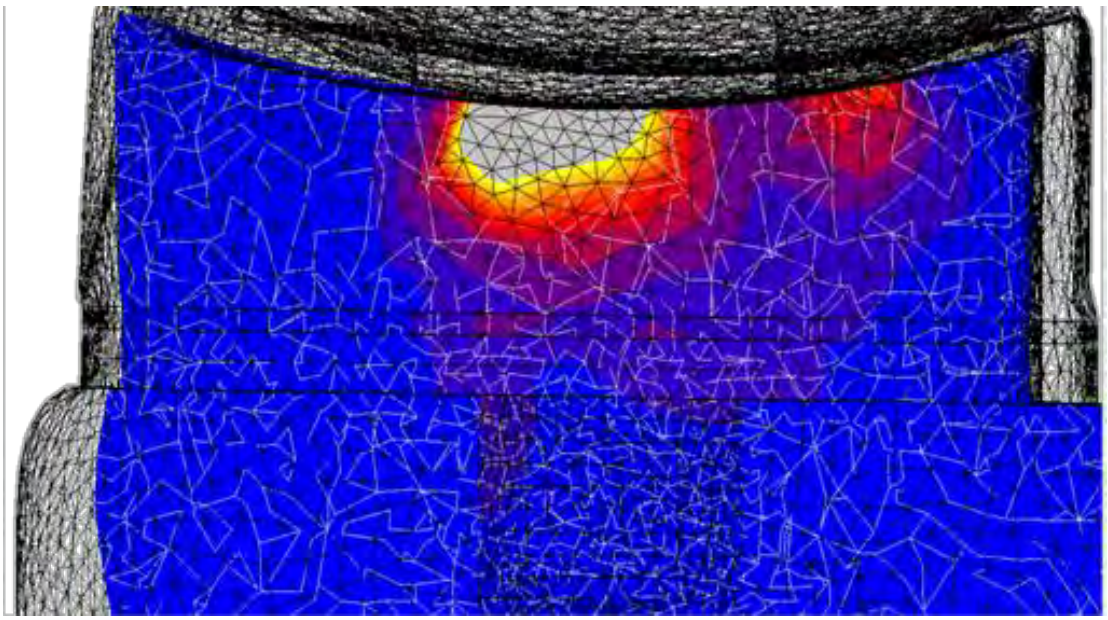

Figure B-3: Distribution of stress into the monoblock implant model when using a femoral component.

The interference fit between the bone and implant has been shown to have an effect. In the clinical setting, it is assumed that. The effect of interference on the stress of the bone was investigated. Interference fit of 50 μm showed stress concentrations on the bone at the edges of the peg. The interference fit of 20 μm showed lower stress at the peg region of the bone (Figure B-4).

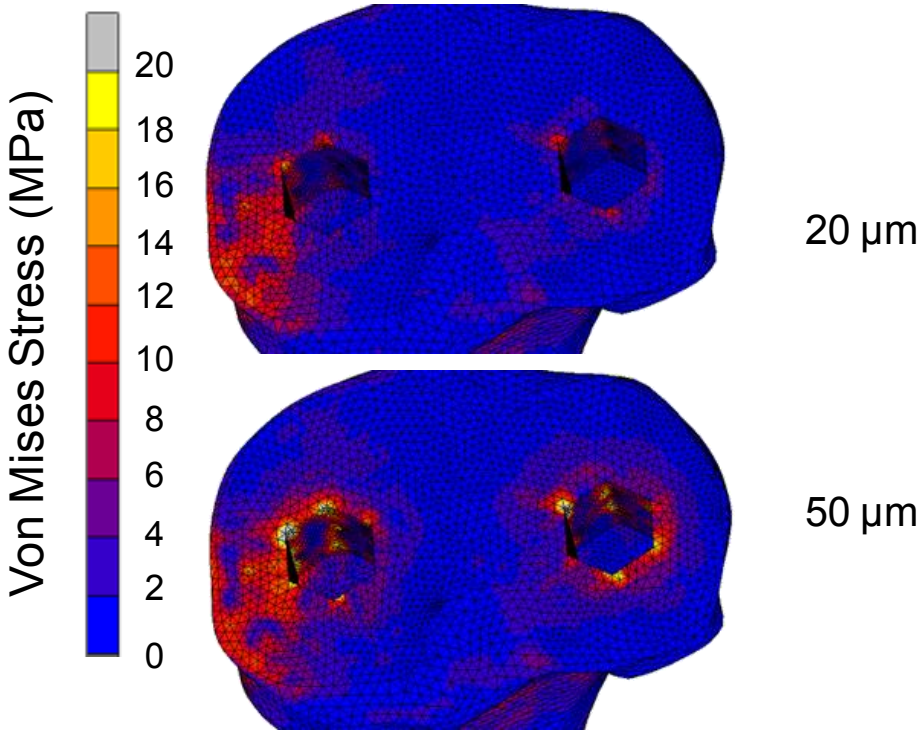

Figure B-4: Bone stress based on interference fit size. Note: High stress concentrations on the bone near the pegs for 50 µm.

The interference fit of 20 um decreased the micromotion at the bone-peg interface and tray region for the monoblock design (Figure B-5).

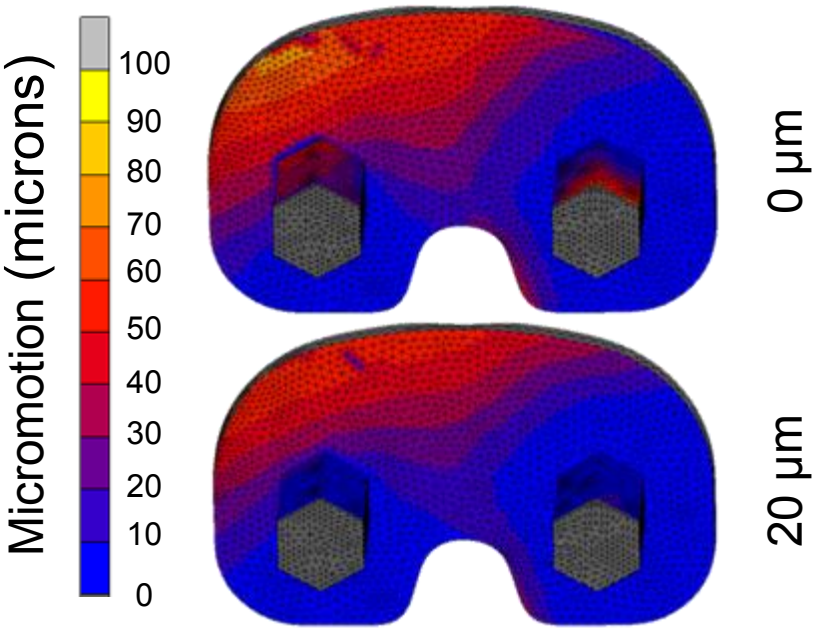

Figure B-5: Interference fit effect on micromotion for the monoblock porous tantalum tibial tray.

The interference fit of 20 um decreased the micromotion at the bone-peg interface and tray region for the modular design (Figure B-6).

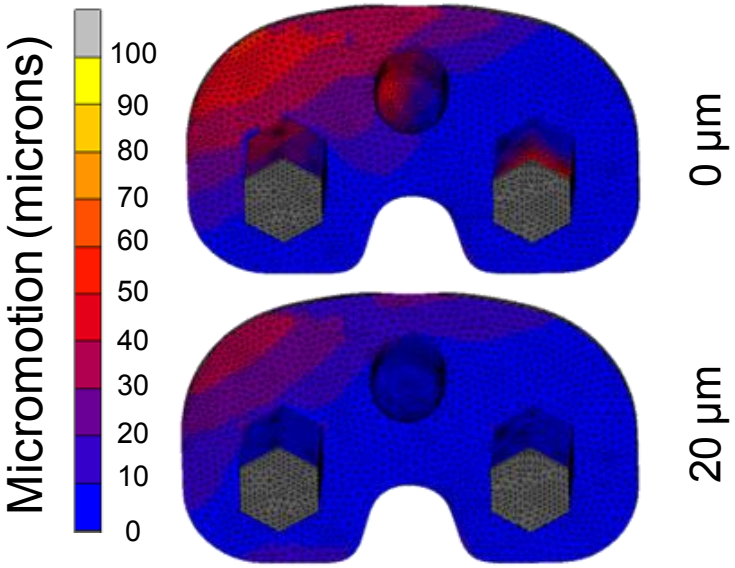

Figure B-6: Interference fit effect on micromotion for the modular porous tantalum tibial tray.

The initial results shows that interference fit can have a large affect on micromotion at the peg region. Micromotion is higher for the monoblock implant compared to the modular implant for walking with normal bone (Figure B-7).

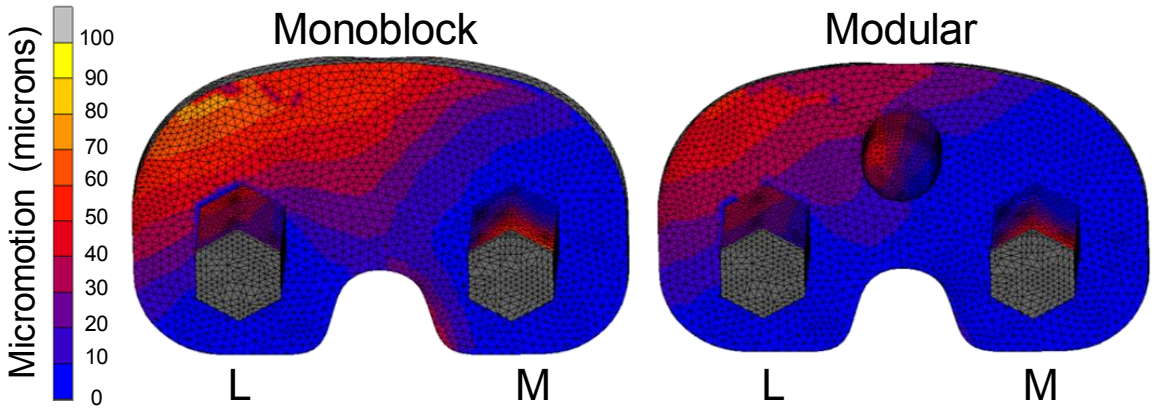

Figure B-7: Micromotion based on implant type for walking with normal bone.

Models that focused on implant properties currently available on the market were also investigated. The properties used for this investigated were outlined below (Table B-1).

Table B-1: Material properties for model design comparison.

	Ti Beads	Fiber Metal	Porous Tantalum	Tritanium®	Biofoam®
Elastic Modulus (GPa)	110*	110*	3.3	110*	2.9
Porosity	40	45	75	72	65
Substrate E-modulus (GPa)	66^	6.9[a]	3.3	2.7	2.9
Coefficient of friction, μ	0.53	0.5[a]	0.88	1.01	0.56

*Elastic modulus from solid metal.
^Estimated [263]
[a][264]

Implant properties showed a minimal affect on micromotion (shear) for the modular design. Comparing the tantalum and Tritanium® to the Biofoam, there is a slight

difference due to coefficient of friction. For the modular design, the effect of coefficient of friction is minimal (Figure B-8).

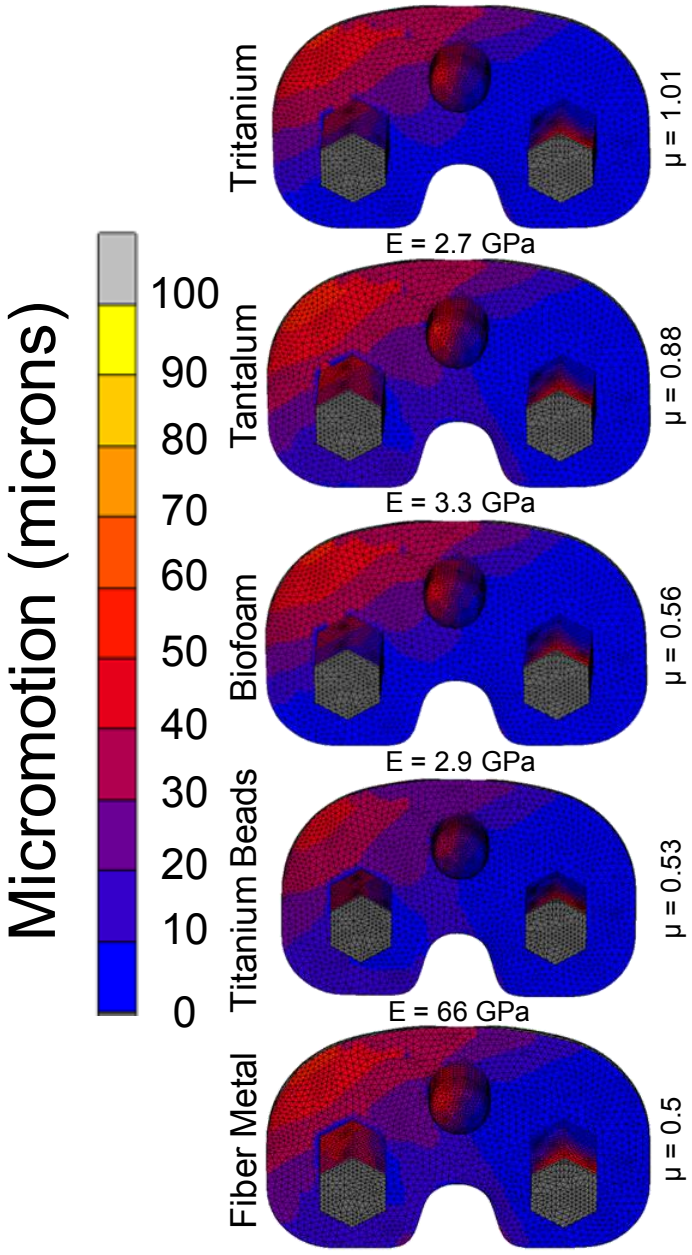

Figure B-8: Modular tibial trays with different properties. Note: Presented with decreasing coefficient of friction.

The change in elastic modulus shows little affect on shear micromotion (Figure B-9).

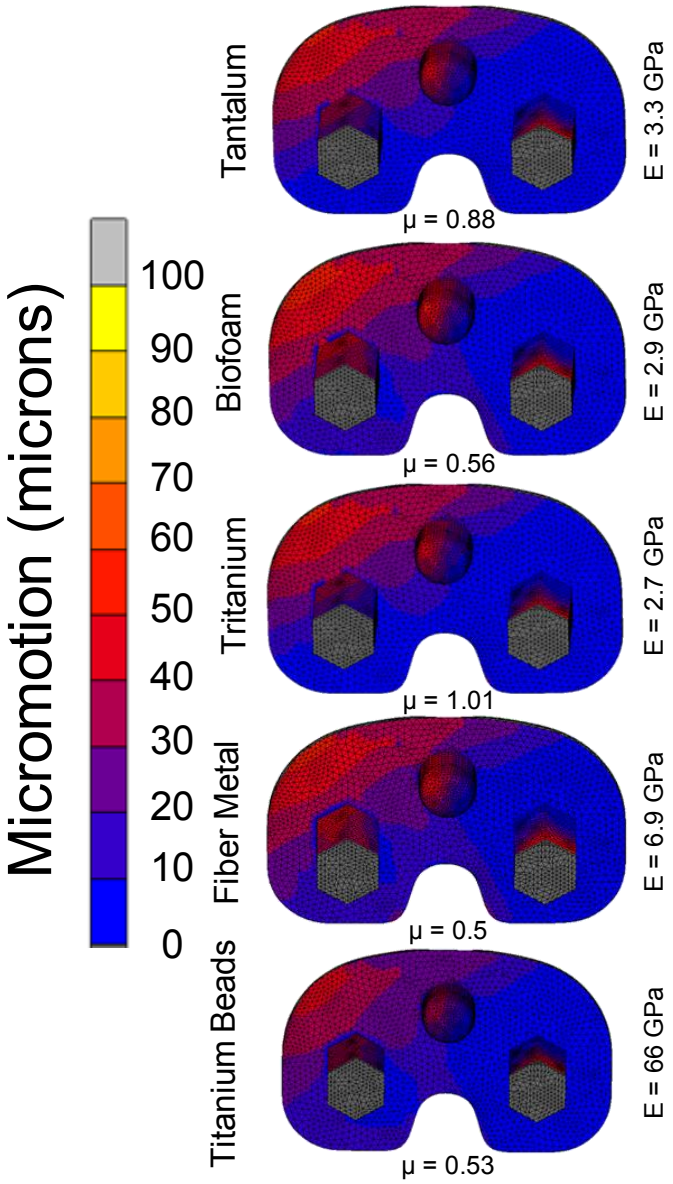

Figure B-9: Modular tibial trays with different properties. Note: Presented with increasing elastic modulus.

For the monoblock design, increasing the elastic modulus showed minimal difference (Figure B-10).

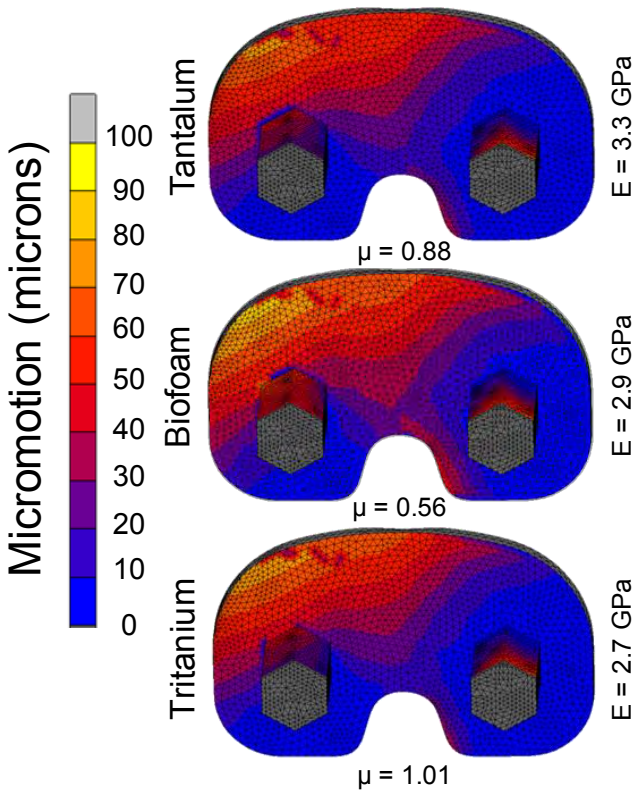

Figure B-10: Monoblock tibial trays with different implant properties. Note: Presented with increasing elastic modulus.

Lower coefficient of friction resulted in higher micromotion when comparing different implant properties for the monoblock design (Figure B-11). There was limited affect seen when the coefficient of friction increased from 0.88 to 1.01 for design properties.

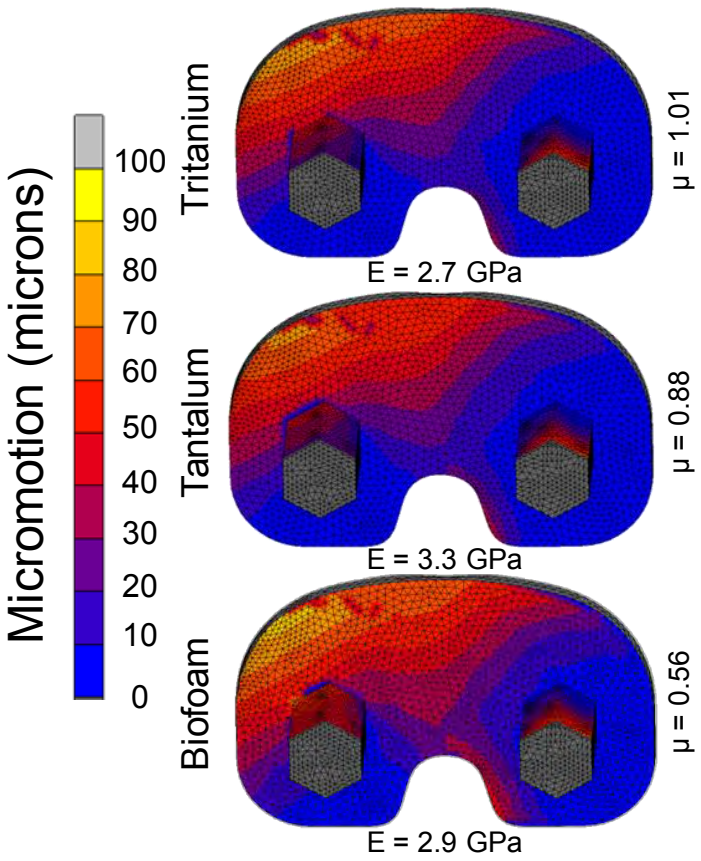

Figure B-11: Monoblock tibial trays with different implant properties. Note: Presented with decreasing coefficient of friction.

Appendix C Bone Remodeling Pilot Study

Develop a model to predict stress and bone remodeling of a porous tantalum tibial tray.

Abstract

Mechanical loosening remains one of the main revision reasons for total knee arthroplasty (TKA). A retrieval analysis study of porous tantalum tibial trays has shown less bone ingrowth into the monoblock design compared to the modular design. Finite element modeling is a technique that can be used to investigate specific factors that affect bone remodeling or stress on the tibial bone. However, models need to be developed that represent the clinical setting. The first objective of this study was to develop a model of a cemented and porous tantalum tibial component with bone remodeling to provide a direct comparison to a previous clinical study. The second objective was to assess the difference in stress on the tibial implant based on implant design type (modular vs monoblock). Case-specific FE models of tibia bone with a cemented component and porous tantalum component were created. A remodeling algorithm was used to determine bone change over time. A modular porous tantalum model was developed to assess the effect of implant design on tibial bone stress. The average bone loss in the cemented clinical study (~45%) was significantly higher than the FE model (~25%). The average bone loss in the cemented clinical study (~33%) was similar to the FE model results (~32%). When comparing the modular and monoblock porous tantalum designs, we saw higher stress on the tibial bone for the modular design. Future work can investigate the effect of loading distribution, bone quality and other implant design factors.

Introduction

Mechanical loosening remains one of the main revision reasons for total knee arthroplasty (TKA) [102]. After TKA, proximal tibial bone resorption, due to stress-

shielding caused by the stiff implanted prosthesis, is a clinical concern. The bone resorption can have detrimental effects on fixation stability and may result in component loosening [265, 266]. To lessen the bone resorption, materials with lower elastic modulus and higher porosity, aimed at achieving solid fixation, have been developed [152]. One of these new coatings, made of tantalum, is designed with a high porosity (75-85%), increasing the potential for bone ingrowth. It has favorable frictional properties ($\mu = 0.88$) to reduce micromotion between the bone and tray, and a low elastic modulus (2.5–3.9 MPa) to reduce stress shielding [151, 153, 164].

A clinical study has shown significantly less decrease in bone mineral density (BMD) when using porous tantalum tibial trays compared to cemented cobalt-chromium tibial components [267]. Our retrieval work has shown that bone ingrowth into porous tantalum tibial implants is significantly less than other porous tantalum implants. Additionally, we saw that bone ingrowth was concentrated in the upper 500 um of the porous substrate. Modular porous tantalum implants also showed a significantly higher amount of bone ingrowth than the monoblock implants.

We wanted to developed finite element models that simulate clinical results and determine if tibial tray implant design affects implant stress. Existing finite element modeling of porous tantalum implants has been limited to 2D glenoid implant ingrowth model [217], microstructural models of the porous tantalum-UHMWPE construct [218] and a femoral stem ingrowth model [210]. The first objective of this study was to develop a model of a cemented and porous tantalum tibial component with bone remodeling to provide a direct comparison to a previous clinical study. The second objective was to assess the difference in stress on the tibial implant based on implant design type (modular vs monoblock).

Methods

Model Creation

A cemented tibial component with titanium properties was created based on the geometry of a previous study [215].

Frictional contact was simulated at the implant-bone interface using a node-to surface contact algorithm (MSC.MARC-Mentat 2013, MSC Software Corporation, Santa Ana, CA, USA). The material properties for the implant and bone-implant contact were based on previous studies [152, 217].

Table C-1. Material properties used in FE models.

Material	Young's Modulus (GPa)	Poisson's Ratio	Bone-Implant Friction Coefficient
UHMWPE	1.174	0.4	N/A
Porous Tantalum w/UHWMPE	4.26	0.35	N/A
Porous Tantalum	3.3	0.31	0.88
Cement	2.1	0.4	1.0

We modified the Orthoload data to fit our implant design [258]. Orthoload is a free public database of forces and moments acting in orthopaedic implants during activities [259]. It should be noted that the implant used in the Orthoload measurements and our finite element models are not of the same design. The coordinate system of the model was defined with the x-axis in the lateral to medial direction, the y-axis in the anterior to posterior direction and z-axis in the superior to inferior direction (Figure C-1).

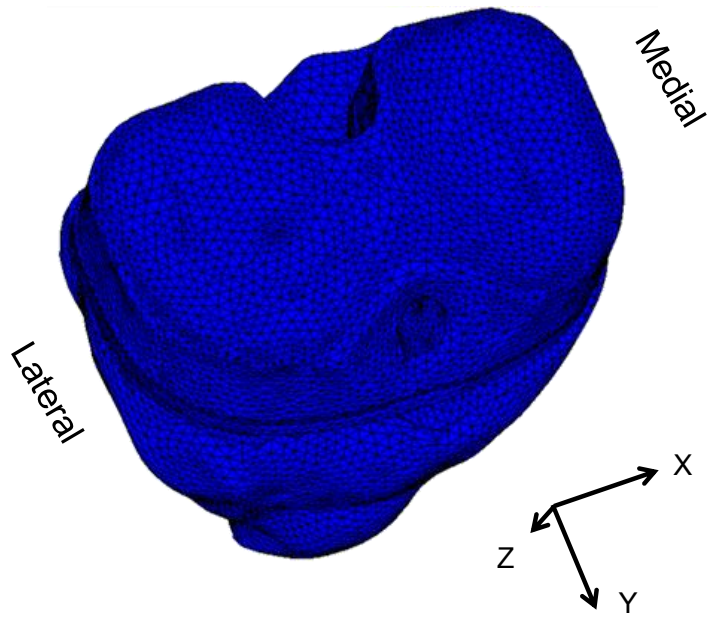

Figure C-1: The coordinate system for the model.

The forces in the x, y and z-direction were applied at the top center of each condyle. For the intact case, we applied the Fx, Fy and Fz force at the maximum Fz during walking. Similarly, we calculated the maximum force for standing up and descending stairs. The intact case served as the reference for the strain adaptive bone remodeling.

Bone Remodeling Simulation

Strain adaptive remodeling theory was used to stimulate changes in bone mineral density in time ($d\rho/dt$) [268]. The strain energy density per unit bone mass, $S=U/\rho$. Where U is the strain energy density and ρ is the apparent density. This is used as a mechanical stimulus to regulate linear remodeling process. Two FE models were created for each comparison. For example, for the monoblock model, we create a S_{ref} model for the intact bone case (Figure C-2) and S_{op} of the tibia with an implant.

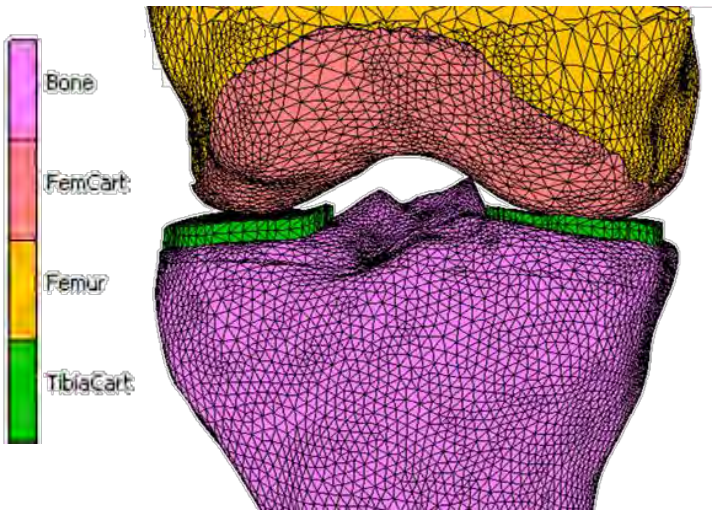

Figure C-2: Intact or Sref model, with a femur, femoral cartilage, tibial cartilage and a tibia.

The S of every element in all locations was generated for two situations of i) intact bone (reference S_{ref}) and ii) implant bone (prosthesis, S_{op}). In each time step of the stimulation, S_{op} was compared with S_{ref} against the remodeling rule. A "Dead zone" was defined with a threshold level "s" set at 0.7 where there would be no bone loss or gain.

The strain-adaptive remodeling algorithm was implemented in Fortran and developed at the Orthopaedic Research Lab, Radboud University Medical Center, Netherlands. The algorithm is based on internal modeling and is site dependent. The difference in local strain energy density per unit bone mass between preoperative (R_{ref}) and postoperative situation was taken as the Stimulus (S) for bone remodeling when outside the dead zone [33] (Figure C-3). When the stimulus is smaller than the dead zone, bone resorption will occur. When the stimulus is larger than the dead zone, bone apposition will take place. The size of the 'dead zone' was based on a previous study [210]. In the current model the remodeling signal was averaged over the three following loading conditions ($S=(S_1+S_2+S_3)/3$). The reconstructions were subjected to a peak loading for walking (S_1), standing up (S_2) and descending stairs (S_3). The local rate of bone mass change was also dependent on the density, based on the assumption that

the remodeling rate depends on the size of the available free bone surface. Typically, the free surface is low in the case of low bone density and high in the case of very high density [269]. Time in the remodeling simulation (computer time unit, ctu) depends on the maximum stimulus per iteration. The time iteration decreases with a greater stimulus.

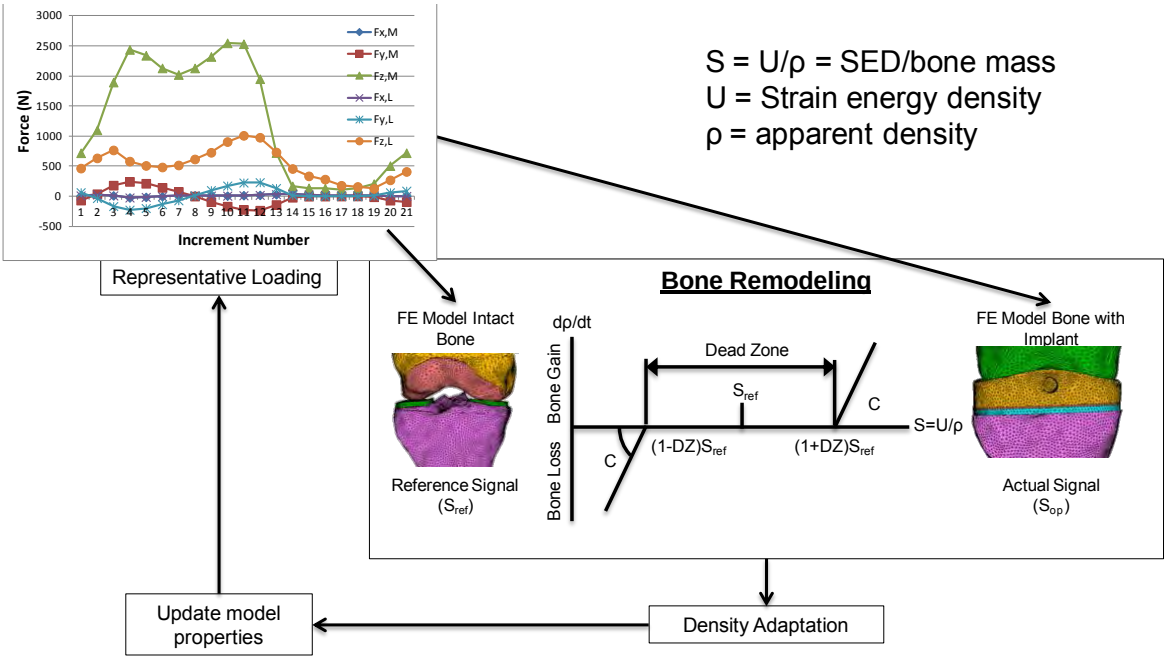

Figure C-3: The process for the bone remodeling simulation.

We compared our remodeling results with a previous DEXA (Dual-energy X-ray absorptiometry) clinical study that compared bone mineral density changes between porous tantalum tibial trays and cemented tibial trays [267]. One study showed significantly less decrease in bone mineral density (BMD) when using porous tantalum tibial trays compared to cemented cobalt-chromium tibial components [267] (Figure C-4

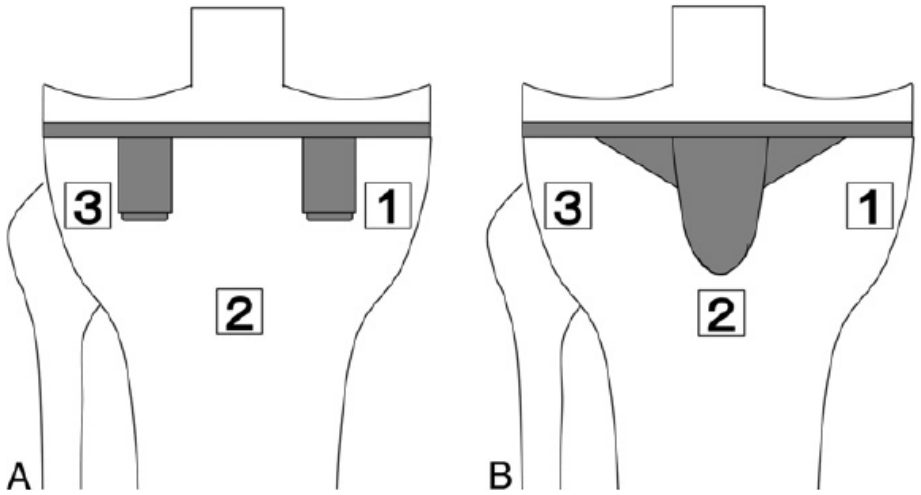

Figure C-4: Bone mineral density measurement location on A) porous tantalum tibial tray and B) cemented tibial tray [267].

To allow for clinically relevant interpretation of the remodeling results, we used an in-house software package (Orthopaedic Research Lab, Radbond University Medical Center, Netherlands, DCMTK MFC 10.8) to project the results of the remodeling simulation onto 2D DEXA images. First, a 3D (X,Y,Z) voxel mesh is mapped onto the FE reconstruction. Subsequently, for each bone tetrahedral element, its intersection volume with each voxel is calculated. The intersection volume is then multiplied by the calcium equivalent of the element and added to the calcium equivalent of the corresponding voxels. Subsequently, a 2D pixel mesh with known a calcium equivalent is created according to the chosen DEXA plane (e.g. (X,Y)). Each pixel has a calcium equivalent value corresponding to the summation of the values of 3D voxels ($X_1,Y_1,Z_{1\div n}$) along the same (X_1,Y_1) coordinates. Non-bone elements do not contribute to the amount of calcium. In fact, if they were present along the (X_1,Y_1) coordinate when converting to the 2D pixel mesh, the pixel will be visualized as a stem pixel on the DEXA. We defined the three zones ([267] and computed bone density (g/cm^2) and local bone mineral content

(BMC) (g) at different time points. We calculated bone density at each location after one, two, three, four and five years postoperatively for the cemented and monoblock model.

Comparisons of the 3 regions (central, lateral and medial) are made between the porous tantalum tibial tray and cemented tibial tray. We also compared the average bone mineral density change for all three locations to the clinical results. A modular implant was created so that the stress distributions on the implant could be compared to determine the effect of implant design.

Results

Our developed FEMs of the cemented tibial tray and porous tantalum monoblock tibial tray model showed overall a similar trend in BMD loss to a previous clinical study [267]. For the cemented case, our simulation showed less bone loss than the actual clinical study. The average bone loss in the cemented clinical study (~45%) was significantly higher than the FE model (~25%). The highest bone loss in the clinical study for the cement implant was in the lateral region (Figure C-6). The cement FE model showed the highest bone loss in the central region (Figure C-5). The FE model for cemented central predicted the bone remodeling of the clinical results (Figure C-5).

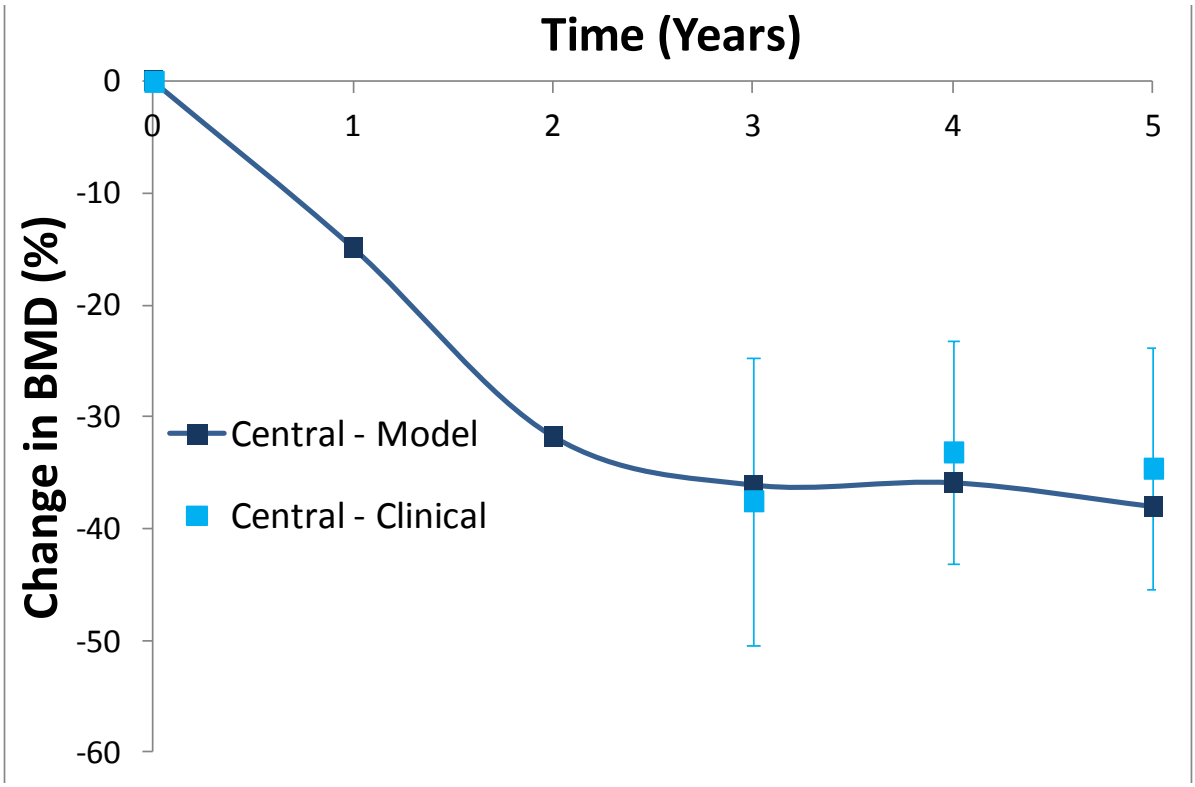

Figure C-5: Change in BMD comparing the clinical and FE model results for the cemented model in the central region. The error bar indicate the reported error in the results from the clinical study [267].

The FE model for cemented predicted lower bone loss at the lateral region compared to the clinical results (Figure C-6).

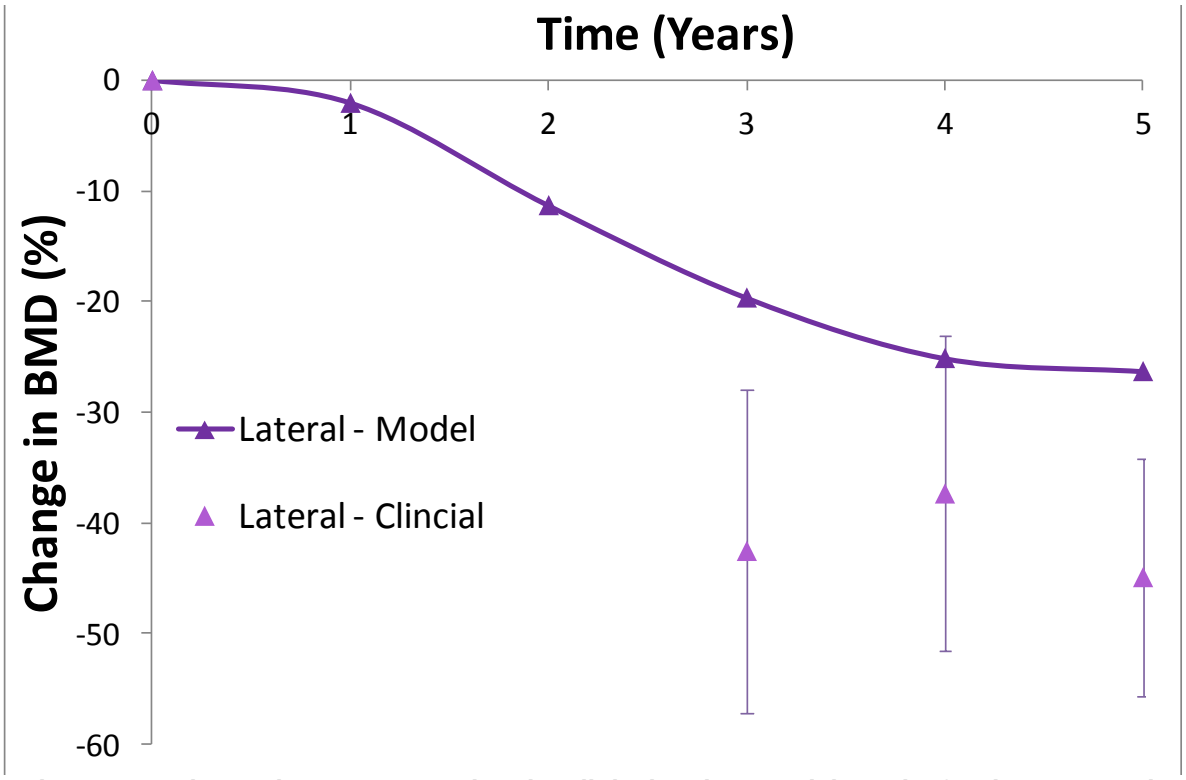

Figure C-6: Change in BMD comparing the clinical and FE model results for the cemented model in the lateral region [267].

The FE model for cemented predicted lower bone loss at the medial region compared to the clinical results (Figure C-7).

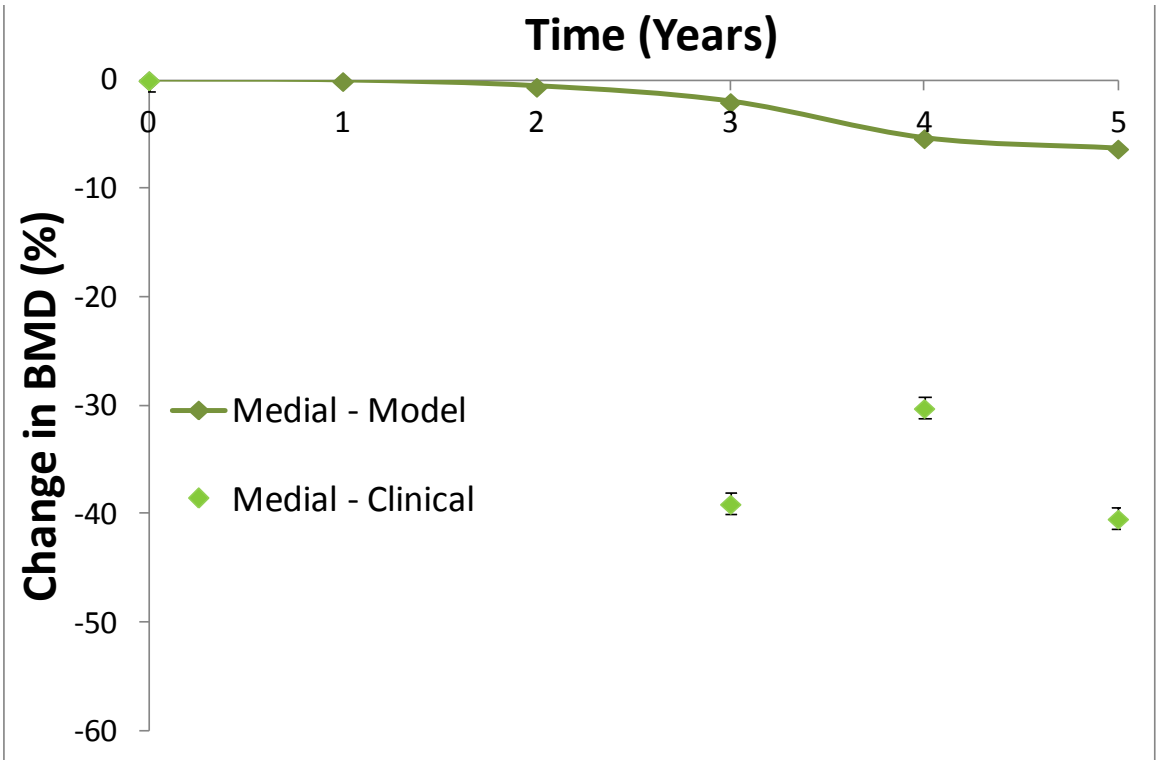

Figure C-7: Change in BMD comparing the clinical and FE model results for the cemented model in the lateral region [267].

The average bone loss in the monoblock porous tantalum clinical study (~33%) was similar to the FE model results (~32%). The FE model for cemented predicted similar bone loss at the central region compared to the clinical results (Figure C-8).

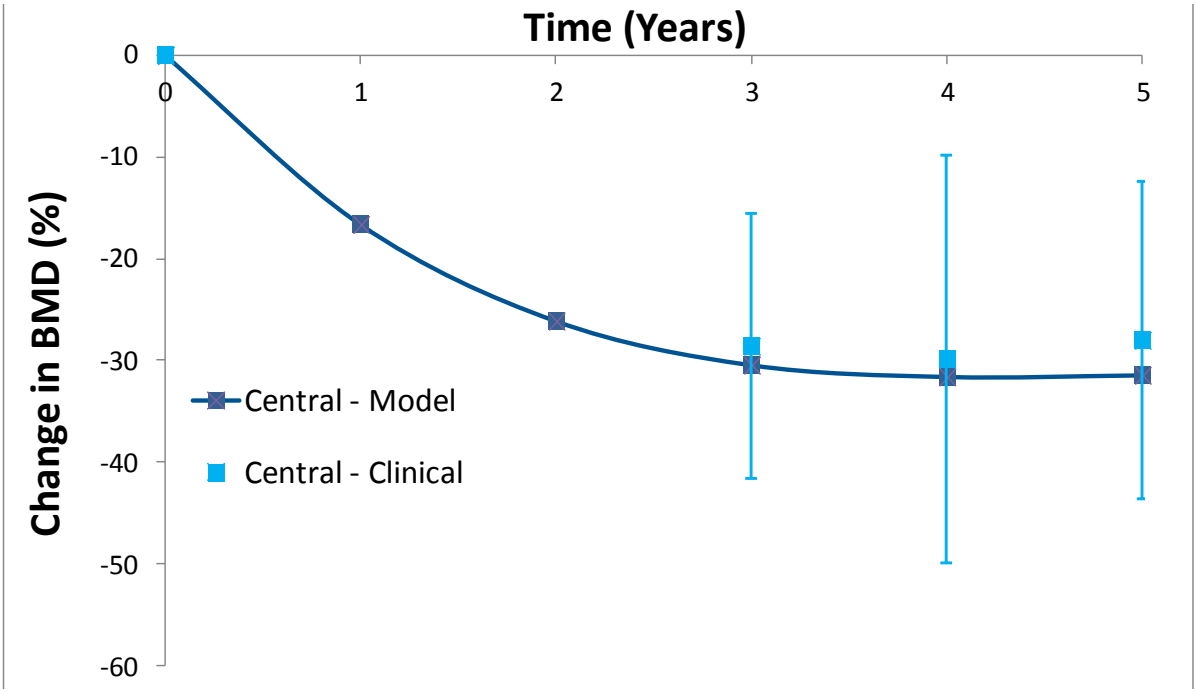

Figure C-8: Change in BMD comparing the clinical and FE model results for the monoblock model in the central region [267].

The FE model for monoblock porous tantalum predicted higher bone loss at the lateral region compared to the clinical results (Figure C-9).

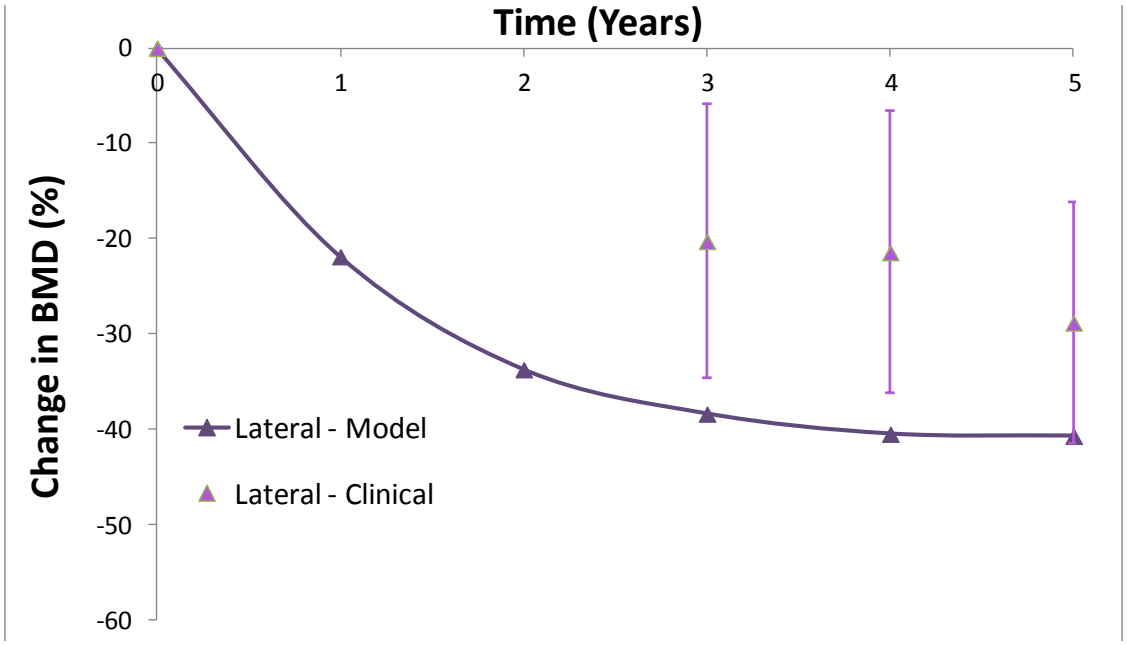

Figure C-9: Change in BMD comparing the clinical and FE model results for the monoblock model in the lateral region [267].

The FE model for monoblock porous tantalum predicted lower bone loss at the medial region compared to the clinical results (Figure C-10).

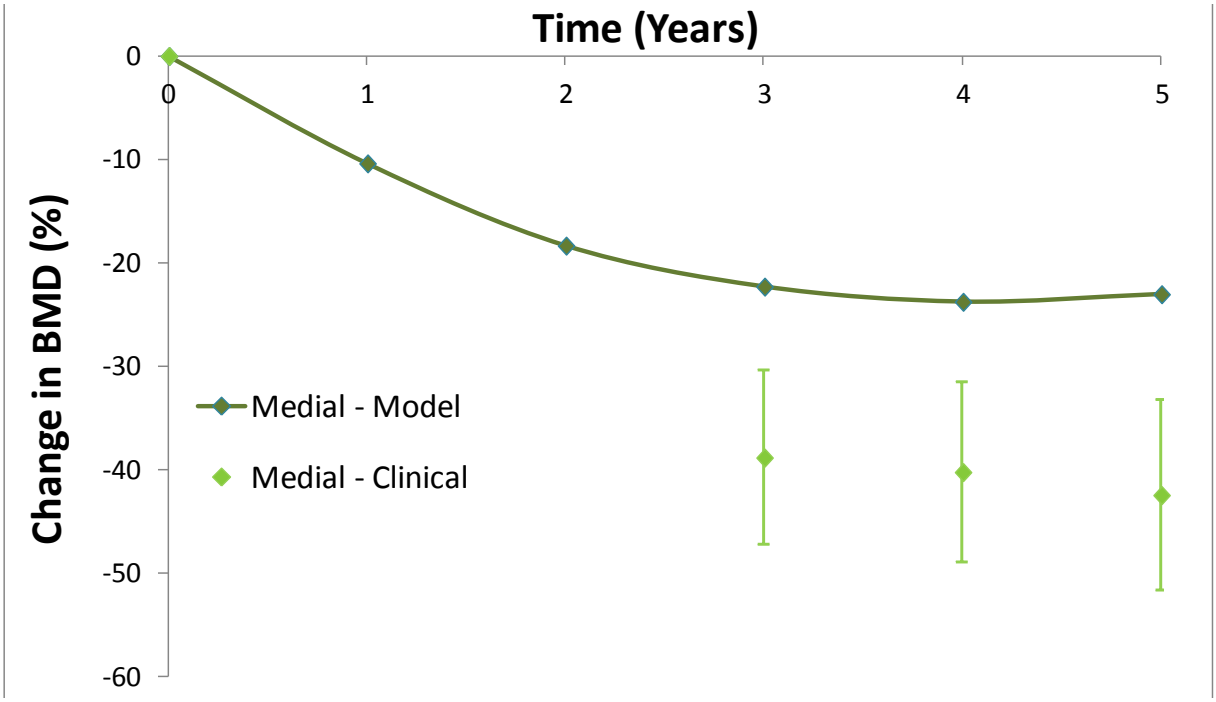

Figure C-10: Change in BMD comparing the clinical and FE model results for the monoblock model in the medial region [267].

Discussion

We developed a finite element models that were able to model the similar trend of bone resorption seen in a clinical study. Our porous tantalum monoblock implant showed similar results to a previous clinical study [267]. Our cemented model showed less bone than the clinical study.

Our study had several limitations due to FEM techniques. These limitations include assumptions on implant material properties, bone properties [270], implant-bone interface conditions and loading conditions [271, 272]. First, the geometries of the implants were estimated and not from original design drawings. Therefore, our modeled implants are not guaranteed to accurately represent all the complexities of the implants. For our model, we only assumed loading on the femur and femoral component. All muscle and ligament forces were neglected. For the loading, we assumed that the load was higher on the medial than lateral side.

The average bone loss in the cemented clinical study (~45%) was significantly higher than the FE model (~25%). The lower bone loss in the FE model may be due to several reasons. The implant geometry for the cement model was not the same implant used in the clinical study. It is possible the difference in the geometry affected the remodeling results. For our model, the contact at the cement-bone interface was modeled as bonded. A previous study of a micro-mechanical model showed that a coefficient of friction of 0.3 was closest to experimental data [273]. For our model, the contact at the implant-cement interface was modeled as bonded. Other studies have shown a coefficient of 0.25-0.5 between the implant-cement interface to be more accurate [274, 275].

The average bone loss in the cemented clinical study (~33%) was similar to the FE model results (~32%). However, there was a significant difference between the remodeling on the medial vs lateral side. This may be due to how the load is applied within our model. It is possible that the loading on the joint pre-surgery and post-surgery for total knee replacement could affect the modeling results. For example, a patient may load the medial side of the joint pre-surgery. After the surgery, loading may then become even between the lateral and medial portion of the joint. Further investigation in the effect of loading may allow the FE models to be more representative of the clinical results [267].

In our model, we assumed that there was no gap between the bone-implant interface. In the clinical setting, it is more likely that there is a gap. FE models that are more representative of the clinical setting may yield further insight into the progression of bone ingrowth into porous tantalum implants.

Vita

Josa Ann Hanzlik, M.S.

Ph.D, Biomedical Engineering, Drexel University, 2015
M.S., Biomedical Engineering, Drexel University, 2013
M.S., Mechanical Engineering, Rochester Institute of Technology, 2008
B.S., Mechanical Engineering, Rochester Institute of Technology, 2008

Drexel Graduate Studies Office: Dissertation Fellowship Spring 2015
Whitaker Fellow: Netherlands 2013-2014
Drexel University: Director's Award for Promotion of Professional and Leadership Development of Women Engineers, March 2014
Calhoun Fellowship, 2008-2010

Publications:

1. **Hanzlik JA**, Day JS, Rimnac CM, Kurtz SM, Ingrowth retrieval study g. Is There A Difference in Bone Ingrowth in Modular Versus Monoblock Porous Tantalum Tibial Trays? J Arthroplasty 30(6): 1073, 2015.

2. Veruva SY, Lanman TH, **Hanzlik JA**, Kurtz SM, Steinbeck Mj. Rare complications of osteolysis and periprosthetic tissue reactions after hybrid and non-hybrid total disc replacement. European Spine Journal. 2014:1-8.

3. **Hanzlik JA**, Day JS and The Ingrowth Retrieval Study Group. Bone Ingrowth into Retrieved Porous Tantalum Implants. Journal of Arthroplasty, 2013; 28 (6): 922-7.

4. Higgs GB, **Hanzlik JA**, MacDonald DW, Gilbert JL, Rimnac CM, Kurtz SM. Is increased modularity associated with increased fretting and corrosion damage in metal-on-metal total hip arthroplasty devices? A retrieval study. J Arthroplasty. 2013; 28:2-6.

5. Higgs GB, **Hanzlik JA**, MacDonald DW, Kane WM, Day JS, Klein GR, Parviz iJ, Mont MA, Kraay MJ, Martell JM, Gilbert JL, Rimnac CM, Kurtz SM. Method of characterizing fretting and corrosion at the various taper connections of retrieved modular components from metal-on-metal total hip arthroplasty. In: Kurtz SM, Greenwald AS, Mihalko WM, Lemons J, editors. Metal-on-Metal Total Hip Replacement Devices, STP 1560. Conshohocken, PA: ASTM; 2013.

6. Day J, **Hanzlik J**, Klein GR, Levine HB, Hartzband MA, Parvizi J, Kraay MJ, Rimnac CM, Kurtz SM. Porous coatings, **Scientific Exhibit No. 18**, 79th Annual Meeting of the American Academy of Orthopaedic Surgeons, San Francisco, CA, February 7–11, 2012.

7. **Hanzlik J**, Patel JD, Ochoa J, Shkolnikov YP, Horn Q, Pavri BB, Greenspon AJ, Kurtz S, Why are Implantable Cardioverter-Defibrillators and Pacemakers Being Revised Today? Proceedings from the Materials and Processes for Medical Devices, Minneapolis, MN, August 8-9th, 2011, 57 - 62.

8. MacDonald D, **Hanzlik J**, Sharkey P, Parvizi J, Kurtz SM. In vivo oxidation and surface damage in retrieved ethylene oxide-sterilized total knee arthroplasties. Clin Orthop Relat Res. 2012;470:1826-1833.

9. **Hanzlik J**, Cretekos E, Lamkin-Kennard KA. Biomimetic Leukocyte Adhesion: A Review of Microfuidic and Computational Approaches and Applications. J Bionic Eng, 2008, 5 (4), 317 - 327.